



Master Thesis

In partial fulfillment of the requirements of the academic degree

Diplom-Ingenieurin

INFLUENCE OF THE CREST WIDTH ON SEISMIC RESPONSE OF ARCH DAMS

In the field of study

Civil Engineering Geotechnical and Hydraulic Engineering

submitted to the

Institute of Hydraulic Engineering and Water Resources Management

Graz University of Technology

Graz, March 2020

Author:

Kerstin GREBENAR

01131050

Supervisor:

Univ.-Prof. Dipl.-Ing. Dr. techn. Gerald ZENZ

Co-Supervisor:

Dipl.-Ing. Edwin STAUDACHER

EIDESSTÄTTLICHE ERKLÄRUNG

Ich erkläre an Eides statt, dass ich die vorliegende Arbeit selbständig verfasst, andere als die angegebenen Quellen/Hilfsmittel nicht benutzt, und die den benutzten Quellen wörtlich und inhaltlich entnommene Stellen als solche kenntlich gemacht habe.

Ich versichere, dass ich dieses Masterarbeitsthema bisher weder im In- noch im Ausland (einer Beurteilerin oder einem Beurteiler) in irgendeiner Form als Prüfungsarbeit vorgelegt habe.

Graz am,

.....

(Unterschrift)

Danksagung

An dieser Stelle möchte ich mich bei allen Menschen bedanken, die mich bei der Erstellung dieser Masterarbeit unterstützt haben.

Großer Dank gebührt Univ.-Prof. Dipl.-Ing. Dr.techn. Gerald Zenz, der mich nicht nur durch mein Masterstudium begleitete, sondern auch meine Masterarbeit betreute. Er war stets meinem Thema sehr angetan und war gespannt auf meine Ergebnisse. Durch seine Hilfestellung während der Besprechungen konnte ich immer auf den richtigen Weg geführt werden und mich wieder besser auf die wesentlichen Fragen konzentrieren.

Des Weiteren möchte ich noch ganz besonders bei meinem betreuenden Assistenten Dipl.-Ing. Edwin Staudacher bedanken, der mich immer unterstützte, immer ein offenes Ohr für mich hatte und der sich immer Zeit für mich nahm, wenn ich eine Frage hatte. Durch seinen Einsatz und seine Hilfsbereitschaft konnte ich meine Masterarbeit in diesem Umfang abschließen.

Zusätzlich möchte ich mich noch bei meinen Eltern bedanken, die mich nicht nur finanziell, sondern auch moralisch unterstützt haben, die immer die richtigen Worte fanden, mich motivierten und immer hinter mir standen.

Kurzfassung

Diese Masterarbeit beschäftigt sich mit dem Einfluss der Mauerstärke auf die Spannungen sowie Verformungen einer Bogenstaumauer, bei seismischer Anregung. Der Gedanke dahinter ist die Bauweise Schweizer Staumauern, welche im Kronenbereich teilweise mit größeren Mauerstärken konzipiert und ausgeführt wurden. Nun gilt es das Verhalten von Kronenverstärkung bei dynamischer Anregung zu untersuchen. In dieser Parameterstudie wird die Geometrie einer 220 m hohen, doppelt gekrümmten Bogenstaumauer mit Hilfe der Finiten-Elemente-Methode diskretisiert. Dabei wird die Dicke im oberen Drittel der Schalenstruktur variiert. Daraus ergeben sich sechs verschiedene Geometrien mit Kronenstärken von 8 bis 20 m. Bei der Berechnung wird davon ausgegangen, dass keine Trennung des Dammkörpers vom Fundamentblock zulässig ist. Zudem wird ein lineares Materialverhalten berücksichtigt, das zu einem linearen Systemverhalten für alle analysierten Geometrien führt. Die Fluid-Struktur-Interaktion wird durch Koppelung der Fluidelemente mit den Volumenelementen der Bogenstaumauer berücksichtigt. Die ermittelten Ergebnisse, Spannungen wie Verformungen, unterscheiden sich im geringen Maße, wodurch für dieselben Geometrien zusätzliche Untersuchungen mit veränderter seismischer Anregung durchgeführt wurden.

Abstract

This master thesis is about the influence of the crest thickness on stresses and deformations of an arch dam, under seismic excitation. The idea behind this is the construction of Swiss dams, of which some were designed and constructed thicker in the crest area. Therefore, the behavior of the increasing crest thickness under dynamic excitation has to be investigated. In this parameter study, the geometry of a 220 m high, double-curved arch dam is discretized by using the finite element method. Thereby the thickness in the upper third of the shell structure is varied. This results in six different geometries with crest thicknesses of 8 to 20 m. During calculation it is assumed that there is no separation of the dam body to the foundation block allowed. In addition, a linear material behavior is considered, which leads to an overall linear system behavior for all analyzed geometries. The fluid-structure interaction is taken into account by coupling the fluid elements with the structure elements of the arch dam. The results obtained, stresses as well as deformations, differ slightly, so that additional studies with changed seismic excitation have been carried out for the same geometries.

Table of Contents

1. Aim and Problem Definition	1
2. Overview of Arch Dams	4
2.1. Introduction to Arch Dams and Dam History [1]	4
2.2. Types of Arch Dams [2]–[4]	5
2.2.1. Constant-Radius Arch Dam	5
2.2.2. Constant-Angle Arch Dam	6
2.2.3. Double-Curvature Arch Dam [3], [4]	7
2.3. Load Cases [1], [5]–[7]	8
2.3.1. Dead Load	8
2.3.2. Hydrostatic Pressure	9
2.3.3. Earthquake - Hydrodynamic Pressure	10
2.3.4. Temperature	11
2.3.5. Ice	11
2.3.6. Silt	12
3. Arch Dams in Austria and Switzerland	13
3.1. Introduction [8], [9]	13
3.2. Dams in Austria [9], [10]	13
3.2.1. General Situation	13
3.2.2. History of Austrian Dams [10]	14
3.2.3. Dam Surveillance	14
3.2.4. Legal Framework and Responsible Committee	15
3.3. Dams in Switzerland [11], [12]	16
3.3.1. General Situation	16
3.3.2. History of Swiss Dams	17
3.3.3. Dam Surveillance	17

3.3.4.	Legal Aspects and Responsible Committee.....	18
3.4.	Shapes of Austrian and Swiss Arch Dams [10], [12].....	19
3.4.1.	Austrian Arch Dams	19
3.4.2.	Swiss Arch Dams.....	21
3.5.	Schlegeis (AT) Compared to Santa Maria (CH) [10], [12]	23
3.5.1.	Schlegeis	24
3.5.2.	Santa Maria.....	24
3.6.	Comparison of the Arch Dams in Austria with Arch Dams in Switzerland [12], [13].....	25
4.	Technical Prerequisites	29
4.1.	Basic Geometric Forms [14], [15].....	29
4.1.1.	Linear Functions	29
4.1.2.	Conic Sections and their Equations Written in Vertex Form.....	30
4.1.3.	Main Form of a Circle.....	35
4.2.	Barlow's Formula [1].....	36
4.3.	Introduction to Structural Dynamics [16]–[19].....	37
4.3.1.	Single Degree of Freedom System	37
4.3.2.	Undamped SDOF System with Free Vibration	38
4.3.3.	Damped SDOF with Free Vibration.....	40
4.3.4.	Multiple Degree of Freedom System (MDOF).....	42
4.3.5.	Undamped MDOF System with Free Vibration	43
4.3.1.	Damped MDOF System with Free Vibration	45
4.3.2.	Rayleigh Damping.....	45
4.4.	The Finite Element Method [20], [21]	47
5.	Numerical Case Studies	53
5.1.	Introduction to the Calculation done with ANSYS	53
5.2.	Geometry and Model [22].....	55
5.3.	Material Parameter.....	56

5.4. Acceleration Time History	57
5.5. Mesh	58
5.6. Element and Node Numbering [23], [24]	60
5.7. Rayleigh Damping	61
5.8. Loading	62
5.9. Results	63
5.10. Summary.....	111
Bibliography	I
List of Figures.....	IV
List of Tables.....	VIII
Appendix A.....	X

1. Aim and Problem Definition

The aim of this master thesis is to examine the influence of the crest width of an arch dams' response on seismic loading. This is achieved by using the simulation program ANSYS. In this program the geometry of the dam is implemented and the response of the arch dam due to seismic ground movement is simulated and investigated. The used geometry is described below. The first arch dam has a crest width of 8 m, which gets in "steps" thicker up to 20 m, to see if there are any differences in the dam behavior.

This master thesis compares the design and geometric shape of arch dams in Switzerland, which are designed and constructed thicker at the dam crest.

The aim of this thesis is to conduct a parameter study and to investigate the sensitivity of the shell structure to seismic loading. Optimizing the geometry is not part of this master thesis.

Geometry of the Arch Dam

The main dimensions of the double curvature arch dam on which the parameter study is based on are listed below.

Key Data for Arch Dam Model:

- Valley width at crest: ~430 m
- Valley width at bottom: ~80 m
- Total Height: 220 m
- Width on the crest: 8 m
- Width in the middle section on bottom: 55 m

The Geometry is a symmetric double curved arch dam:



Figure 1: Geometry of Arch Dam Model

For the Foundation Model a symmetric block is used.

Data for Foundation Model:

- Length: 1000 m
- Width: 1000 m
- Height: 500 m

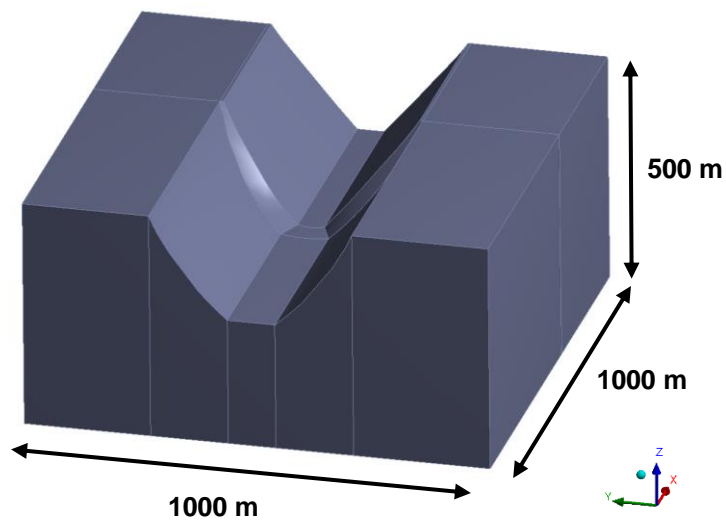


Figure 2: Geometry of Foundation Model

The minimum length of the Reservoir Model is created by choosing twice the height of the dam.

Data for Reservoir Model:

- ~450 m in the vertex of the reservoir (>2x Height of the Dam)

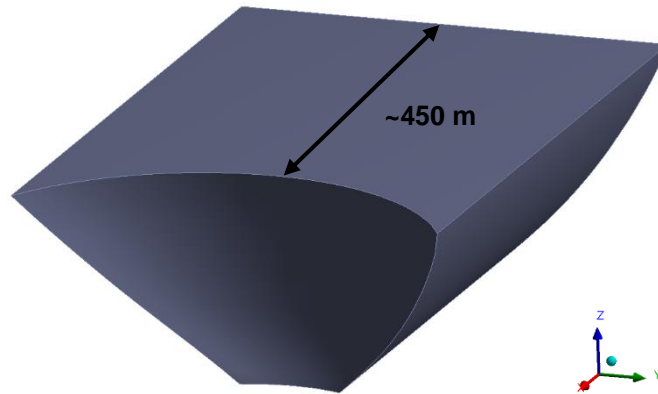


Figure 3: Geometry of Reservoir Model

2. Overview of Arch Dams

2.1. Introduction to Arch Dams and Dam History [1]

A dam is a natural or man-made structure, which can vary in size and form depending on the width of the river or of the valley, with the purpose to impound a river and to store water. These water retaining structures provide storage of water, not only to produce electricity by hydropower, but also for drinking water and irrigation purpose. They are also an attraction for recreational activities.

The first dam remains were found in Azerbaijan and Jawa. These small natural earth dams date back to 4000 B.C. and were built to provide small surrounding towns with approximately 2000 inhabitants with water. The oldest arch dam known of is the Glanum Dam, also known as Vallon de Baume Dam in France. It is 12 m high and 18 m in length and dates back to the Roman times. It was built out of two masonry walls and its purpose was to supply the nearby town Glanum with water.

Based on the shape of the valley and the given foundation, the construction materials for dams are sand, soil or rock and concrete or Rolled Compacted Concrete (RCC). By piling up the fill material the so-called earth and rock filled dams are created which can be built as fill dams with central core or surface sealing. Concrete dams can differ in form, such as the gravity dam, the arch gravity dam and the arch dam. An arch dam is slender shape optimized shell structure with the main principle of transferring horizontal acting loads towards the valley flanks.

This master thesis is specifically devoted to arch dams, in particular on double curvature arch dams.

2.2. Types of Arch Dams [2]–[4]

Ancient dams were not very tall. Over time the knowledge to design and construct these structures improved and due to that it was possible to build higher dams. At the moment the tallest dam in the world is Jinping I the arch dam in China, with a maximum height of 305 m and a crest length of 569 m. With modern calculation processes, complex arch dam shapes can be designed by experienced engineers. If the foundation at the dam location has sufficient bearing capacity, the optimum shape of the arch dam must be found. This is achieved by adapting the geometry to the local conditions, by changing the angle, the radius and the curvature of the dam.

These three main types of arch dams are called: the constant-radius arch dam, the constant-angle arch dam and the double-curvature arch dam.

2.2.1. Constant-Radius Arch Dam

The geometry of this dam is defined by a circular arch and its radius is constant over the dam's height. As a result, the upstream face is of cylindrical shape. The thickness increases from the crest to the base of the dam, based on the corresponding hydrostatic water pressure in the reservoir.

By transforming the Barlow's formula, the thickness of the arch dam can be calculated for preliminary designs.

$$d = \frac{p(z) * r}{\sigma} \quad (1-1)$$

with:

d [m] ...thickness of the dam

$p(z)$ [MPa] ...hydrostatic pressure

r [m] ...radius of the arch, referring to the center of the arch ($d/2$)

σ [MN/m²] ...hoop stress

A minimum of volume can be reached by minimizing the area of the cross-section of the arch dam. This gives an ideal opening angle of 133°. Deviations of this angle have only a slightly impact on the volume. Because of that, angles between 120° and 140° can be chosen. This leads to a limitation concerning the adaption of the dam to the topographic conditions of the valley.

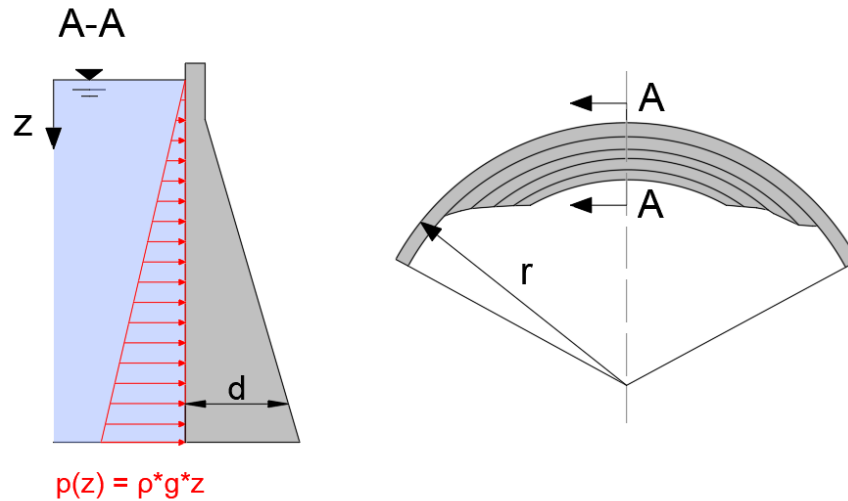


Figure 4: Constant-radius arch dam - layout and cross section, cf. [3]

2.2.2. Constant-Angle Arch Dam

Unlike the constant-radius arch dam, the radii of the arches of the constant-angle arch dam vary. The central angle over the whole arch stays the same. As a result of this setup, the dam is curved on its upstream side and has a vertical downstream face in the main section of the dam. The opening angle should be between 100° and 130°.

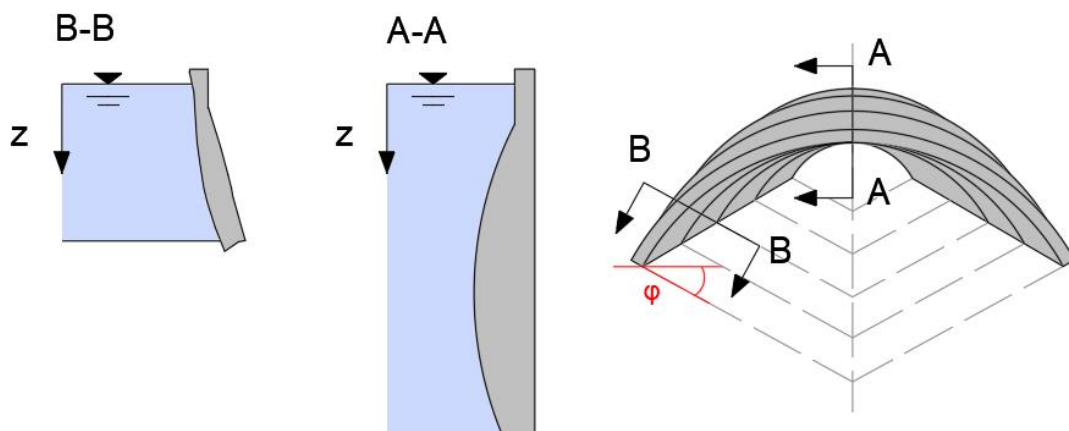


Figure 5: Constant-angle arch dam - layout and cross section, cf. [3]

2.2.3. Double-Curvature Arch Dam [3], [4]

The upstream and downstream faces of this dam are curved in cross stream and vertical direction. The double curvature dam design allows a reduction of volume and reduces the thickness of the dam structure. The construction of this kind of dam is more sophisticated, compared to the other designs. Double curved arch dams are suitable for narrow as well as for wide spanned valleys.

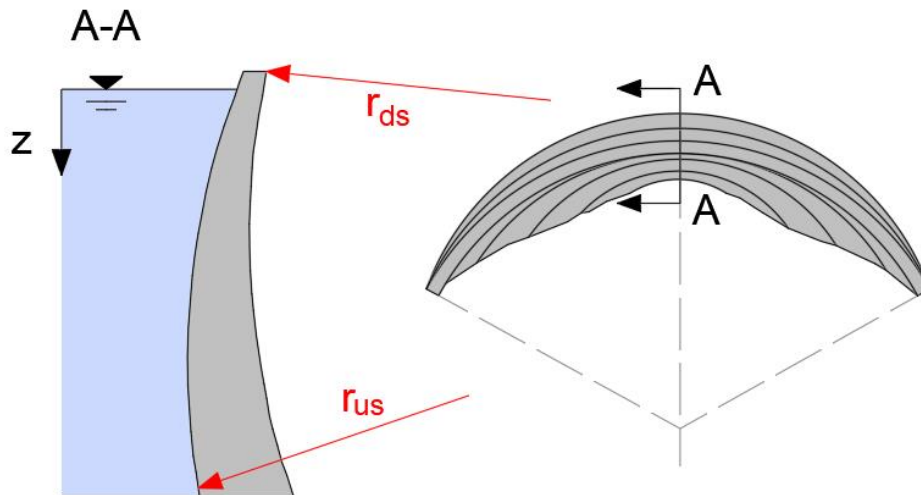


Figure 6: Double-curvature arch dam - layout and cross section, cf. [3]

2.3. Load Cases [1], [5]–[7]

Like every statically indeterminate system, the loads acting on the construction can be summarized as loads acting permanently, which are permanent loads, and as restrained stresses which are created due to the restraint of deformation or due a change in the volume. Permanent loads are such as the dead load and the water pressure, acting normal on the dam surface. Also, sedimentation and ice pressure rate among permanent loads. Restrained stresses can appear as deformations of the ground due to the water load and joint water pressure. Temperature changes of the water and the air, or during hardening of the concrete can also cause restrained stresses, as well as shrinkage and swelling of the concrete.

2.3.1. *Dead Load*

To construct concrete dams, blocks of concrete are poured which are separated by vertical contraction joints. Continuously poured concrete dams are made of Roller Compacted Concrete (RCC). RCC is often used because of its low shrinkage potential. The construction method is decisive for the calculation of the static system. The blocks can be calculated as detached vertical cantilevers, if the blocks are poured separately and the block joints are grouted after completion of the dam, afterwards the reservoir can be filled. If the reservoir is already filled in stages during concreting, but is emptied before the horizontal block joint injection, the blocks can be assumed to be detached. Another construction method is filling the reservoir immediately after concreting without reducing the water level. This leads to a different stress distribution because of the dead load of the newly poured blocks acts on the continuous arch below.

To calculate the dead load, the formula below can be used:

$$G = m_d * g \quad (2-1)$$

with:

G [N] ...dead load

m_d [kg] ...mass of the dam

g [m/s²] ...gravitational acceleration

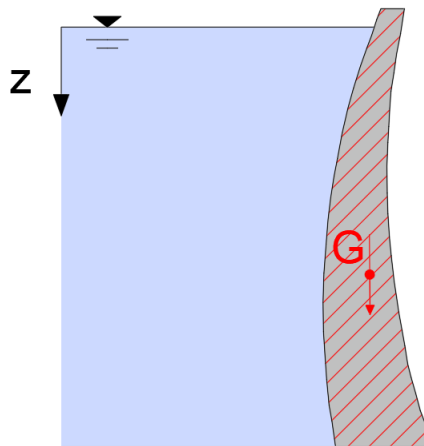


Figure 7: Dead load of an arch dam, cf. [6]

2.3.2. Hydrostatic Pressure

There are two types of water pressures. First, the pressure on surfaces and secondly, the pressures in joints or cracks. The water pressure acting on the dam body acts permanently and is given with the water level of the reservoir and is normal to the upstream surface.

The joint water pressure, at the base joint, is defined through the maximum water level and the water conductivity of the underground. This water conductivity depends on constructive measures such as the position of the ground curtain, or on the local stresses. This leads to a change of conductivity while operating the dam. The joint water pressure acts orthogonal to the structure of the joint system.

The hydrostatic pressure can be calculated with the pressure distribution. It depends on the height of the water and is therefore the largest at the bottom of the dam. The water pressure is always perpendicular to the surface on which it is applied. This leads to a vertical and horizontal water pressure, if the arch dam is curved on the upstream face.

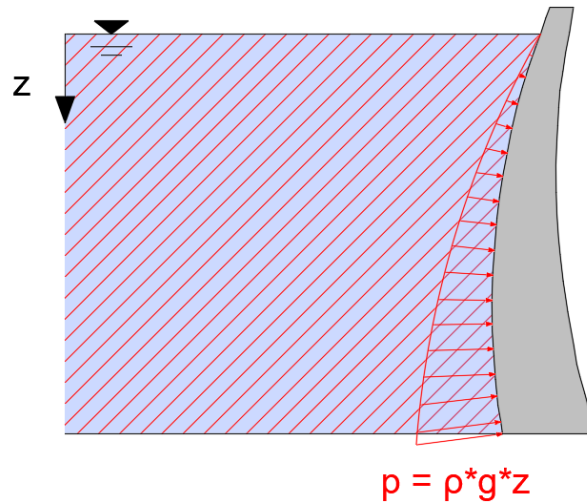


Figure 8 Hydrostatic pressure distribution, cf. [6]

2.3.3. Earthquake - Hydrodynamic Pressure

Under earthquake loading, it is necessary to estimate the magnitude and the location of the earthquake and determine the response of the dam, which can be done with time-history methods or a response spectrum. Complex dynamic models are needed to describe the effects and movements of an earthquake.

To describe the force which is caused by an earthquake the “pseudo static” method can be used.

$$F_{eq} = m * a_{eq} \tag{2-2}$$

with:

F_{eq} [N] ...force due to an earthquake

m [kg] ...mass of water

a_{eq} [m/s²] ...acceleration caused by an earthquake

2.3.4. *Temperature*

Temperature loads have an impact on an arch dams, if the temperature of the concrete changes. This leads to a volume change of a block which is restrained by the abutments and adjacent blocks. This can happen directly after the construction of the dam, which is called closure temperature, or during operation of the dam, when a difference between the temperature of the air on the downstream side and the temperature of the water on the upstream side leads to a temperature change in the structure. Closure temperatures has to be incorporated into the design and can be determined with the results of the stress analyses. The concrete temperatures can be determined with temperature heat analyses, which includes the surrounding air temperatures the temperature of the water and the solar radiation.

Loading due to temperature changes is no considered in this master thesis.

2.3.5. *Ice*

This load can occur in regions where the temperature drops below zero degrees in winter. The pressure acts against the face of the dam and is a result of thermal expansion of the ice. It can also develop due to wind drag. Thermal expansion depends on the thickness and the rise of temperature of the ice, on the coefficient of the thermal expansion, the elastic modulus and its strength. The pressure which is caused by wind drag depends on the velocity and direction of the wind, on the shape of the area and on the roughness of the surface.

As this load can be a significant loading case for arch dams, the ice load needs to be taken into account either by considering the action of forces or by taking measures to reduce the likelihood of ice interaction. Such measures can be aeration or ice cutting.

2.3.6. Silt

Siltation depends on the geology in the catchment areas of the streams that feed the reservoir. Therefore, silt pressure depends on the location and can also not occur at all. Before taking silt pressure into account, the designer needs to check the geological and hydrological conditions.

There are several hypotheses to determine the pressure due to sedimentation. A safe way to calculate it is with the specific weight of the silt, under consideration of the buoyancy, and with the earth pressure at rest.

The lateral earth pressure is:

$$e_{h,z} = z * \gamma_{u,s} * K_0 \quad (2-3)$$

With the vertical earth pressure and the earth coefficient:

$$K_0 = 1 - \sin(\varphi_s) \quad (2-4)$$

with:

$e_{h,z}$	[MPa]	...horizontal earth pressure
K_0	[-]	...earth pressure at rest
$\gamma_{u,s}$	[MN/m ³]	...specific weight of saturated silt
φ_s	[°]	...friction angle of silt
z	[m]	...depth in which horizontal pressure appears

3. Arch Dams in Austria and Switzerland

3.1. Introduction [8], [9]

Austria and Switzerland are both countries which are rich in water resources. The percentage of hydropower which is used for electricity generation is in Switzerland at 57% and accounts with 96% nearly the total renewable energy. In Austria this percentage is at 63% out of the total electrical energy generation.

In Europe the countries with the largest amount of electricity, produced by hydropower, are Norway and Iceland. The alpine countries Austria and Switzerland are very comparable regarding the amount of produced hydro power. Austria produces around 42.900 GWh/year, while Switzerland, which has an area slightly half of Austria, is able to generate almost the same amount of hydropower, with around 36.500 GWh per year.

The next pages show the general situation, the differences and similarities of arch dams in both countries and gives a brief overview of the history of dam design and construction. Also, the arch dams higher than 100 m are listed and depicted, to compare the design of the arch dams of both countries with each other.

3.2. Dams in Austria [9], [10]

3.2.1. General Situation

The main purpose of Austrian dams is to store water for generation and storage of electricity. There are also dams used for storing drinking water, preventing flood events and controlling debris flow. The type, function and location of the dam depends on the topography. In Austria run-of-river plants, high head power plants and pumped-storage power plants can be found. The high head and the pumped-storage power plants are in the mountainous regions of Austria, while the run-of-river plants can be found on the main rivers in Austria.

As the water flow of Austrian rivers and streams is not constant and the required electricity is usually higher in the winter than in the summer, dams with big storage volumes are needed. The tallest dam that impounds Austria's biggest reservoir is named Kölnbreinsperre with a height of 200 m and an active storage of 200 hm³.

Austria has 206 dams of which 23 of those are arch dams. Only two of those are arch-gravity dams. Most of the arch dams in Austria are double curved.

3.2.2. History of Austrian Dams [10]

In the year 1882 hydroelectricity started to develop. Between 1908 and 1911 the first dam in Austria was build, a 37 m high gravity dam. In 1918 the annual power generation was already at 1765 GWh, where 895 GWh came from hydro energy and 870 GWh came from thermal energy. The oldest arch dam in Austria is with 72 years the Limberg arch dam next to the rivers Kapruner Ache and Salzach.

The first bigger hydroelectric projects were implemented in the mountain region of the federal states Tyrol and Vorarlberg. The national grid to supply the east of Austria was set up a few years later, leading to a policy of co-operation with the grid of southern and western Germany. At the beginning of 1930 the development of hydropower decreased and slowly started to recover and grow after World War II. In comparison with Switzerland, Austria had a lower growth rate over the years. The reason for that was, that the government focused more on thermal power stations supplied with coal, natural gas and oil than on storage power programs.

3.2.3. Dam Surveillance

Dam safety depends on the design of the dam and on the implementation of the dam in the surrounding topography, and additionally it relays on recognizing potential hazards and alterations while operating the dam. To monitor the dam structure and its behavior, it is necessary to have a surveillance system, which must be installed before the first impounding during the construction of the dam.

The data for large dams which are recorded in Austria are: the construction data, the main design data, the observations and all readings. Surveillance includes the visual inspections, which refers to the dam body itself, the foreland of the dam and to the reservoir slopes. Also, the appurtenant works are inspected and tested regularly by the dam attendants together with the dam safety engineer in charge.

By providing a constant imperviousness of dam and foundation, a safety check would already be given. If movements are detected on the valley slopes of the reservoir, the number of measuring devices and the quantity of measurements need to be increased together with a sound theoretical model to interpret the observations and to be able to prevent sudden failure modes.

3.2.4. Legal Framework and Responsible Committee

The Austrian Water Law regulates the construction and operation of dams in Austria. The law states that the public interests regarding the dam safety and the rights of third parties must not be violated by the construction or operation of the dam. Furthermore, the dam and the devices used for supervision must meet the current state of the art or must be adjusted if the state of the art changes, due to new findings or research evidence.

If the newly built dam falls into the category “large dams”, this is the case if the dam height exceeds 15 m or if the reservoir capacity is above 500,000 m³, then the dam must be examined and evaluated by the Austrian Commission on Dams (ACD). This organization was founded 1918 to prevent future dam failure, after 1917 basic regulations for fundamental guidelines were established. The evaluation from the ACD is needed because of new structures or in case of existing dams for extensive rehabilitation works. The ACD is also responsible to elaborate specific guidelines related to hydraulic structures.

A Dam Safety Engineer (DSE) and his deputies must be designated by the owner of the dam to ensure the safety of the dam. The DSE, which needs to be approved by the federal dam authority, needs to make sure that the dam safety is always given.

3.3. Dams in Switzerland [11], [12]

3.3.1. General Situation

There are approximately 1200 dams in Switzerland. According to the International Commission on Large Dams (ICOLD), 182 of them are large dams. Most of the dams were built for producing electric power by storing and regulating water, ten of those have a different purpose. Three of them were built for flood control, three dams are used for water supply and the other four dams are constructed for flood protection. 127 out of the 182 dams are arch dams. 25 of these 182 dams are higher than 100 m. The tallest dam in Switzerland, which is also the tallest gravity dam in the world is the 285 m high Grande-Dixence gravity dam. The highest arch dam is the Mauvoisin arch dam with 237 m. Around 40% of the large dams are arch dams. The distribution of arch dams regarding their height can be seen in the figure 9 below.

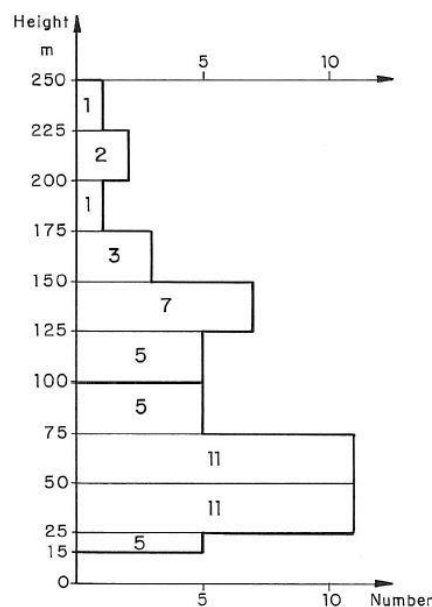


Figure 9: Distribution of the arch dams in Switzerland over their height [11]

3.3.2. *History of Swiss Dams*

Most of the dams in Switzerland were built between 1950 and 1970. Afterwards not many dams were built anymore. Therefore, a strong decline in dam construction took place. There are only a few dams in Switzerland which are built before 1950. The oldest dam, which is still in operation, is a 14.5 m high embankment dam, build in 1822. The oldest arch dam in Switzerland is the Montsalvens dam, built in 1920. Before it became known that the Corfino arch dam, located in Italy, has been built before the Montsalvens dam, it was considered to be the oldest modern large arch dam of Europe. The Schräh dam, a 112 m high concrete dam was also known to be the tallest dam of the world for a long period of time. Very impressive is that during the years 1957 till 1965 four dams were built which exceed 200 m in height. This was the arch dam Mauvoisin, built in 1957 with a height of 237 m, which was raised to 250 m in the year 1990, the Grande Dixence, a 285 m high gravity dam, built in the year 1961, the Luzzone arch dam which was constructed in 1963 with a height of 208 m which was also raised in 1998 to 225 m and the Contra arch dam, built in 1965, with a total height of 220 m.

In Switzerland already 90 % of the realizable hydropower potential is in operation. The last 10 % are difficult or impossible to realize, meaning that todays dam engineering is more focused on maintaining of the existing dams in the highest possible way and providing their engineering expertise in foreign countries.

3.3.3. *Dam Surveillance*

Same as for the Austrian Dams the dam surveillance is divided in visual inspection and measurements and in analyzing the measurement result, which has to be done by an experienced engineer who needs to perform an in-depth safety review. This is done every 5 years for a dam with a height of 40 m minimum, or at least 10 m if the reservoir contains more than 1 million m³. By following these measures, it can be assured that all of the gates of the dam and the spillway work properly. Predictive behavior models are also used to forecast the behavior and the deformation of the dam.

3.3.4. Legal Aspects and Responsible Committee

After the attack on German dams in the Ruhr area during World War II, the legislation regarding the dam safety during war was established. The legislation changed to a common law legislation, which should ensure dam safety during operation, with the end of the war.

In 1957 the ordinance passed and was released. It indicates the kind of dams for which it has to be applied, the right surveillance, structural safety and the emergency plans, the implementation and the concluding clauses.

It is defined, that only dams with a height of at least 10 m, or at least 5 m with a storage capacity over 50,000 m³, are a hazard and therefore need to be investigated by the Federal Council.

The Swiss Federal Council Office of Energy (SFOE) is assigned to ensure that the legislation is executed correctly. This includes the direct safety supervision of 222 dams in Switzerland together with the preparation of technical documents and the development and adaption of the safety concept and the safety requirements of the dams. The individual cantons are responsible for safety and supervision of smaller dams, under the supervision of the SFOE.

3.4. Shapes of Austrian and Swiss Arch Dams [10], [12]

3.4.1. Austrian Arch Dams

To compare the arch dams in Austria with the arch dams in Switzerland, only dams exceeding 100 m in height were chosen. Austria has 6 arch dams which are higher than 100 m:

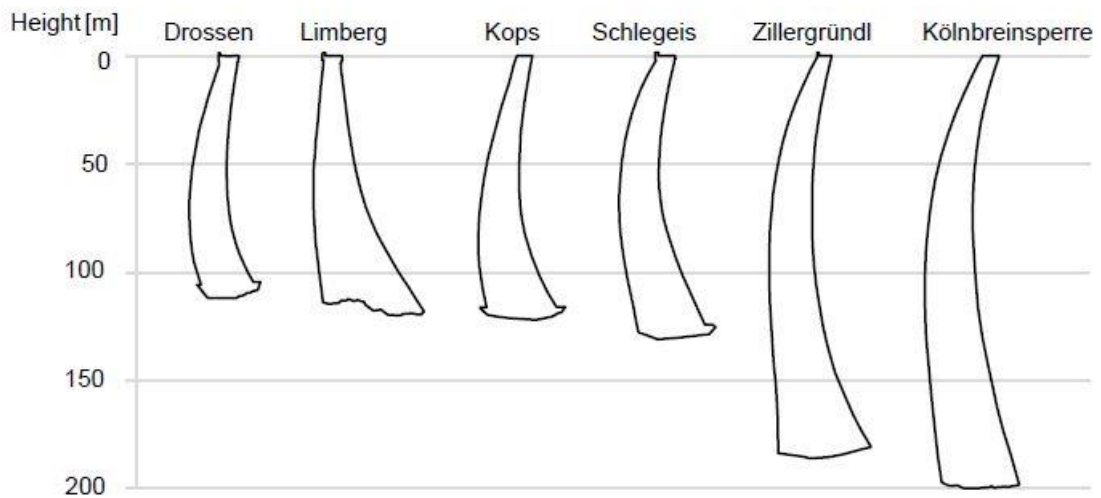


Figure 10: Austrian arch dams, cf. [10]

Dams in Austria	Dam height [m]	Crest length [m]	Concrete volume [m ³]
Drossen	112	357	355000
Limberg	120	357	446000
Kops	122	400	663000
Schlegeis	131	725	960000
Zillergründl	186	506	1370000
Kölnbrein	200	626	1580000

Table 1: Austrian dams, higher than 100 m, sorted by their height [10]

The Drossen dam is a double-curvature constant-angle arch dam, which was finished in 1955 and is close to the town Kaprun in Salzburg. It has a height of 112 m and has a crest length of 357 m. It is 7 m wide at the crest and has a base thickness of 25 m. Drossen arch dam together with Mooser dam provide the reservoir Mooserboden with an active storage capacity of 84.9 hm³.

3. Arch Dams in Austria and Switzerland

The dam Limberg was built close to the town Zell am See and forms the reservoir Limberg. It has a height of 120 m with a crest length of 357 m. The construction of this double-curvature arch dam was finished in 1951. The Limberg dam is a constant-angle dam with a crest thickness of 6 m and a base thickness of 37 m. The amount of the active storage is at 81.2 hm³.

The arch dam Kops was constructed between 1962 and 1969 and is located in Vorarlberg near Schruns. The dam is 122 m high and 400 m long at its crest. It has a concrete volume of 485,000 m³ and a reservoir area of 1 km². At the time of its construction it was the tallest dam in Austria.

The dam Schlegeis is close to the town Mayrhofen in Tyrol. It is 131 m high and is with a crest width of 725 m one of the widest dams in Austria. The construction of this arch dam was finished in 1971. The volume of this dam sums up in total to 980,000 m³ and the reservoir area is 2.2 km².

Another dam close to the town Mayrhofen is the arch dam Zillergründl. It was built 1986 and has a height of 186 m. The crest length is with 506 m not as impressive as the crest length from the arch dam Schlegeis but is still very long. The dam Zillergründl is the second biggest arch dam in Austria and has a dam volume of 1,370,000 m³ and a reservoir area of 1.41 km².

The tallest arch dam in Austria is the Kölnbrein dam with 200 m. It is located in Carinthia, close to the town Gmünd. The construction of this dam was finished in the year 1977. 1,580,000 m³ concrete was needed for the dam volume. The length of the crest is with 626 m also very impressive. The reservoir area for this dam is 2.25 km².

3.4.2. Swiss Arch Dams

Switzerland has 15 arch dams which are higher than 100 m. The following pictures show these dams ordered by their height. The cross section in the bottom picture on the right is the cross section of the used geometry. It is drawn next to the dams of Switzerland to compare it with the other cross sections.

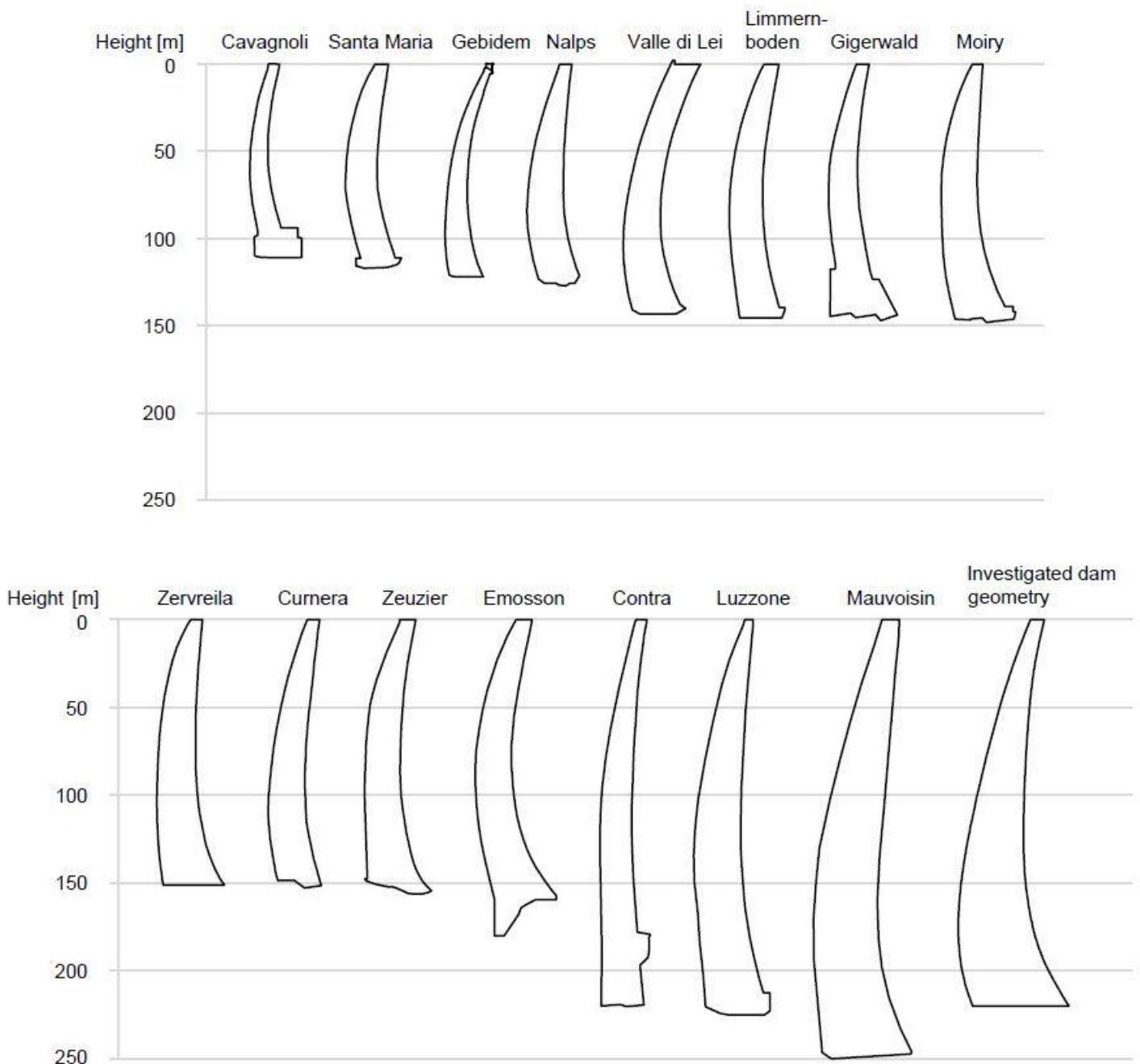


Figure 11: Swiss dams, higher than 100 m, cf. [12]

3. Arch Dams in Austria and Switzerland

Dams in Switzerland	Dam height [m]	Crest length [m]
Cavagnoli	111	320
Contra	220	380
Curnera	153	350
Emosson	180	554
Gebidem	122	327
Gigerwald	147	430
Limmernboden	146	370
Luzzone	225	510
Mauvoisin	250	520
Moiry	148	610
Nalps	127	480
Santa Maria	117	560
Valle di Lei	143	690
Zervreila	151	504
Zeuzier	156	256
Investigated dam geometry	220	430

Table 2: Swiss arch dams sorted by their height including the investigated dam geometry [12]

Due to Switzerland's topography a lot of the built dams are arch dams. Mauvoisin is with 250 m the tallest arch dam in Switzerland.

Despite the fact that the dams in Switzerland are very tall, only a few had problems due to their height. The arch dam Zeuzier is one of the only tall dams which developed cracks on its downstream face. These cracks didn't develop due to its height, but due to a movement in the rock foundation. This happened because of a lower water level in the rock foundation due to the construction of a tunnel close by.

3.5. Schlegeis (AT) Compared to Santa Maria (CH) [10], [12]

The Austrian arch dam Schlegeis and the Swiss arch dam Santa Maria are compared with each other due to their similarity in size and form.

Arch Dams	Dam height [m]	Crest length [m]	Crest thickness [m]	Relation Crest length/Height	Relation Height/Crest thickness
Schlegeis	131	725	9	5.53	14.56
Santa Maria	117	560	8	4.79	14.63

Table 3: Listing of the geometry data of both dams

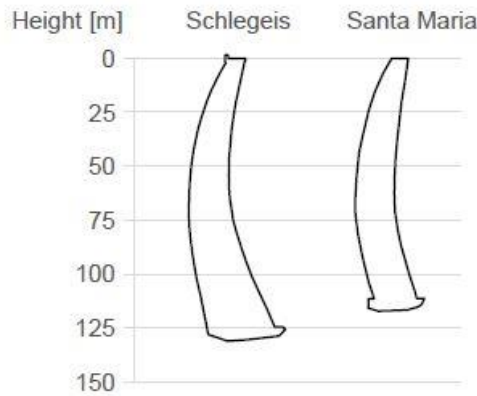


Figure 12: Cross sections of the arch dams Schlegeis and Santa Maria [10][12]

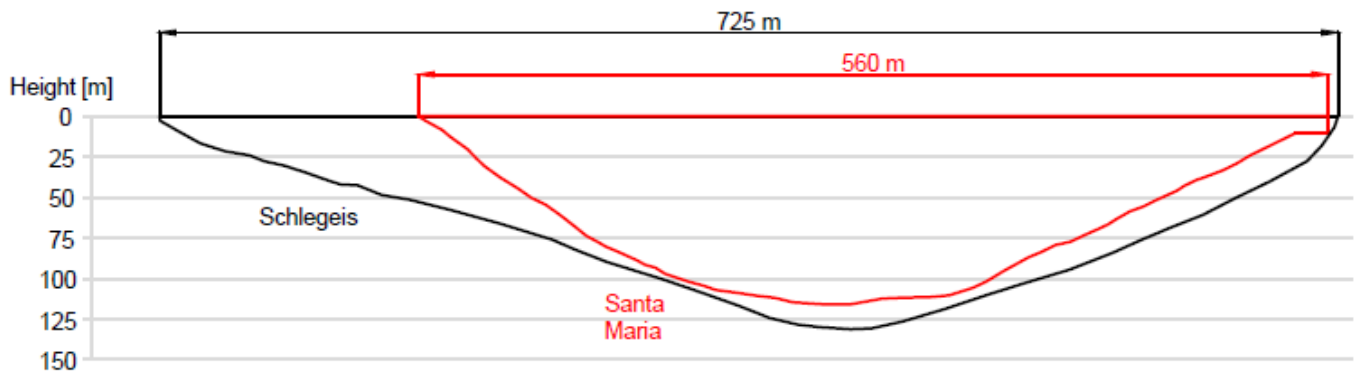


Figure 13: Comparison of the longitudinal sections across the valley of both dams [10][12]

3.5.1. *Schlegeis*

Geometry

The double-curvature arch-gravity dam Schlegeis has due to favorable site geology a unusual crest length/height ratio of 5.53. The horizontal sections were executed elliptical, to fit perfectly into the unsymmetrical valley configuration. The dam consists of 43 blocks with a width of 17 m each. Between these blocks vertical joints are built in. Four horizontal inspection galleries and a base gallery located on the foundation rock are provided in the dam.

Surveillance

The dam has a large span in relation to its height and is monitored in its performance very closely. This is done with a wide range of instrumentation, such as five shafts with direct and inverted pendulums that expend to a depth of 80 m below the dam, 50 uplift pressure gauges and more than 70 extensometers which are located at seven sections in the foundation.

3.5.2. *Santa Maria*

Geometry

The company Vorderrhein AG uses the waterpower of the Vorderrhein and its inflows back till Tavanasa. This results in a catchment area of 315.8 km². The reservoir of the parabolic arch dam Santa Maria communicates with the reservoir Nalps and Curnera, of which the arch dam Santa Maria is the smallest with 117 m, but has the greatest span with 560 m.

Surveillance

Many extensive researches at the end of the 1990s confirmed the safety of the wide arch dam. The surveillance network was extended during the NEAT-Project. The observation was intensified after construction of the Gotthard base tunnel, which was built only 2.2 km in horizontal and 1.3 km in vertical distance away from the dam.

3.6. Comparison of the Arch Dams in Austria with Arch Dams in Switzerland [12], [13]

The shape and the design of an arch dam depend on the topography and its purpose. To compare these different dams the equation of the “coefficient of slenderness” from Lombardi is be used:

$$C = \frac{F^2}{V * H} \quad (3-1)$$

with:

C	$[-]$	<i>...slenderness coefficient</i>
F	$[m^2]$	<i>...area of the mean surface of the arch dam</i>
V	$[m^3]$	<i>...volume of the concrete</i>
H	$[m]$	<i>...height of the dam</i>

This slenderness coefficient shows, that dams with a higher coefficient are more likely to develop stability problems. The highest slenderness coefficient that can occur without expecting any troubles is 20. A more appropriate and therefore more conservative dam layout is given with a slenderness factor is 15. The picture below shows the slenderness coefficient for larger dams in Austria and Switzerland over their height. The dotted line indicates an area which should not be exceeded when designing an arch dam.

The slenderness factor for this master thesis is with 10.42 low and close to the arch dam Luzzone in Switzerland.

3. Arch Dams in Austria and Switzerland

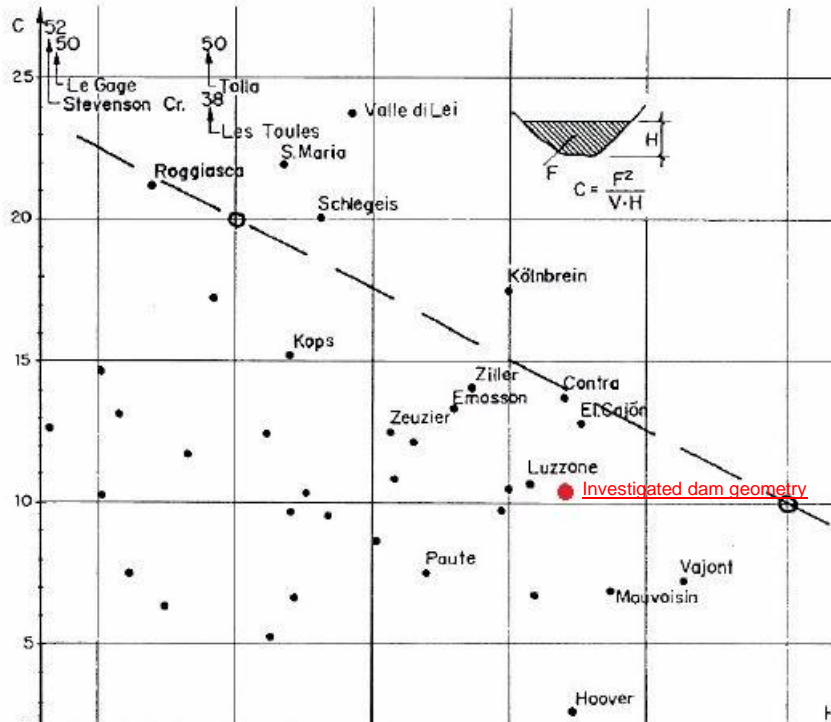


Figure 14: Slenderness factor of large dams in Austria and Switzerland over the height with the slenderness factor for the geometry used for this master thesis [13]

Another possibility to compare the different dams with each other is by using the relation of the crest length to the height of the dam and to compare the height of the dam to the thickness of the dam crest.

Dams in Switzerland	Dam height [m]	Crest length [m]	Crest thickness [m]	Relation Crest length/Height	Relation Height/Crest thickness
Cavagnoli	111	320	5	2.88	22.20
Contra	220	380	7	1.73	31.43
Curnera	153	350	7	2.29	21.86
Emosson	180	554	9	3.08	20.00
Gebidem	122	327	3	2.68	40.67
Gigerwald	147	430	7	2.93	21.00
Limmernboden	146	370	9	2.53	16.22
Luzzone	225	510	5.6	2.27	40.18
Mauvoisin	250	520	12	2.08	20.83
Moiry	148	610	7	4.12	21.14
Nalps	127	480	7	3.78	18.14
Santa Maria	117	560	8	4.79	14.63
Valle di Lei	143	690	15	4.83	9.53
Zervreila	151	504	7	3.34	21.57
Zeuzier	156	256	7	1.64	22.29
			Mean value:	3.00	22.78

Table 4: Swiss dams over 100 m in alphabetical order [12]

3. Arch Dams in Austria and Switzerland

Dams in Austria	Dam height [m]	Crest length [m]	Crest thickness [m]	Relation Crest length/height	Relation Height/Crest thickness
Drossen	112	357	7	3.19	16.00
Limberg	120	357	6	2.98	20.00
Kops	122	400	6	3.28	20.33
Schlegeis	131	725	9	5.53	14.56
Zillergründl	186	506	6	2.72	31.00
Kölnbrein	200	626	7.6	3.13	26.32
			Mean value:	3.47	21.37

Table 5: Austrian dams over 100 m in alphabetical order [12]

For the dams in Switzerland five dams stand out. The Contra arch dam with a low crest length to height ratio of 1.73, the Moiry arch dam with a high crest length/height relation of 4.12, the Santa Maria arch dam with a crest length to height ratio of 4.79, the Valle di Lei arch dam with the highest ratio of 4.83 and the Zeuzier arch dam with the lowest ratio of 1.64.

The arch dam Contra is with 220 m the second highest arch dam in Switzerland. Due to its height the ratio of the crest length to the height is very small. The relation of the height to the crest thickness is with 31.43 also a bit higher, than the average with 22.78.

The arch dam Moiry has the second longest crest length of the arch dams in Switzerland. Due to the 610 m long crest length, the relation between the crest length and the height is higher than the average with 3.00.

The Santa Maria arch dam is compared to its length not very tall. This leads to a high ratio of the crest length divided by the height. The smaller height explains also the relatively small ratio value of 14.63 of the height to the crest thickness.

The arch dam Valle die Lei has an impressive length of 690 m. This explains the high crest length/height ratio. The Valle di Lei arch dam has also the widest crest with 15 m. The crest of this arch dam was built thicker than usual as a safety measure after the second world war. This high crest thickness leads also to the lowest height/crest thickness ratio of 9.53.

The Zeuzier arch dam was built in a narrow valley and is therefore not very wide. With only a length of 256 m the ratio of the crest length to the height turns out to be the smallest.

3. Arch Dams in Austria and Switzerland

For the Austrian dams, the Schlegeis arch dam stands out. It has a crest length of 725 m and has therefore a high crest-length to dam height ratio of 5.53. The optimal dam configuration had to be found with the help of comprehensive design studies.

4. Technical Prerequisites

4.1. Basic Geometric Forms [14], [15]

4.1.1. Linear Functions

The equation of a linear function is:

$$y = f(x) = mx + n \quad (4-1)$$

Its graph is a straight line and can be described by only using two points $P_1(x_1, y_1)$ and $P_2(x_2, y_2)$. The parameter “m” from the equation (4-1) describes the gradient and the parameter “n” stands for the value where the line intercepts with the y-axis.

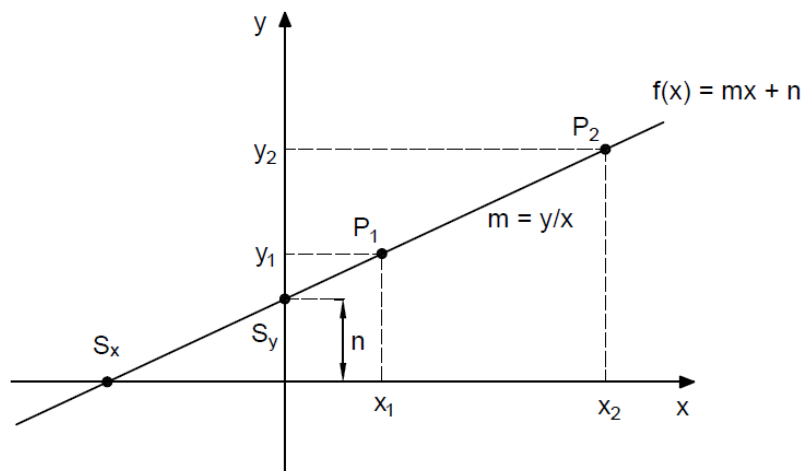


Figure 15: Graph of the linear function, cf. [14]

S_x is the point of intersection with the x-axis: $S_x \left(\frac{-n}{m} / 0 \right)$ and S_y is the intersection point on the y-axis: $S_y(0/n)$.

The gradient can be calculated by simply inserting the x- and y-values for P₂ and deduct these with the x- and y-values from the Point P₁ into the formula $m = \frac{y}{x}$.

$$m = \frac{y_2 - y_1}{x_2 - x_1} \quad (4-2)$$

With the known parameter m, the distance of the intersection point S_y to the x-axis can be calculated:

$$n = y - mx \quad (4-3)$$

By inserting the equation (4-2) and (4-3) in the formula (4-1) with the known points x₁ and y₁ for x and y the following equation is formed:

$$f(x) = \frac{y_2 - y_1}{x_2 - x_1} * x_1 + \left(y_1 - \frac{y_2 - y_1}{x_2 - x_1} * x_1 \right) \quad (4-4)$$

4.1.2. Conic Sections and their Equations Written in Vertex Form

The vertex of the conic section needs to be shifted to the center of the coordinate system to receive the vertex equation.

Circle

If the circle has its centre in the origin of the coordinate system, the equation is written as follows:

$$r^2 = x^2 + y^2 \quad (4-5)$$

If the circle does not have its centre in the origin, the coordinate x must be edited:

$$r^2 = (x - a)^2 + y^2 \quad (4-6)$$

With $r = a$ the formula above can be rewritten as:

$$y^2 = 2rx - x^2 \quad (4-7)$$

The vertex formula of a circle can be reached by replacing r with p and adding $(\epsilon^2 - 1)$ to x^2 in the formula (4-7):

$$y^2 = 2px + (\epsilon^2 - 1)x^2 \quad (4-8)$$

With the numerical eccentricity $\epsilon = 0$

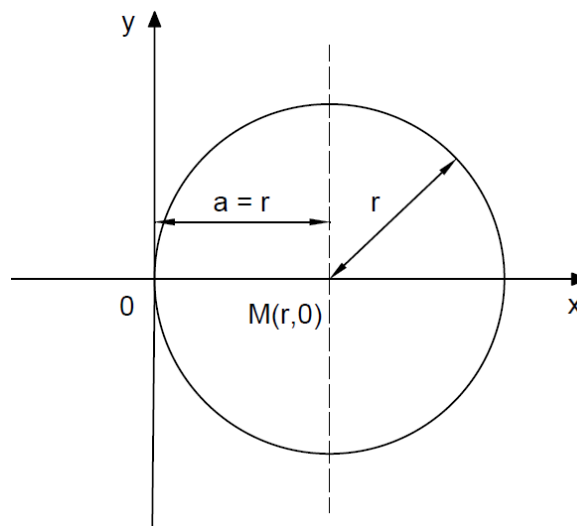


Figure 16: Circle with shifted centre along the x-axis, cf. [15]

Ellipse

The normal form of an ellipse is as follows:

$$\frac{x^2}{a^2} + \frac{y^2}{b^2} = 1 \quad (4-9)$$

This occurs when the coordinate axes are the same as the axes of the ellipse and the centre of the ellipse is at the coordinate origin.

The coordinate x must be edited if the ellipse does not have its centre in the origin:

$$\frac{(x - a)^2}{a^2} + \frac{y^2}{b^2} = 1 \quad (4-10)$$

The formula above can be rewritten as:

$$y^2 = 2 * \frac{b^2}{a} * x + \frac{b^2}{a^2} * x^2 \quad (4-11)$$

With the known half parameter $p = \frac{b^2}{a}$ and the numerical eccentricity as $\varepsilon = \frac{\sqrt{a^2 - b^2}}{a}$ the vertex form of the equation of an ellipse is:

$$y^2 = 2 * p * x + (\varepsilon^2 - 1) * x^2 \quad \text{with: } 0 < \varepsilon < 1 \quad (4-12)$$

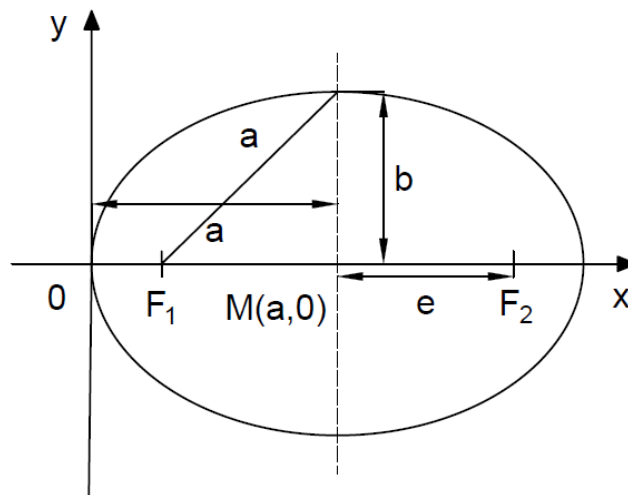


Figure 17: Ellipse with shifted centre along the x-axis, cf. [15]

Parabola

If the opening of a parabola is on the right side, then the general equation of a parabola is:

$$y^2 = 2 * p * x \quad x \geq 0 \quad (4-13)$$

The general vertex form can be reached by adding $(\varepsilon^2 - 1) * x^2$ to the equation (4-13).

$$y^2 = 2 * p * x + (\varepsilon^2 - 1) * x^2 \quad \text{with: } \varepsilon = 1 \quad (4-14)$$

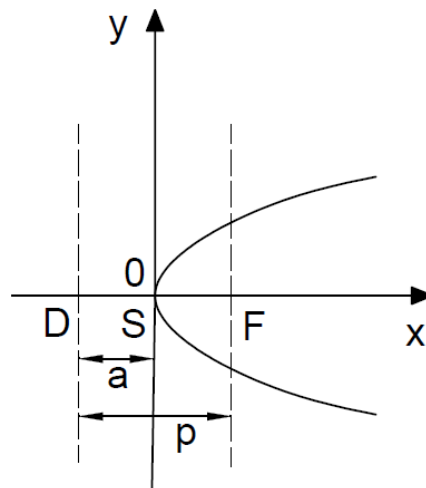


Figure 18: Parabola ellipse with shifted centre along the x-axis, cf. [15]

Hyperbola

If the hyperbola has its centre in the origin of the coordinate system, its equation is written as follows:

$$\frac{x^2}{a^2} - \frac{y^2}{b^2} = 1 \quad (4-15)$$

After shifting the hyperbola along the x-axis, the formula (4-15) looks as follows:

$$\frac{(x + a)^2}{a^2} - \frac{y^2}{b^2} = 1 \quad (4-16)$$

After solving the equation for y^2 :

$$y^2 = 2 * \frac{b^2}{a} * x - \frac{b^2}{a^2} * x^2 \quad (4-17)$$

With the same half parameter $p = \frac{b^2}{a}$ as the ellipse (hyperbola: $2p = \frac{2b^2}{a}$) and with $\varepsilon = \frac{\sqrt{a^2+b^2}}{a}$, the vertex form of the equation of a hyperbola is:

$$y^2 = 2 * p * x + (\varepsilon^2 - 1) * x^2 \quad \text{with: } \varepsilon > 1 \quad (4-18)$$

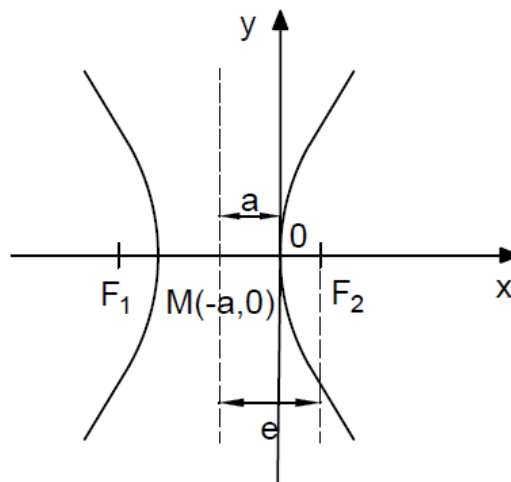


Figure 19: Hyperbola with shifted centre along the x-axis, cf. [15]

Every equation of the vertex form of every conic section is the same at the end. This means that the equation:

$$y^2 = 2 * p * x + (\varepsilon^2 - 1) * x^2 \quad (4-19)$$

can always be applied. The only difference is the numerical eccentricity ε which varies with the different shapes.

4.1.3. Main Form of a Circle

If the circle does not have its centre along the x-axis, meaning that it is shifted up along the y-axis as well, the equation (4-6) is also edited for the y coordinate:

$$r^2 = (x - x_m)^2 + (y - y_m)^2 \quad (4-20)$$

Solving the equation for y results in:

$$y = \sqrt{r^2 - (x - x_m)^2} + y_m \quad (4-21)$$

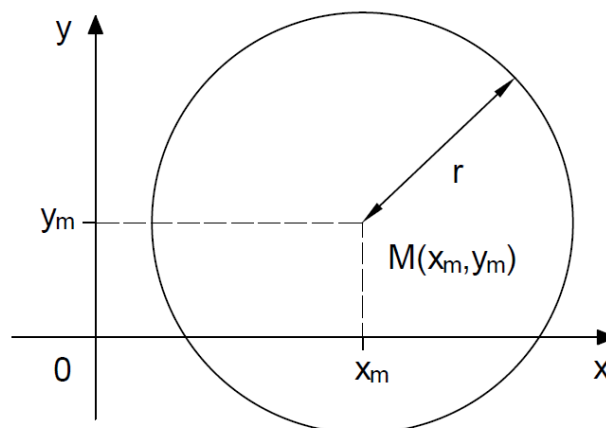


Figure 20: Circle with shifted centre along the x- and y-axis, cf. [15]

4.2. Barlow's Formula [1]

To calculate the needed thickness for an arch dam, the heel formula, or Barlow's formula is used:

$$\sigma = \frac{p(z) * r}{d} \quad (4-22)$$

with:

σ [MN/m²] ...hoop stress

$p(z)$ [MPa] ...hydrostatic pressure

r [m] ...radius of the arch

d [m] ...thickness of the dam

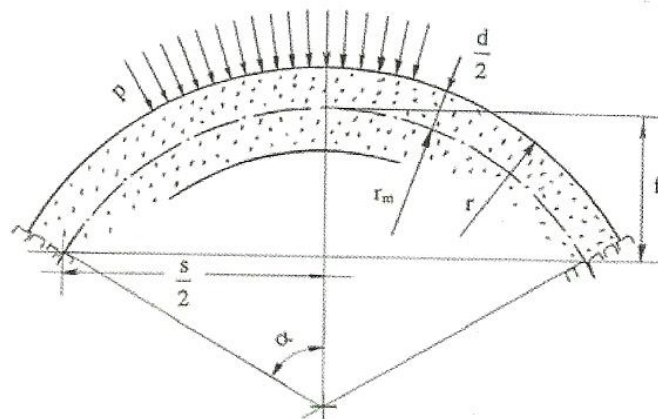


Figure 21: Geometry of the arch with its parameters [1]

4.3. Introduction to Structural Dynamics [16]–[19]

As this master thesis is about the seismic response of arch dams, the next pages are about the dynamic behavior and the calculation of a dynamic loading.

A dynamic load can be a transient load, a periodic load, a harmonic load or an impulsive load. The temporal course of the transient load depends on the time and does not repeat itself. The time course at the periodic load repeats itself after a certain period time T . A harmonic load is a periodic load with a sine/cosine time course. The impact load has a short abrupt impact load on the building with a limited exposure time.

4.3.1. Single Degree of Freedom System

As the name indicates, the single degree of freedom system is a system which has a restricted motion by only a single independent function or coordinate. It is often used to describe a more complex structure approximately.

With Newton's second law of motion:

$$F = m * a \quad \text{or} \quad f_{(t)} = m\ddot{u} \quad (4-24)$$

the governing equation of motion of a SDOF System is:

$$m\ddot{u} + c\dot{u} + ku = f_{(t)} \quad (4-25)$$

Where k is the stiffness coefficient, c is the damping coefficient, m describes the mass and $f_{(t)}$ is the external force.

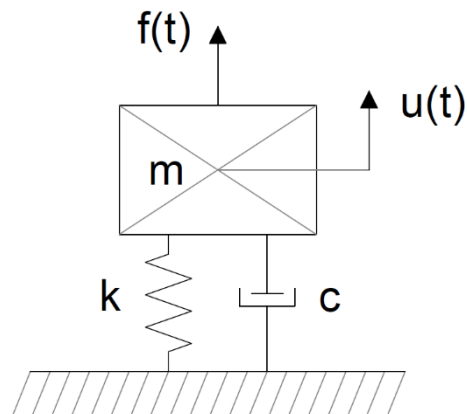


Figure 22: SDOF system with external force, cf. [16]

4.3.2. Undamped SDOF System with Free Vibration

By taking the formula (4-25), the differential equation of the undamped free vibration system is:

$$m\ddot{u} + ku = 0 \quad (4-26)$$

when $f_{(t)} = 0$ and if there is no damping.

For the approach of the solution the following formula is chosen:

$$u = e^{\lambda t} \quad (4-27)$$

After inserting (4-27) into (4-26):

$$(m\lambda^2 + k)e^{\lambda t} = 0 \quad (4-28)$$

The equation above can be written as:

$$m\lambda^2 + k = 0 \quad (4-29)$$

as the exponential term is never zero.

With the equation:

$$\omega_n = \sqrt{\frac{k}{m}} \quad (4-30)$$

inserted into (4-29) and after solving the formula for λ , the characteristic equation is:

$$\lambda_{1,2} = \pm i\omega_n \quad \text{with } i = \sqrt{-1} \quad (4-31)$$

By substituting equation (4-31) into the general equation:

$$u(t) = a_1 e^{\lambda_1 t} + a_2 e^{\lambda_2 t} \quad (4-32)$$

which can be rewritten:

$$u(t) = a_1 e^{i\omega_n t} + a_2 e^{-i\omega_n t} \quad (4-33)$$

By using the Euler relations:

$$e^{ix} = \cos(x) + i * \sin(x) \quad (4-34)$$

the formula (4-33) turns into:

$$u(t) = A * \cos(\omega_n t) + B * \sin(\omega_n t) \quad (4-35)$$

The integration constants A and B depend on the different boundary conditions.

4.3.3. Damped SDOF with Free Vibration

If the single degree of freedom system is damped, the equation is as follows:

$$m\ddot{u} + c\dot{u} + ku = 0 \quad (4-36)$$

With the solution from the equation (4-27):

$$m\lambda^2 + c\lambda + k = 0 \quad (4-37)$$

This gives the solution for the equation:

$$u(t) = e^{-\frac{c}{2m}t} \left(A * e^{\sqrt{\left(\frac{c}{2m}\right)^2 - \frac{k}{m}}t} + B e^{-\sqrt{\left(\frac{c}{2m}\right)^2 - \frac{k}{m}}t} \right) \quad (4-38)$$

It is known, that the system and its damped behavior depends on the value in the radical of the equation (4-38). Therefore, a critical damping coefficient is used which sets this radical to zero and gives a reference quality.

$$\left(\frac{c_c}{2m}\right)^2 - \frac{k}{m} = 0 \quad (4-39)$$

Solving for c_c :

$$c_c = 2\sqrt{km} = 2m\omega_n \quad (4-40)$$

Where c_c is the critical damping, k is the stiffness, m describes the mass and ω_n is the natural circular frequency.

The damping ratio:

$$\zeta = \frac{c}{c_c} = \frac{c}{2m\omega_n} \quad (4-41)$$

describes the damping properties in the system.

Due to the value of the damping ratio, following three damping cases can occur:

- $\zeta < 1.0$ *system is underdamped*
- $\zeta = 1.0$ *system is critical damped*
- $\zeta > 1.0$ *system is overdamped*

For a damped oscillator the quickest way to reach zero is through critical damping. As shown in the graph below, with underdamping the function reaches zero quicker than the critical damped one but doesn't stay there and oscillates around it. With the overdamped function, zero is reached, but it takes longer than with the critical damping.

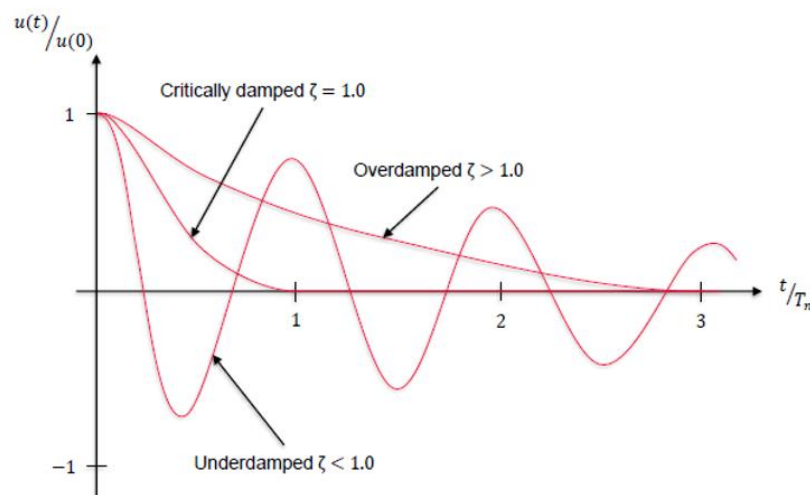


Figure 23: Damping cases [18]

Critical damping is the line that divides the oscillatory from the non-oscillatory motion. The damping coefficient c_c is the smallest value of c that prevents the oscillation completely and is therefore called critical damping ratio.

4.3.4. Multiple Degree of Freedom System (MDOF)

Not every system can be described by a single degree of freedom system. In this case, a system with discrete masses, that needs two or more coordinates to describe their motion, the multiple degree of freedom system, is used.

As the system consists more masses, the differential equation needs to be done for every mass:

$$m_n \ddot{u} + \sum_{j=1}^n c_{nj} \dot{u}_j + \sum_{j=1}^n k_{nj} u_j = f_n(t) \quad (4-42)$$

This differential equation can be described with matrices:

$$[M]\{\ddot{U}\} + [C]\{\dot{U}\} + [K]\{U\} = \{F(t)\} \quad (4-43)$$

With $[M]$ as the mass matrix, $[C]$ as the damping matrix, $[K]$ as the stiffness matrix and $\{F(t)\}$ as the load vector, multiplied with the corresponding vectors $\{\ddot{U}\}$, $\{\dot{U}\}$ and $\{U\}$, which describe the acceleration, the velocity and the displacement.

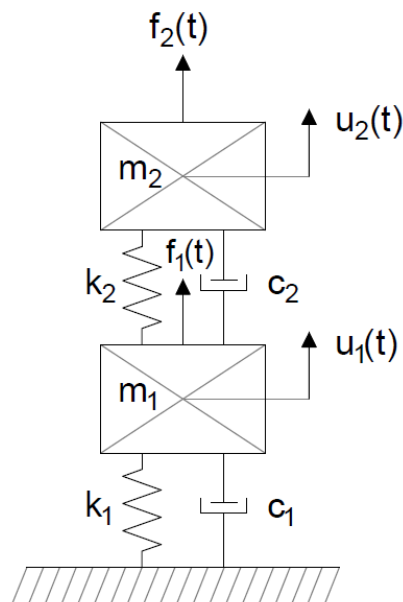


Figure 24: MDOF system with external force, cf. [16]

4.3.5. Undamped MDOF System with Free Vibration

The differential equation (4-33) without the damping matrix and the load vector is:

$$[M]\{\ddot{U}\} + [K]\{U\} = \{0\} \quad (4-44)$$

The solution approach for this differential equation is:

$$\{U\} = \varphi \cos(\omega t - \theta) \quad (4-45)$$

After solving the homogeneous differential equation:

$$([K] - \omega^2[M])\varphi = \{0\} \quad (4-46)$$

the equation above can be written as:

$$[K] - \omega^2[M] = \{0\} \quad (4-47)$$

This is a polynomial of the n^{th} degree with n Eigenvalues. This means n solutions, which can only be considered as ratio values, since it is a homogeneous system of equations.

These solutions are called Eigenmodes and show the relative deviation. By putting all Eigenmodes of all n -Eigenfrequencies together and sort them by size, starting with the smallest Eigenfrequency, the modal matrix or transformation matrix forms.

$$[\psi] = [\{\psi_1\}, \{\psi_2\}, \dots, \{\psi_n\}] \quad (4-48)$$

The orthogonality applies to these Eigenmodes (with $i \neq j$):

$$\{\psi_i\}^T [M] \{\psi_j\} = 0 \quad (4-49)$$

$$\{\psi_i\}^T [K] \{\psi_j\} = 0 \quad (4-50)$$

This leads to diagonal matrices but only applies for the mass and stiffness matrices.

The following formula describes the total deformation as a linear combination of the Eigenmodes:

$$\{u_{(t)}\} = \sum_{i=1}^n \psi_i Y_{i(t)} = [\psi] \{Y_{(t)}\} \quad (4-51)$$

With this equation inserted into the first formula (4-44) and by multiplying it with $\{\psi_i\}^T$ the differential equation for the undamped MDOF system can be described:

$$\{\psi_i\}^T [M] [\psi] \{\ddot{Y}_{(t)}\} + \{\psi_i\}^T [K] [\psi] \{Y_{(t)}\} = \{0\} \quad (4-52)$$

After considering the orthogonality the differential equation can be written as:

$$\{\psi_i\}^T [M] \{\psi_i\} \{\ddot{Y}_{(t)}\} + \{\psi_i\}^T [K] \{\psi_i\} \{Y_{(t)}\} = \{0\} \quad (4-53)$$

4.3.1. Damped MDOF System with Free Vibration

If the multiple degree of freedom system is damped and the orthogonality is considered, then the equation is:

$$\{\psi_i\}^T [C] \{\psi_j\} = 0 \quad (4-54)$$

This is only an approximation, since the damping matrix is basically fully occupied. If the differential equation is written with associated damping and by choosing an approach as before for the undamped case, complex Eigenvectors and Eigenvalues can be reached. To avoid this case, the differential equation is solved. First for the undamped case and afterwards with damping.

$$\{\psi_i\}^T [M] \{\psi_j\} \{\ddot{Y}_{(t)}\} + \{\psi_i\}^T [C] \{\psi_j\} \{\dot{Y}_{(t)}\} + \{\psi_i\}^T [K] \{\psi_j\} \{Y_{(t)}\} = \{0\} \quad (4-55)$$

4.3.2. Rayleigh Damping

Damping is expressed in this master thesis through Rayleigh damping, which is proportional to the mass and stiffness matrices.

$$[C] = \alpha [M] + \beta [K] \quad (4-56)$$

α describes the mass-proportional damping coefficient and β describes the stiffness-proportional damping coefficient.

The damping ratio can be calculated with:

$$\zeta_n = \frac{1}{2\omega_n} \alpha + \frac{\omega_n}{2} \beta \quad (4-57)$$

Where ζ_n is the damping ratio of the n^{th} mode and ω_n is the natural frequency of the n^{th} mode.

The damping coefficients α and β are:

$$\alpha = \omega_i \omega_j \beta \quad (4-58)$$

$$\beta = \frac{2\zeta}{\omega_i + \omega_j} \quad (4-59)$$

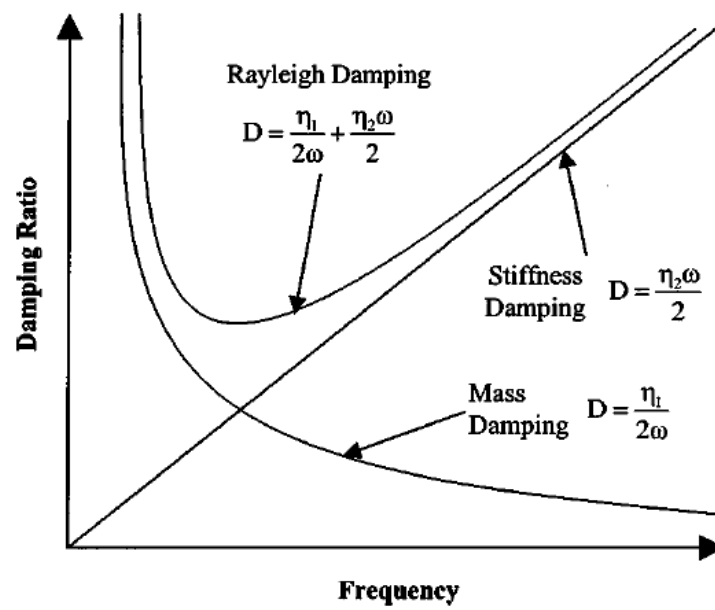


Figure 25: Rayleigh damping [19]

4.4. The Finite Element Method [20], [21]

To calculate complex geometries and their behavior due to certain loads, a software is needed which is able to solve such systems numerically. As analytical methods are often insufficient, an approximate solution is used. With the Finite Element Method, as this approximate solution, the most difficult and complicated problems can be solved by using a finite number of clearly defined components. It should, though, be kept in mind that this method gives just an approach of the solution of the problem.

The geometry can be described by dividing it in a finite number of defined components or “elements”. This procedure is called discretizing. If the problem can only be solved by using mathematical fiction of an infinitesimal, the procedure is called continuous, as the number of elements is infinite. Independent of the number of the elements of a system, a computer can always solve a discrete problem. Continuous problems can only be solved exactly by mathematical manipulation, as the capacity of computers is finite. Various methods of discretization have been proposed to overcome the intractability of continuous problems. The involved approximation in these methods approach the true continuum solution as the number of discrete variables increase. With an increase of variables, the approximation of the solution of a problem gets more and more precise.

The topic of the Finite Element Method is extensive. Therefore, the next pages explain only the approach of the Finite Element Method for a two-dimensional structure.

First, the geometry is separated into elements. The global coordinates of the nodes on the elements are transformed into a local coordinate system which allows to calculate the potential energy:

$$\{x_{(\xi,\eta)}\}^e = \sum_n N_{n(\xi,\eta)} \{x\}_n^e \quad (4-60)$$

with:

$x_{(\xi,\eta)}$...coordinates of the local coordinate system

$N_{n(\xi,\eta)}$...shape function

x ...coordinates of the global coordinate system

n ...number of nodes per element

For the displacement the same equation is used as for the geometry:

$$\{u_{(\xi,\eta)}\}^e = \sum_n N_{n(\xi,\eta)} \{u\}_n^e \quad (4-61)$$

with:

$u_{(\xi,\eta)}$...displacement of the node in the local coordinate system

u ...displacement in the global coordinate system

With the known displacement the strains can be calculated as followed:

$$\varepsilon_x = \frac{\delta u_x}{\delta x} = \frac{\sum_n N_{n(\xi,\eta)} u_{x_n}^e}{\delta x} \quad (4-62)$$

$$\varepsilon_y = \frac{\delta u_y}{\delta y} = \frac{\sum_n N_{n(\xi,\eta)} u_{y_n}^e}{\delta y} \quad (4-63)$$

$$\gamma_{xy} = \frac{\delta u_x}{\delta y} + \frac{\delta u_y}{\delta x} = \frac{\sum_n N_{n(\xi,\eta)} u_{x_n}^e}{\delta y} + \frac{\sum_n N_{n(\xi,\eta)} u_{y_n}^e}{\delta x} \quad (4-64)$$

With the derivatives of the form functions the so-called B – matrix can be set up:

$$[B] = \begin{bmatrix} \frac{\delta N_{1(\xi,\eta)}}{\delta x} & 0 & 0 \\ 0 & \frac{\delta N_{1(\xi,\eta)}}{\delta y} \dots & \frac{\delta N_n}{\delta x} \\ \frac{\delta N_{1(\xi,\eta)}}{\delta y} & \frac{\delta N_{1(\xi,\eta)}}{\delta x} & \frac{\delta N_n}{\delta y} \end{bmatrix} \quad (4-65)$$

With the B-matrix known the strains are:

$$\{\varepsilon\}^e = [B]^e \{u\}^e \quad (4-66)$$

With the Hooke's law the stresses of each element can be calculated:

$$\sigma_x = \frac{E}{1 - \nu^2} (\varepsilon_x + \nu * \varepsilon_y) \quad (4-67)$$

$$\sigma_y = \frac{E}{1 - \nu^2} (\varepsilon_y + \nu * \varepsilon_x) \quad (4-68)$$

$$\tau_x = \frac{E}{2(1 - \nu^2)} \gamma_{xy} \quad (4-69)$$

with:

E [MPa] ...Young's modulus

ν [-] ...Poisson ratio

By separating the material dependent parameters E and ν from the strains, the so-called D - matrix is formed:

$$[D] = \frac{E}{1 - \nu^2} \begin{bmatrix} 1 & \nu & 0 \\ \nu & 1 & 0 \\ 0 & 0 & \frac{1 - \nu}{2} \end{bmatrix} \quad (4-70)$$

The stress vector rewritten with matrices is:

$$\{\sigma\}^e = [D]^e \{\varepsilon\}^e \quad (4-71)$$

For the total potential energy, the internal and external potential are needed. The internal potential energy is already included in eq (4-71):

$$\Pi_i = \frac{1}{2} \int_{-1}^1 \int_{-1}^1 \{\varepsilon\}^T \{\sigma\}^e |J| d\xi d\eta \quad (4-72)$$

The external energy is:

$$\Pi_e = \{P\}^e \{u\}^e \quad (4-73)$$

Therefore, the total potential energy is:

$$\Pi = \Pi_i + \Pi_e = \frac{1}{2} \int_{-1}^1 \int_{-1}^1 \{\varepsilon\}^T \{\sigma\}^e |J| d\xi d\eta + \{P\}^e \{u\}^e \quad (4-74)$$

With the Jacobi Matrix:

$$[J] = \begin{bmatrix} \frac{\delta x}{\delta \xi} & \frac{\delta y}{\delta \xi} \\ \frac{\delta x}{\delta \eta} & \frac{\delta y}{\delta \eta} \end{bmatrix} \quad (4-75)$$

to transform the B-matrix, because the local shape functions cannot be derived from the global coordinates.

By forming the minimum of the potential energy by partially deriving the equation and by setting it to zero, the system is getting balanced and the equation can be solved:

$$\frac{\delta \Pi}{\delta \{u\}^e} = \frac{\Pi_i}{\delta \{u\}^e} + \frac{\Pi_e}{\delta \{u\}^e} = 0 \quad (4-76)$$

The equation above is, after derivation, and with $\frac{\Pi_e}{\delta \{u\}^e} = \{P\}^e$:

$$[K]^e \{u\}^e - \{P\}^e = 0 \quad (4-77)$$

With K as the stiffness matrix and P as the load vector per element. The stiffness matrix can be written as:

$$[K] = \int_{-1}^1 \int_{-1}^1 [B]^T [D] [B] |J| d\xi d\eta \quad (4-78)$$

With the known stiffness of an element and the known external forces, that act on the element, the displacement can be calculated. Afterwards the stresses and strains can be determined in the post processing.

Fluid Structure Interaction (FSI)

This method is used to define the interaction between the dam body and the fluid. As this is a topic is extensive only the equations which are used for the coupled system are listed below.

Dynamic elemental equation:

$$[M_s]\{\ddot{u}_e\} + [C_s]\{\dot{u}_e\} + [K_s]\{u_e\} - [R]\{p_e\} = \{f_s\} \quad (4-79)$$

The fluid is described with the discretized wave equation:

$$[M_F]\{\ddot{p}_e\} + [C_F]\{\dot{p}_e\} + [K_F]\{p_e\} + \vec{p}_0[R]^T\{\ddot{u}_{e,F}\} = \{f_F\} \quad (4-80)$$

Equation (4-79) and (4-80) in matrix notation are:

$$\begin{bmatrix} [M_s] & 0 \\ \vec{p}_0[R]^T & [M_F] \end{bmatrix} \begin{Bmatrix} \{\ddot{u}_e\} \\ \{\ddot{p}_e\} \end{Bmatrix} + \begin{bmatrix} [C_s] & 0 \\ 0 & [C_F] \end{bmatrix} \begin{Bmatrix} \{\dot{u}_e\} \\ \{\dot{p}_e\} \end{Bmatrix} + \begin{bmatrix} [K_s] & -[R] \\ 0 & [K_F] \end{bmatrix} \begin{Bmatrix} \{u_e\} \\ \{p_e\} \end{Bmatrix} = \begin{Bmatrix} \{f_s\} \\ \{f_F\} \end{Bmatrix} \quad (4-81)$$

Equation (4-81) describes the complete finite element discretized equations for the FSI problem. The subscript F in the equation above stands for all submatrices which will be generated by the acoustic fluid element. The S indicates all submatrices which are generated by the structural element used in the model.

To get further information about this topic the dissertation by Markus Goldgruber is highly recommended. In his dissertation, he did an intensely research about the fluid modelling methods which he explains it in detail.

5. Numerical Case Studies

5.1. Introduction to the Calculation done with ANSYS

The commercial Finite Element Software package Ansys Mechanical Workbench has been used to discretize the initial arch dam geometry as well as its alternations. Furthermore, the pre- and postprocessing has been done with the same package.

Six dams are created in total with the program ANSYS. The crest width increased in the different models from 8 m to 9 m, 10 m, 12 m up to 14 m and finally to 20 m. First the different Mode shapes and Eigenfrequencies are calculated and viewed. After that, an acceleration in x-, y- and z-direction on the bottom of the arch dam is applied to simulate the earthquake load. By doing this, the behavior of the dam regarding the different internal stresses due to an increased weight on the top of the dam and due the higher location of the centre of gravity is examined.

In order to implement this, the linear analysis is applied for the dynamic behavior. The dam and the foundation are modeled by higher order 3-D solid elements, which exhibits quadratic displacement behavior. The reservoir is modeled by 3-D acoustic elements. To simulate the water load, the hydrostatic pressure is applied as a pressure load on the structure.

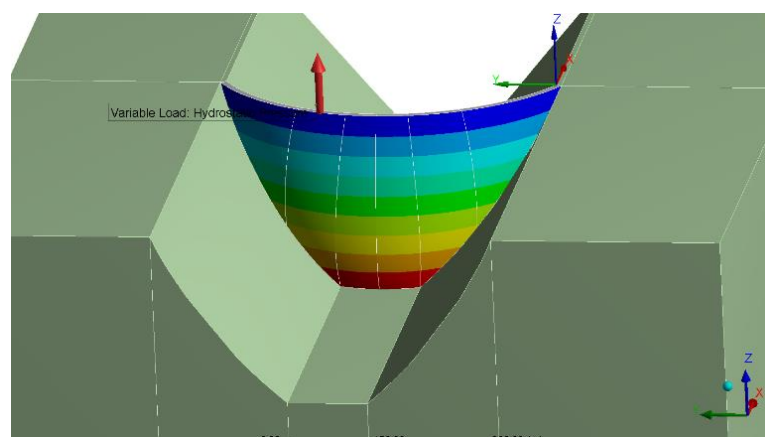


Figure 26: Hydrostatic pressure

For the reservoir the boundary condition of zero pressure on the free surface of the water is defined. Also, the reservoir is set to be nonreflecting at the end, which is obtained by using the Impedance Boundary. The fluid-structure interaction (FSI) analysis is taken into account to describe the interaction of the water with the dam.

Uniform reduced integration is used over the whole system. The foundation rock and the arch dam were assumed to be linear elastic.

To connect the different nodes and degrees of freedom together the multipoint constraint approach (MPC) is used to create a connection between the dam and the foundation and between the dam and the reservoir.

Structural damping is applied to the materials by using Rayleigh-Damping.

5.2. Geometry and Model [22]

The dimensions of the geometry of the dam, of the foundation and of the reservoir are described in Chapter 1. The dimensions of the foundation and reservoir are based on the dimensions of the 12th International Benchmark Workshop on numerical analysis of dams. The geometry of the dam is not the same but has the same dimensions as the arch dam in the ICOLD proceedings.

The reservoir is created, by extruding the part on the upstream side of the dam. In this master thesis the reservoir is assumed to have no freeboard. Then the part in front of the dam is cut out to create the final geometry:

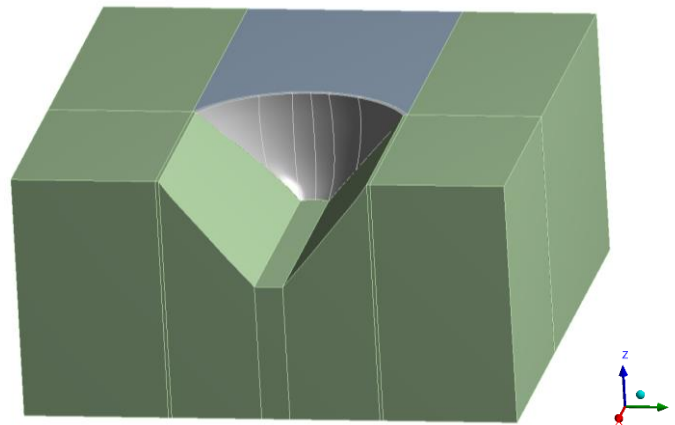


Figure 27: Final geometry

This given geometry is modified by widening the dam crest and the top third of the dam, 70 m from the crest down, to generate six different dams. This is done by using a linear approach with which the geometry is changed every 10 m, starting from the top at 220 m.

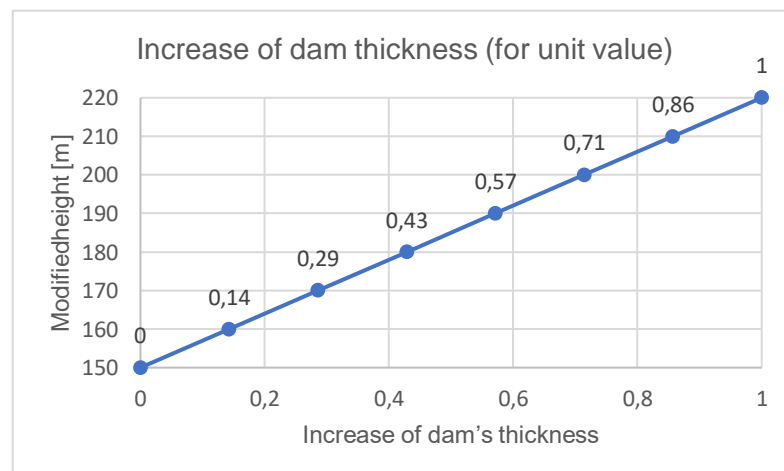


Figure 28: Increase of dam thickness (for unit value) depending on the dam's elevation

By multiplying these values with the wanted thickness (for example: $8+1*4 = 12$ m) a new dam is created. The height in this diagram is referring to the first 70 m from the top of the dam downwards, this means the 220 m mark is at the dam crest and the 150 m mark is 70 m below the dam crest. The figure below illustrates that.

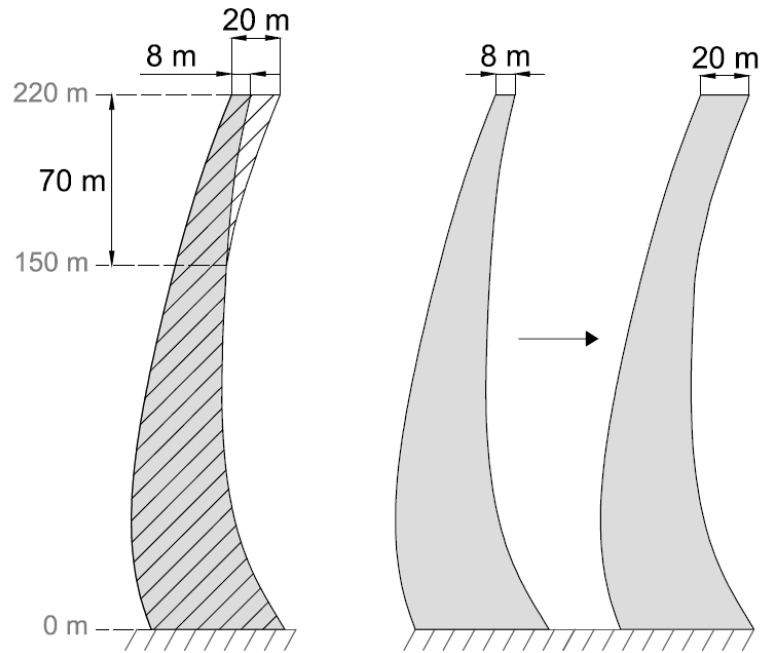


Figure 29: Cross section of the main section of the arch dam with an 8 m and 20 m crest width

5.3. Material Parameter

Following Material properties are used:

Arch Dam		Rock Mass		Water	
Density [kg/m ³]	2400	Density [kg/m ³]	0.0	Density [kg/m ³]	1000
Poisson - ratio [-]	0.167	Poisson - ratio [-]	0.2	Bulk - modulus [MPa]	2200
Youngs - modulus [MPa]	27000	Youngs - modulus [MPa]	25000		

Table 6: Material parameter

5.4. Acceleration Time History

The used acceleration is shown in the figures below. It is an acceleration spreading in x-, y- and z-direction. It is given in m/s^2 for a time span of 20 sec. The maximum acceleration of the time series is around 1m/s^2 .

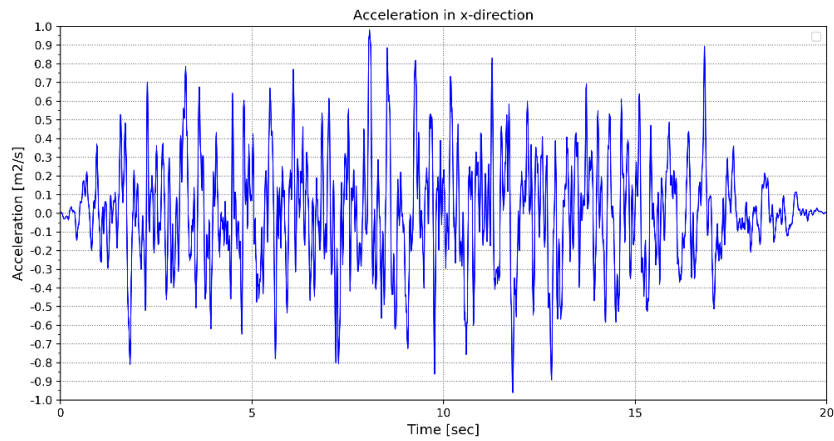


Figure 31: Acceleration in x-direction

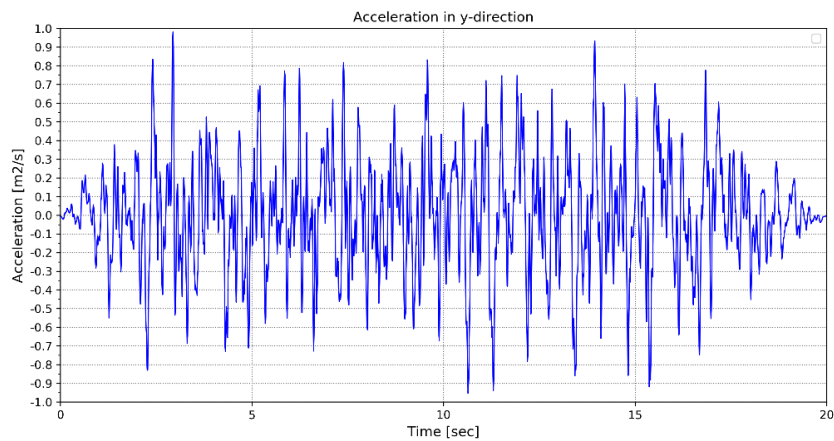


Figure 30: Acceleration in y-direction

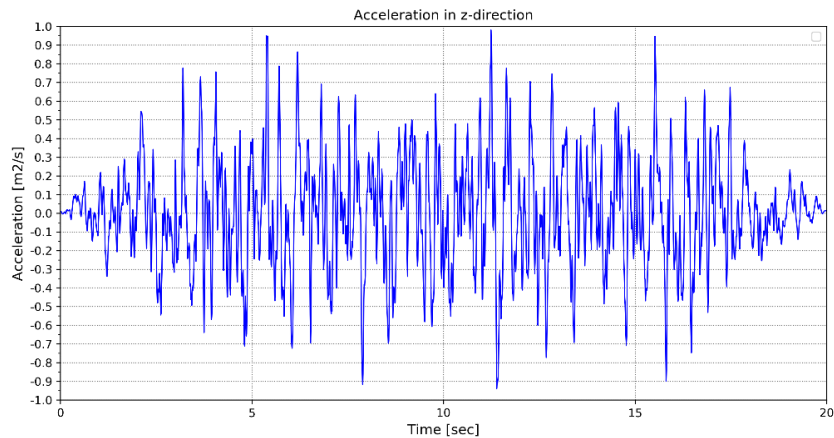


Figure 32: Acceleration in z-direction

5.5. Mesh

The mesh sensitivity is examined by using the arch dam with a crest thickness of 8 m. Only the mesh of the dam itself is refined, the foundation and the reservoir stayed the same. Therefore Figure 34 and Figure 35 below show only the arch dam.

First the arch dam, the reservoir and the foundation are meshed with an element size of 30 m, then the dam is refined with an element size of 20 m and the finest mesh of the dam is created with 15 m elements.

Coarse Mesh (30 m element size):

Coarse Mesh	Rock	Arch Dam	Fluid
Number of Nodes	26865	4049	7701
Number of Elements	5792	768	1584

Table 7: Nodes and elements for the coarse mesh

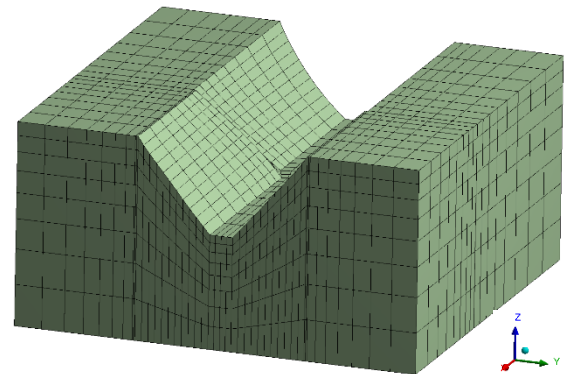
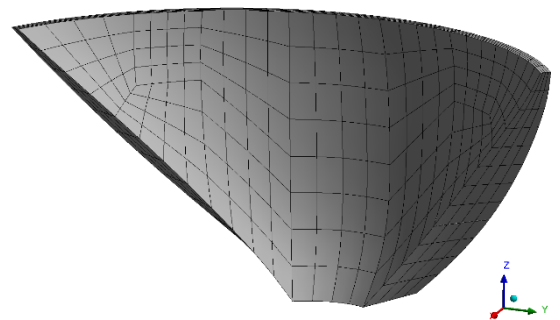
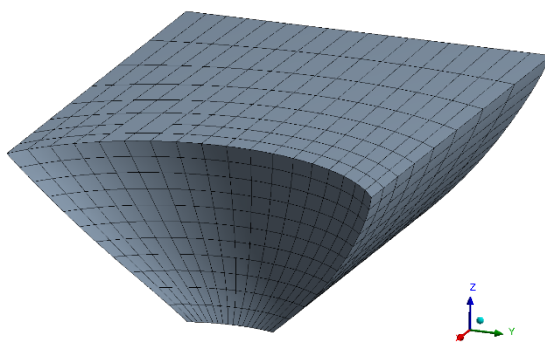


Figure 33: Coarse mesh for arch dam, reservoir and foundation

Medium Mesh (20 m element size):

Medium Mesh	Rock	Arch Dam	Fluid
Number of Nodes	26865	8805	7701
Number of Elements	5792	1728	1584

Table 8: Nodes and elements for the medium mesh

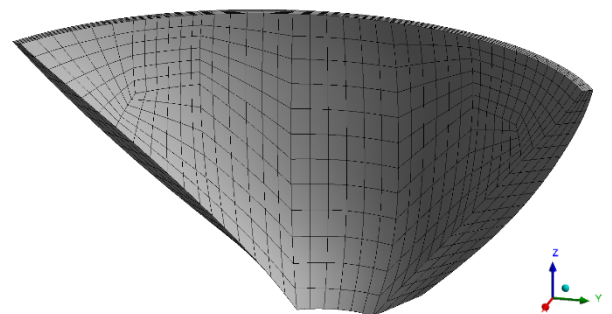


Figure 34: Medium mesh

Fine Mesh (15 m element size):

Fine Mesh	Rock	Arch Dam	Fluid
Number of Nodes	26865	14113	7701
Number of Elements	5792	2816	1584

Table 9: Nodes and elements for the fine mesh

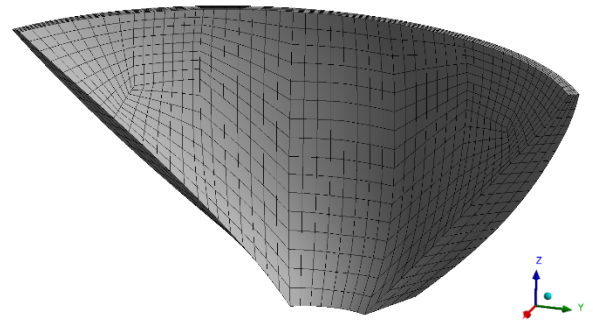


Figure 35: Fine mesh

To decide which mesh is suitable for the simulation, the horizontal stresses, the vertical stresses and the deformation of the dams with different mesh sizes are compared. The difference between the mesh with an element size of 20 m and 15 m is minimal. Therefore, the mesh with an element size of 20 m is used for the calculation.

The figure below shows the chosen mesh for all bodies.

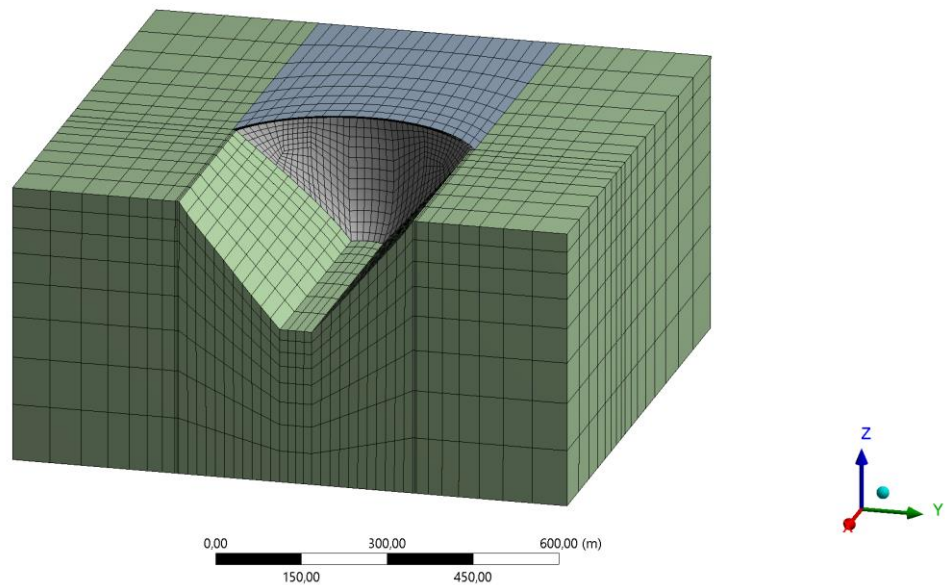


Figure 36: Chosen mesh for the whole geometry for the arch dam with 8 m crest width

5.6.Element and Node Numbering [23], [24]

The element type “Solid186” is used for the arch dam and for the rock foundation. It is a homogeneous structural solid element which is well suited for modeling irregular meshes. The 20-node element exhibits quadratic displacement behavior and uses uniform flow. For the reservoir, the higher order 3-D solid element “Fluid220” is used, which is also a 20-node element. This quadratic element is used to model the fluid medium and to describe the interface in the fluid structure interaction problems.

The figure below shows the geometry of the Solid186 and the Fluid220 elements, as both are 20-nodes elements.

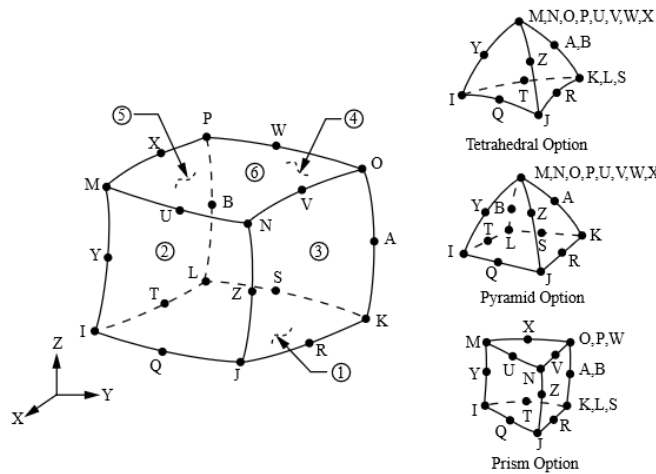


Figure 37: Geometry of the element “Solid186” an “Fluid220” [22]

5.7. Rayleigh Damping

The dam's damping behavior during seismic loading conditions is defined with the considered Rayleigh damping. With an assumed structural damping ratio of 5 %, the mass and stiffness proportional damping parameters, calculated based on equation (4-58) and (4-59), are:

Geometry						
	d = 8 m	d = 9 m	d = 10 m	d = 12 m	d = 14 m	d = 20 m
β	0.00326	0.00322	0.00318	0.00310	0.00302	0.00286
α	0.65013	0.65446	0.65885	0.66758	0.67625	0.69728

Table 10: Alpha and beta values for the 6 geometries, with d as the crest thickness

The effective mass is for the geometries with a crest thickness of 8 m to 14 m the highest for the 2nd and 9th frequency. This changed only for the last dam with the crest thickness of 20 m, where the effective mass for the 2nd and 10th frequency contributes the most.

The next picture shows the Rayleigh damping for the dam with a crest thickness of 8 m.

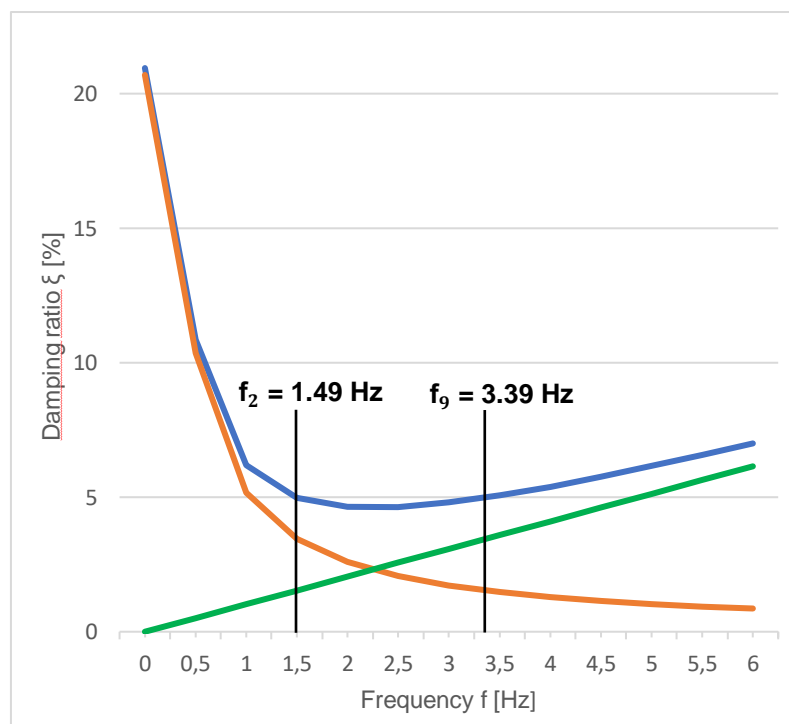


Figure 38: Rayleigh damping for initial geometry

5.8. Loading

Gravity, hydrostatic water pressure and seismic loading are taken into account for the following results. Gravity and hydrostatic pressure are applied together in the first step.

The vertical stresses, the hoop stresses and the minimum and maximum principal stresses are examined in the main, the right and the left section for the static load and the seismic loads. The main section is in the middle of the arch dam and the left and right sections are in a 45 degrees angle next to the main section. The static load is, if not separately written down, the line in the middle of the figures and the minimal and maximal seismic loads are the lines on the left side (minimal seismic load) and on the right side (maximal seismic load) of the static load.

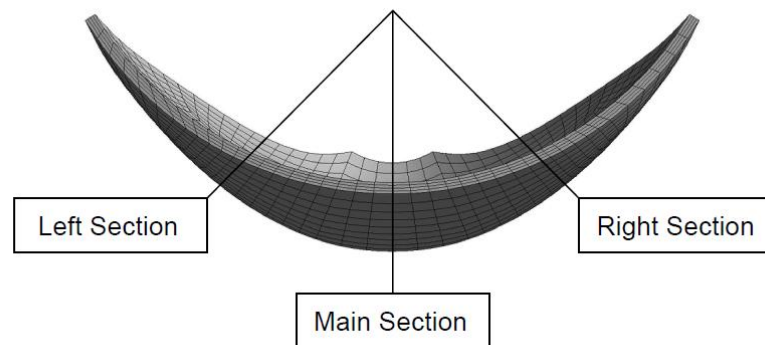


Figure 39: Location of the three evaluation sections

5.9. Results

The next table shows the first ten Eigenfrequencies for each dam. The interaction with the reservoir is considered.

Mode	Frequency [Hz]					
	d = 8 m	d = 9 m	d = 10 m	d = 12 m	d = 14 m	d = 20 m
1	1.48	1.48	1.48	1.48	1.48	1.51
2	1.49	1.49	1.49	1.50	1.51	1.53
3	2.00	2.01	2.01	2.02	2.03	2.05
4	2.19	2.20	2.20	2.23	2.25	2.34
5	2.51	2.51	2.51	2.51	2.51	2.52
6	2.68	2.72	2.75	2.83	2.91	3.14
7	3.17	3.18	3.18	3.19	3.19	3.20
8	3.20	3.20	3.21	3.22	3.23	3.27
9	3.39	3.45	3.52	3.64	3.76	3.92
10	3.91	3.91	3.91	3.91	3.91	4.03

Table 11: Table of the first ten Eigenfrequencies for every arch dam with d as the crest thickness

The Eigenfrequencies are also illustrated in the figure below, to show that there is little, or no difference between the Eigenfrequencies of the six different dams. Only the 6th, 9th and 10th Eigenfrequency of the arch dam with a crest thickness of 20 m are larger than the other Eigenfrequencies.

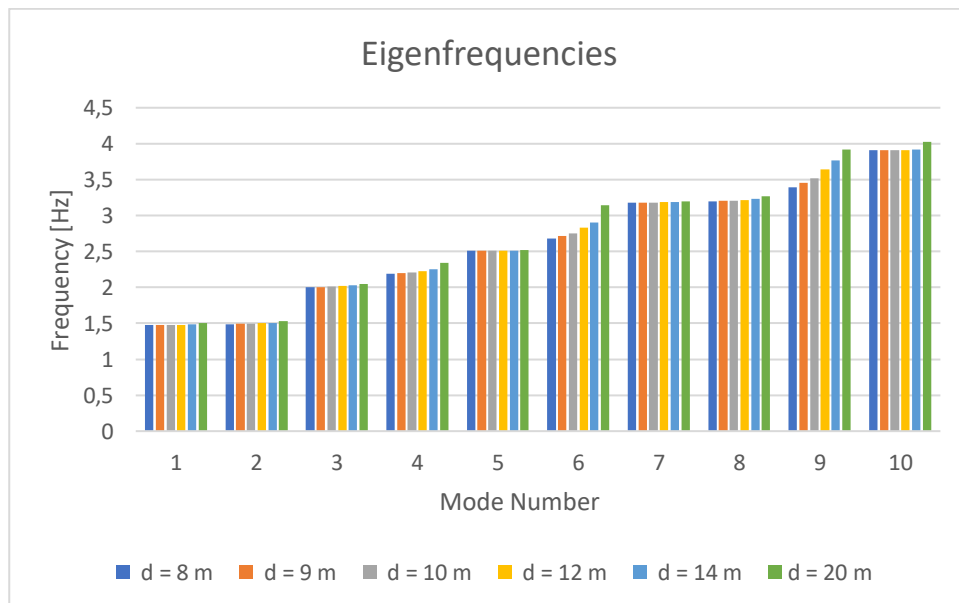


Figure 40: First 10 Eigenfrequencies of the arch dams, with d as the crest thickness

Mode shapes

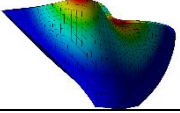
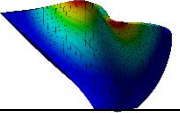
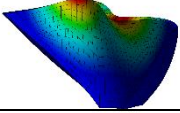
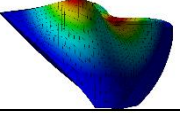
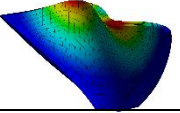
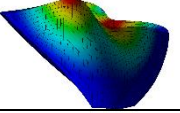
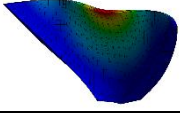
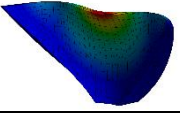
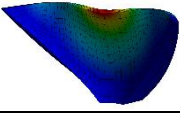
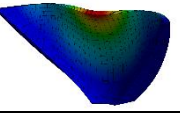
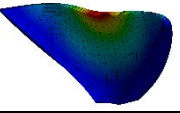
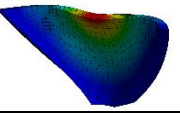
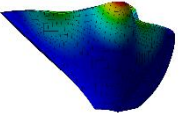
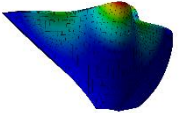
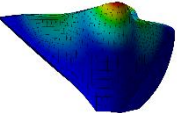
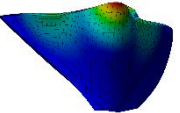
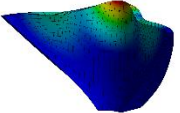
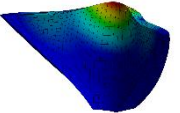
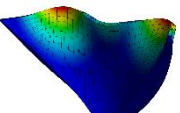
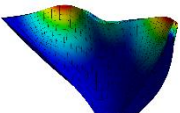
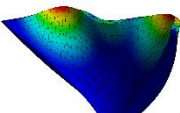
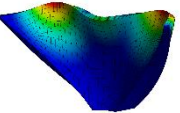
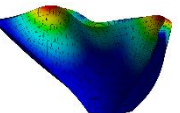
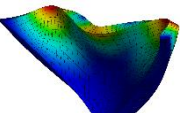
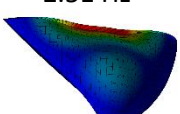
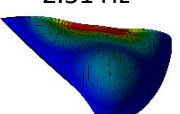
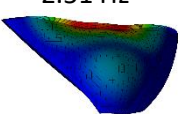
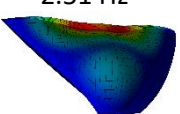
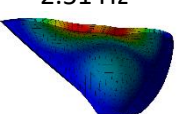
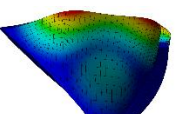
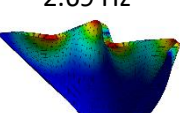
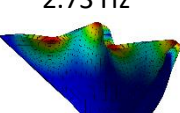
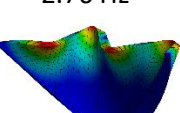
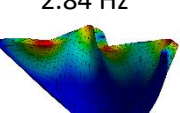
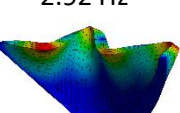
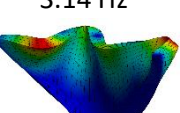
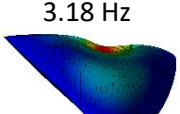
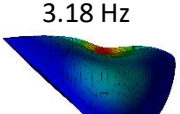
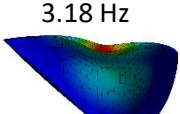
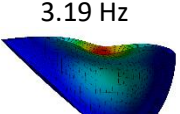
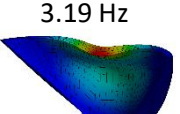
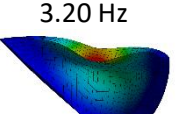
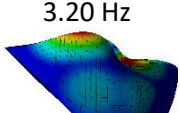
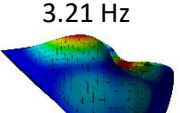
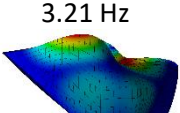
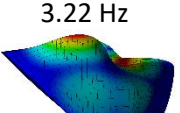
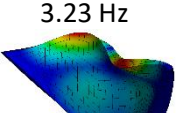
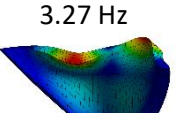
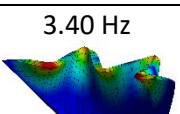
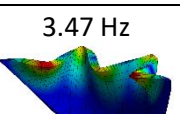
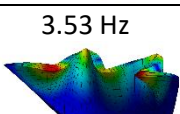
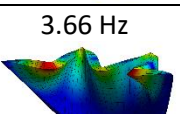
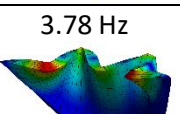
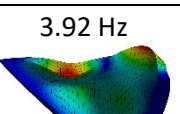
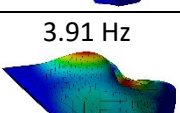
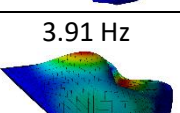
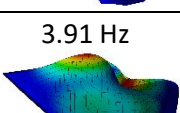
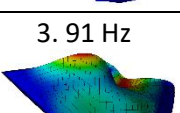
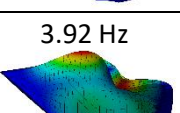
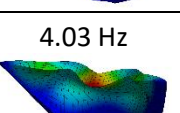
Mode Number	d = 8 m	d = 9 m	d = 10 m	d = 12 m	d = 14 m	d = 20 m
1	1.48 Hz 	1.48 Hz 	1.48 Hz 	1.48 Hz 	1.49 Hz 	1.51 Hz 
2	1.49 Hz 	1.49 Hz 	1.50 Hz 	1.50 Hz 	1.51 Hz 	1.53 Hz 
3	2.00 Hz 	2.01 Hz 	2.01 Hz 	2.02 Hz 	2.03 Hz 	2.05 Hz 
4	2.19 Hz 	2.20 Hz 	2.21 Hz 	2.23 Hz 	2.26 Hz 	2.34 Hz 
5	2.51 Hz 	2.51 Hz 	2.51 Hz 	2.51 Hz 	2.51 Hz 	2.52 Hz 
6	2.69 Hz 	2.73 Hz 	2.76 Hz 	2.84 Hz 	2.92 Hz 	3.14 Hz 
7	3.18 Hz 	3.18 Hz 	3.18 Hz 	3.19 Hz 	3.19 Hz 	3.20 Hz 
8	3.20 Hz 	3.21 Hz 	3.21 Hz 	3.22 Hz 	3.23 Hz 	3.27 Hz 
9	3.40 Hz 	3.47 Hz 	3.53 Hz 	3.66 Hz 	3.78 Hz 	3.92 Hz 
10	3.91 Hz 	3.91 Hz 	3.91 Hz 	3.91 Hz 	3.92 Hz 	4.03 Hz 

Table 12: Mode shapes of the different arch dams, with d as the crest thickness

The mode shapes 1 to 4 are for all arch dams the same. For mode number 5 the mode shapes, for the first five dams ($d = 8$ m to $d = 14$ m, with d as crest thickness) are the same, only the thickest dam with the crest of 20 m has a different mode shape.

The following diagrams show the results of the hoop stresses, which are oriented along the y -axis, the vertical stresses along the z -axis, the minimum and maximum principal stresses and the deformation of the different dams which its orientation along the x -axis. The middle line represents the stresses and displacement as a result of the static load. The left and the right lines represent the minima and maxima of the time series. The six dams are illustrated in six different colors. The colors for each dam are described in the legend, which is included in the diagram.

The geometry is cut in three sections, the main, right and left section. For the main section the global coordinate is used. The left and right section use each a coordinate system which is orientated along the left or the right section cut.

The used acceleration time series for the upstream and the downstream side of the arch dam is pictured in the chapter “5.4 Acceleration Time History”. The maximum acceleration of the time series is around 1 m/s^2 .

The diagrams below show the results of deformation along the main section on the downstream and the upstream side of the arch dam with regard to the global coordinate system. The deformation is only shown in the main section and not in the left and the right section, as the displacements are significant higher in the main section, due to the height of the dam. This directional deformation is analyzed for the x -direction. Therefore, the positive results are towards the downstream face and the negative results are in the direction of the upstream face of the dam.

Deformation – Main Section – Downstream

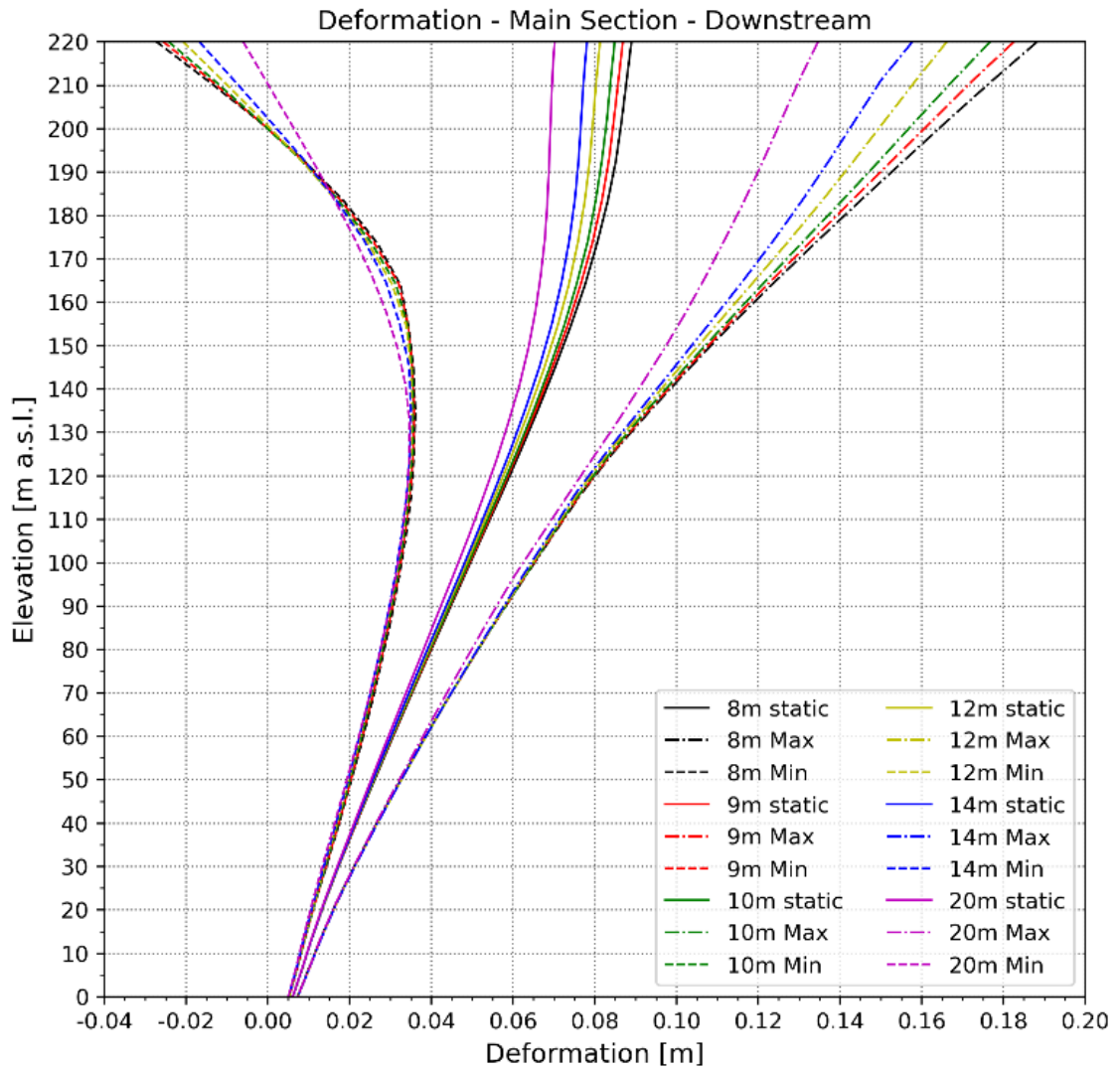
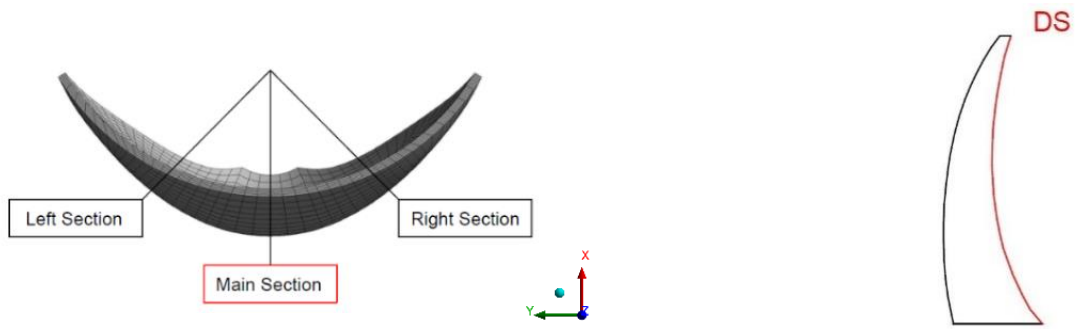


Figure 41: Deformation of the six dams in the main section along the downstream face

Deformation (Only Static Load) – Main Section – Downstream

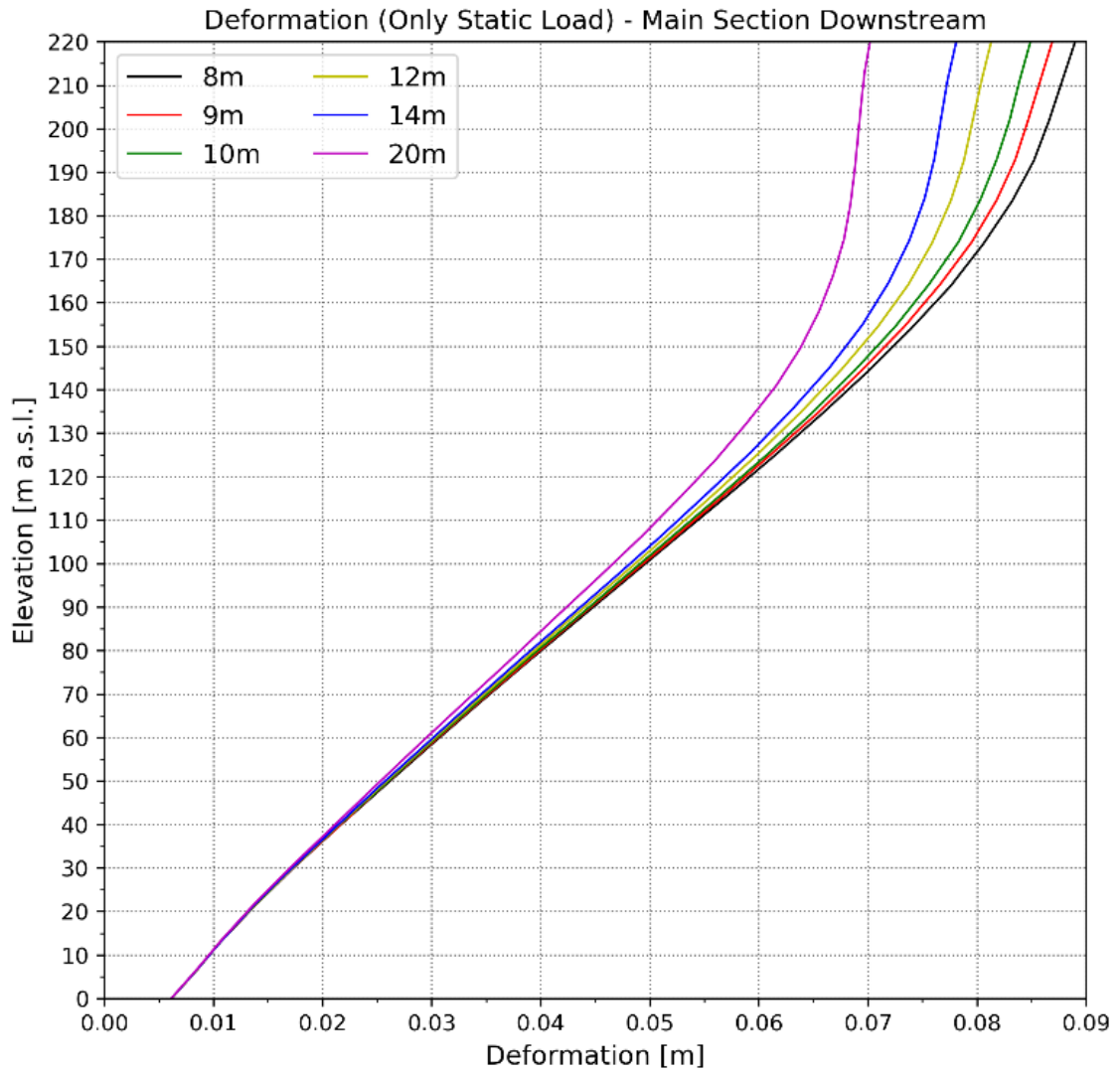
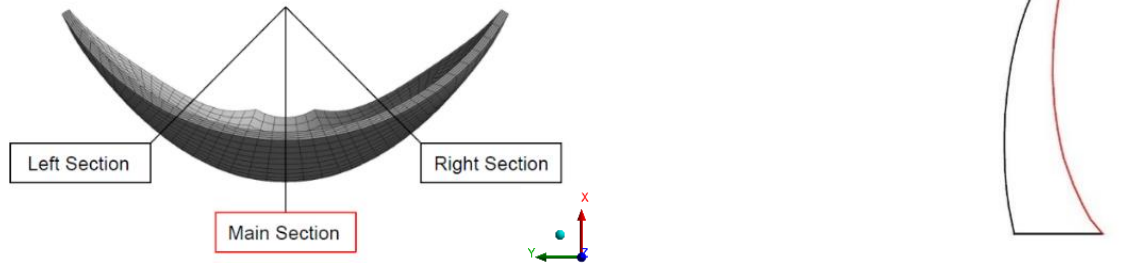


Figure 42: Static load of the deformation of the six dams in the main section along the downstream side

Deformation (Only Dynamic Load) – Main Section

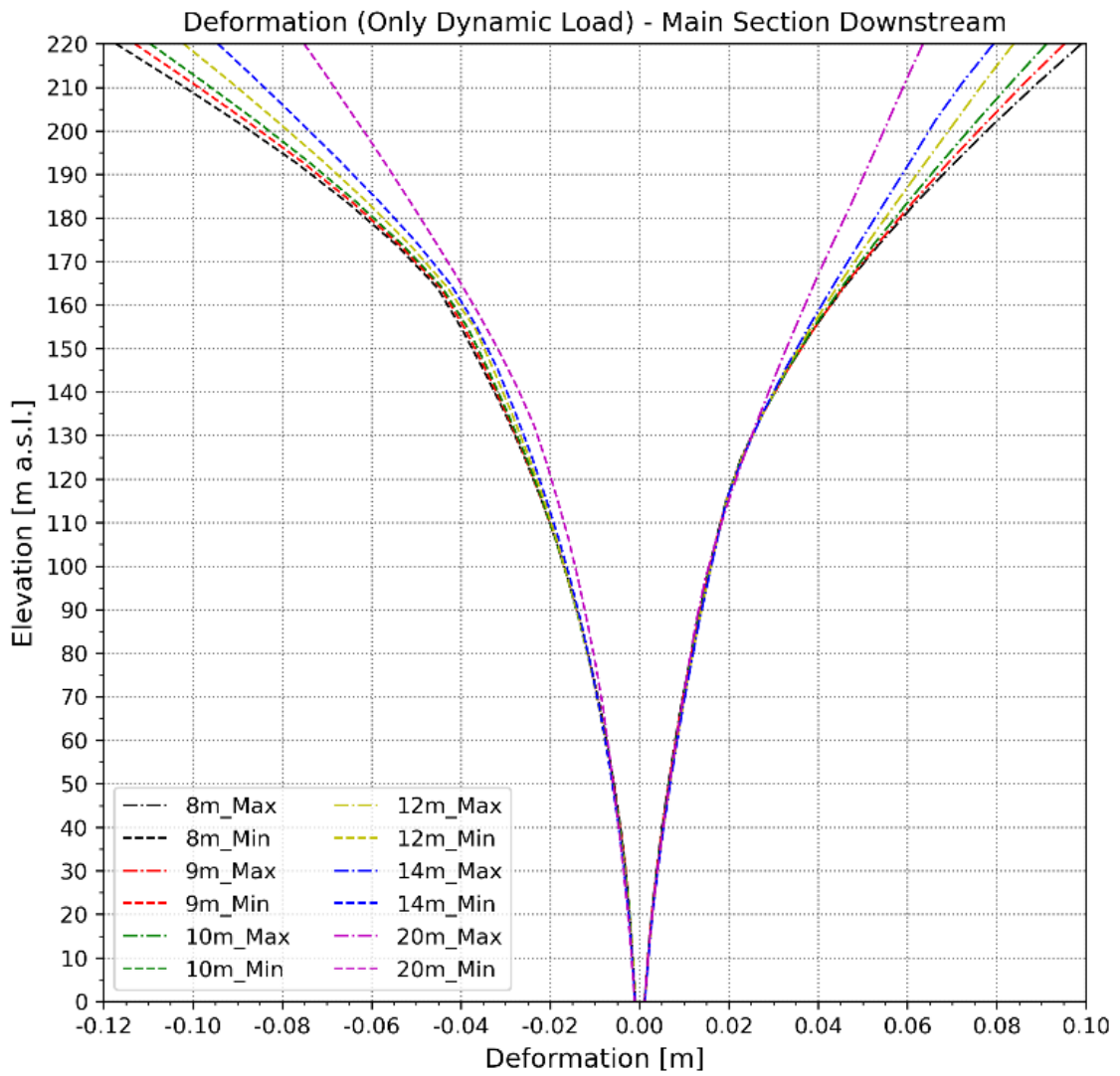
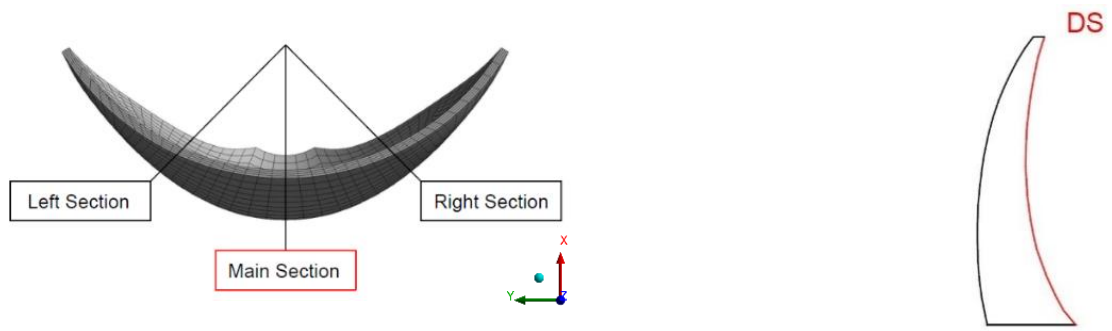


Figure 43: Dynamic load of the deformation of the six dams in the main section along the downstream side

Deformation – Main Section – Upstream

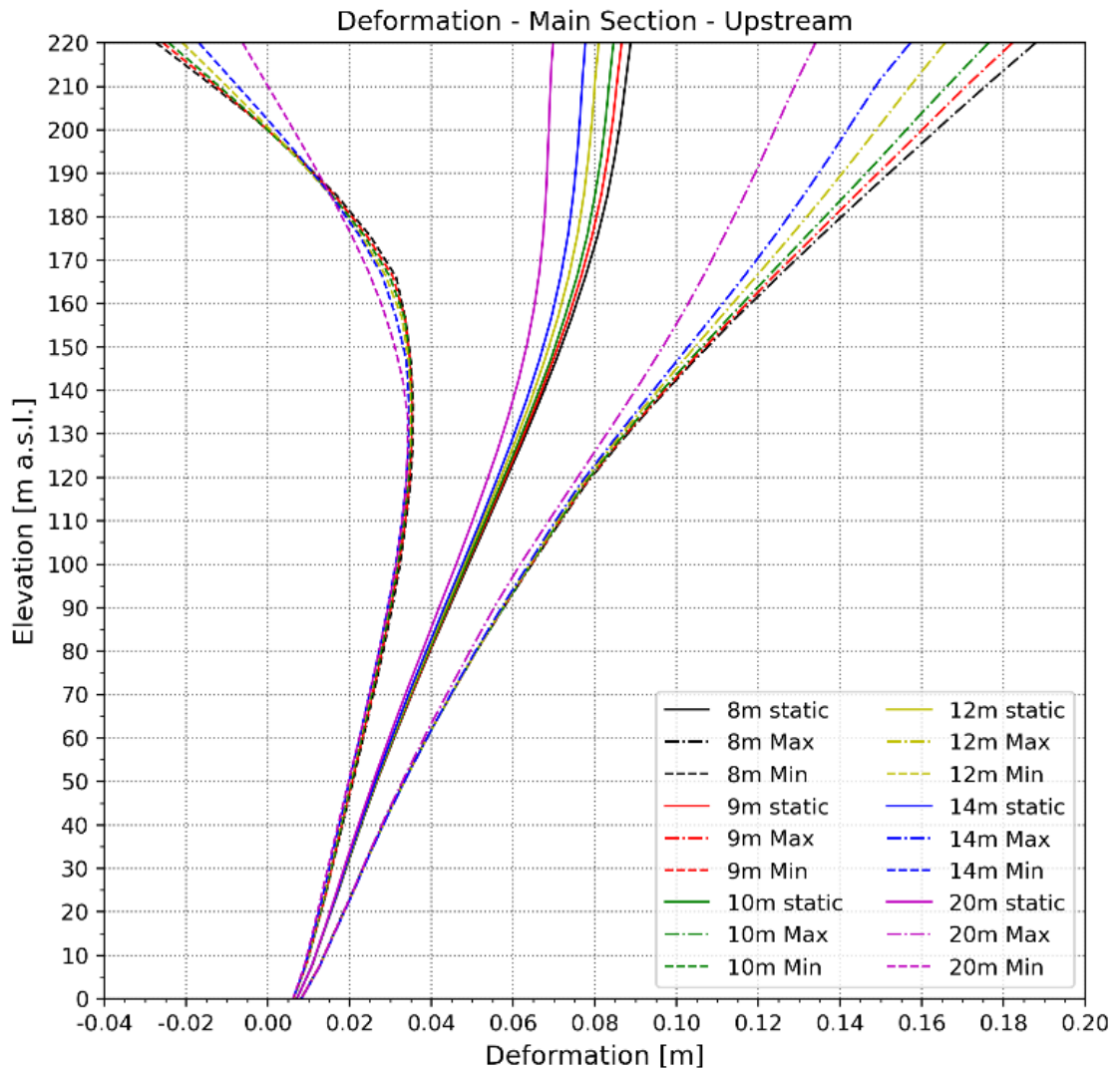
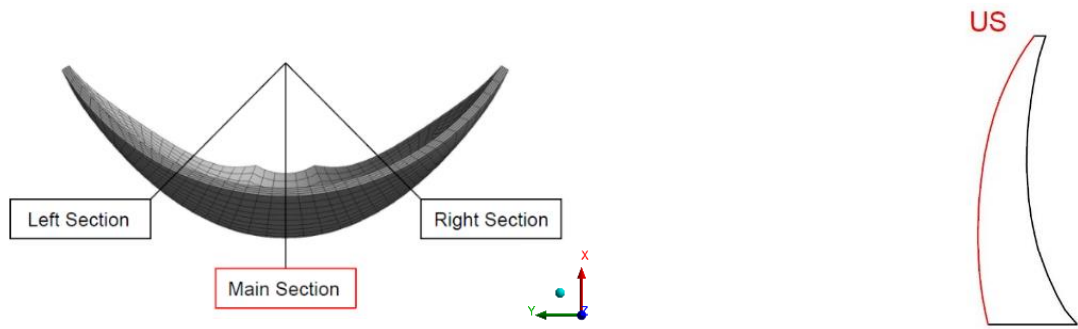


Figure 44: Deformation of the six dams in the main section along the upstream side

The tables below describe the displacements of all dams. The values are taken in the point where the biggest difference between the stresses in the diagrams are. The following tables show the difference between the results of the static load and the results of the minima and maxima of the time series. The differences are then shown in percentage, with the base geometry as reference.

The height of the taken values can be seen in the left corner written in gray. For the first table the values are taken at the dam crest (220 m).

Deformation - Main Section - US					
220 m	Static load	dynamic load			
Crest thickness	Displacement [cm]	min. Displacement [cm]	Difference from static load in %	max. Displacement [cm]	Difference from static load in %
8 m	8.88	-2.74	100.0	18.80	100.0
9 m	8.66	-2.57	96.6	18.20	96.2
10 m	8.46	-2.43	93.7	17.60	92.1
12 m	8.10	-2.09	87.7	16.60	85.7
14 m	7.77	-1.69	81.4	15.70	79.9
20 m	6.98	-0.62	65.4	13.40	64.7

Table 13: Deformation at the main section – upstream

Deformation - Main Section - DS					
220 m	Static load	dynamic load			
Crest thickness	Displacement [cm]	min. Displacement [cm]	Difference from static load in %	max. Displacement [cm]	Difference from static load in %
8 m	8.90	-2.73	100.0	18.80	100.0
9 m	8.69	-2.56	96.7	18.30	97.1
10 m	8.49	-2.43	93.9	17.70	93.0
12 m	8.13	-2.10	88.0	16.60	85.6
14 m	7.81	-1.68	81.6	15.80	80.7
20 m	7.02	0.13	59.2	13.50	65.5

Table 14: Deformation at the main section - downstream

Deformation - Main Section - DS and US

Figure 41 and Figure 44 show that the deformation along the downstream and the upstream face decreases when the thickness of the dam increases. This can clearly be explained by an increase of the systems stiffness. In Figure 41 a significant reduction of the maximum deformation between the arch dam with a dam crest of 8 m (18.8 cm) and the arch dam with a thickness of 20 m (13.5 cm) can be seen.

Throughout the entire process of changing the thickness from 8m to 20m the tendency is consistent. Due to the stiffer crest, the deformations reduce on the upstream and downstream face, and are the lowest at the elevation of the dam crest, at 220 m. The results of the upstream and the downstream face of the main section do not differ significantly.

The change in displacements are plausible as more volume of the arch dams leads to a higher stiffness of the system. Therefore, the arch dams with a thicker crest width can't be deformed as much as the arch dams with a thinner crest width.

Hoop Stress – Main section – Upstream

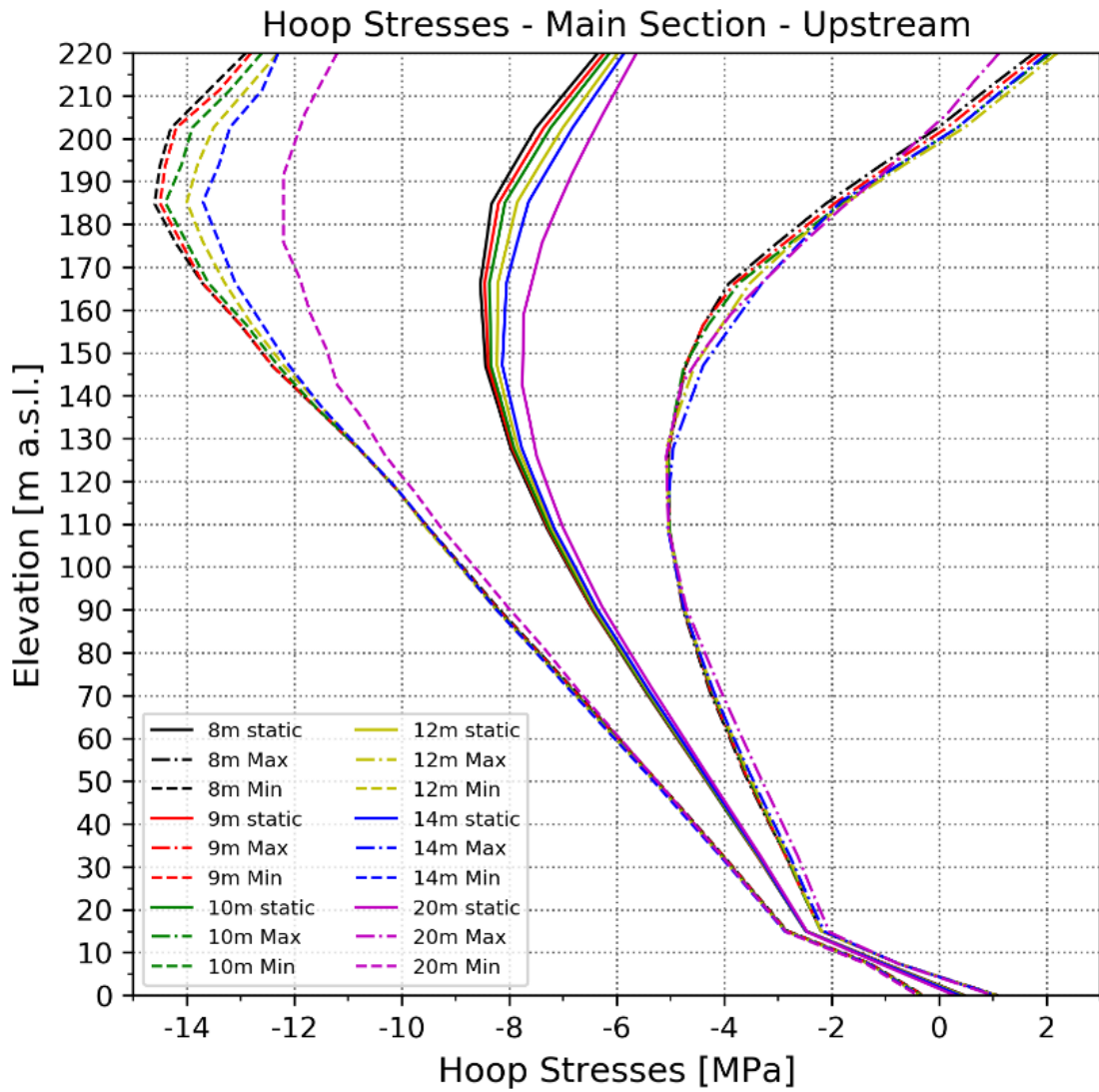
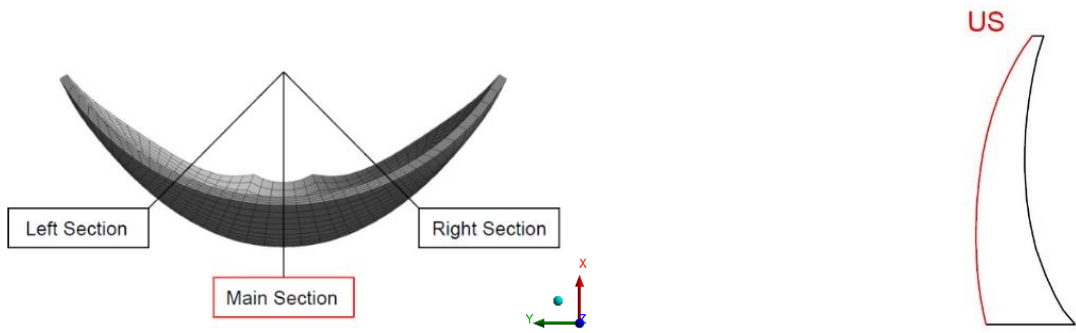


Figure 45: Hoop stresses of the six dams in the main section along the upstream side

Hoop Stresses (Only Static Load) – Main Section – Upstream

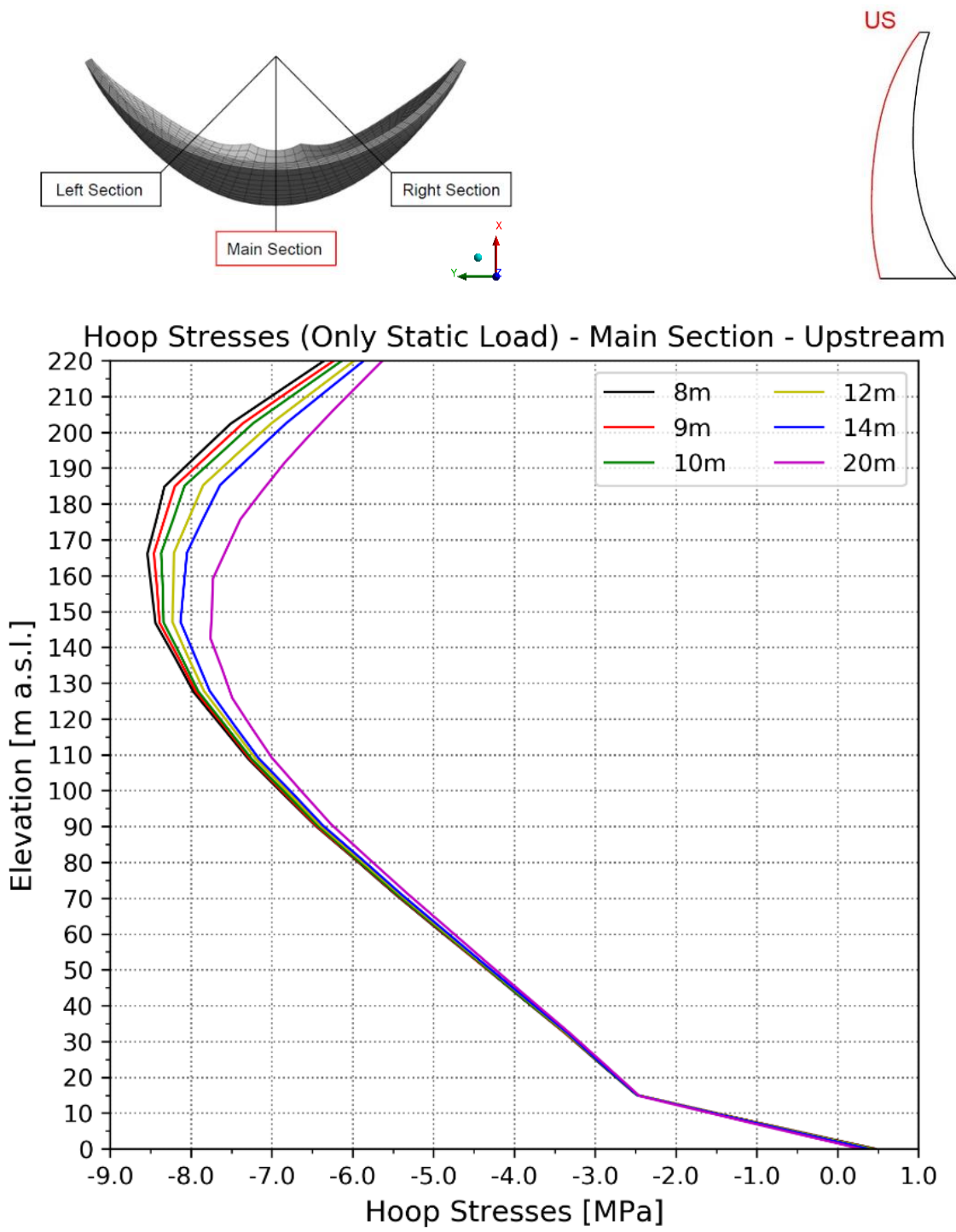


Figure 46: Static load of the hoop stresses of the six dams in the main section along the upstream side

Hoop Stresses (Only Dynamic Load) – Main Section – Upstream

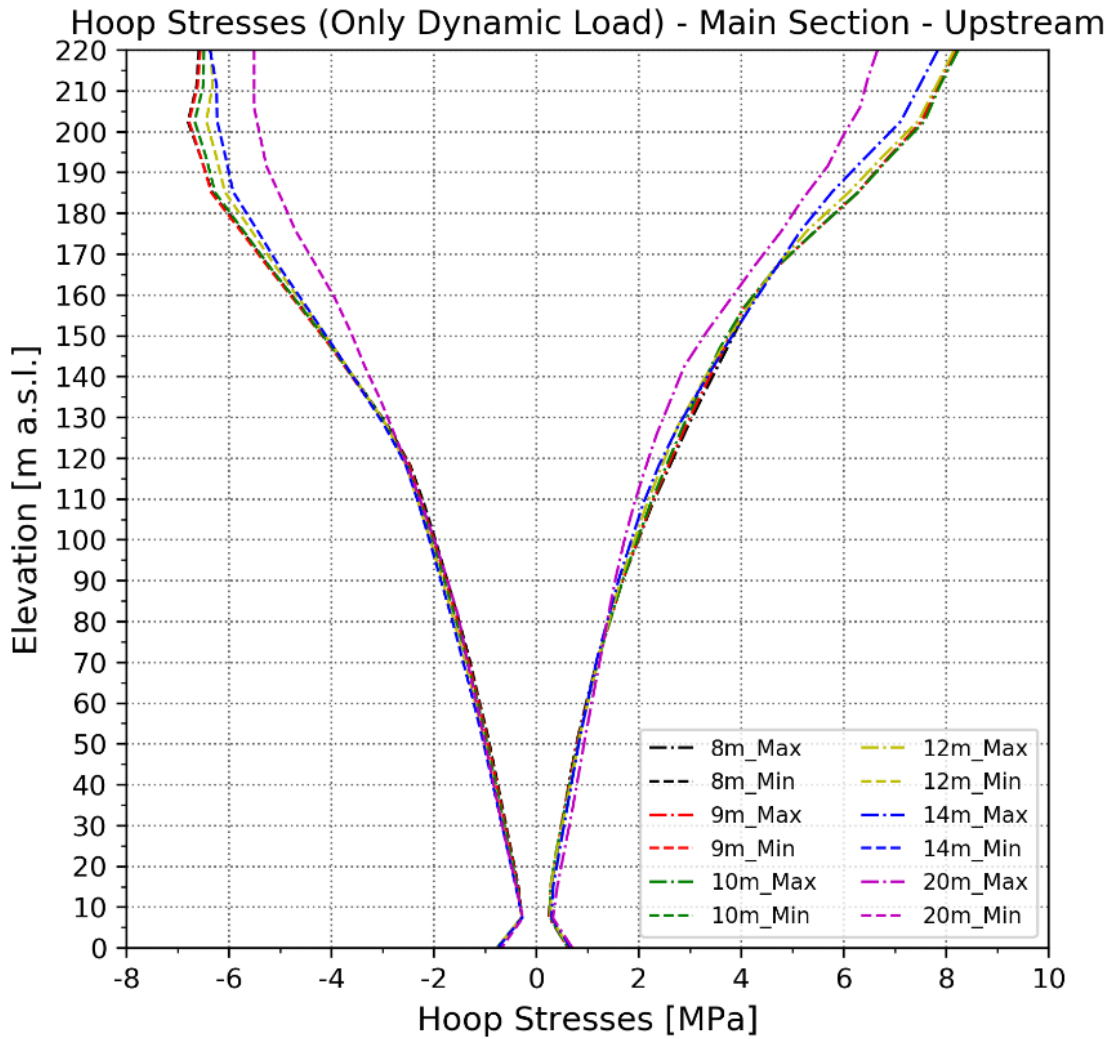
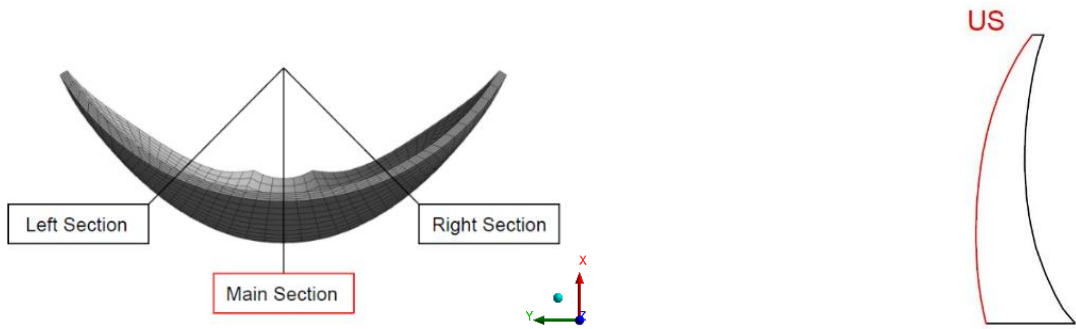


Figure 47: Dynamic load of the hoop stresses of the six dams in the main section along the upstream side

Hoop Stress – Main section – Downstream

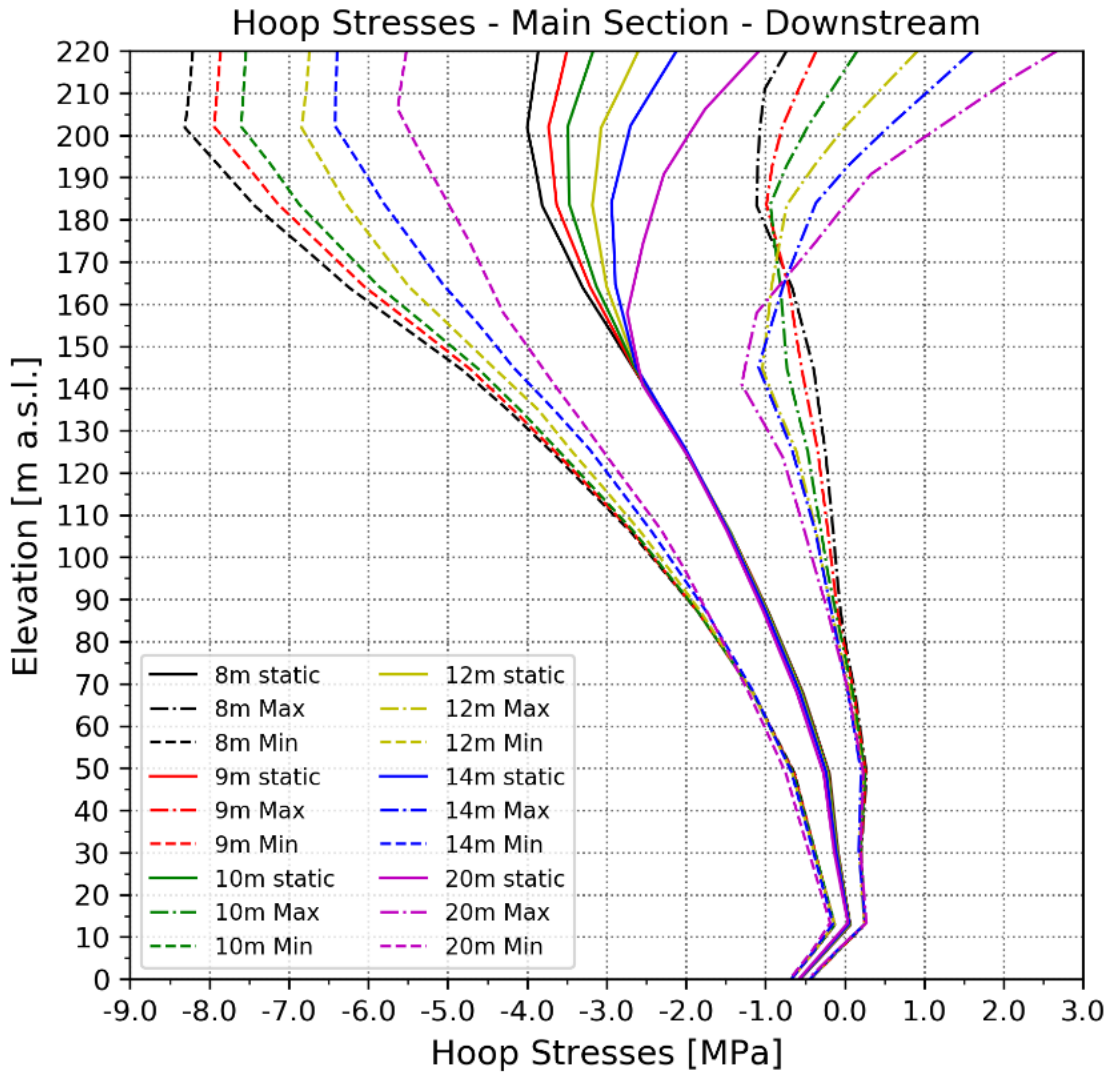
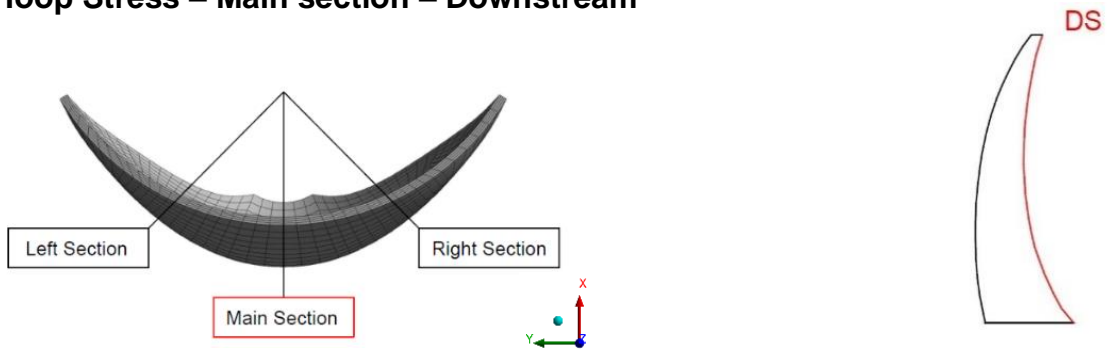


Figure 48: Hoop stresses of the six dams in the main section along the downstream side

Hoop Stresses – Left Section – Upstream

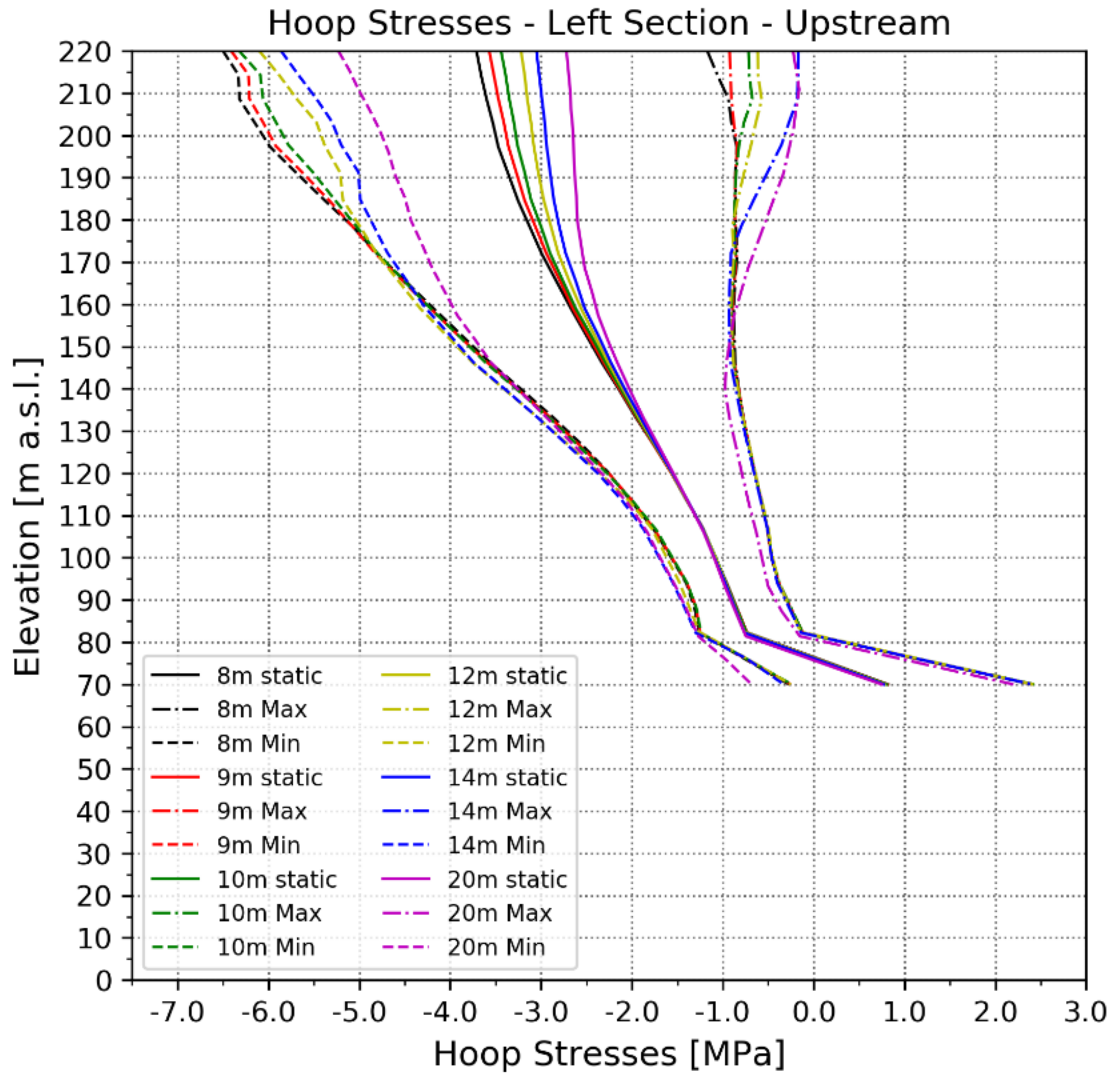
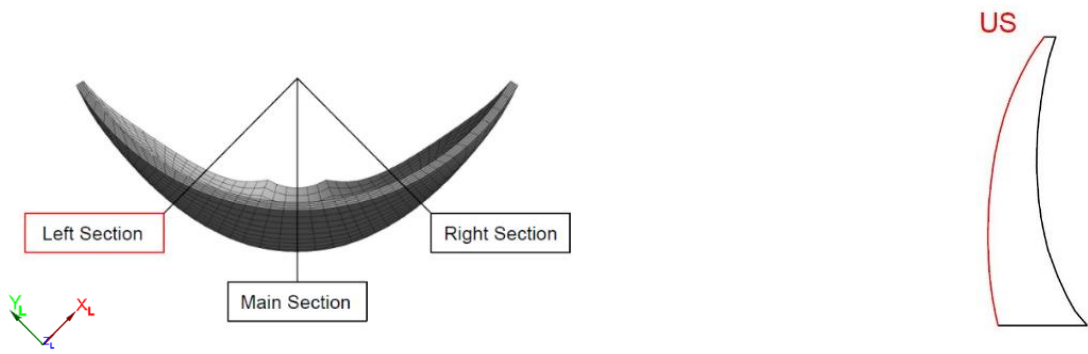


Figure 49: Hoop stresses of the six dams in the left section along the upstream side

Hoop Stresses – Left Section – Downstream

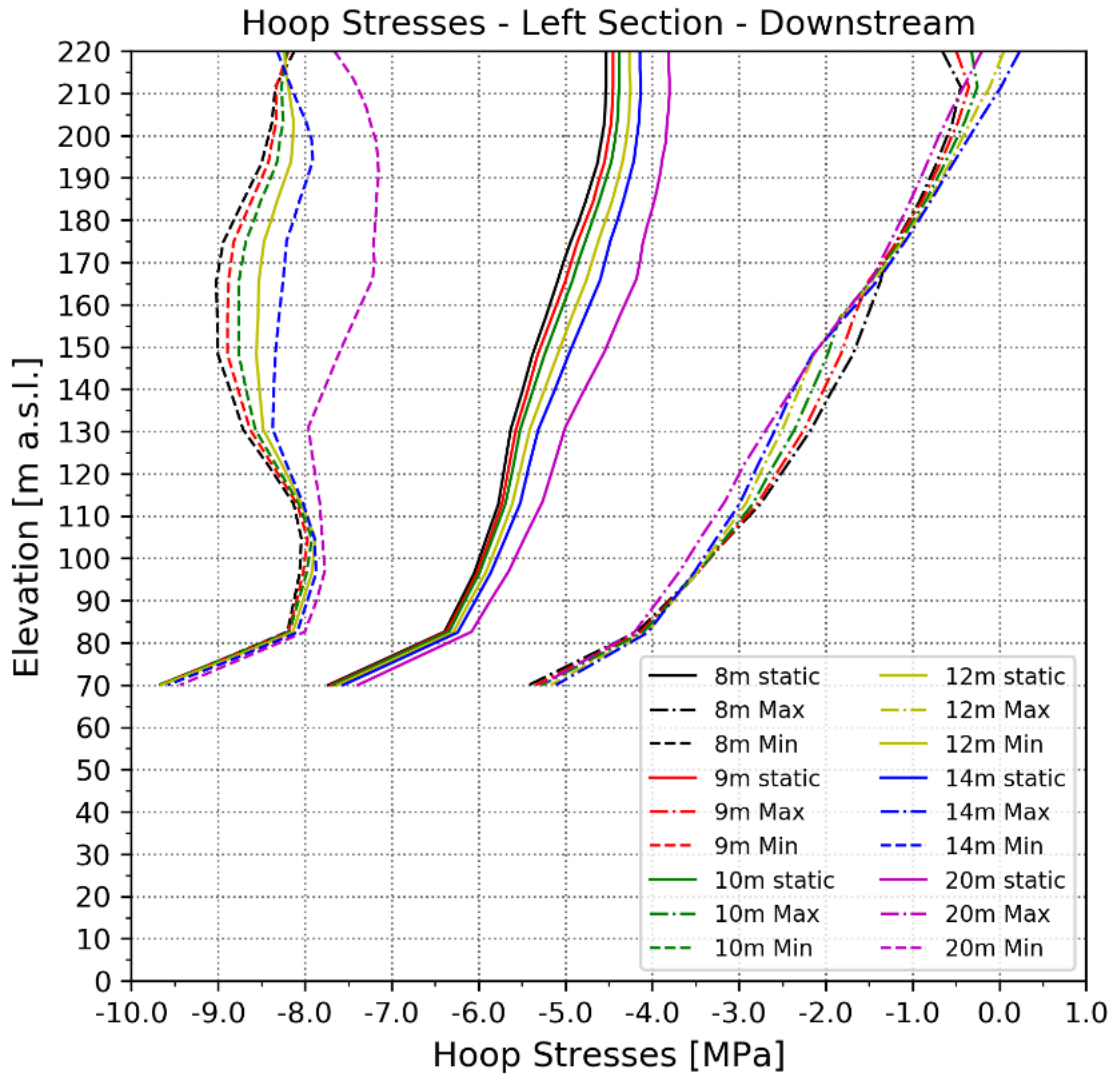
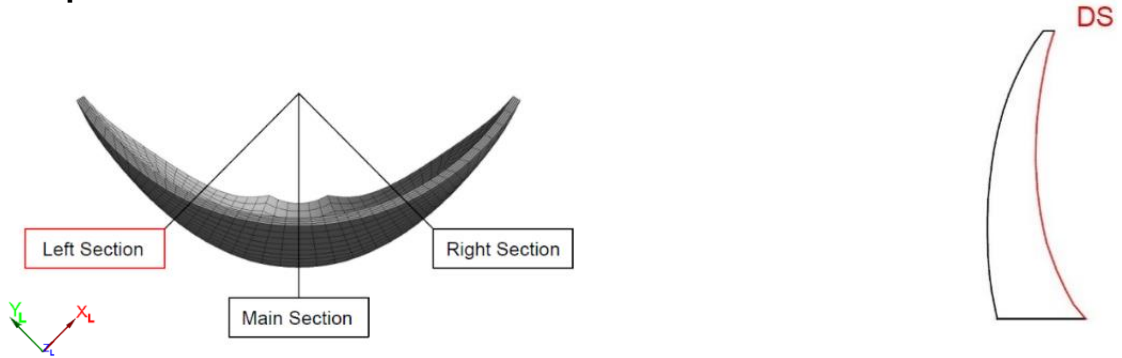


Figure 50: Hoop stresses of the six dams in the left section along the downstream side

Hoop Stresses – Right Section – Upstream

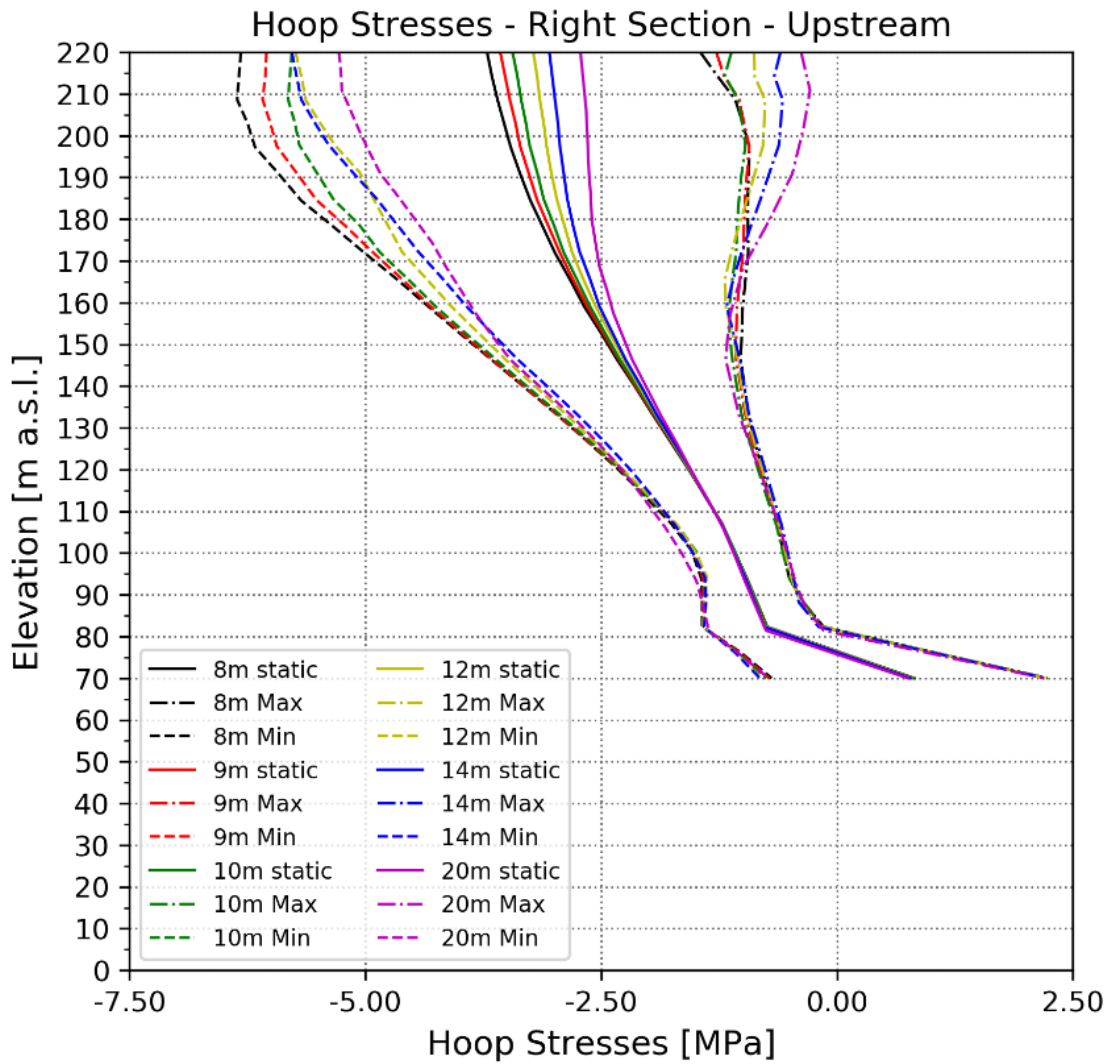
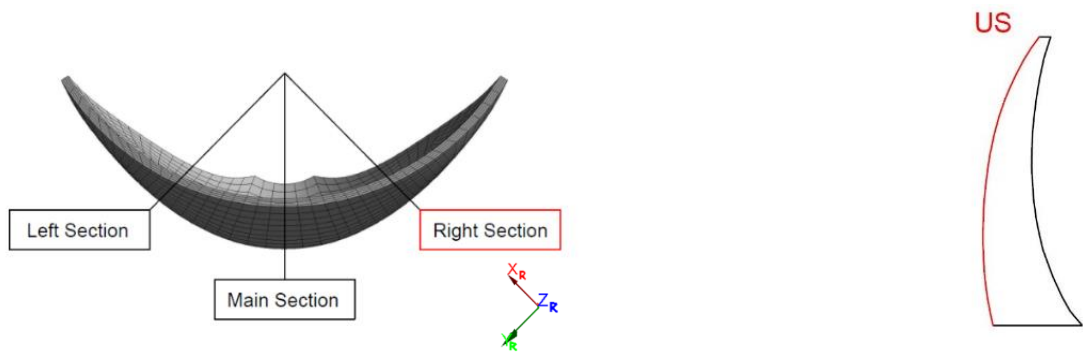


Figure 51: Hoop stresses of the six dams in the right section along the upstream side

Hoop Stresses – Right Section – Downstream

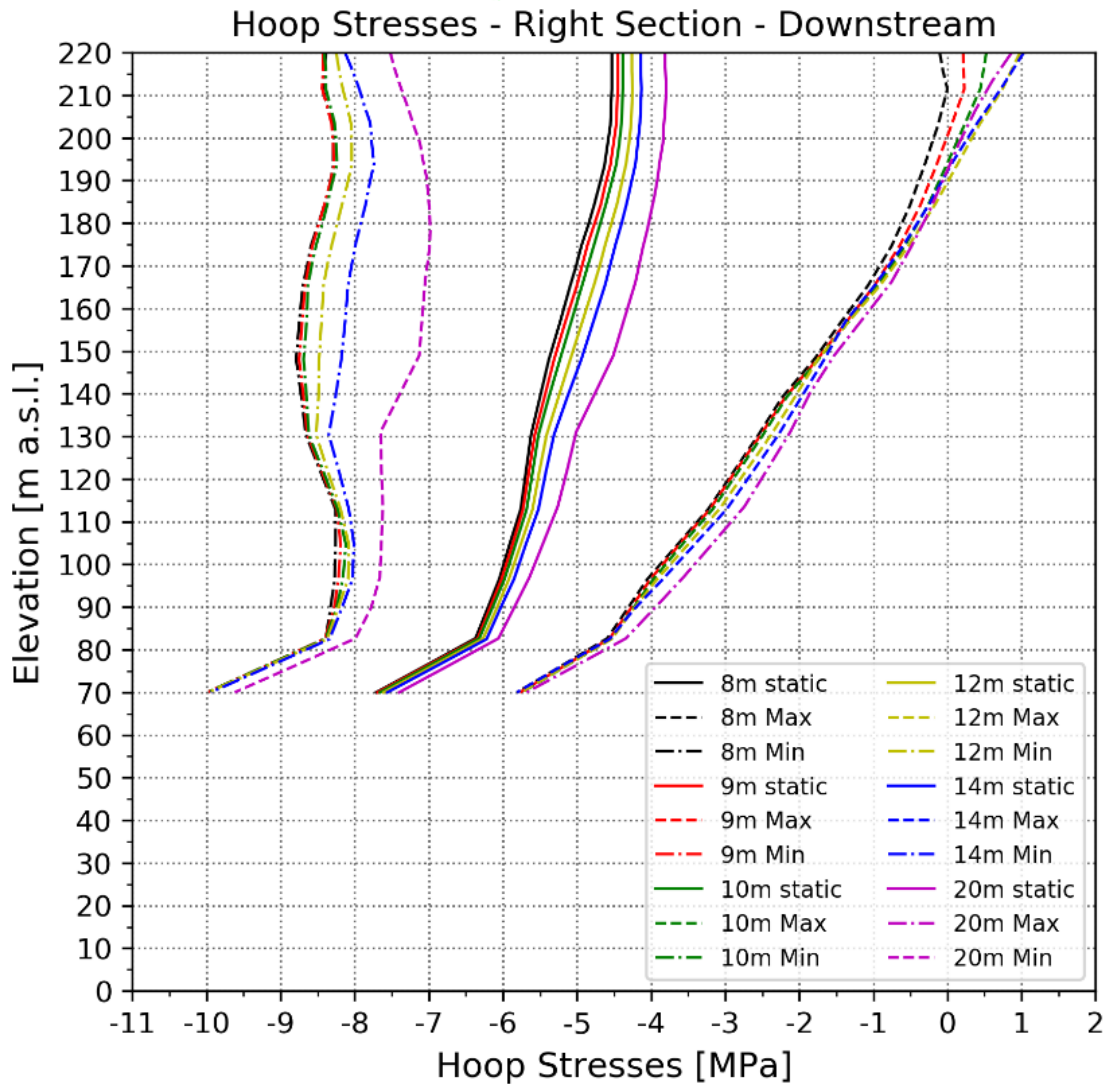
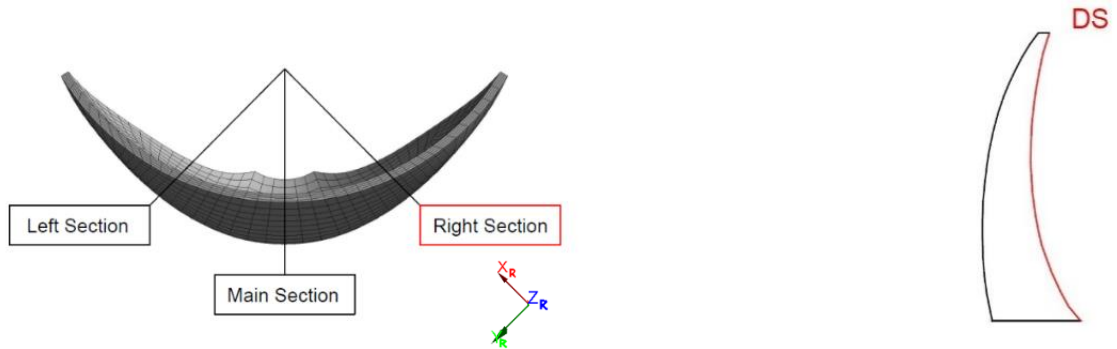


Figure 52: Hoop stresses of the six dams in the right section along the downstream side

5. Numerical Case Studies

Hoop Stress - Main Section - US					
180 m	Static load	dynamic load			
Crest thickness	Hoop Stress [MPa]	min. Hoop Stress [MPa]	Difference from static load in %	max. Hoop Stress [MPa]	Difference from static load in %
8 m	-8.40	-14.50	100.0	-3.00	100.0
9 m	-8.30	-14.30	98.4	-2.80	101.9
10 m	-8.20	-14.20	98.4	-2.77	100.6
12 m	-8.00	-13.80	95.1	-2.70	98.1
14 m	-7.80	-13.50	93.4	-2.60	96.3
20 m	-7.30	-12.20	80.3	-2.50	88.9

Table 15: Hoop stresses at the main section – upstream

Hoop Stress - Main Section - DS					
220 m	Static load	dynamic load			
Crest thickness	Hoop Stress [MPa]	min. Hoop Stress [MPa]	Difference from static load in %	max. Hoop Stress [MPa]	Difference from static load in %
8 m	-3.86	-8.21	100.0	-0.74	100.0
9 m	-3.50	-7.86	100.2	-0.36	100.6
10 m	-3.17	-7.54	100.5	0.16	106.7
12 m	-2.60	-6.74	95.2	0.92	112.8
14 m	-2.12	-6.39	98.2	1.61	119.6
20 m	-1.08	-5.52	102.1	2.67	120.2

Table 16: Hoop stresses at the main section – downstream

Hoop Stress - Left Section - US					
220 m	Static load	dynamic load			
Crest thickness	Hoop Stress [MPa]	min. Hoop Stress [MPa]	Difference from static load in %	max. Hoop Stress [MPa]	Difference from static load in %
8 m	-3.71	-6.50	100.0	-1.17	100.0
9 m	-3.57	-6.41	101.8	-0.92	104.3
10 m	-3.44	-6.32	103.2	-0.72	107.1
12 m	-3.22	-6.10	103.2	-0.61	102.8
14 m	-3.05	-5.86	100.7	-0.17	113.4
20 m	-2.72	-5.23	90.0	-0.23	98.0

Table 17: Hoop stresses at the left section - upstream

5.Numerical Case Studies

Hoop Stress - Left Section - DS					
180 m	Static load	dynamic load			
Crest thickness	Hoop Stress [MPa]	min. Hoop Stress [MPa]	Difference from static load in %	max Hoop Stress [MPa]	Difference from static load in %
8 m	-4.85	-8.83	100.0	-1.06	100.0
9 m	-4.77	-8.72	99.2	-1.04	98.4
10 m	-4.69	-8.59	98.0	-1.00	97.4
12 m	-4.54	-8.39	96.7	-0.96	94.5
14 m	-4.40	-8.13	93.7	-0.93	91.6
20 m	-4.00	-7.18	79.9	-1.50	66.0

Table 18: Hoop stresses at the left section – downstream

Hoop Stress - Right Section - US					
220 m	Static load	dynamic load			
Crest thickness	Hoop Stress [MPa]	min. Hoop Stress [MPa]	Difference from static load in %	max. Hoop Stress [MPa]	Difference from static load in %
8 m	-3.71	-6.32	100.0	-1.45	100.0
9 m	-3.56	-6.05	95.4	-1.28	100.9
10 m	-3.44	-5.78	89.7	-1.12	102.7
12 m	-3.22	-5.74	96.6	-0.88	103.5
14 m	-3.05	-5.78	104.6	-0.60	108.4
20 m	-2.72	-5.28	98.1	-0.38	103.5

Table 19: Hoop stresses at the right section – upstream

Hoop Stress - Right Section - DS					
180 m	Static load	dynamic load			
Crest thickness	Hoop Stress [MPa]	min. Hoop Stress [MPa]	Difference from static load in %	max. Hoop Stress [MPa]	Difference from static load in %
8 m	-4.85	-8.50	100.0	-0.63	100.0
9 m	-4.77	-8.49	101.9	-0.50	101.2
10 m	-4.69	-8.44	102.7	-0.40	101.7
12 m	-4.54	-8.24	101.4	-0.34	99.5
14 m	-4.40	-7.82	93.7	-0.41	94.5
20 m	-4.00	-7.00	82.2	-0.35	86.5

Table 20: Hoop stresses at the right section - downstream

Hoop Stresses - Downstream

Figure 48 shows the hoop stresses of the main section of all investigated geometries along the downstream face. The results of the static load of the six geometries are the same till 150 m. After that the results differ due to the change in the geometry.

Table 16 shows that the compressive stresses on the dam crest decrease, when the thickness of the arch dam increases. This lets the dam leans towards the upstream face of the arch dam.

The minimum hoop stresses show a kink around the dam elevation of 200 m. This is due to the shape of the geometry and is the result of a discontinuity which occurs at this point.

The lines on the right in Figure 48 represents the maximum hoops stresses, which intersect at about elevation 165 m. This can be explained due to a different centre of gravity for the thicker dams, which shows higher values than for the thinner dams and moves further to the downstream face.

The static load of the hoop stresses on the left side are parallel to each other. The pressure is the highest at the base joint and decreases with increasing height of the dam.

The investigated sections close to the right and left abutments show similar results as the results in the main section.

Hoop Stress - Main Section - DS					
220 m	Static load	dynamic load			
Crest thickness	Hoop Stress [MPa]	min. Hoop Stress [MPa]	Difference from static load in %	max. Hoop Stress [MPa]	Difference from static load in %
8 m	-3.86	-8.21	100.0	-0.74	100.0
20 m	-1.08	-5.52	102.1	2.67	120.2

Table 21 Hoop stresses of the dam with the thinnest and thickest dam crest at the main section – downstream

The table above shows the hoop stresses for the arch dam with a crest thickness of 8 and 20 m at the main section along the downstream face of the dam. It can

be seen that there is a negative effect in tension due to the higher stiffness of the dam. This means that the tensile stresses increase when the crest of the arch dam increases.

Hoop Stresses - Upstream

Figure 45 shows that the compressive stresses on the upstream face also decrease in the upper third of the arch dam, as the stiffness increased due to more volume of the dam. Due to that a high difference of 2.3 MPa can be seen in the results of the minimum dynamic load concerning the thickest arch dam with a crest thickness of $d = 20$ m and the dam with a crest thickness of $d = 8$ m.

The results for the static load in the main section are for all investigated geometries nearly the same.

The results of the hoop stresses on the left side do not differ much from each other. Figure 49 illustrates that.

Vertical Stress – Main Section – Upstream

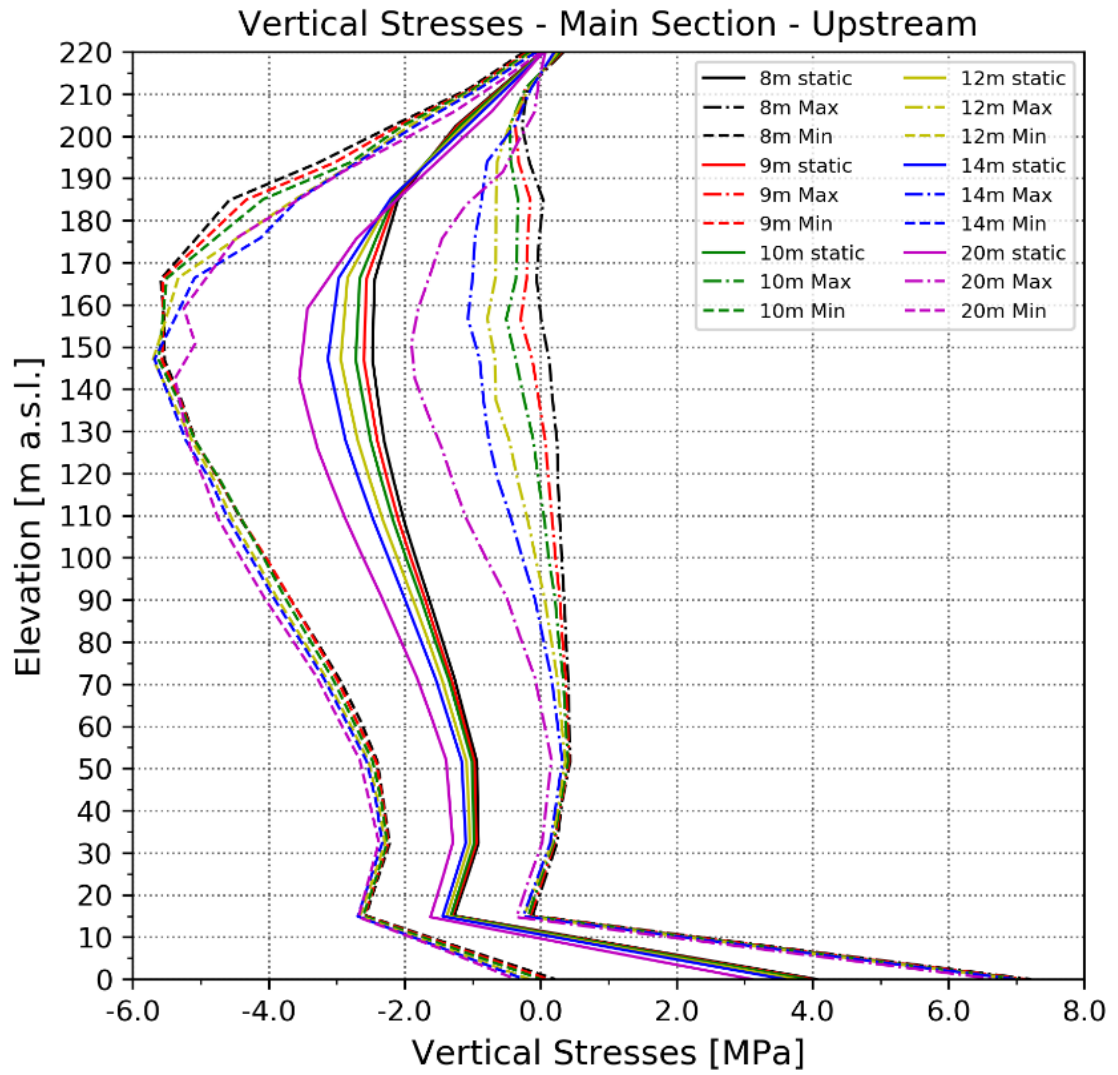
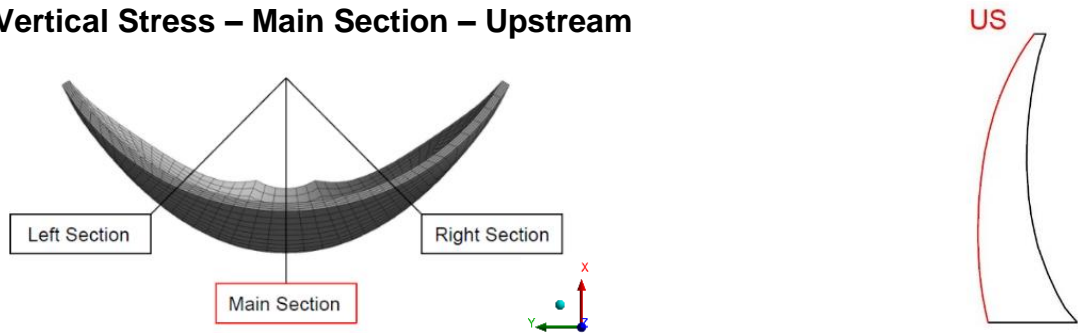


Figure 53: Vertical stresses of the six dams in the main section along the upstream side

Vertical Stress – Main Section – Downstream

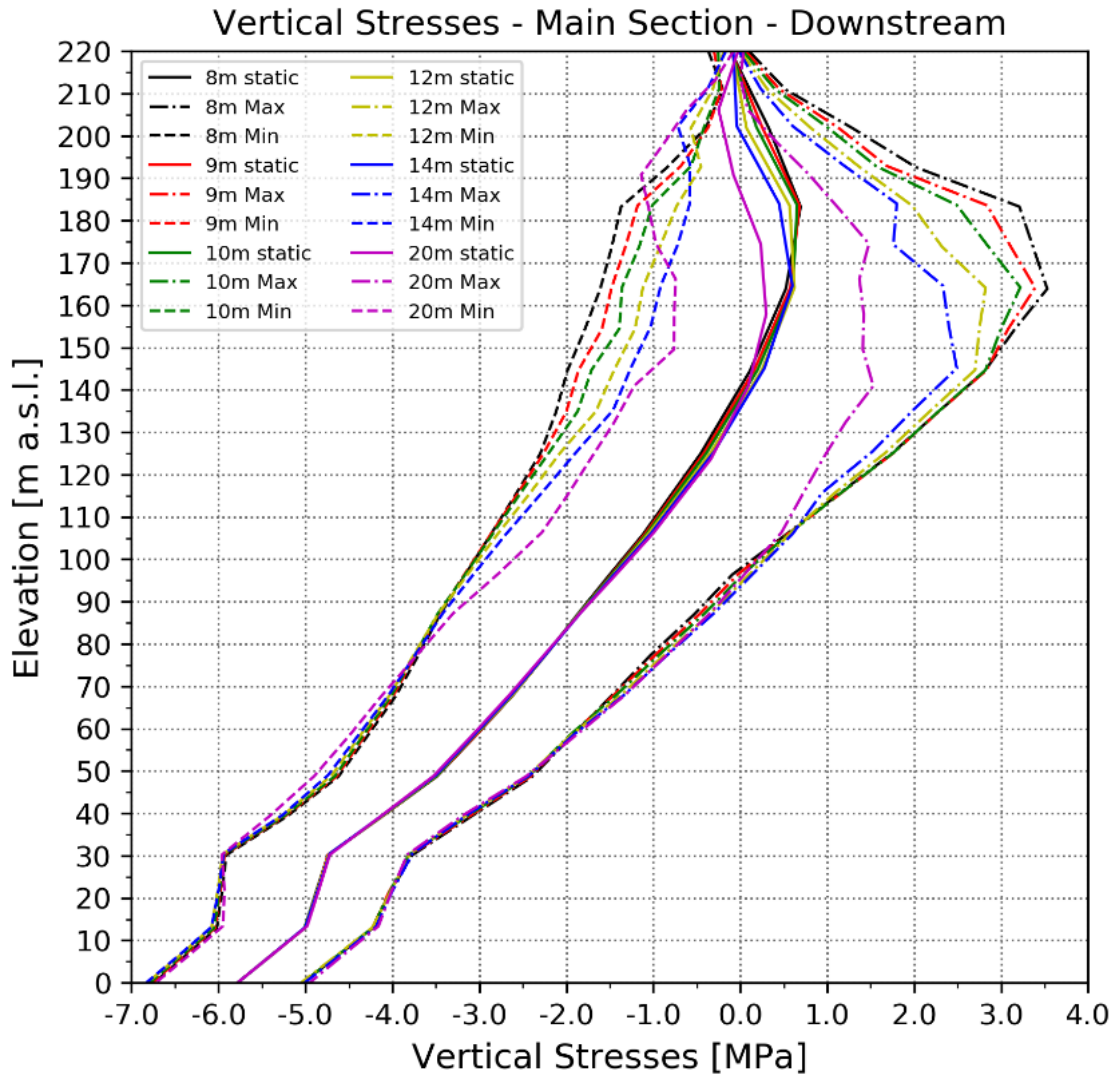
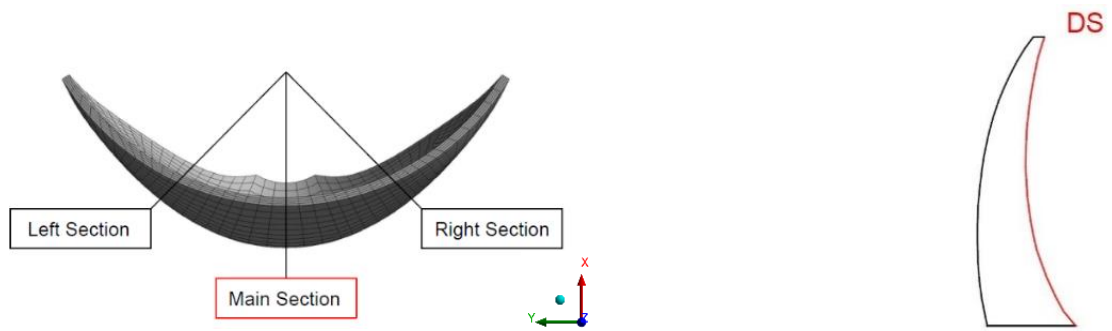


Figure 54: Vertical stresses of the six dams in the main section along the downstream side

Vertical Stresses – Left Section – Upstream

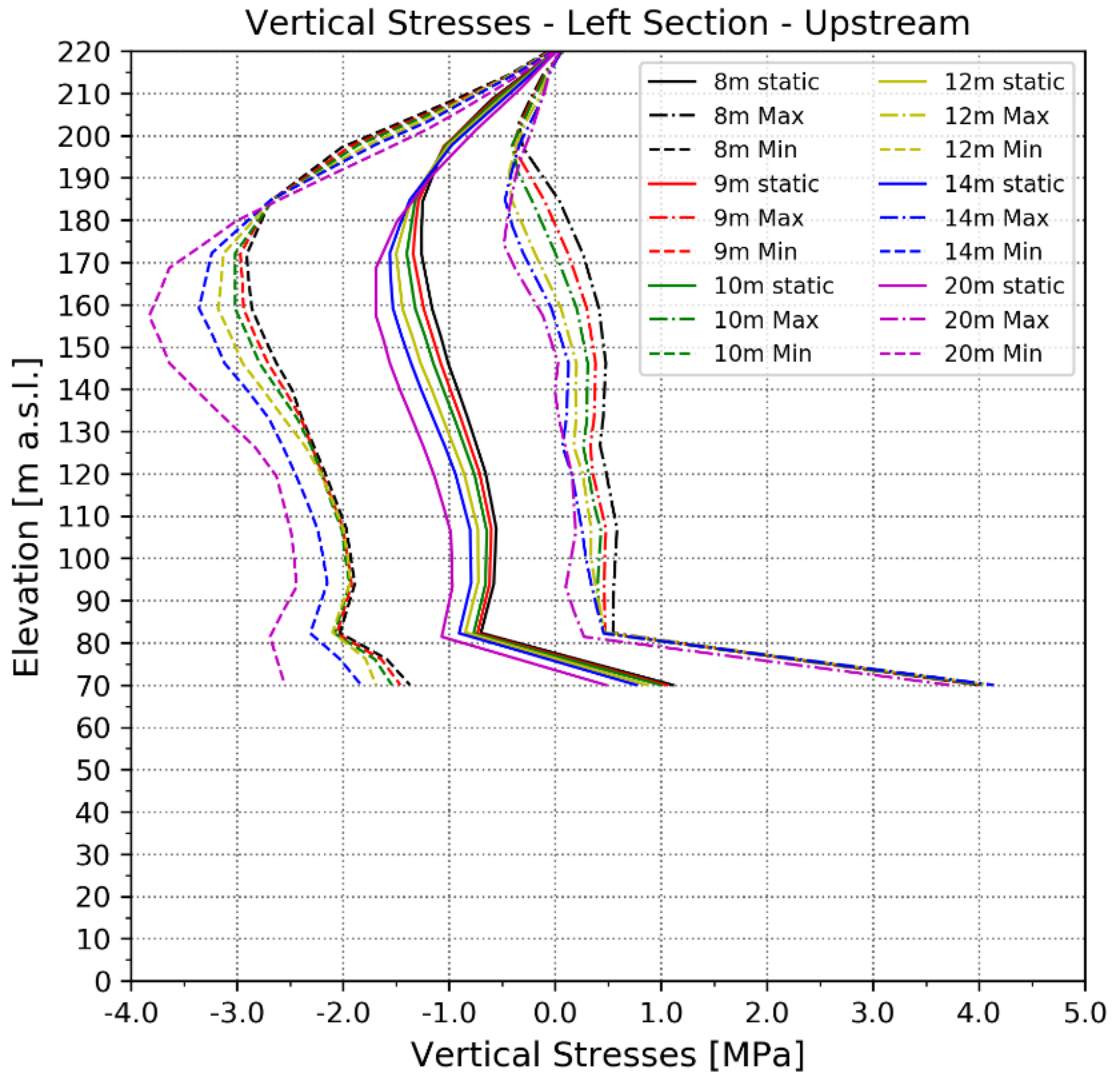
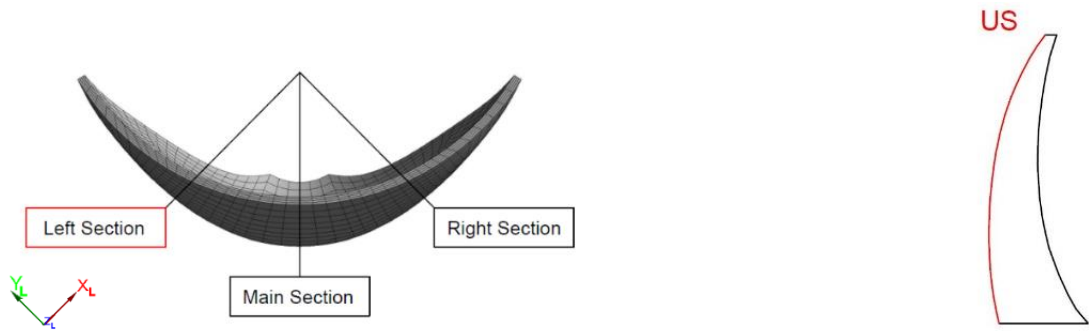


Figure 55: Vertical stresses of the six dams in the left section along the upstream side

Vertical Stresses – Left Section – Downstream

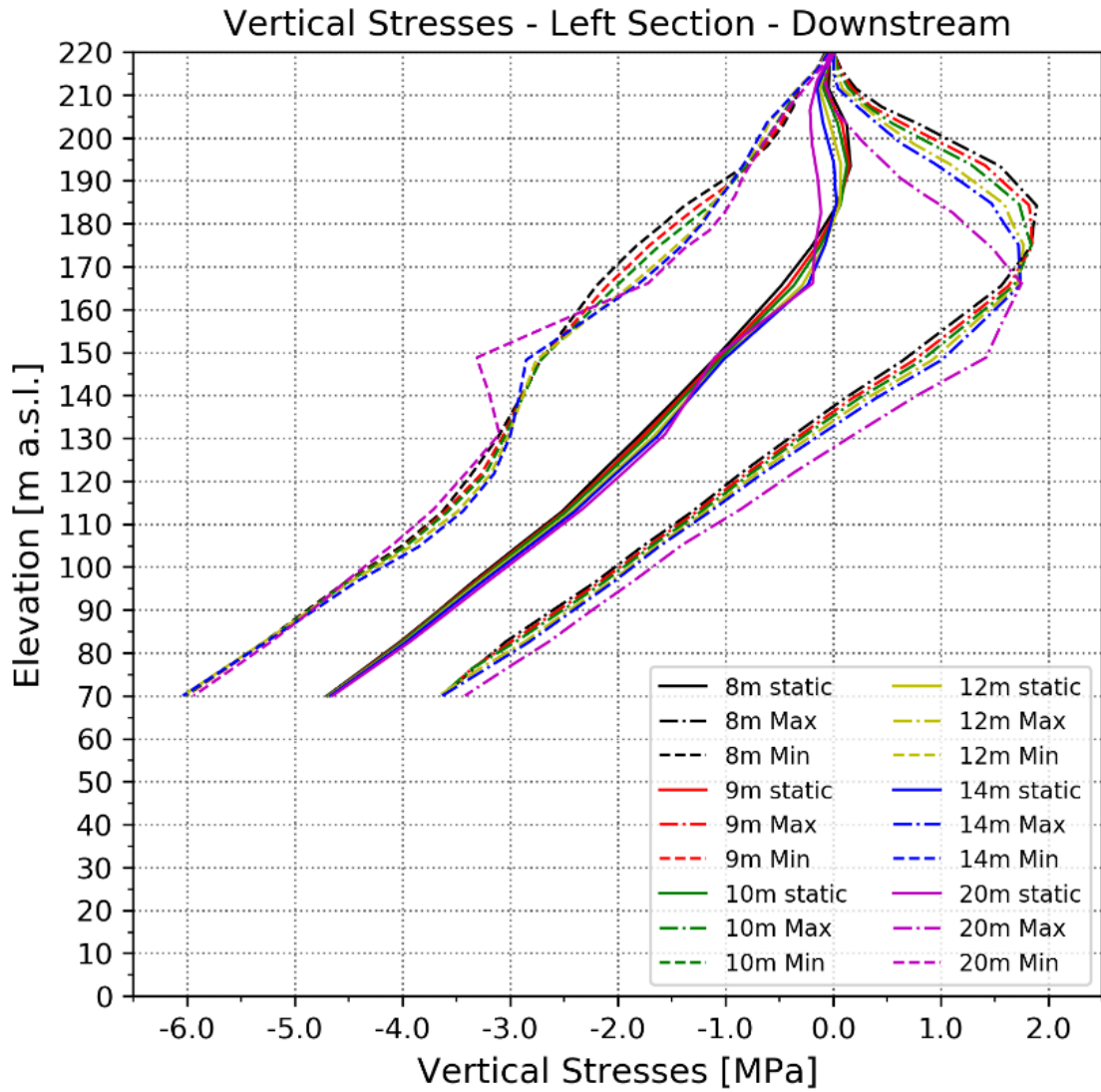
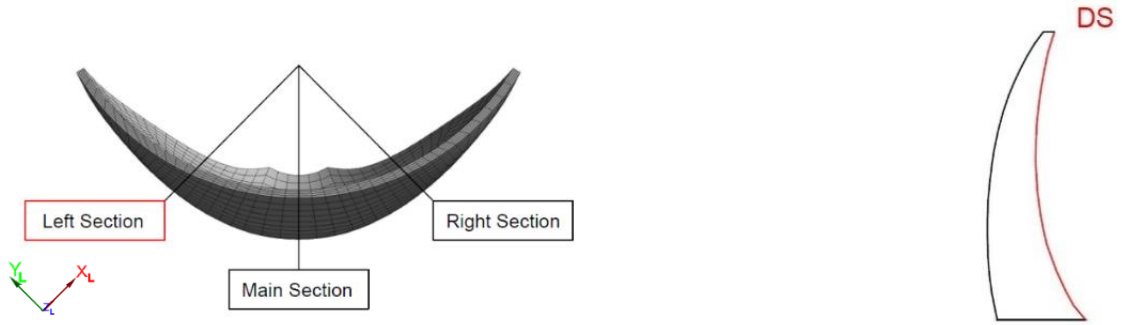


Figure 56: Vertical stresses of the six dams in the left section along the downstream side

Vertical Stresses – Right Section – Upstream

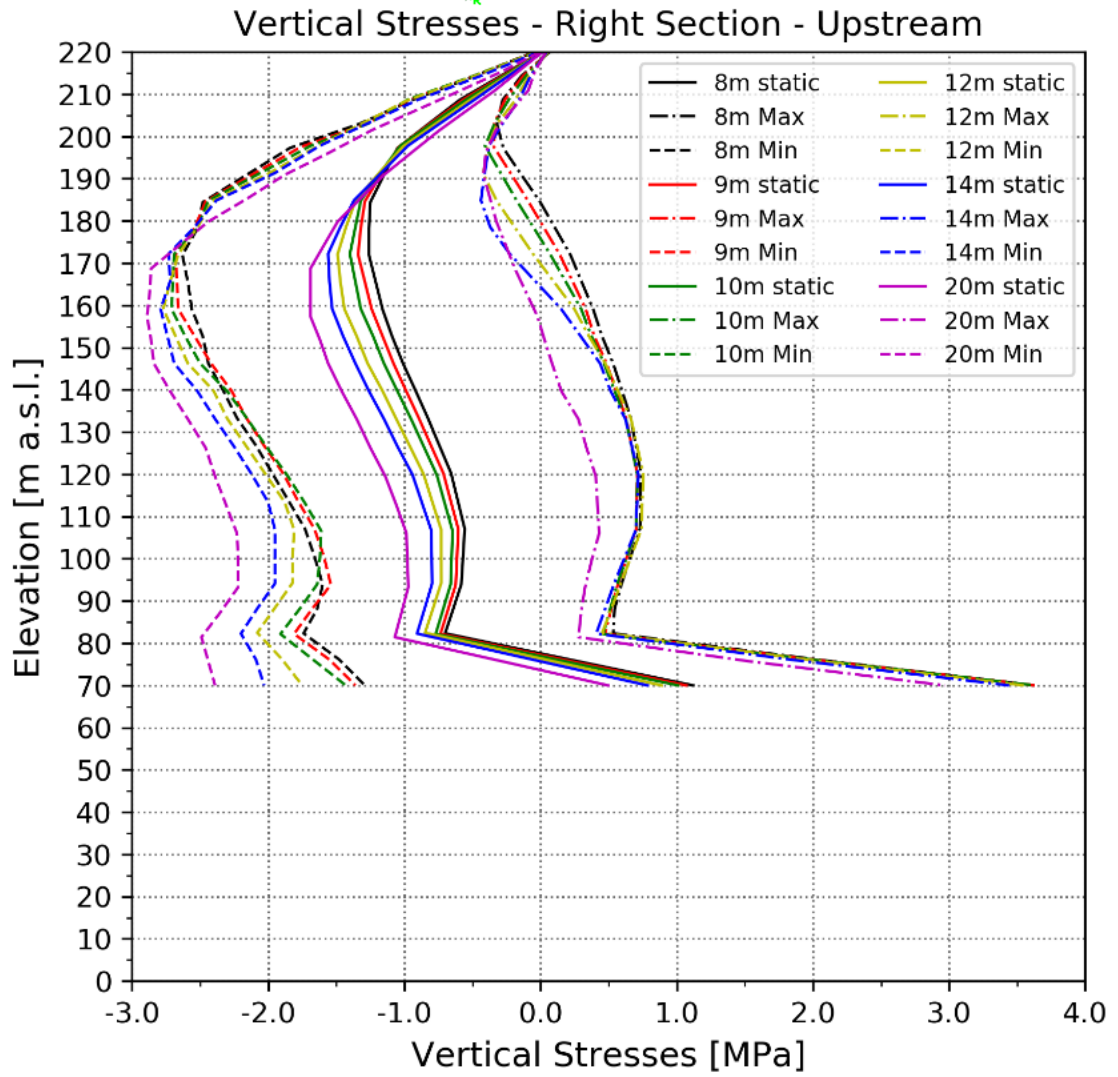
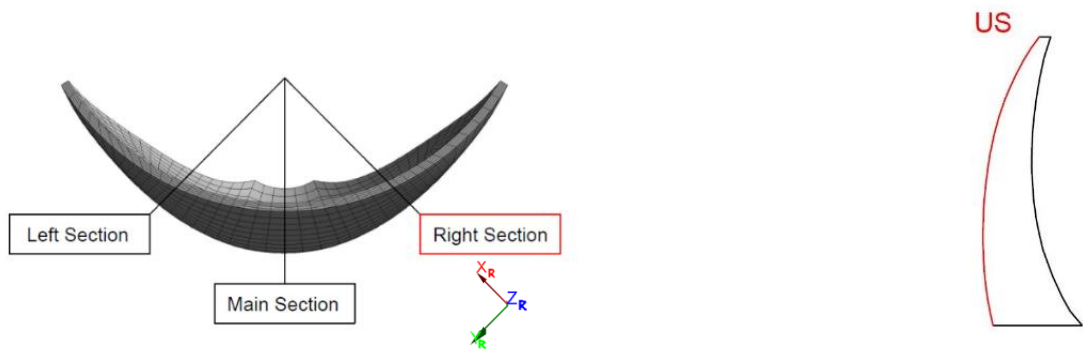


Figure 57: Vertical stresses of the six dams in the right section along the upstream side

Vertical Stresses – Right Section – Downstream

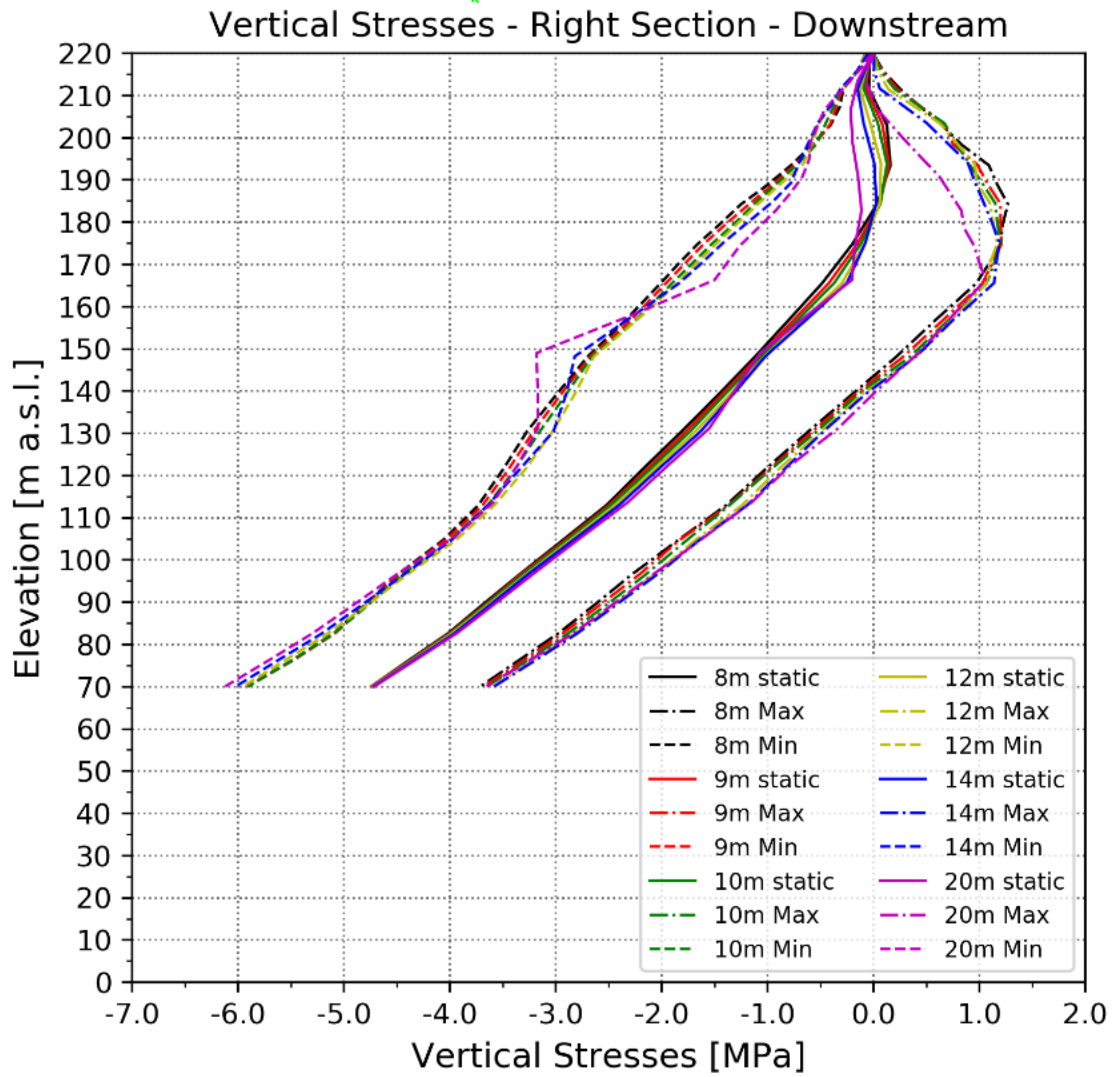
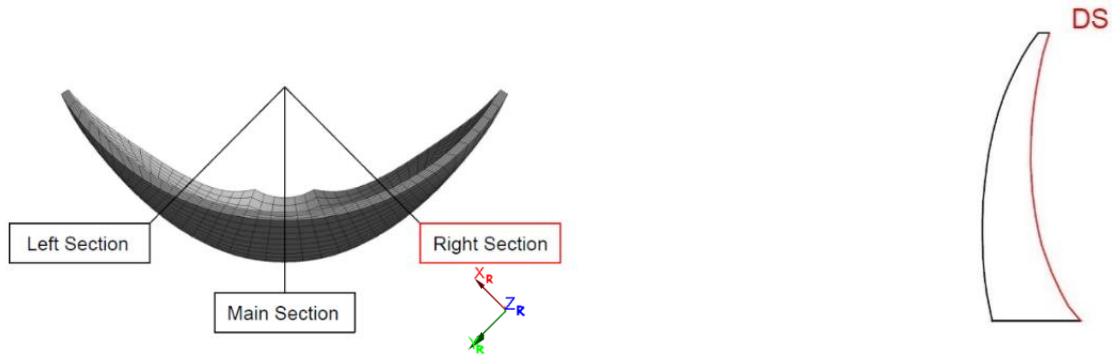


Figure 58: Vertical stresses of the six dams in the right section along the downstream side

Vertical Stress - Main Section - US					
160 m	Static load	dynamic load			
Crest thickness	Vertical Stress [MPa]	min. Vertical Stress [MPa]	Difference from static load in %	max. Vertical Stress [MPa]	Difference from static load in %
8 m	-2.45	-5.55	100.0	0.00	100.0
9 m	-2.57	-5.55	96.1	-0.29	93.1
10 m	-2.68	-5.53	91.9	-0.50	89.0
12 m	-2.87	-5.40	81.6	-0.75	86.5
14 m	-3.00	-5.30	74.2	-1.00	81.6
20 m	-3.43	-5.25	58.7	-1.80	66.5

Table 22: Vertical stresses at the main section – upstream

Vertical Stress - Main Section - DS					
170 m	Static load	dynamic load			
Crest thickness	Vertical Stress [MPa]	min. Vertical Stress [MPa]	Difference from static load in %	max. Vertical Stress [MPa]	Difference from static load in %
8 m	0.58	-1.55	100.0	3.40	100.0
9 m	0.60	-1.40	93.9	3.20	92.2
10 m	0.62	-1.30	90.1	3.00	84.4
12 m	0.60	-1.00	75.1	2.70	74.5
14 m	0.58	-0.90	69.5	2.00	50.4
20 m	0.25	-0.75	46.9	1.40	40.8

Table 23: Vertical stresses at the main section – downstream

Vertical Stress - Left Section - US					
160 m	Static load	dynamic load			
Crest thickness	Vertical Stress [MPa]	min. Vertical Stress [MPa]	Difference from static load in %	max. Vertical Stress [MPa]	Difference from static load in %
8 m	-1.16	-2.86	100.0	0.42	100.0
9 m	-1.24	-2.94	100.0	0.30	97.5
10 m	-1.32	-3.04	101.2	0.20	96.2
12 m	-1.44	-3.18	102.4	0.06	94.9
14 m	-1.53	-3.36	107.6	-0.04	94.3
20 m	-1.69	-3.83	125.9	-0.12	99.4

Table 24: Vertical stresses at the left section - upstream

Vertical Stress - Left Section - DS					
180 m	Static load	dynamic load			
Crest thickness	Vertical Stress [MPa]	min. Vertical Stress [MPa]	Difference from static load in %	max. Vertical Stress [MPa]	Difference from static load in %
8 m	-0.08	-1.60	100.0	1.86	100.0
9 m	-0.04	-1.48	94.7	1.84	96.9
10 m	-0.02	-1.37	88.8	1.78	92.8
12 m	-0.01	-1.24	80.9	1.67	86.6
14 m	-0.02	-1.22	78.9	1.59	83.0
20 m	-0.14	-1.15	66.4	1.29	73.7

Table 25: Vertical stresses at the left section – downstream

Vertical Stress - Right Section - US					
160 m	Static load	dynamic load			
Crest thickness	Vertical Stress [MPa]	min. Vertical Stress [MPa]	Difference from static load in %	max. Vertical Stress [MPa]	Difference from static load in %
8 m	-1.16	-2.56	100.0	0.39	100.0
9 m	-1.24	-2.66	101.4	0.33	101.3
10 m	-1.32	-2.71	99.3	0.30	104.5
12 m	-1.44	-2.77	95.0	0.25	109.0
14 m	-1.53	-2.79	90.0	-0.15	89.0
20 m	-1.69	-2.88	85.0	-0.02	107.7

Table 26: Vertical stresses at the right section – upstream

Vertical Stress - Right Section - DS					
180 m	Static load	dynamic load			
Crest thickness	Vertical Stress [MPa]	min. Vertical Stress [MPa]	Difference from static load in %	max. Vertical Stress [MPa]	Difference from static load in %
8 m	-0.08	-1.45	100.0	1.22	100.0
9 m	-0.04	-1.39	98.5	1.20	95.4
10 m	-0.02	-1.31	94.2	1.17	91.5
12 m	-0.01	-1.28	92.7	1.13	87.7
14 m	-0.02	-1.19	85.4	1.12	87.7
20 m	-0.14	-1.09	69.3	0.86	76.9

Table 27: Vertical stresses at the right section - downstream

Vertical Stresses - Downstream

In Figure 54 can be seen that the tensile stresses along the downstream face decrease. The tendency of the reduction of the tensile stresses is significant. Table 23 shows that there is a difference of 2 MPa between the arch dam with a crest thickness of 8 m and the arch dam with a crest thickness of 20 m. This means that likelihood of crack development in the horizontal concrete joints is reduced drastically when the volume of the arch dam increases.

The results of the vertical stresses on the downstream face are for the right and the left side very similar. A kink can be seen at the dam elevation of 150 m for both sides. This is due to the width of the geometry, which increases at this point.

Vertical Stresses - Upstream

Same as for the vertical stresses along the downstream face, it can be seen that the compressive stresses in the main section increase with an increasing dam crest. The results in the main section show a small kink at the dam elevation of 150 m, where the thickness of the geometry increases.

The results of the static and dynamic load for the left and the right side are also similar to each other.

Minimum Principal Stresses – Main Section – Upstream

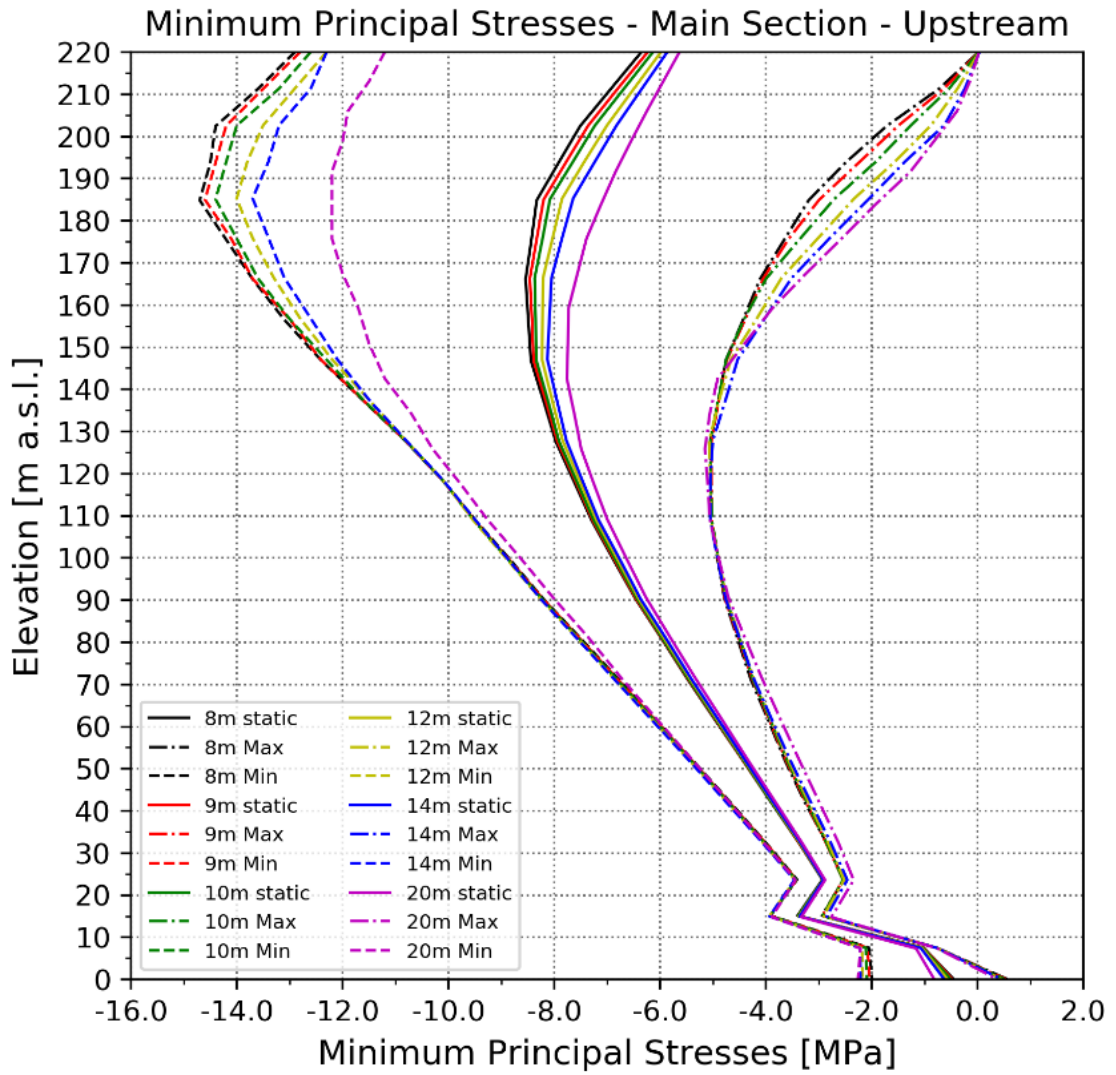
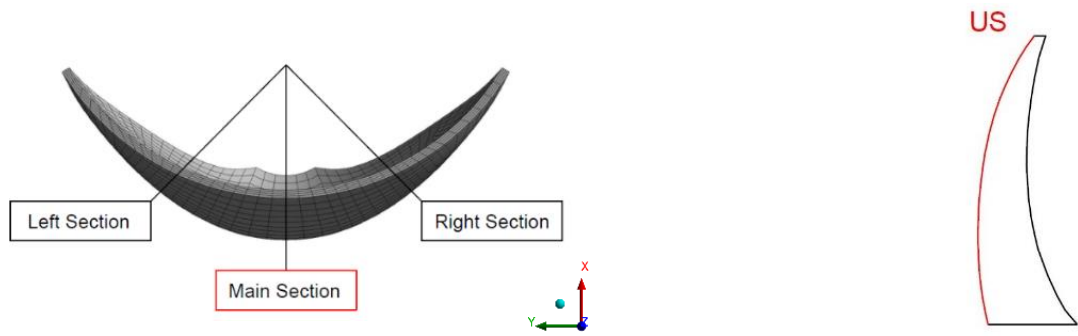


Figure 59: Minimum principal stresses of the six dams in the main section along the upstream side

Minimum Principal Stresses – Main Section – Downstream

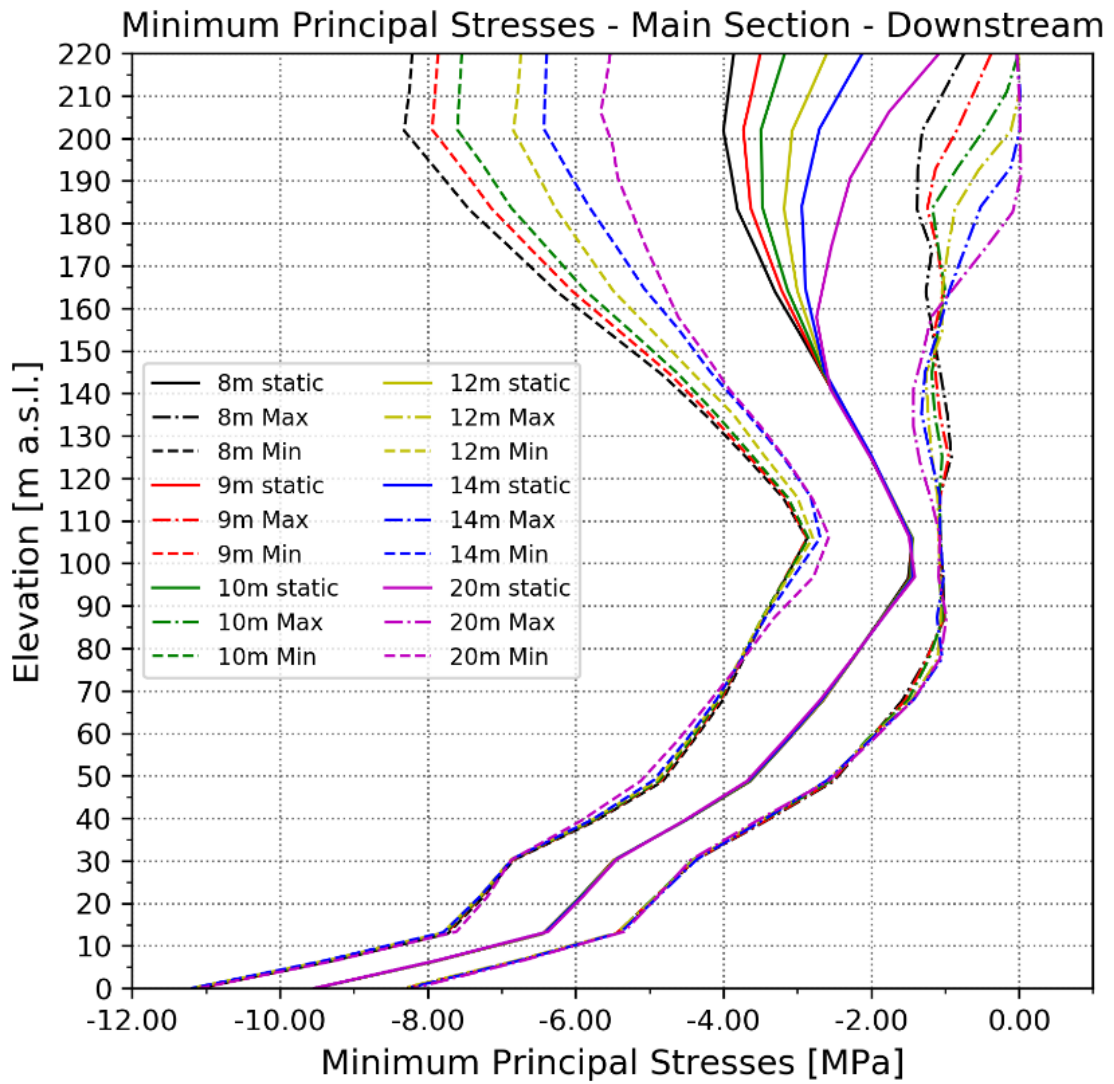
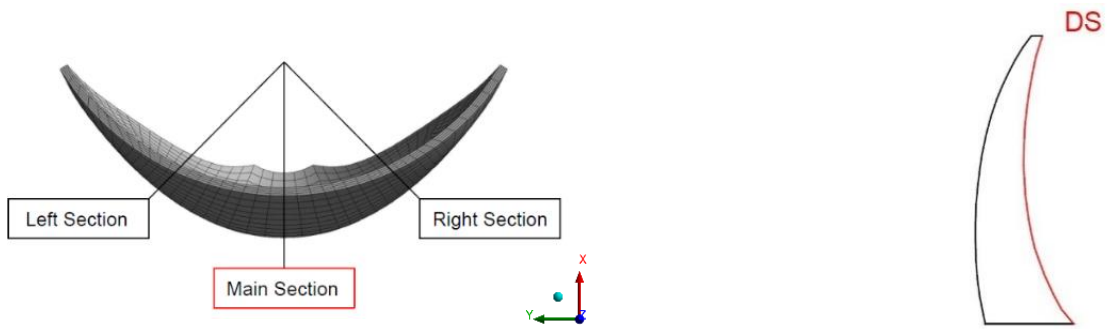


Figure 60: Minimum principal stresses of the six dams in the main section along the downstream side

Minimum Principal Stresses – Left Section – Upstream

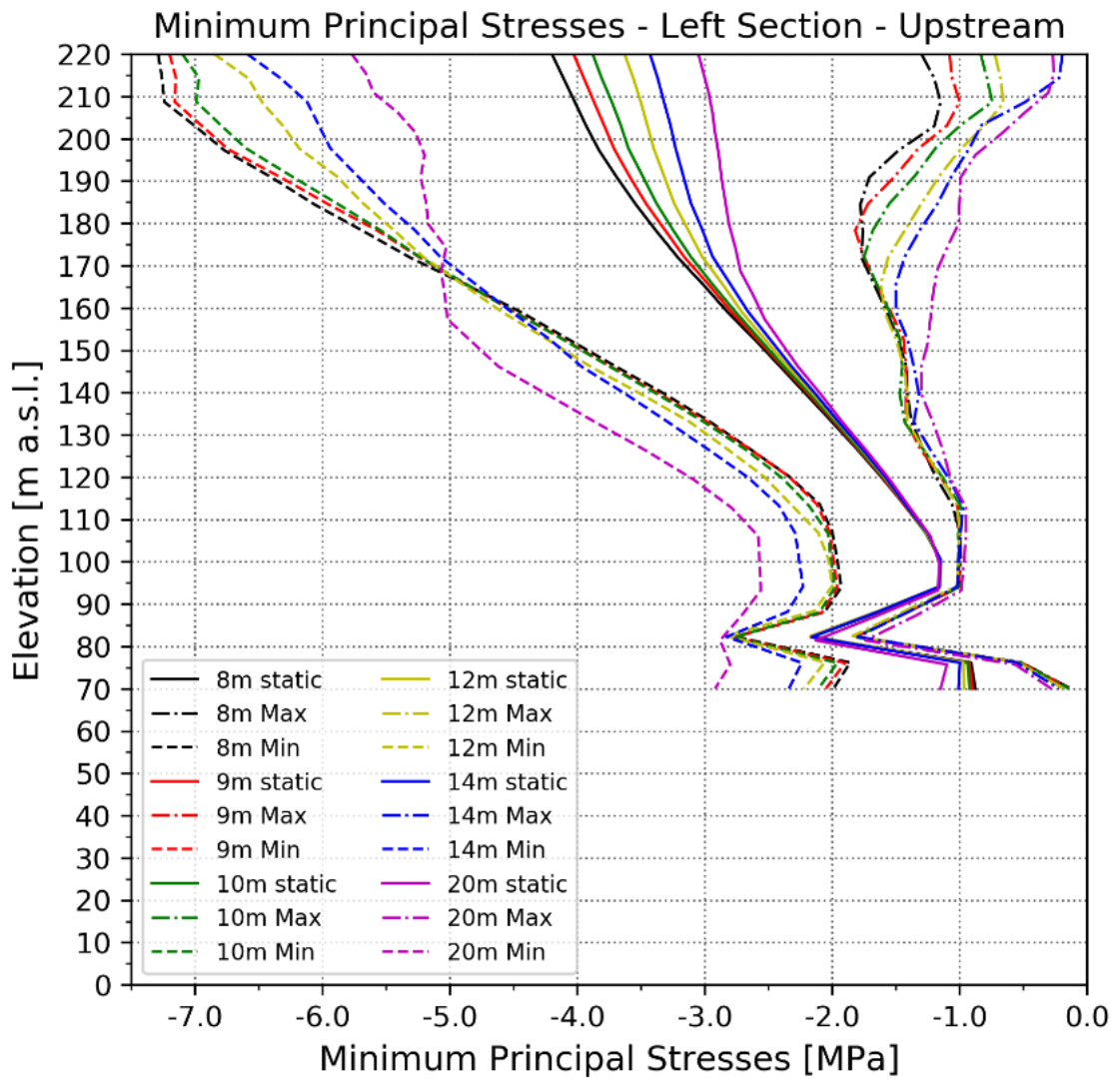
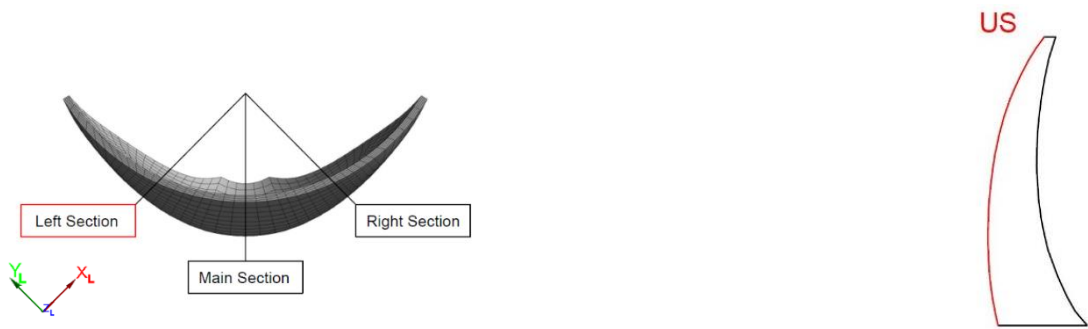


Figure 61: Minimum principal stresses of the six dams in the left section along the upstream side

Minimum Principal Stresses – Left Section – Downstream

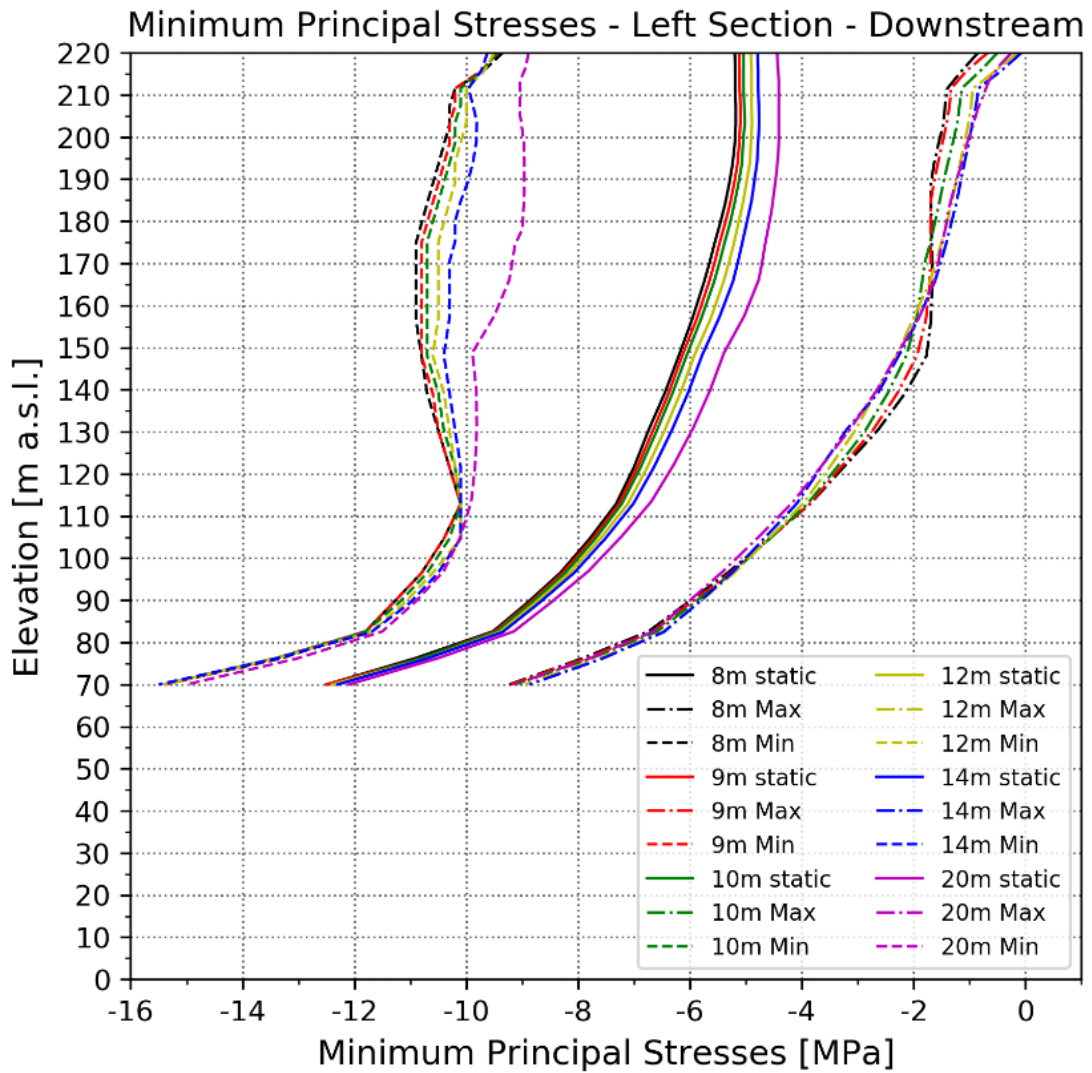
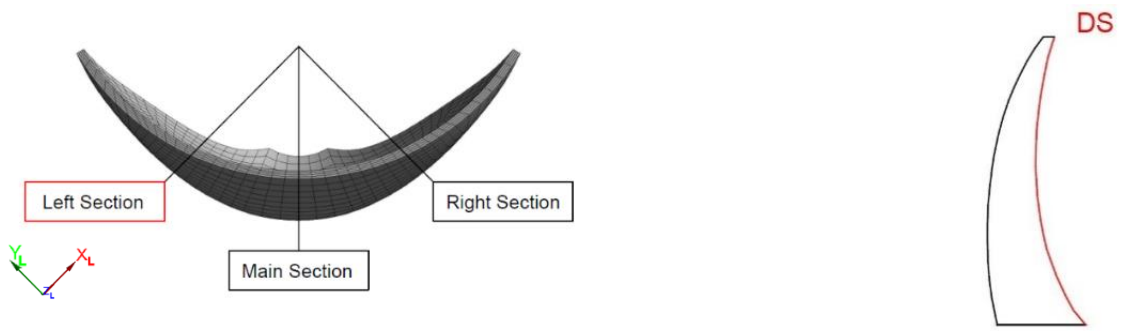


Figure 62: Minimum principal stresses of the six dams in the left section along the downstream side

Minimum Principal Stresses – Right Section – Upstream

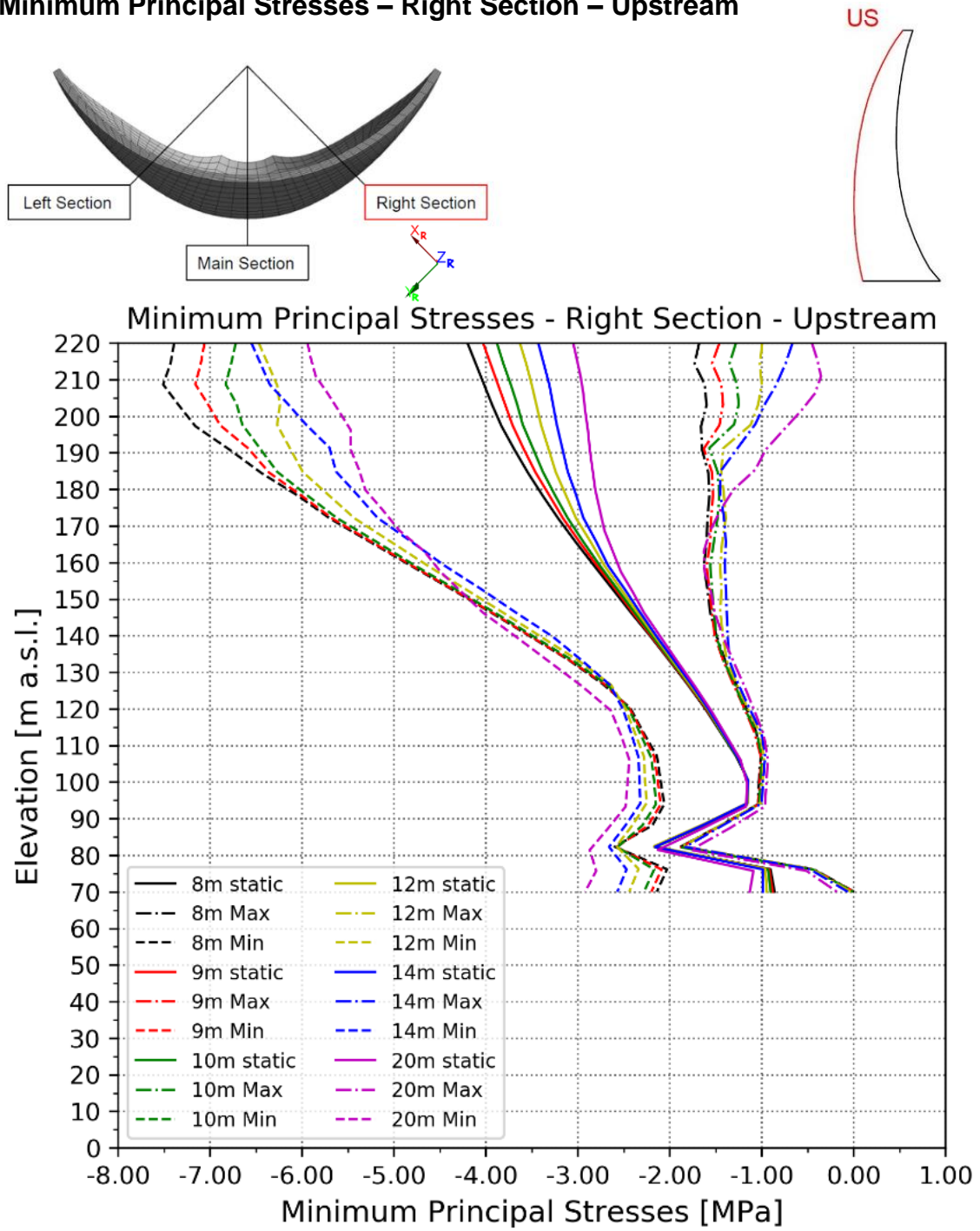


Figure 63: Minimum principal stresses of the six dams in the right section along the upstream side

Minimum Principal Stresses – Right Section – Downstream

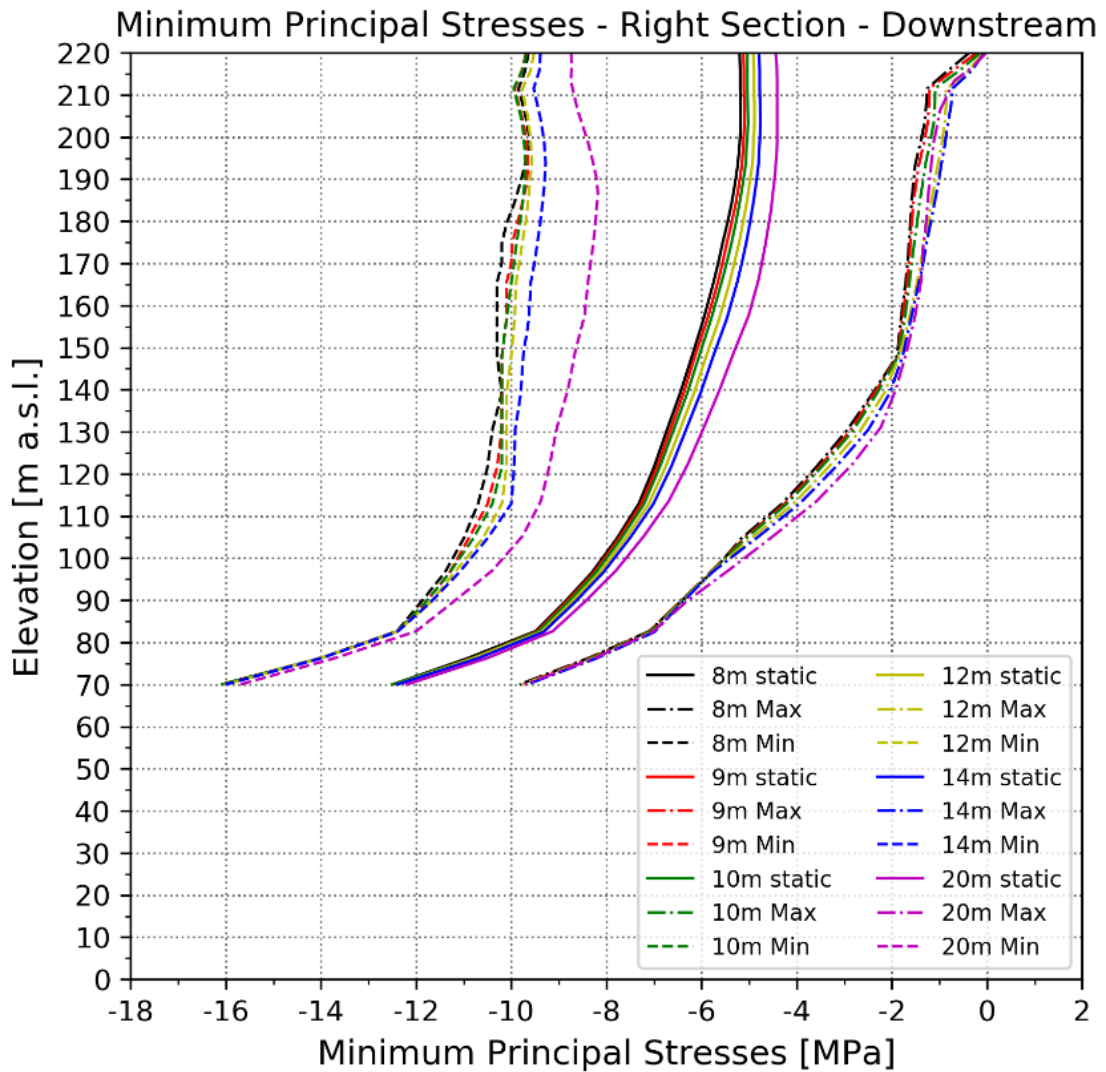
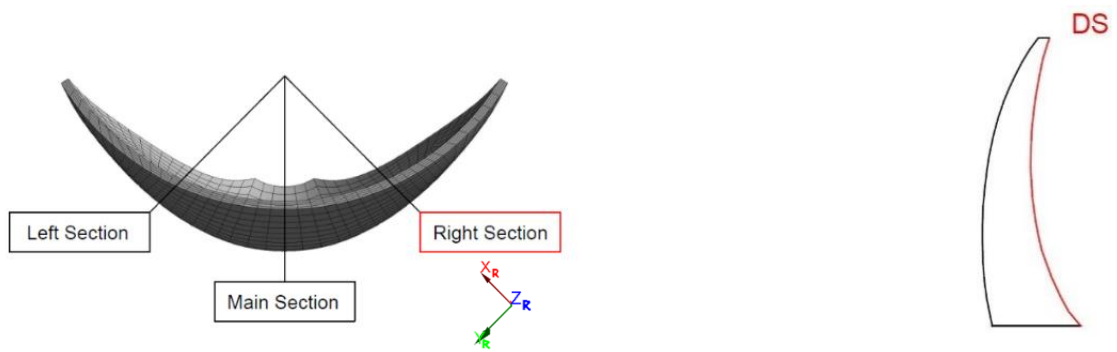


Figure 64: Minimum principal stresses of the six dams in the right section along the downstream side

Minimum Principal Stress - Main Section - US					
180 m	Static load	dynamic load			
Crest thickness	Minimum Principal Stress [MPa]	min. Minimum Principal Stress [MPa]	Difference from static load in %	max. Minimum Principal Stress [MPa]	Difference from static load in %
8 m	-8.40	-14.50	100.0	-3.50	100.0
9 m	-8.20	-14.40	101.6	-3.40	98.0
10 m	-8.10	-14.30	101.6	-3.20	100.0
12 m	-8.00	-13.90	96.7	-2.90	104.1
14 m	-7.80	-13.50	93.4	-2.70	104.1
20 m	-7.30	-12.20	80.3	-2.50	98.0

Table 28: Minimum principal stresses at the main section – upstream

Minimum Principal Stress - Main Section - DS					
220 m	Static load	dynamic load			
Crest thickness	Minimum Principal Stress [MPa]	min. Minimum Principal Stress [MPa]	Difference from static load in %	max. Minimum Principal Stress [MPa]	Difference from static load in %
8 m	-3.86	-8.21	100.0	-0.74	100.0
9 m	-3.50	-7.86	100.2	-0.38	100.0
10 m	-3.17	-7.54	100.5	-0.07	99.4
12 m	-2.60	-6.74	95.2	-0.01	83.0
14 m	-2.12	-6.39	98.2	-0.03	67.0
20 m	-1.08	-5.53	102.3	-0.03	33.7

Table 29: Minimum principal stresses at the main section – downstream

Minimum Principal Stress - Left Section - US					
220 m	Static load	dynamic load			
Crest thickness	Minimum Principal Stress [MPa]	min. Minimum Principal Stress [MPa]	Difference from static load in %	max. Minimum Principal Stress [MPa]	Difference from static load in %
8 m	-4.20	-7.29	100.0	-1.30	100.0
9 m	-4.03	-7.20	102.6	-1.08	101.7
10 m	-3.88	-7.10	104.2	-0.84	104.8
12 m	-3.63	-6.85	104.2	-0.72	100.3
14 m	-3.43	-6.59	102.3	-0.19	111.7
20 m	-3.05	-5.77	88.0	-0.27	95.9

Table 30: Minimum principal stresses at the left section - upstream

Minimum Principal Stress - Left Section - DS					
180 m	Static load	dynamic load			
Crest thickness	Minimum Principal Stress [MPa]	min. Minimum Principal Stress [MPa]	Difference from static load in %	max. Minimum Principal Stress [MPa]	Difference from static load in %
8 m	-5.46	-10.80	100.0	-1.68	100.0
9 m	-5.37	-10.70	99.8	-1.70	97.1
10 m	-5.28	-10.60	99.6	-1.62	96.8
12 m	-5.13	-10.40	98.7	-1.40	98.7
14 m	-4.98	-10.20	97.8	-1.32	96.8
20 m	-4.60	-9.00	82.4	-1.40	84.7

Table 31: Minimum principal stresses at the left section – downstream

Minimum Principal Stress - Right Section - US					
220 m	Static load	dynamic load			
Crest thickness	Minimum Principal Stress [MPa]	min. Minimum Principal Stress [MPa]	Difference from static load in %	max. Minimum Principal Stress [MPa]	Difference from static load in %
8 m	-4.20	-7.39	100.0	-1.68	100.0
9 m	-4.03	-7.06	95.0	-1.46	102.0
10 m	-3.88	-6.72	89.0	-1.30	102.4
12 m	-3.63	-6.47	89.0	-1.28	93.3
14 m	-3.43	-6.55	97.8	-0.99	96.8
20 m	-3.05	-5.94	90.6	-0.66	94.8

Table 32: Minimum principal stresses at the right section – upstream

Minimum Principal Stress - Right Section - DS					
180 m	Static load	dynamic load			
Crest thickness	Minimum Principal Stress [MPa]	min. Minimum Principal Stress [MPa]	Difference from static load in %	max. Minimum Principal Stress [MPa]	Difference from static load in %
8 m	-5.70	-10.20	100.0	-1.67	100.0
9 m	-5.56	-10.00	98.7	-1.64	97.3
10 m	-5.50	-9.94	98.7	-1.58	97.3
12 m	-5.30	-9.83	100.7	-1.39	97.0
14 m	-5.15	-9.51	96.9	-1.34	94.5
20 m	-4.73	-8.33	80.0	-1.36	83.6

Table 33: Minimum principal stresses at the right section - downstream

Minimum Principal Stresses - Downstream

The minimum principal stresses are getting smaller when the dam is getting thicker. Figure 60 shows that the top half of the diagram is the same as the hoop stresses on the downstream side. Only the minimal Minimum Principal Stresses are cut at 0 MPa due to the dead weight. The dead weight is also the reason, why the loads change and get smaller at the elevation of 110 m.

The results of the left and the right section do not vary much from each other. Only the minimum dynamic load for the dam with a 20 m crest width has a kink on the left side at the dam elevation of 150 m.

Minimum Principal Stresses - Upstream

The resulting lines of the static load differ not much from each other, regarding the main section of the dam. The results of the dams due to the maxima of the time series vary not much from each other either. Only the results of the minimum dynamic load for the arch dam $d = 20$ m is with 12.2 MPa slightly smaller than the other loads.

The tensile stresses on the upstream side of the dam get bigger when the dam crest increases.

Maximum Principal Stresses – Main Section – Upstream

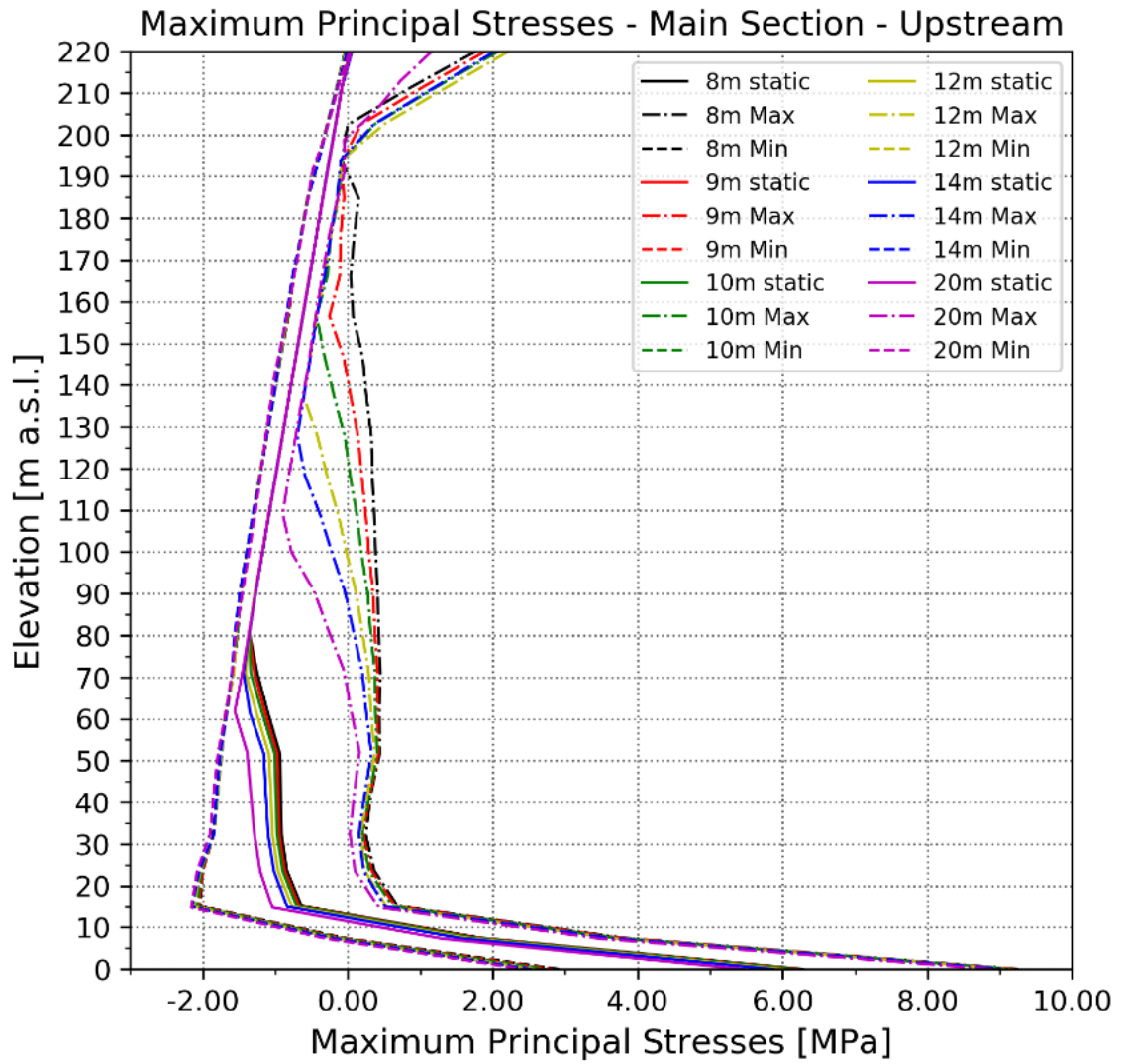
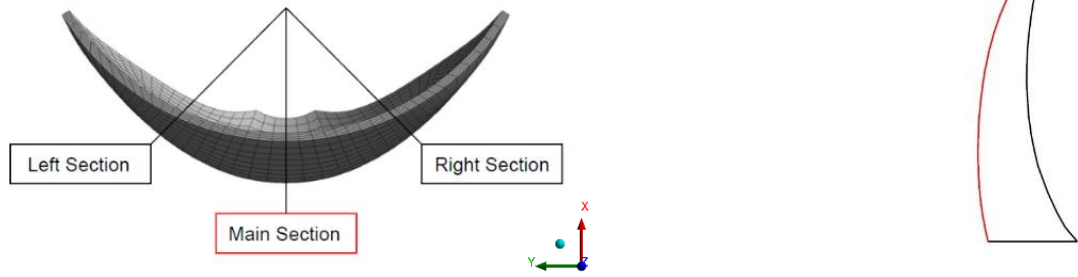


Figure 65: Maximum principal stresses of the six dams in the main section along the upstream side

Maximum Principal Stresses – Main Section – Downstream

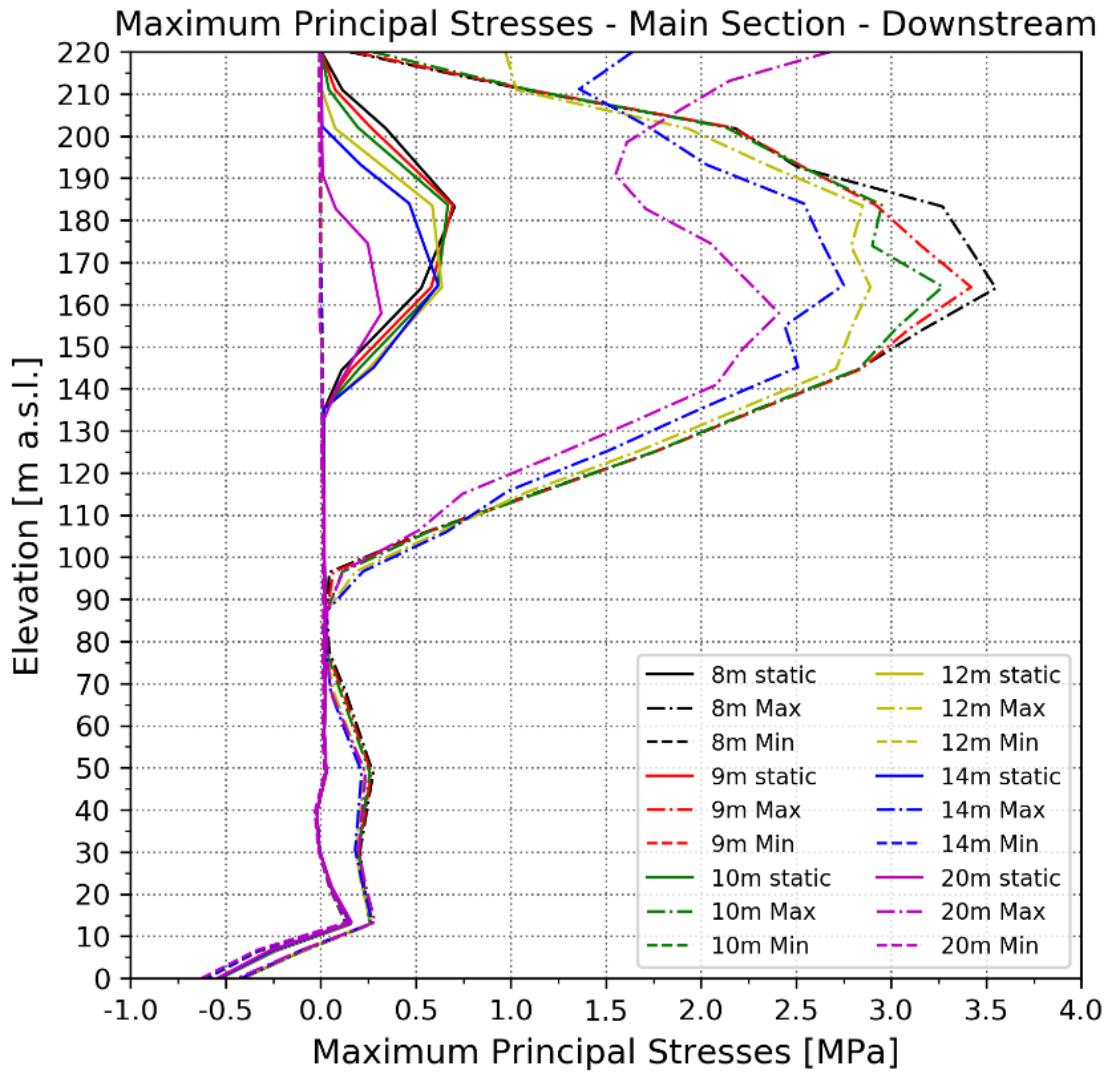
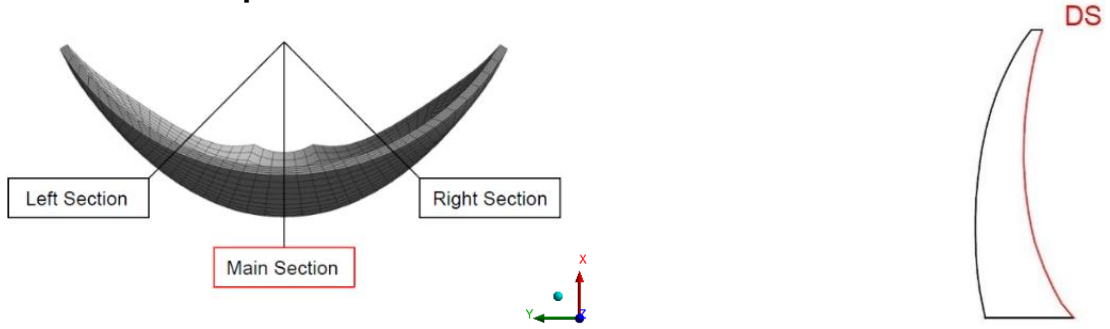


Figure 66: Maximum principal stresses of the six dams in the main section along the downstream side

Maximum Principal Stresses – Left Section – Upstream

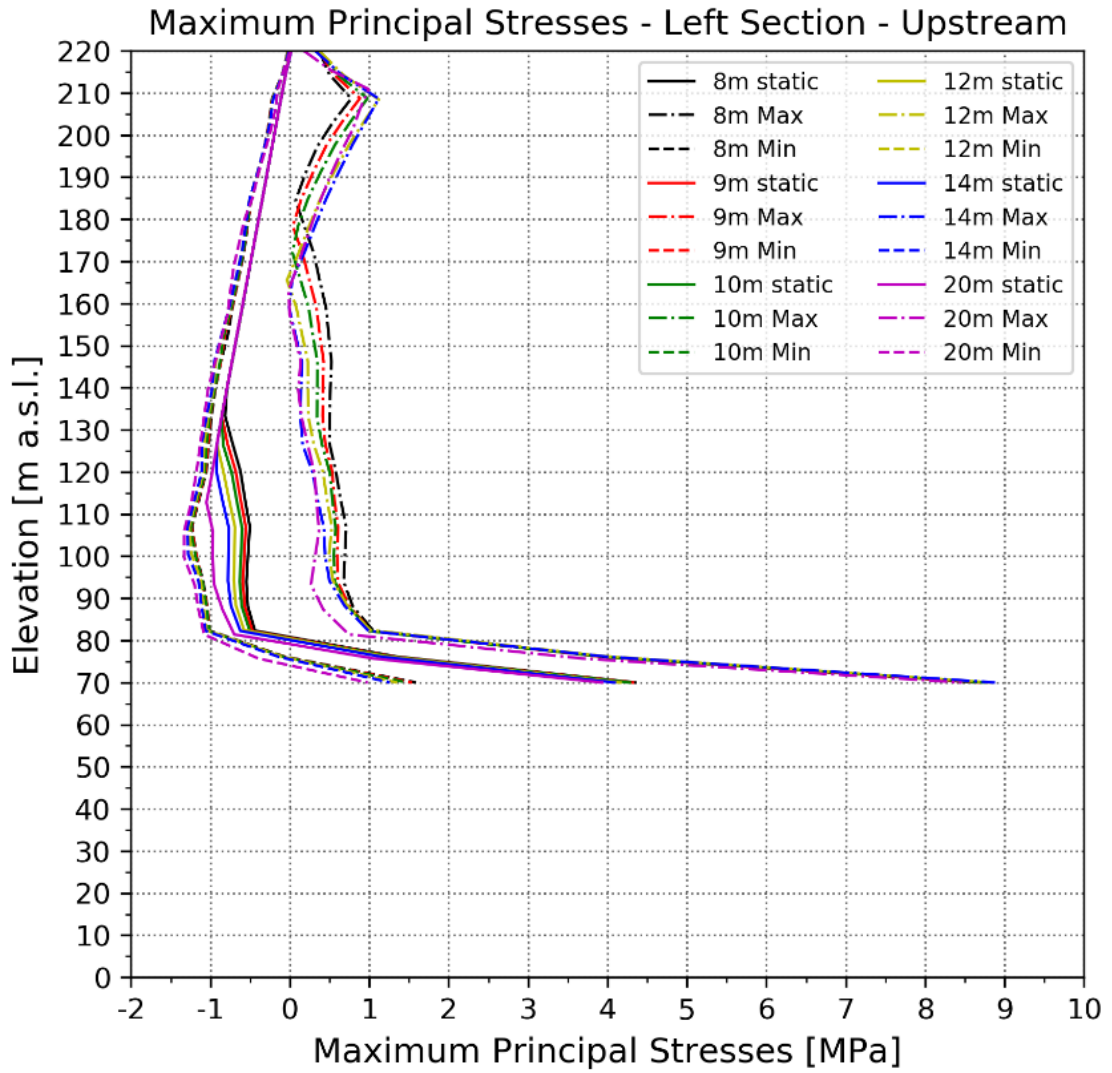
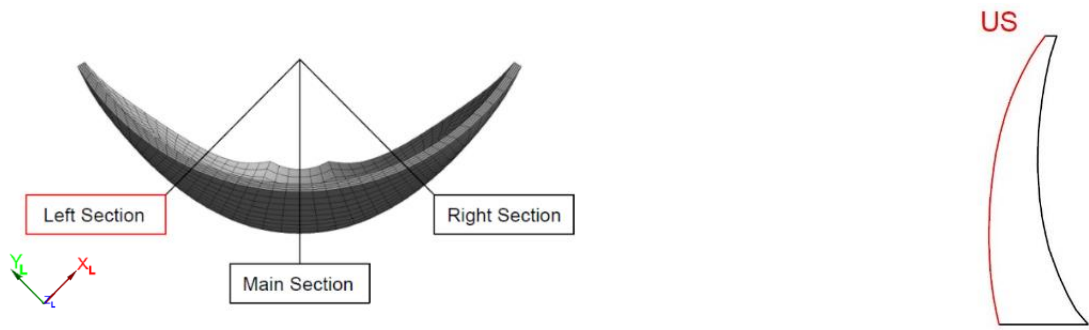


Figure 67: Maximum principal stresses of the six dams in the left section along the upstream side

Maximum Principal Stresses – Left Section – Downstream

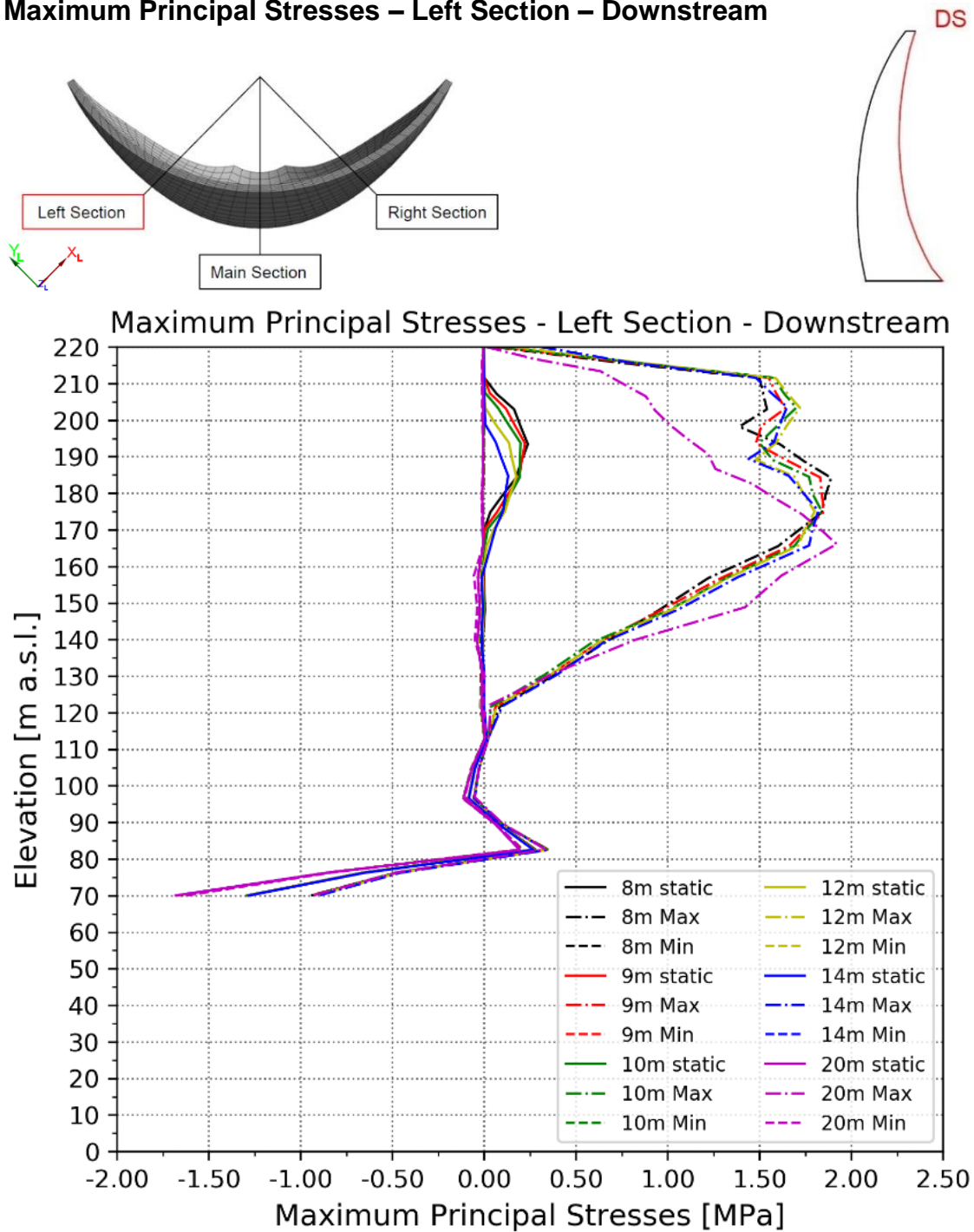


Figure 68: Maximum principal stresses of the six dams in the left section along the downstream side

Maximum Principal Stresses – Right Section – Upstream

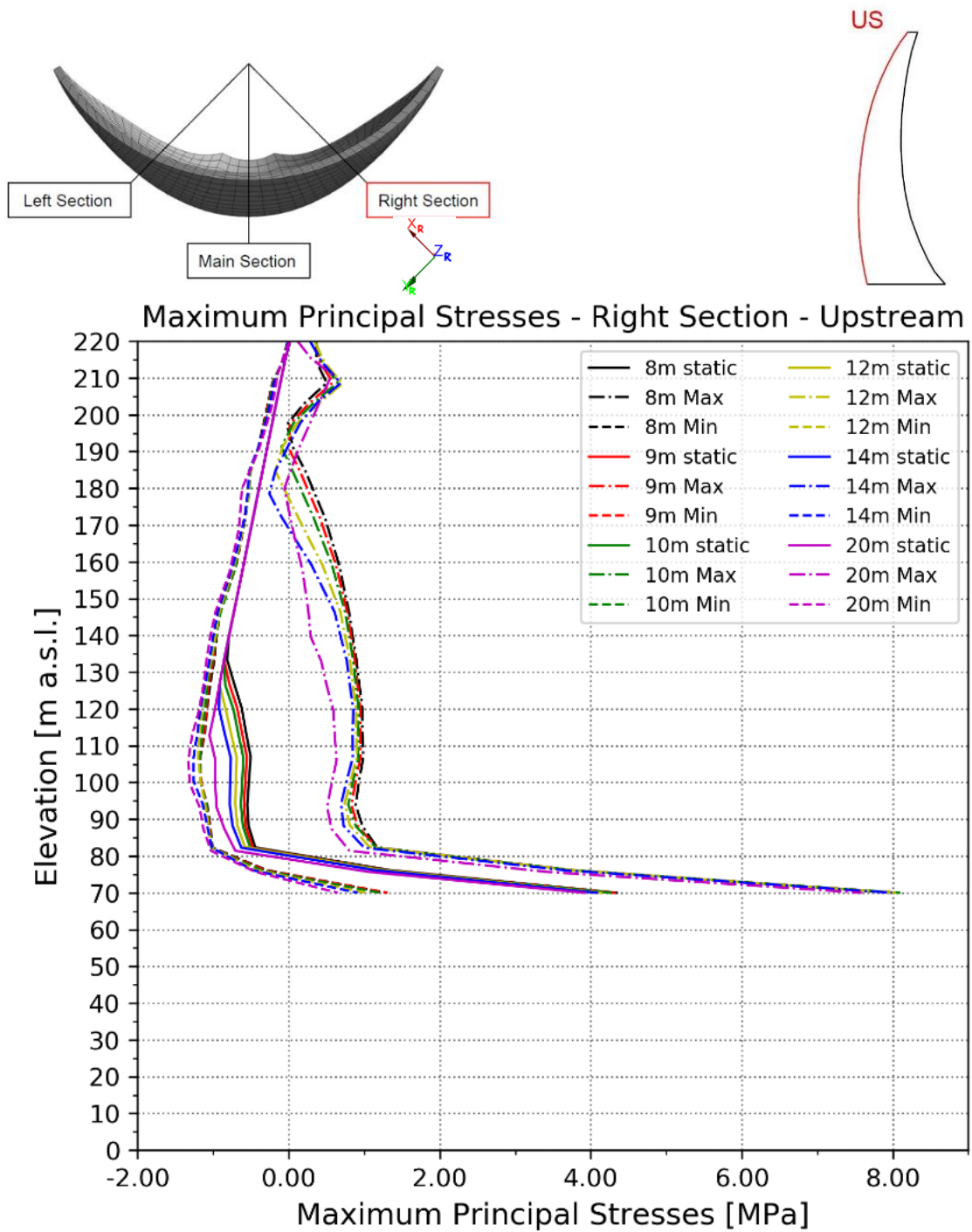


Figure 69: Maximum principal stresses of the six dams in the right section along the upstream side

Maximum Principal Stresses – Right Section – Downstream

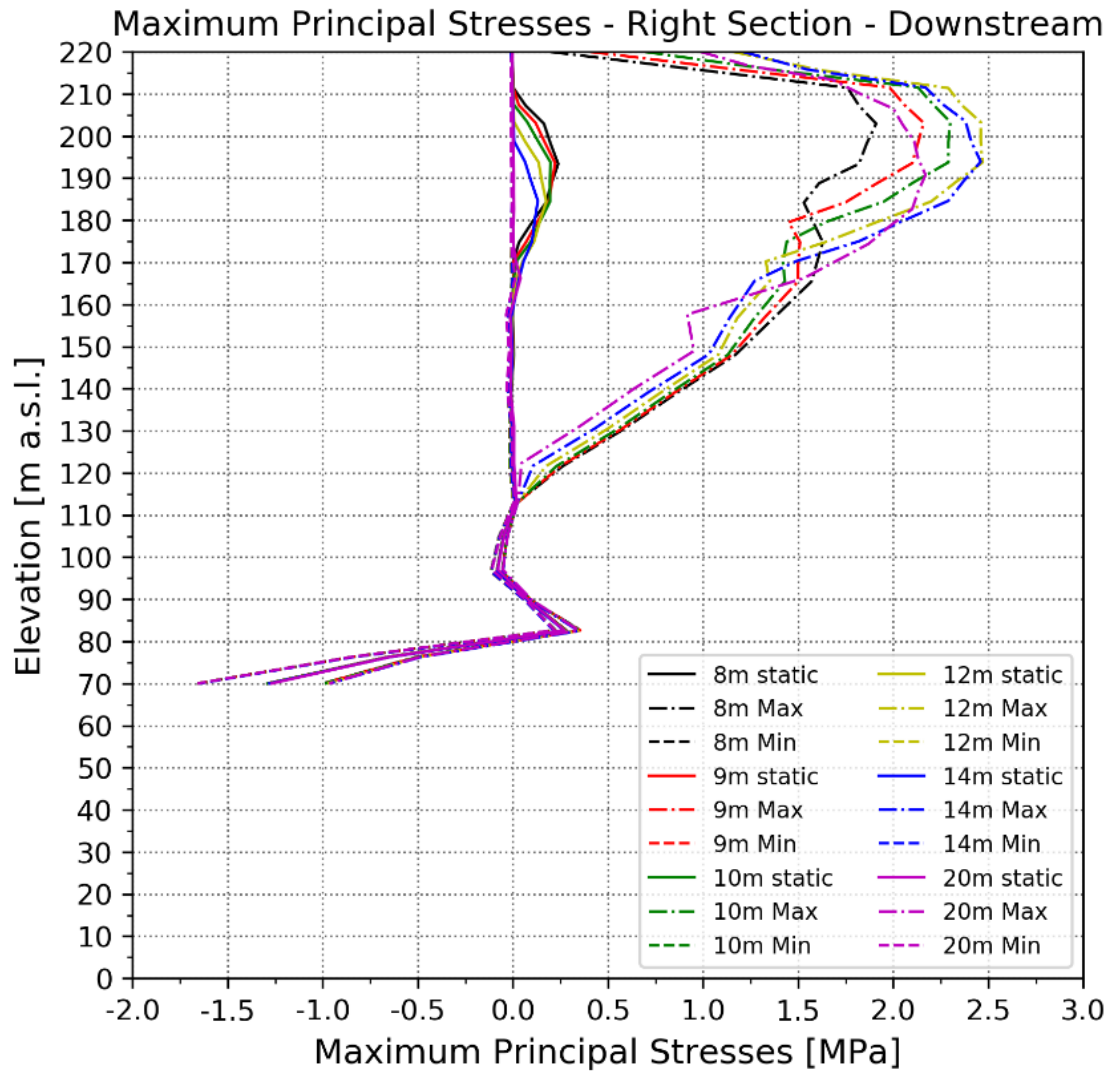
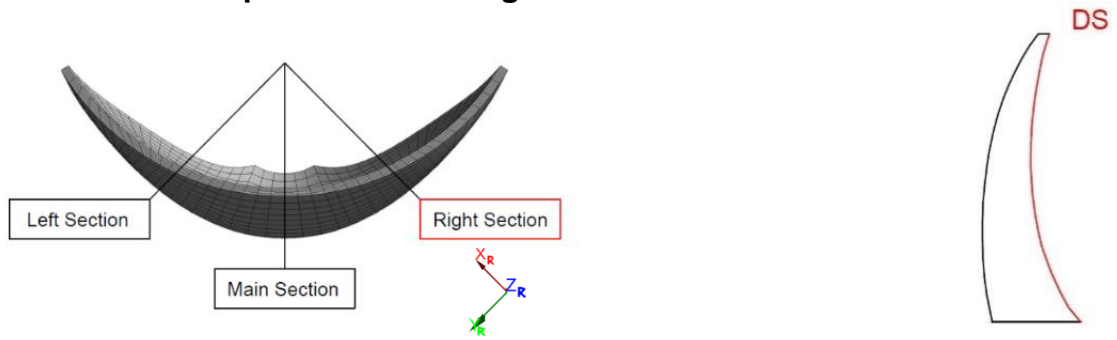


Figure 70: Maximum principal stresses of the six dams in the right section along the downstream side

Maximum Principal Stress - Main Section - US					
50 m	Static load	dynamic load			
Crest thickness	Maximum Principal Stress [MPa]	min. Maximum Principal Stress [MPa]	Difference from static load in %	max. Maximum Principal Stress [MPa]	Difference from static load in %
8 m	-0.94	-1.74	100.0	0.44	100.0
9 m	-0.97	-1.76	98.8	0.42	100.7
10 m	-1.01	-1.77	95.0	0.41	102.9
12 m	-1.09	-1.75	82.5	0.37	105.8
14 m	-1.16	-1.76	75.0	0.32	107.2
20 m	-1.35	-1.79	55.0	0.16	109.4

Table 34: Maximum principal stresses at the main section – upstream

Maximum Principal Stress - Main Section - DS					
170m	Static load	dynamic load			
Crest thickness	Maximum Principal Stress [MPa]	min. Maximum Principal Stress [MPa]	Difference from static load in %	max. Maximum Principal Stress [MPa]	Difference from static load in %
8 m	0.62	0.00	100.0	3.41	100.0
9 m	0.63	0.00	101.6	3.16	90.7
10 m	0.64	0.00	103.2	2.90	81.0
12 m	0.61	0.00	98.4	2.80	78.5
14 m	0.55	0.00	88.7	2.65	75.3
20 m	0.26	0.00	41.9	2.00	62.4

Table 35: Maximum principal stresses at the main section – downstream

Maximum Principal Stress - Left Section - US					
100 m	Static load	dynamic load			
Crest thickness	Maximum Principal Stress [MPa]	min. Maximum Principal Stress [MPa]	Difference from static load in %	max. Maximum Principal Stress [MPa]	Difference from static load in %
8 m	-0.53	-1.18	100.0	0.69	100.0
9 m	-0.57	-1.18	93.8	0.60	95.9
10 m	-0.62	-1.19	87.7	0.55	95.9
12 m	-0.70	-1.24	83.1	0.50	98.4
14 m	-0.77	-1.28	78.5	0.44	99.2
20 m	-0.97	-1.33	55.4	0.32	105.7

Table 36: Maximum principal stresses at the left section - upstream

Maximum Principal Stress - Left Section - DS					
190m	Static load	dynamic load			
Crest thickness	Maximum Principal Stress [MPa]	min. Maximum Principal Stress [MPa]	Difference from static load in %	max. Maximum Principal Stress [MPa]	Difference from static load in %
8 m	0.20	0.00	100.0	1.74	100.0
9 m	0.20	0.00	100.0	1.65	94.2
10 m	0.20	0.00	100.0	1.57	89.0
12 m	0.15	0.00	75.0	1.48	86.4
14 m	0.09	0.00	45.0	1.44	87.7
20 m	0.00	0.00	0.0	1.22	79.2

Table 37: Maximum principal stresses at the left section – downstream

Maximum Principal Stress - Right Section - US					
100 m	Static load	dynamic load			
Crest thickness	Maximum Principal Stress [MPa]	min. Maximum Principal Stress [MPa]	Difference from static load in %	max. Maximum Principal Stress [MPa]	Difference from static load in %
8 m	-0.53	-1.17	100.0	0.93	100.0
9 m	-0.57	-1.16	92.2	0.88	99.3
10 m	-0.62	-1.17	85.9	0.85	100.7
12 m	-0.70	-1.17	73.4	0.82	104.1
14 m	-0.78	-1.26	75.0	0.77	106.2
20 m	-0.97	-1.31	53.1	0.57	105.5

Table 38: Maximum principal stresses at the right section – upstream

Maximum Principal Stress - Right Section - DS					
190m	Static load	dynamic load			
Crest thickness	Maximum Principal Stress [MPa]	min. Maximum Principal Stress [MPa]	Difference from static load in %	max. Maximum Principal Stress [MPa]	Difference from static load in %
8 m	0.20	0.00	100.0	1.70	100.0
9 m	0.20	0.00	100.0	1.90	113.3
10 m	0.19	0.00	95.0	2.11	128.0
12 m	0.15	0.00	75.0	2.33	145.3
14 m	0.09	0.00	45.0	2.37	152.0
20 m	0.00	0.00	0.0	2.17	144.7

Table 39: Maximum principal stresses at the right section - downstream

Maximum Principal Stresses - Downstream

Figure 66 shows that the maximum principal stresses decrease with an increase of the width of the arch dam. This applies for the main the right and the left section. The results of the maximum principal stresses for the left and the right section vary not much from each other. The pressure at the base joint is smaller in the main section than the pressure at the abutment on the left and right side.

For the dam with the widest dam crest a kink can be seen at the dam elevation of 150 m in the right section.

Maximum Principal Stresses - Upstream

The tensile stresses on the upstream side also decrease with a higher volume of the dam. The pressure on the upstream face is in the main section at the base joint and at the dam crest higher than at the left and right section.

5.10. Summary

It was recognized that some arch dams in Switzerland are designed thicker at the crest. This thesis investigates the influence of the stiffness of the upper arch dam part under dynamic earthquake loading.

At the beginning arch dams located in Austria and Switzerland, which exceed 100 m, are compared with each other to see a difference in design and construction of the different dams. For this kind of stiffness influenced bearing behavior an initial geometry, a double curved arch dam with a height of 220 m and a crest thickness of 8 m, is modified. It is changed in “steps” by thickening the top third of the geometry, starting from the dam crest and going 70 m down. This procedure is done five times, leading to six geometries, including the initial geometry. After discretization of the chosen geometry with ANSYS Mechanical Workbench, the dead load, the water pressure and the acceleration are applied. The dynamic water pressure during the earthquake is simulated, by coupling the acoustic elements with the solid elements by using the Fluid Structure Interaction (FSI). It is assumed that there is no separation of the dam body to the foundation block allowed. Furthermore, linear material behavior is accounted which leads to an overall linear system behavior for all analyzed geometries.

The geometries have been investigated in the main, the left and in the right section of the dam, regarding the displacement and the stresses on the upstream and downstream face of the dam. The results of the displacement and stresses due to the static load and the dynamic load of the investigated geometries are then illustrated in diagrams to compare the results with each other.

The results show that the by increasing the crest thickness, which leads to a higher stiffness of the system, the deformations along the upstream and the downstream face decrease. The hoop stresses show an increase of tensile stresses along the downstream and the upstream face of the dam when the width of the crest increases. By increasing the volume of the dam, the vertical tensile stresses along the upstream and downstream face decrease and therefore the likelihood of crack development in the horizontal concrete joints decreases as well.

To gain more and different results further studies are obtained with a changed seismic excitation. The idea behind that is to gain higher differences in the results as the new acceleration has an excitation frequency close to the Eigenfrequency, which could lead to resonance and could be fatal for the system. To compare the Eigenfrequencies with the excitation frequencies a frequency response spectrum was created by using the discrete Fourier Transform. The maximum acceleration of the time series for the used acceleration and the acceleration used for the second calculation is around 1 m/s^2 . Appendix A shows the results for the second calculation.

It has to be noted that this calculation is only done for one specific dam structure. The results will differ if a different geometry is used. Also, this calculation is done with the program ANSYS Mechanical Workbench, by using the linear method. A different program or a different calculation method can also lead to different results.

To obtain more information regarding the influence of the crest thickness on seismic response of the arch dams, further investigations can be done by allowing a separation between the dam body and the foundation block as well as block joint opening. This will reduce the horizontal tension in the upper part by redistribution of the stresses due to the joint opening. The calculation should be conducted with the same geometries, and with the same acceleration time series to be able to compare the results with the results of this master thesis.

In addition, a discrete crack on the bed joint on the downstream face of the arch dam can be discretized to determine the influence of the crack regarding to the response of the arch dam geometries.

Another calculation can also be made by using the nonlinear analysis instead of the linear method.

Bibliography

- [1] R. Widmann, *Die Talsperren Österreichs, Large Dams in Austria, Arch Dams*, Vol. 35. Salzburg: Austrian National Committee on Large Dams - ATCOLD, 2005.
- [2] T. Strobl and F. Zunic, *Wasserbau: aktuelle Grundlagen - Neue Entwicklungen*. Berlin: Springer, 2006.
- [3] H. H. Thomas, *The Engineering of Large Dams*, Vol. 1. John Wiley & Sons, 1976.
- [4] J. L. Serafim and R. W. Clough, *Arch Dams*. Rotterdam: A.A.Balkema, 1990.
- [5] Bureau of Reclamation United States Department of Interior, Ed., "Design Criteria for Concrete Arch and Gravity Dams," Washington, D.C., 1977.
- [6] M. Pagitsch, *Arch Dam Design and Optimization*. 2012.
- [7] Bundesministerium für Land- und Forstwirtschaft, Umwelt und Wasserwirtschaft and Österreichische Staubeckenkommission, *Richtlinie zum Nachweis der Tragsicherheit von Betonsperren*. 2016.
- [8] Schweizer Wasserwirtschaftsverband (n. d.), "Wasserkraft Schweiz," Retrieved on September 25th 2019. from: <https://www.swv.ch/fachinformationen/wasserkraft-schweiz/>
- [9] G. Zenz, Ed., *Pumped Storage Hydropower in Austria*. Graz: Verlag der Technischen Universität Graz, 2018.
- [10] F. Huber, Ed., *Dams in Austria*. Vienna: Österreichisches Nationalkomitee für Talsperren, 1991.
- [11] G. Lombardi, "On Swiss Arch Dams," in Proceedings of the Conference BNCOLD, London, 1989.

- [12] Swiss Committee on Dams, *Dams in Switzerland - Source for Worldwide Swiss Dam Engineering*. 2011.
- [13] G. Lombardi, "Querkraftbedingte Schäden in Bogensperren," *Wasser-Energie-Luft*, Heft 5/6, CH-5401 Baden, 1988.
- [14] A. Kemnitz, *Mathematik zum Studienbeginn*, 9. Auflage. Vieweg+Teubner, 2010.
- [15] H.-J. Bartsch, *Taschenbuch Mathematischer Formeln*, 20. Auflage. Fachbuchverlag Leipzig, 2004.
- [16] D. D. Pfaffinger, *Tragwerksdynamik*. Springer-Verlag Wien New York, 1989.
- [17] D. Dinkler, *Einführung in die Strukturdynamik: Modelle und Anwendungen*, 2. Auflage. Wiesbaden: Springer Vieweg, 2017.
- [18] A. K. Chopra, *Dynamics of structures: theory and applications to earthquake engineering*. Harlow: Pearson Education, 2014.
- [19] A. Zerwer, G. Cascante, and J. Hutchinson, *Parameter Estimation in Finite Element Simulations of Rayleigh Waves*. 2002.
- [20] O. C. Zienkiewicz, R. L. Taylor, and J. Z. Zhu, *The Finite Element Method: Its Basis and Fundamentals*, 7th Edition. Butterworth Heinemann, 2013.
- [21] M. Goldgruber, *Nonlinear seismic modelling of concrete dams - Doctoral thesis*. TU Graz, 2015.
- [22] G. Zenz and M. Goldgruber, Proceedings of the 12th international benchmark workshop on numerical analysis of dams, *ICOLD - 12th International benchmark workshop on numerical analysis of dams*, 2014.
- [23] ANSYS, © Academic Research Mechanical, Release 19.2, Help System, Chapter 7: Element Library – Solid186 Element Description, ANSYS, Inc.

[24] ANSYS, ® Academic Research Mechanical, Release 19.2, Help System,
Chapter 7: Element Library – FLUID220 Element Description, ANSYS, Inc.

List of Figures

Figure 1: Geometry of Arch Dam Model.....	2
Figure 2: Geometry of Foundation Model.....	2
Figure 3: Geometry of Reservoir Model	3
Figure 4: Constant-radius arch dam - layout and cross section, cf. [3].....	6
Figure 5: Constant-angle arch dam - layout and cross section, cf. [3].....	6
Figure 6: Double-curvature arch dam - layout and cross section, cf. [3]	7
Figure 7: Dead load of an arch dam, cf. [6]	9
Figure 8 Hydrostatic pressure distribution, cf. [6]	10
Figure 9: Distribution of the arch dams in Switzerland over their height [11]....	16
Figure 10: Austrian arch dams, cf. [10]	19
Figure 11: Swiss dams, higher than 100 m, cf. [12]	21
Figure 12: Cross sections of the arch dams Schlegeis and Santa Maria [10][12]	23
Figure 13: Comparison of the longitudinal sections across the valley of both dams [10][12].....	23
Figure 14: Slenderness factor of large dams in Austria and Switzerland over the height with the slenderness factor for the geometry used for this master thesis [13].....	26
Figure 15: Graph of the linear function, cf. [14]	29
Figure 16: Circle with shifted centre along the x-axis, cf. [15]	31
Figure 17: Ellipse with shifted centre along the x-axis, cf. [15].....	32
Figure 18: Parabola ellipse with shifted centre along the x-axis, cf. [15].....	33
Figure 19: Hyperbola with shifted centre along the x-axis, cf. [15]	34
Figure 20: Circle with shifted centre along the x- and y-axis, cf. [15]	35
Figure 21: Geometry of the arch with its parameters [1]	36
Figure 22: SDOF system with external force, cf. [16].....	38
Figure 23: Damping cases [18]	41

Figure 24: MDOF system with external force, cf. [16]	42
Figure 25: Rayleigh damping [19]	46
Figure 26: Hydrostatic pressure	53
Figure 27: Final geometry	55
Figure 28: Increase of dam thickness (for unit value) depending on the dam's elevation.....	55
Figure 29: Cross section of the main section of the arch dam with an 8 m and 20 m crest width	56
Figure 30: Acceleration in y-direction	57
Figure 31: Acceleration in x-direction	57
Figure 32: Acceleration in z-direction	57
Figure 33: Coarse mesh for arch dam, reservoir and foundation	58
Figure 34: Medium mesh	58
Figure 35: Fine mesh	59
Figure 36: Chosen mesh for the whole geometry for the arch dam with 8 m crest width.....	59
Figure 37: Geometry of the element "Solid186" an "Fluid220" [22]	60
Figure 38: Rayleigh damping for initial geometry	61
Figure 39: Location of the three evaluation sections	62
Figure 40: First 10 Eigenfrequencies of the arch dams, with d as the crest thickness	63
Figure 41: Deformation of the six dams in the main section along the downstream face	66
Figure 42: Static load of the deformation of the six dams in the main section along the downstream side	67
Figure 43: Dynamic load of the deformation of the six dams in the main section along the downstream side	68
Figure 44: Deformation of the six dams in the main section along the upstream side	69
Figure 45: Hoop stresses of the six dams in the main section along the upstream side	72

Figure 46: Static load of the hoop stresses of the six dams in the main section along the upstream side.....	73
Figure 47: Dynamic load of the hoop stresses of the six dams in the main section along the upstream side.....	74
Figure 48: Hoop stresses of the six dams in the main section along the downstream side.....	75
Figure 49: Hoop stresses of the six dams in the left section along the upstream side	76
Figure 50: Hoop stresses of the six dams in the left section along the downstream side	77
Figure 51: Hoop stresses of the six dams in the right section along the upstream side	78
Figure 52: Hoop stresses of the six dams in the right section along the downstream side.....	79
Figure 53: Vertical stresses of the six dams in the main section along the upstream side.....	84
Figure 54: Vertical stresses of the six dams in the main section along the downstream side.....	85
Figure 55: Vertical stresses of the six dams in the left section along the upstream side	86
Figure 56: Vertical stresses of the six dams in the left section along the downstream side.....	87
Figure 57: Vertical stresses of the six dams in the right section along the upstream side	88
Figure 58: Vertical stresses of the six dams in the right section along the downstream side.....	89
Figure 59: Minimum principal stresses of the six dams in the main section along the upstream side.....	93
Figure 60: Minimum principal stresses of the six dams in the main section along the downstream side	94
Figure 61: Minimum principal stresses of the six dams in the left section along the upstream side.....	95
Figure 62: Minimum principal stresses of the six dams in the left section along the downstream side	96

Figure 63: Minimum principal stresses of the six dams in the right section along the upstream side.....	97
Figure 64: Minimum principal stresses of the six dams in the right section along the downstream side	98
Figure 65: Maximum principal stresses of the six dams in the main section along the upstream side.....	102
Figure 66: Maximum principal stresses of the six dams in the main section along the downstream side	103
Figure 67: Maximum principal stresses of the six dams in the left section along the upstream side.....	104
Figure 68: Maximum principal stresses of the six dams in the left section along the downstream side	105
Figure 69: Maximum principal stresses of the six dams in the right section along the upstream side.....	106
Figure 70: Maximum principal stresses of the six dams in the right section along the downstream side	107

List of Tables

Table 1: Austrian dams, higher than 100 m, sorted by their height [10]	19
Table 2: Swiss arch dams sorted by their height including the investigated dam geometry [12]	22
Table 3: Listing of the geometry data of both dams	23
Table 4: Swiss dams over 100 m in alphabetical order [12]	26
Table 5: Austrian dams over 100 m in alphabetical order [12]	27
Table 6: Material parameter	56
Table 7: Nodes and elements for the coarse mesh	58
Table 8: Nodes and elements for the medium mesh	58
Table 9: Nodes and elements for the fine mesh	59
Table 10: Alpha and beta values for the 6 geometries, with d as the crest thickness	61
Table 11: Table of the first ten Eigenfrequencies for every arch dam with d as the crest thickness	63
Table 12: Mode shapes of the different arch dams, with d as the crest thickness	64
Table 13: Deformation at the main section – upstream	70
Table 14: Deformation at the main section - downstream	70
Table 15: Hoop stresses at the main section – upstream	80
Table 16: Hoop stresses at the main section – downstream	80
Table 17: Hoop stresses at the left section - upstream	80
Table 18: Hoop stresses at the left section – downstream	81
Table 19: Hoop stresses at the right section – upstream	81
Table 20: Hoop stresses at the right section - downstream	81
Table 21 Hoop stresses of the dam with the thinnest and thickest dam crest at the main section – downstream	82
Table 22: Vertical stresses at the main section – upstream	90

Table 23: Vertical stresses at the main section – downstream	90
Table 24: Vertical stresses at the left section - upstream	90
Table 25: Vertical stresses at the left section – downstream	91
Table 26: Vertical stresses at the right section – upstream	91
Table 27: Vertical stresses at the right section - downstream	91
Table 28: Minimum principal stresses at the main section – upstream	99
Table 29: Minimum principal stresses at the main section – downstream.....	99
Table 30: Minimum principal stresses at the left section - upstream	99
Table 31: Minimum principal stresses at the left section – downstream.....	100
Table 32: Minimum principal stresses at the right section – upstream	100
Table 33: Minimum principal stresses at the right section - downstream	100
Table 34: Maximum principal stresses at the main section – upstream	108
Table 35: Maximum principal stresses at the main section – downstream.....	108
Table 36: Maximum principal stresses at the left section - upstream	108
Table 37: Maximum principal stresses at the left section – downstream.....	109
Table 38: Maximum principal stresses at the right section – upstream	109
Table 39: Maximum principal stresses at the right section - downstream	109

Appendix A

As shown before, the results of the displacement and the stresses do not vary too much from each other. To see a possible larger influence in the stresses and in the displacement, a different acceleration with an excitation frequency close to the Eigenfrequency is used.

First three different accelerations are examined if their excitation frequency is close to the Eigenfrequency of the dams. This is done by using the discrete Fourier Transform.

The acceleration below is used because it has an excitation frequency close to the Eigenfrequency in z-direction.

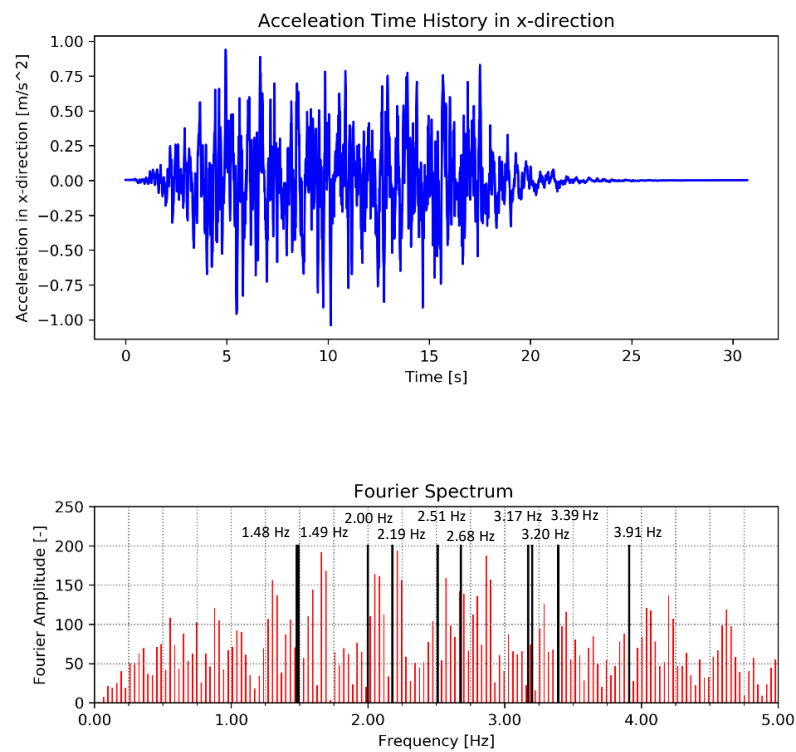


Figure 71: Acceleration in x-direction

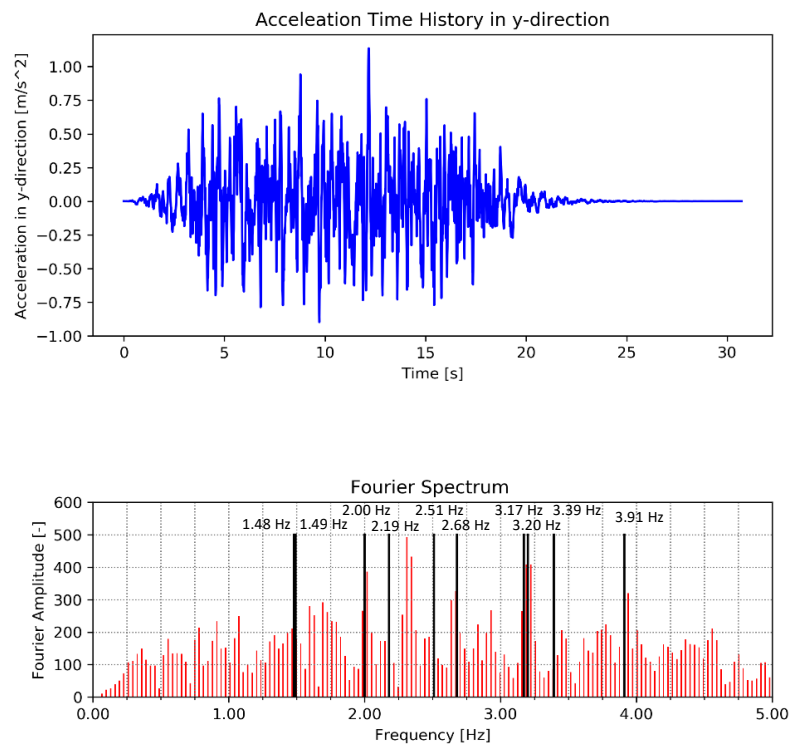


Figure 72: Acceleration in y-direction

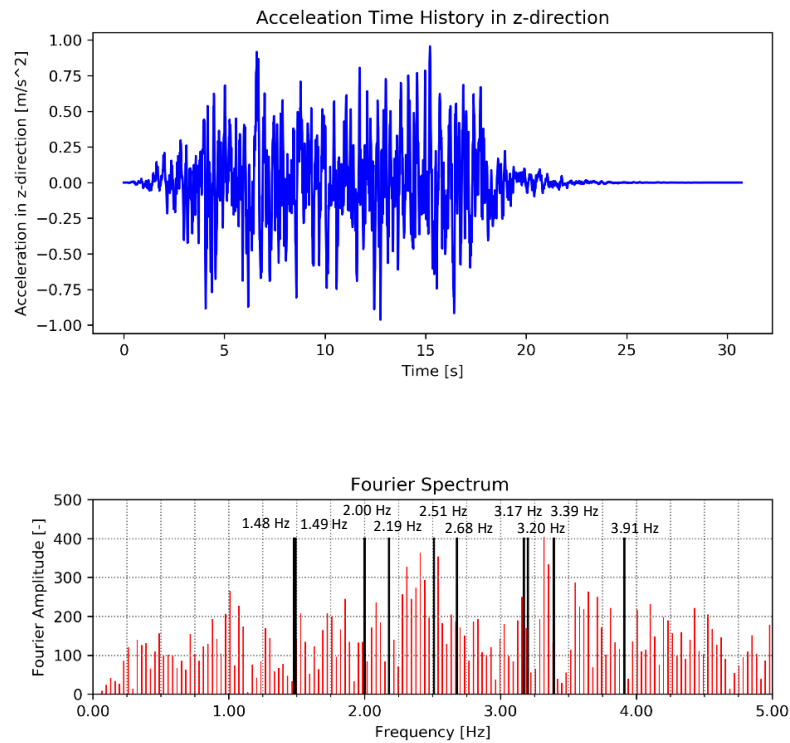


Figure 73: Acceleration in z-direction

The results of the deformations with the given acceleration above are as following:

Deformation – Main Section – Downstream

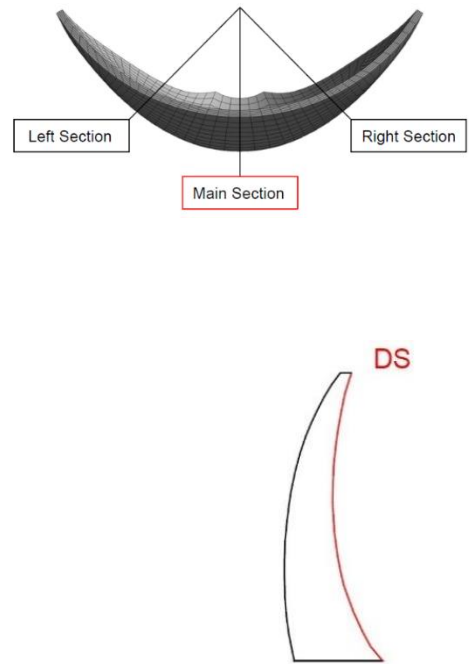
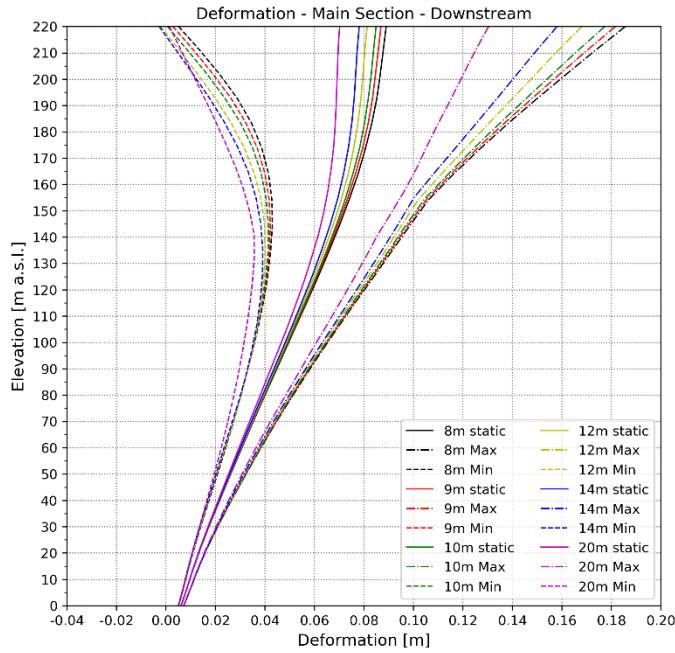


Figure 74: Deformation at the main section - downstream

Deformation – Main Section – Upstream

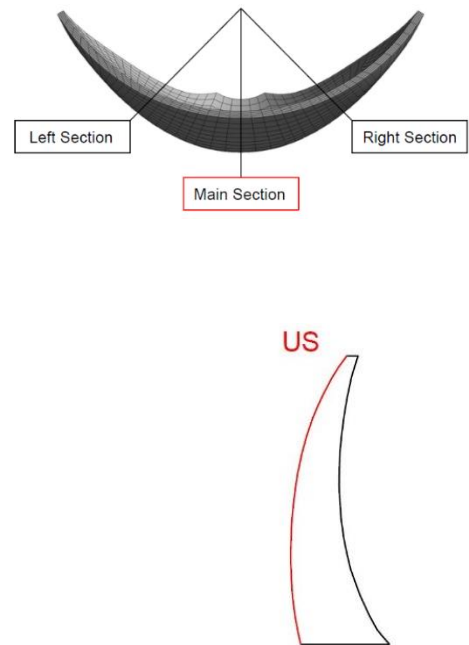
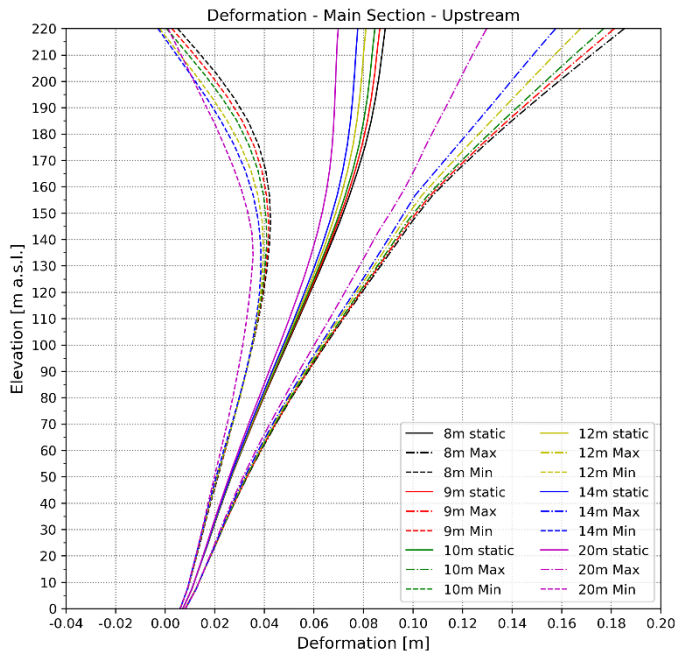


Figure 75: Deformation at the main section - upstream

For a better understanding and to illustrate the difference between the results of the calculation made with the acceleration before and of the calculation with the acceleration which has the excitation frequency close to the Eigenfrequency of the dams, only the results of the dam with a crest width of 8 m and 20 m are plotted in one diagram. The results of the arch dam with a crest width of 8 m is shown in blue and the red lines describes the results for the arch dam with a crest width of 20 m.

Deformation – Main Section – Downstream

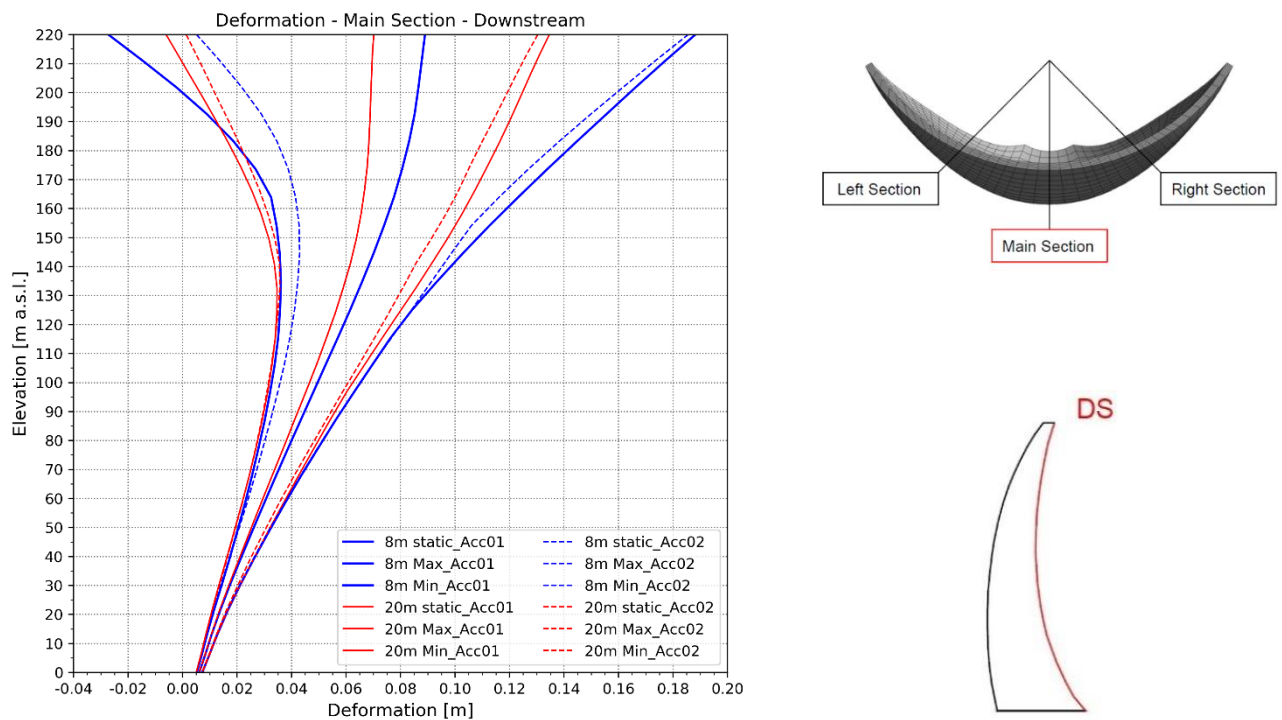


Figure 76: Deformation of the dams with an 8 m crest width and a 20 m crest width in the main section along the downstream face

Deformation – Main Section – Upstream

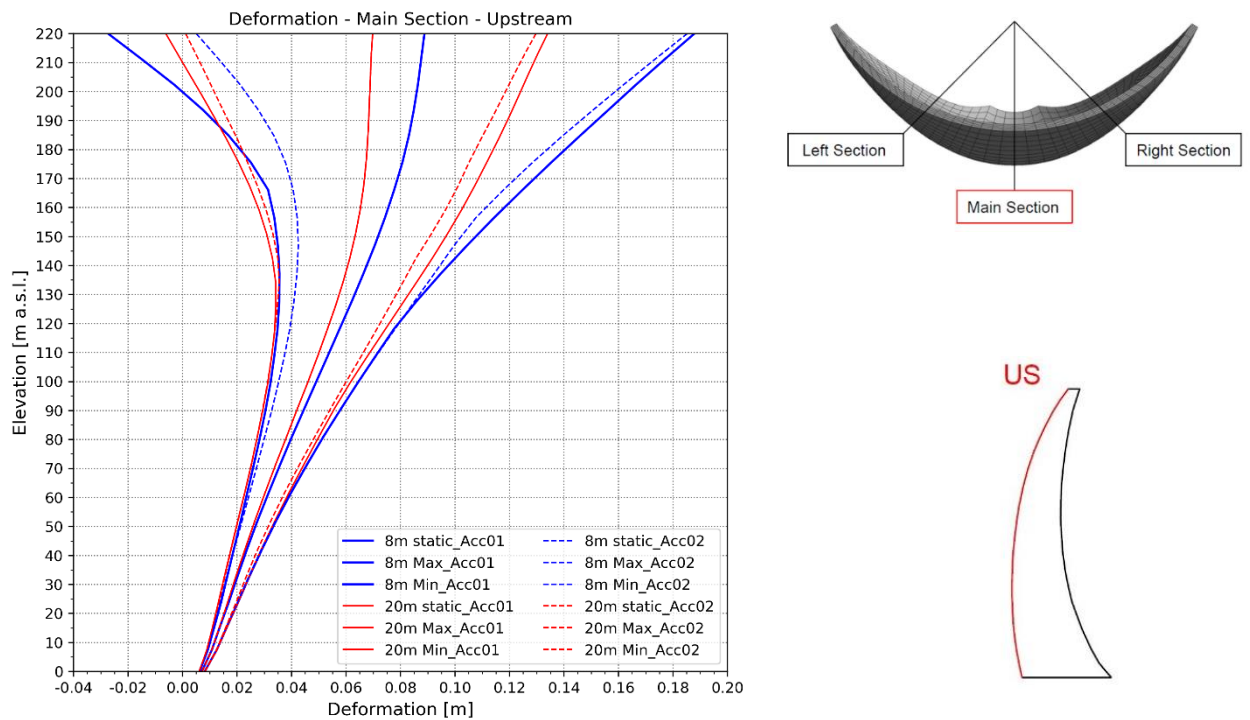


Figure 77: Deformation of the dams with an 8 m crest width and a 20 m crest width in the main section along the upstream face

Same as for the results before, the following tables show the deformation or stresses due to the static and dynamic load for the six different arch.

Deformation - Main Section - US					
220 m	Static load	dynamic load			
Crest thickness	Displacement [cm]	min. Displacement [cm]	Difference from static load in %	max. Displacement [cm]	Difference from static load in %
8 m	8.88	0.50	100.0	18.53	100.0
9 m	8.66	0.27	100.1	18.13	98.1
10 m	8.46	0.05	100.4	17.70	95.8
12 m	8.10	-0.23	99.4	16.77	89.8
14 m	7.77	-0.29	96.2	15.76	82.8
20 m	6.98	0.12	81.9	12.98	62.2

Table 40: Deformation at the main section – upstream

Deformation - Main Section - DS					
220 m	Static load	dynamic load			
Crest thickness	Displacement [cm]	min. Displacement [cm]	Difference from static load in %	max. Displacement [cm]	Difference from static load in %
8 m	8.90	0.51	100.0	18.57	100.0
9 m	8.69	0.28	100.2	18.17	98.0
10 m	8.49	0.06	100.5	17.74	95.7
12 m	8.13	-0.22	99.5	16.81	89.8
14 m	7.81	-0.28	96.4	15.81	82.7
20 m	7.02	0.13	82.1	13.04	62.3

Table 41: Deformation at the main section – downstream

Deformation - Downstream and Upstream

Figure 76 shows that the deformations of the second calculation in the main section decrease. This is the case for the upstream and the downstream face of the dam. The lines on the right indicate the results due to the minimum time series. It can be seen that the deformation decreases more when the dam is thicker at the dam crest.

Hoop Stress – Main section – Upstream

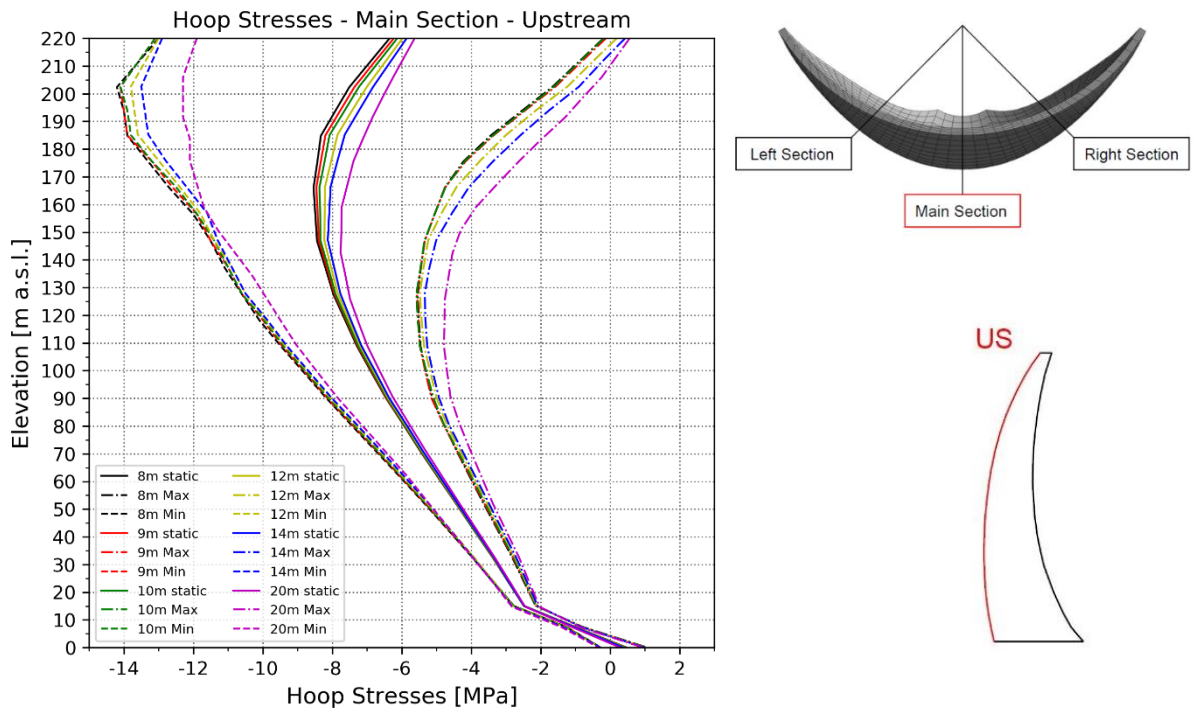


Figure 78: Hoop stresses at the main section - upstream

Hoop Stress – Main section – Downstream

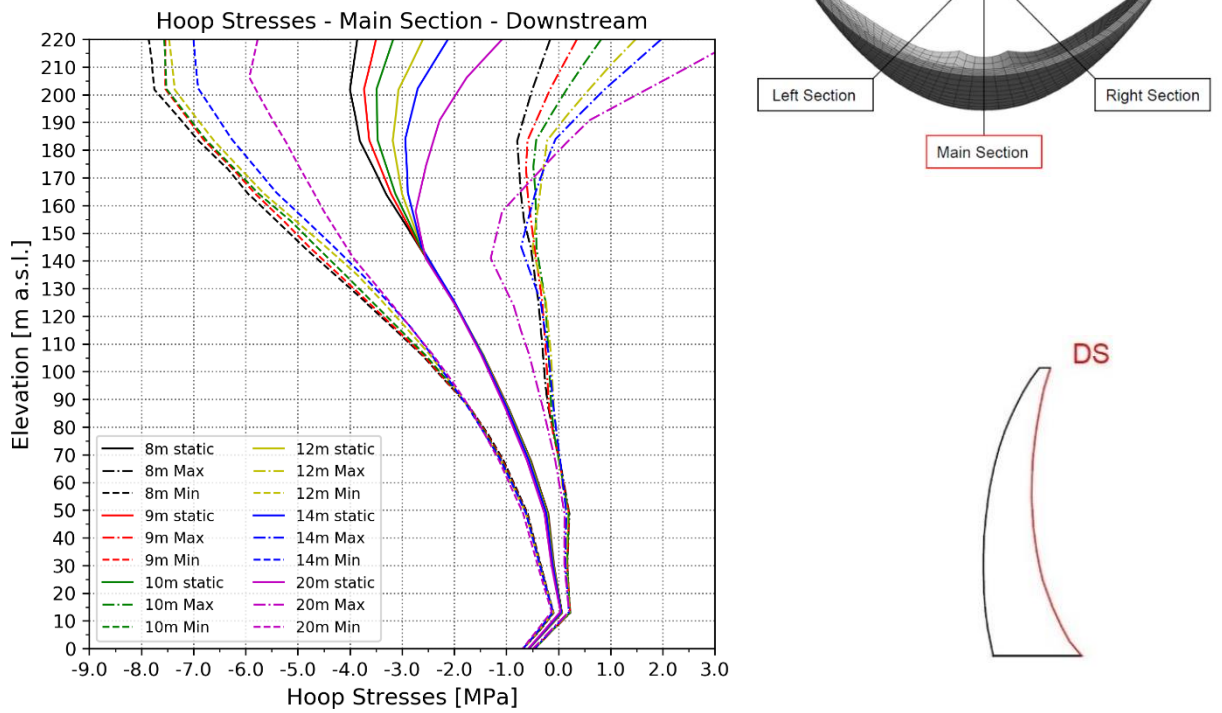


Figure 79: Hoop stresses at the main section - downstream

Hoop Stresses – Left Section – Upstream

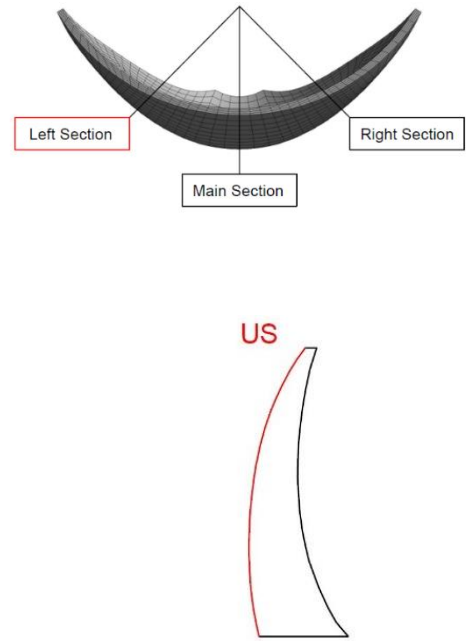
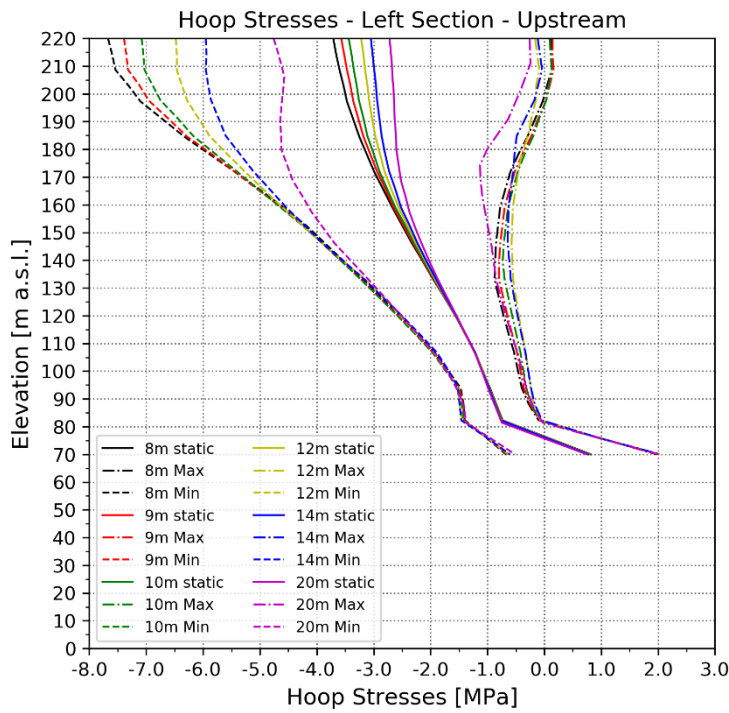


Figure 80: Hoop stresses at the left section - upstream

Hoop Stresses – Left Section – Downstream

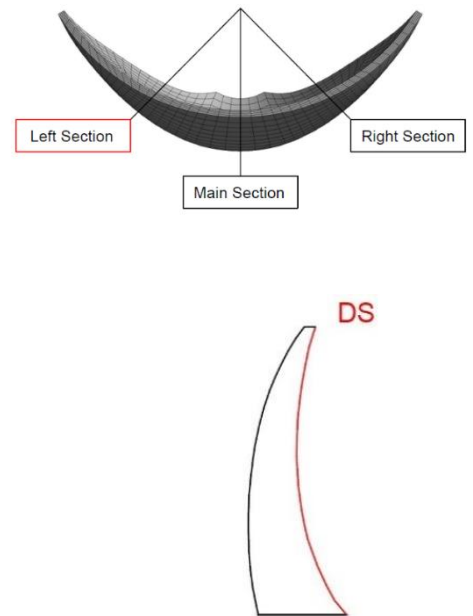
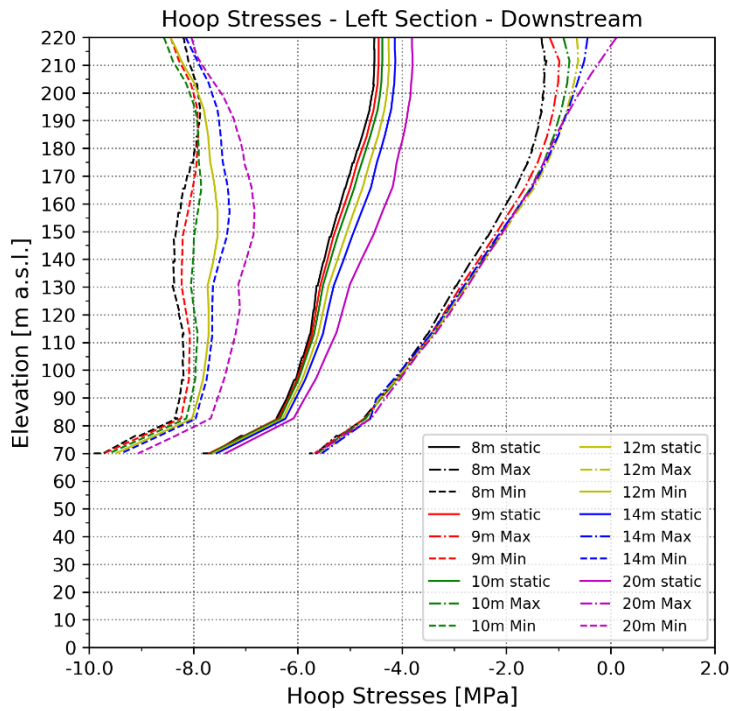


Figure 81: Hoop stresses at the left section - downstream

Hoop Stresses – Right Section – Upstream

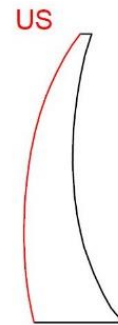
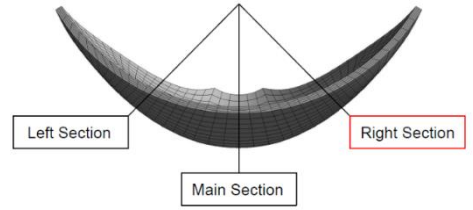
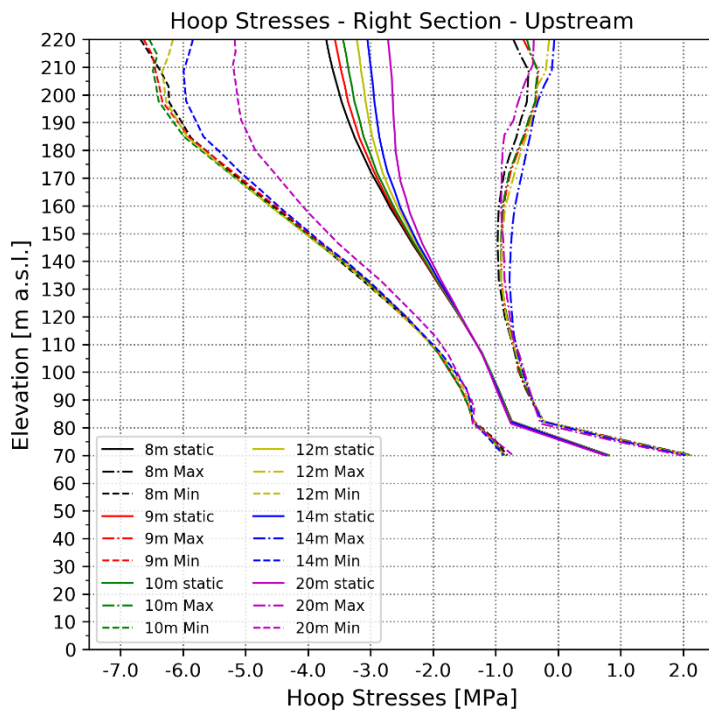


Figure 82: Hoop stresses at the right section - upstream

Hoop Stresses – Right Section – Downstream

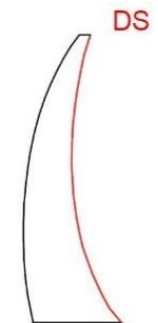
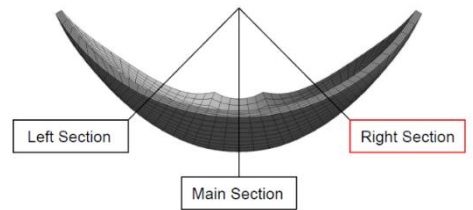
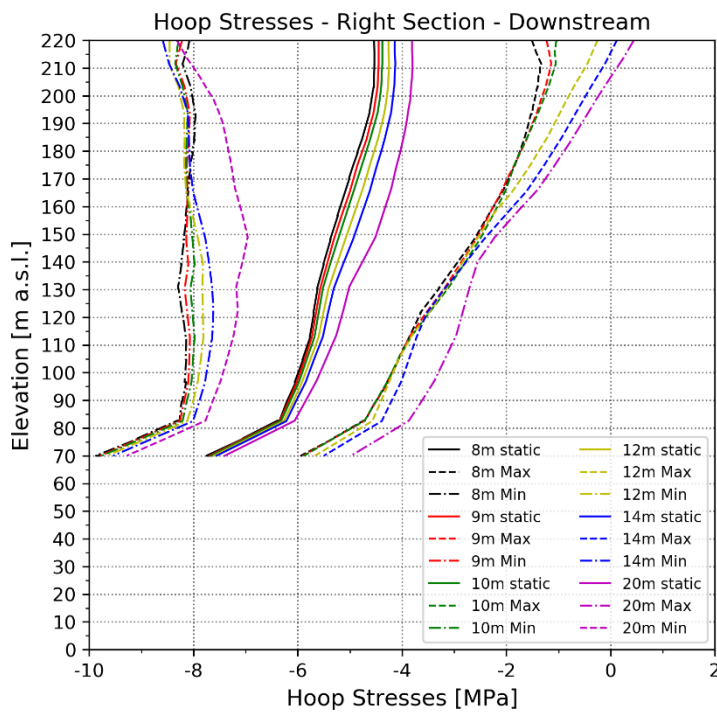


Figure 83: Hoop stresses at the right section - downstream

Hoop Stress – Main section – Upstream

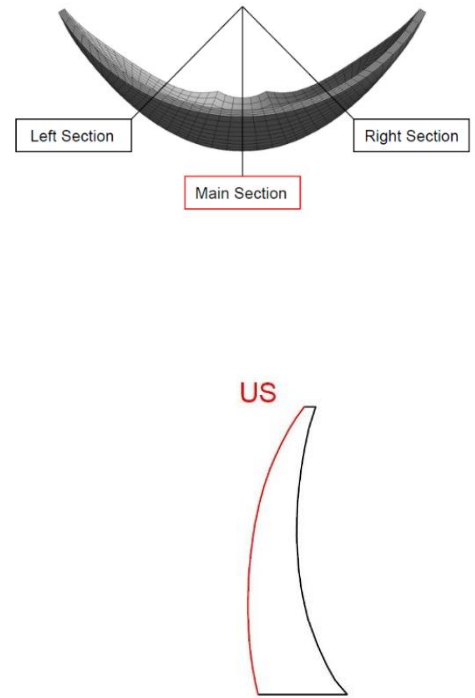
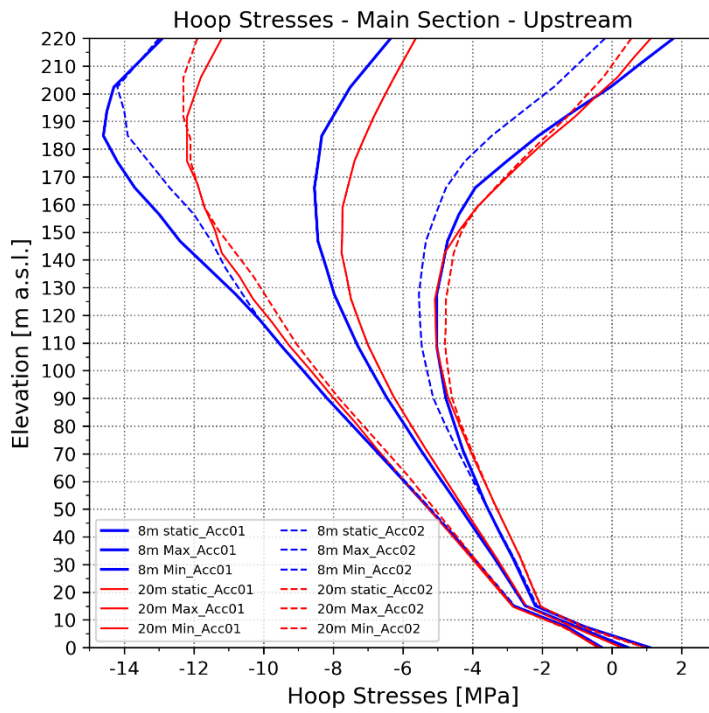


Figure 84: Hoop stresses of the dams with an 8 m crest width and a 20 m crest width in the main section along the upstream face

Hoop Stress – Main section – Downstream

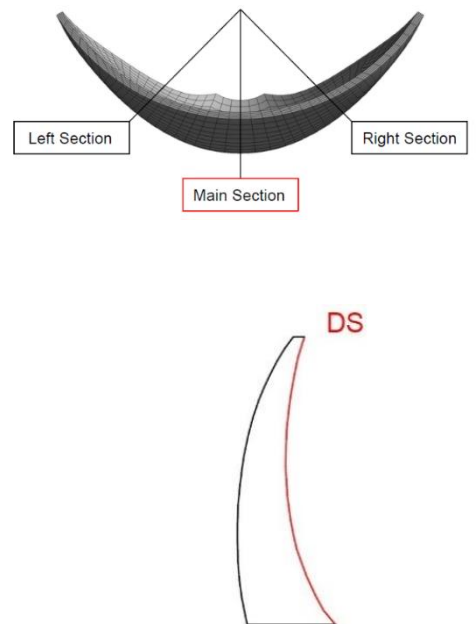
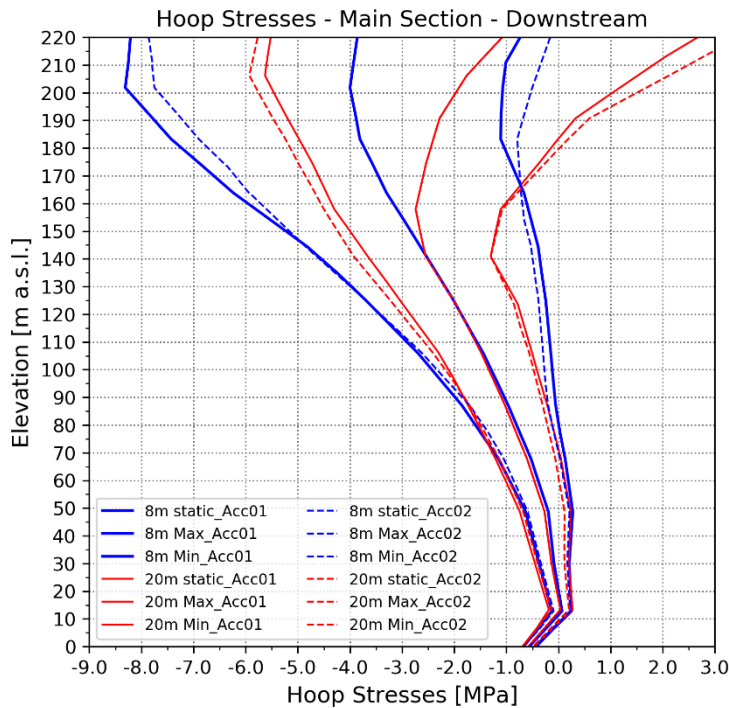


Figure 85: Hoop stresses of the dams with an 8 m crest width and a 20 m crest width in the main section along the downstream face

Hoop Stresses – Left Section – Upstream

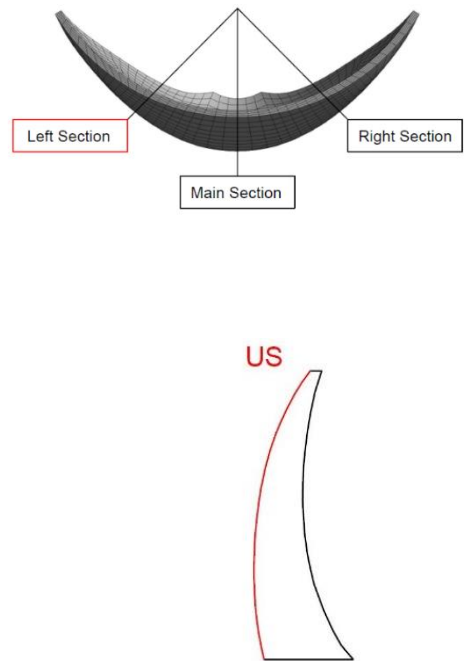
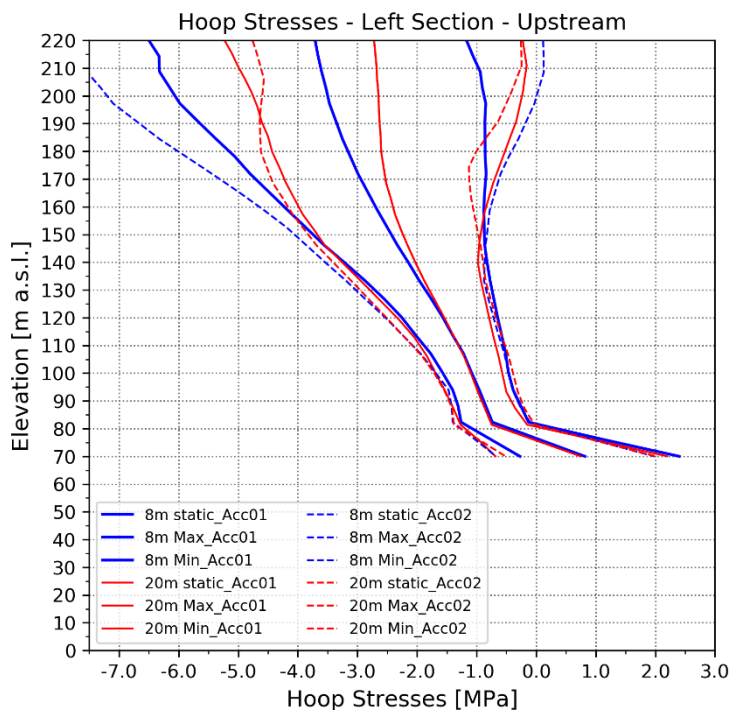


Figure 86: Hoop stresses of the dams with an 8 m crest width and a 20 m crest width in the left section along the upstream face

Hoop Stresses – Left Section – Downstream

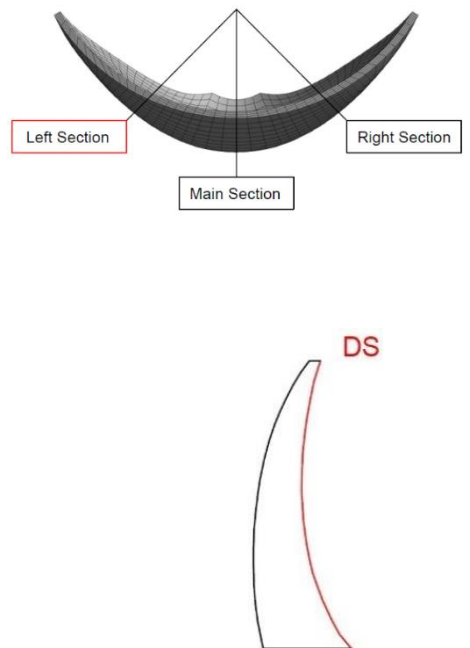
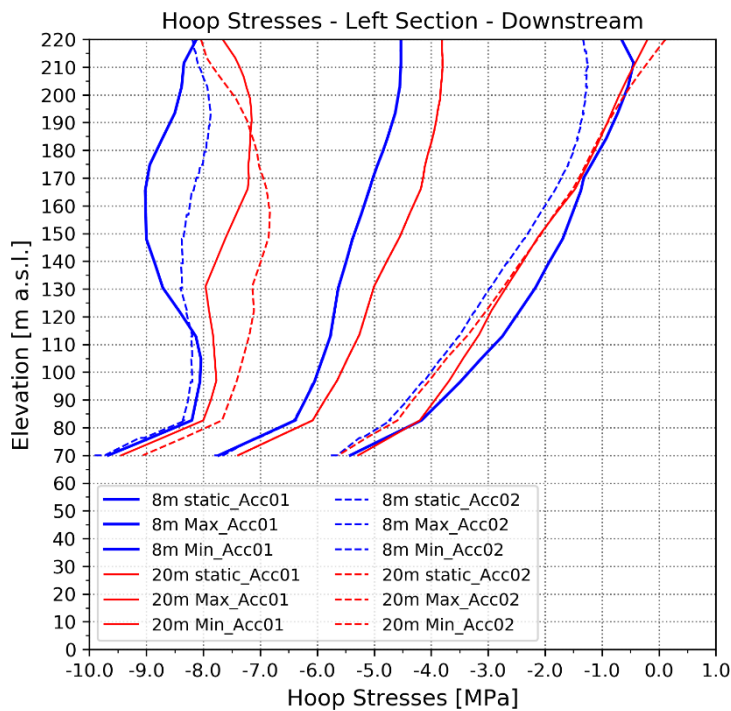


Figure 87: Hoop stresses of the dams with an 8 m crest width and a 20 m crest width in the left section along the downstream face

Hoop Stresses – Right Section – Upstream

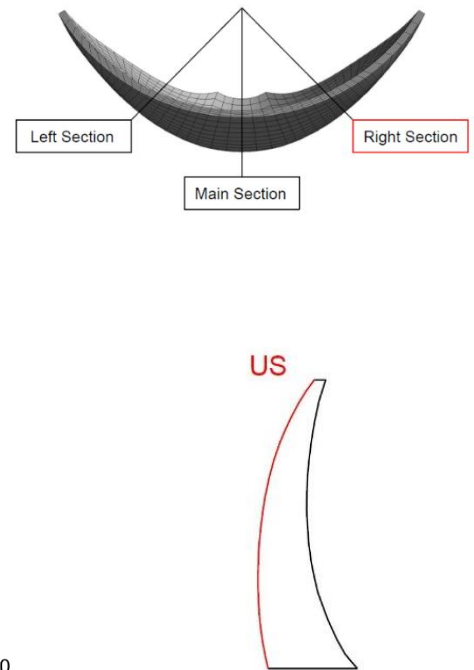
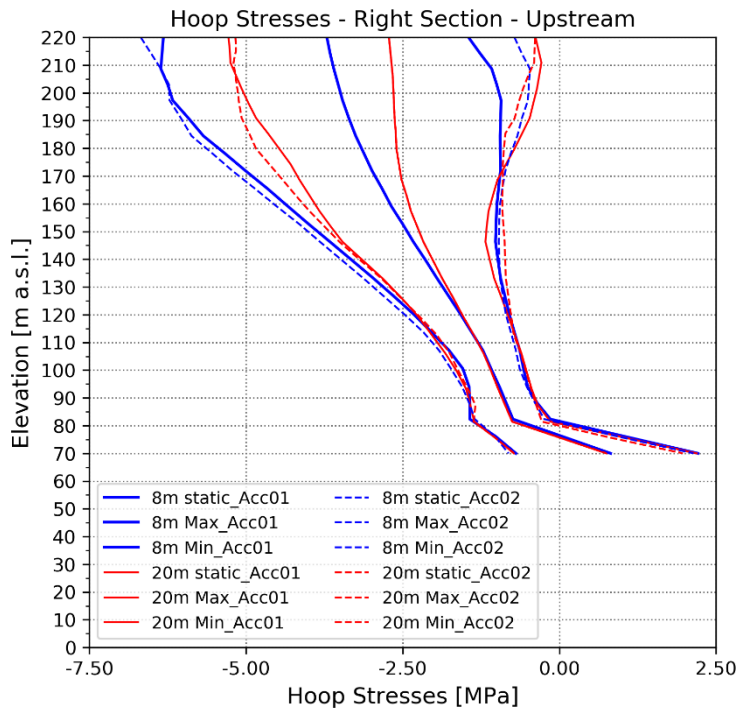


Figure 88: Hoop stresses of the dams with an 8 m crest width and a 20 m crest width in the right section along the upstream face

Hoop Stresses – Right Section – Downstream

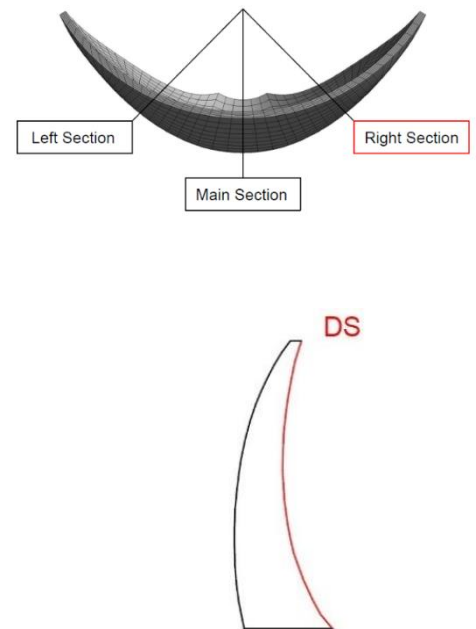
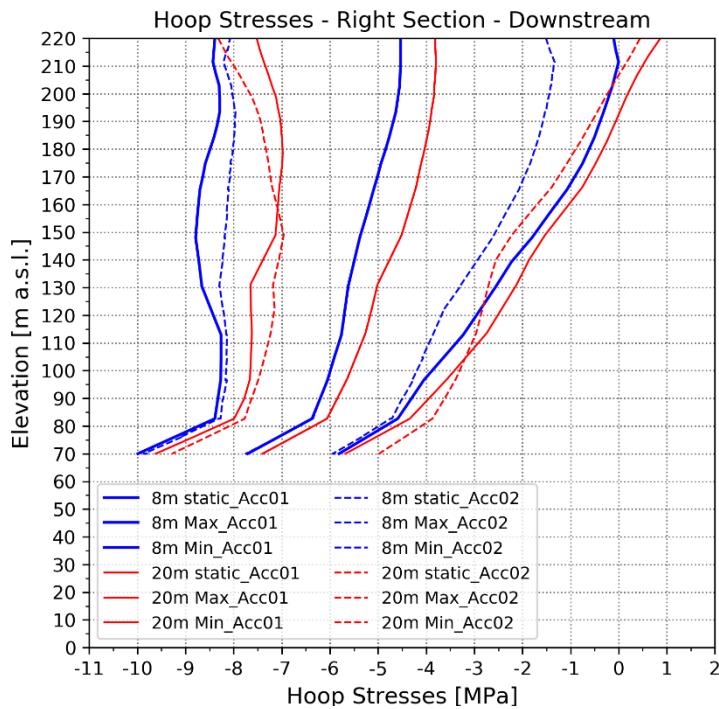


Figure 89: Hoop stresses of the dams with an 8 m crest width and a 20 m crest width in the right section along the downstream face

Hoop Stress - Main Section - US					
180 m	Static load	dynamic load			
Crest thickness	Hoop Stress [MPa]	min. Hoop Stress [MPa]	Difference from static load in %	max. Hoop Stress [MPa]	Difference from static load in %
8 m	-8.40	-13.34	100.0	-4.00	100.0
9 m	-8.30	-13.34	102.0	-3.90	100.0
10 m	-8.20	-13.30	103.2	-3.90	97.7
12 m	-8.00	-13.20	105.3	-3.50	102.3
14 m	-7.80	-13.00	105.3	-3.00	109.1
20 m	-7.30	-12.20	99.2	-2.50	109.1

Table 42: Hoop stresses at the main section – upstream

Hoop Stress - Main Section - DS					
220 m	Static load	dynamic load			
Crest thickness	Hoop Stress [MPa]	min. Hoop Stress [MPa]	Difference from static load in %	max. Hoop Stress [MPa]	Difference from static load in %
8 m	-3.86	-7.83	100.0	-0.16	100.0
9 m	-3.50	-7.54	101.8	0.35	104.1
10 m	-3.17	-7.56	110.6	0.82	107.8
12 m	-2.60	-7.47	122.7	1.48	110.3
14 m	-2.12	-7.00	122.9	1.97	110.5
20 m	-1.08	-5.77	118.1	3.46	122.7

Table 43: Hoop stresses at the main section – downstream

Hoop Stress - Left Section - US					
220 m	Static load	dynamic load			
Crest thickness	Hoop Stress [MPa]	min. Hoop Stress [MPa]	Difference from static load in %	max. Hoop Stress [MPa]	Difference from static load in %
8 m	-3.71	-7.67	100.0	0.16	100.0
9 m	-3.57	-7.39	96.5	0.15	96.1
10 m	-3.44	-7.08	91.9	0.09	91.2
12 m	-3.22	-6.48	82.3	-0.16	79.1
14 m	-3.05	-5.95	73.2	-0.12	75.7
20 m	-2.72	-4.76	51.5	-0.26	63.6

Table 44: Hoop stresses at the left section – upstream

Hoop Stress - Left Section - DS					
180 m	Static load	dynamic load			
Crest thickness	Hoop Stress [MPa]	min. Hoop Stress [MPa]	Difference from static load in %	max Hoop Stress [MPa]	Difference from static load in %
8 m	-4.85	-7.95	100.0	-1.56	100.0
9 m	-4.77	-7.93	101.9	-1.31	105.2
10 m	-4.69	-7.90	103.5	-1.19	106.4
12 m	-4.54	-7.70	101.9	-1.10	104.6
14 m	-4.40	-7.46	98.7	-1.12	99.7
20 m	-4.00	-7.05	98.4	-1.20	85.1

Table 45: Hoop stresses at the left section - downstream

Hoop Stress - Right Section - US					
220 m	Static load	dynamic load			
Crest thickness	Hoop Stress [MPa]	min. Hoop Stress [MPa]	Difference from static load in %	max. Hoop Stress [MPa]	Difference from static load in %
8 m	-3.71	-6.68	100.0	-0.72	100.0
9 m	-3.56	-6.63	103.4	-0.56	100.3
10 m	-3.44	-6.54	104.4	-0.50	98.3
12 m	-3.22	-6.16	99.0	-0.14	103.0
14 m	-3.05	-5.84	93.9	-0.06	100.0
20 m	-2.72	-5.17	82.5	-0.39	77.9

Table 46: Hoop stresses at the right section – upstream

Hoop Stress - Right Section - DS					
180 m	Static load	dynamic load			
Crest thickness	Hoop Stress [MPa]	min. Hoop Stress [MPa]	Difference from static load in %	max. Hoop Stress [MPa]	Difference from static load in %
8 m	-4.85	-8.00	100.0	-1.75	100.0
9 m	-4.77	-8.11	106.0	-1.73	98.1
10 m	-4.69	-8.14	109.5	-1.74	95.2
12 m	-4.54	-8.18	115.6	-1.39	101.6
14 m	-4.40	-8.08	116.8	-1.11	106.1
20 m	-4.00	-7.32	105.4	-0.95	98.4

Table 47: Hoop stresses at the right section – downstream

Hoop Stress - Downstream

The tensile stresses in the main section are higher than in the calculation before. Figure 83 shows that the tendency of the hoop stresses on the right is the same as the results gained before. The compressive stresses decrease if the volume of the dam increases. Same appears on the left side. The tensile stresses in the main section increase, when the crest width increases.

Compared to the results before, the hoop stresses gained with the maximum time series, which were obtained in this calculation, decrease in the left and the right section.

Hoop Stress - Upstream

In the main section along the upstream face of the dam, the tensile stresses decrease, compared to the results from the calculation before.

The hoop stresses on the upstream face show for the left and right side the same characteristics as the hoop stresses on the downstream side.

Vertical Stress – Main Section – Upstream

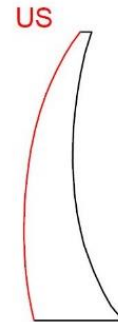
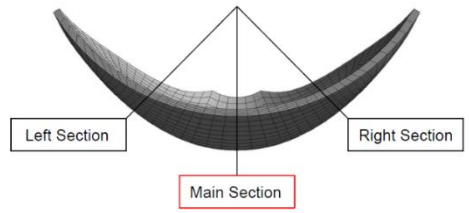
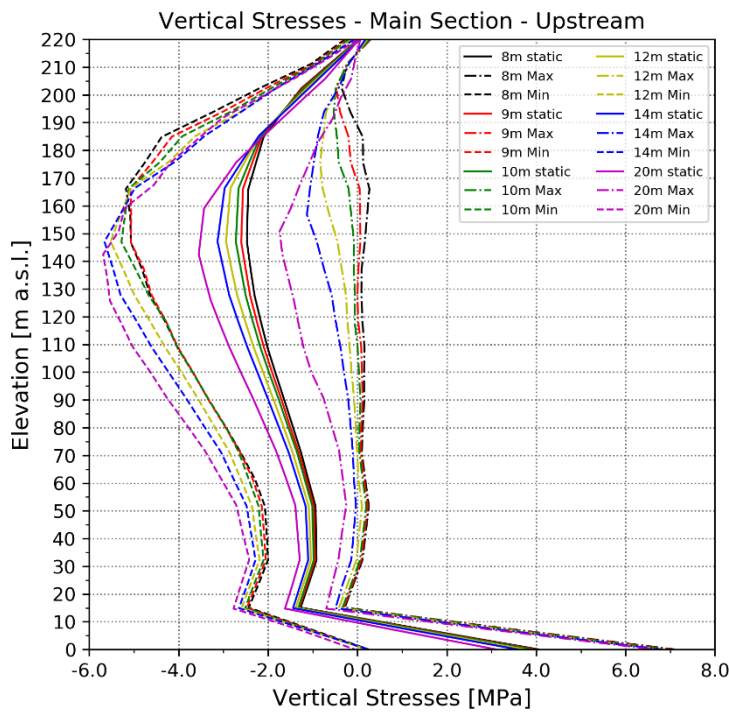


Figure 90: Vertical stresses at the main section - upstream

Vertical Stress – Main Section – Downstream

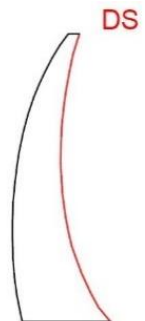
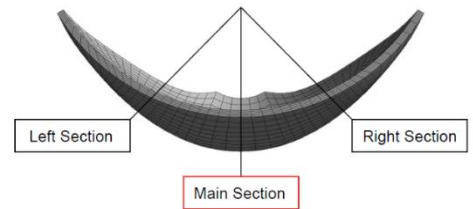
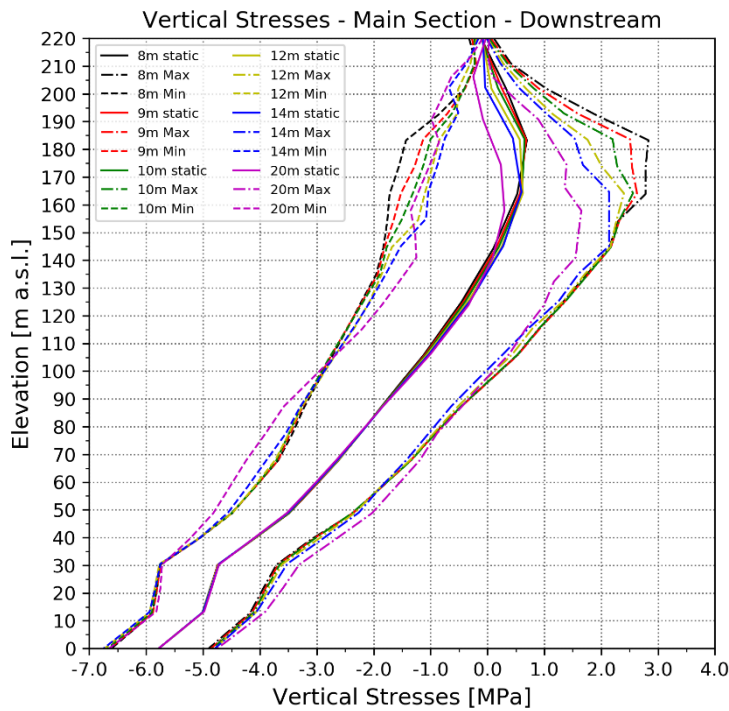


Figure 91: Vertical stresses at the main section - downstream

Vertical Stresses – Left Section – Upstream

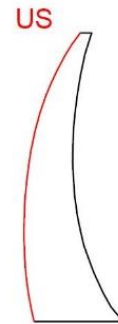
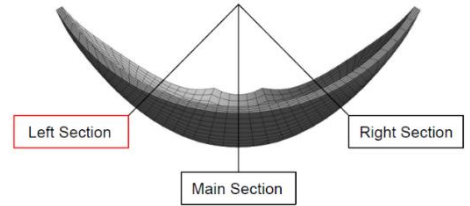
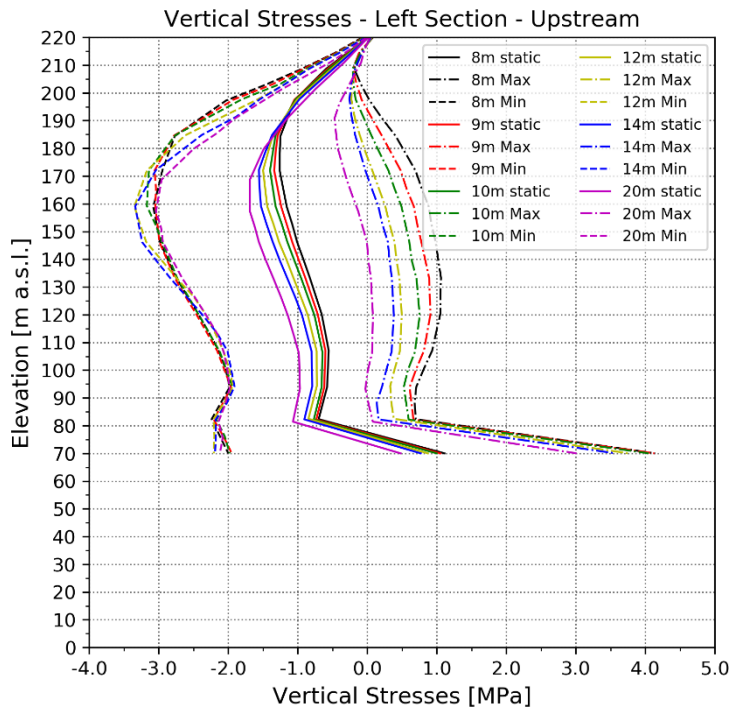


Figure 92: Vertical stresses at the left section - upstream

Vertical Stresses – Left Section – Downstream

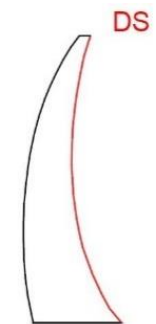
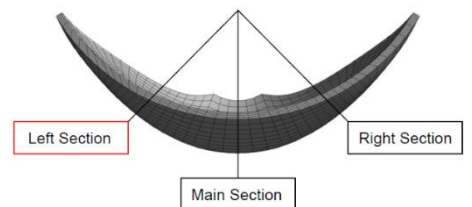
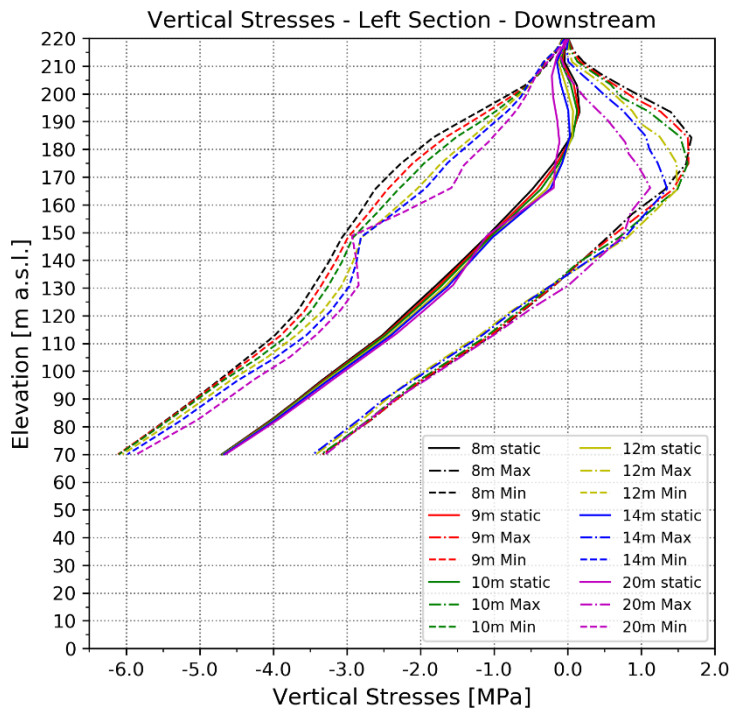


Figure 93: Vertical stresses at the left section - downstream

Vertical Stresses – Right Section – Upstream

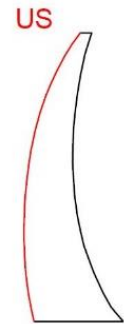
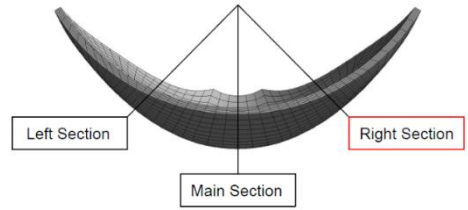
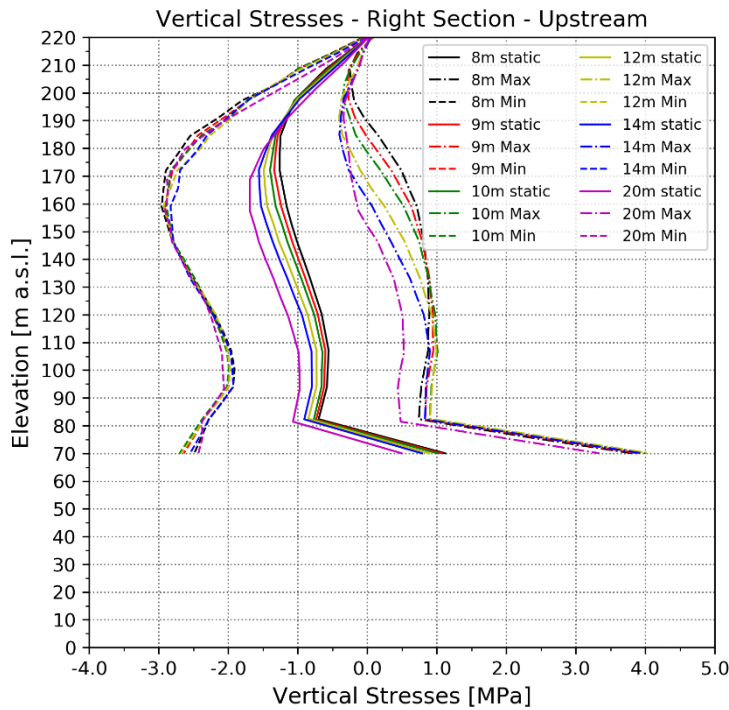


Figure 94: Vertical stresses at the right section - upstream

Vertical Stresses – Right Section – Downstream

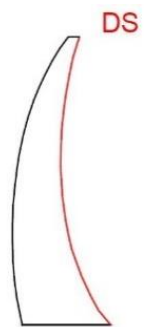
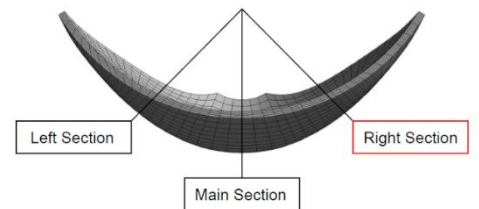
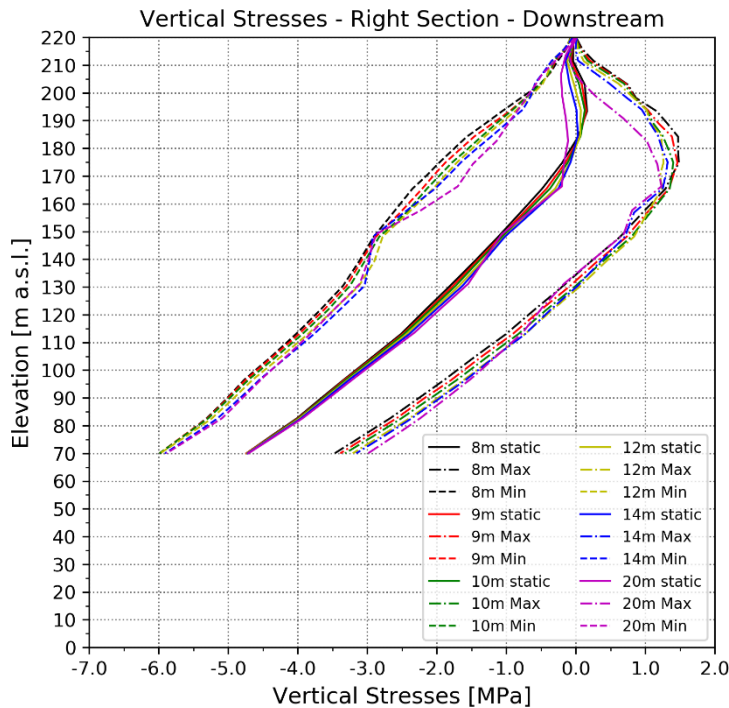


Figure 95: Vertical stresses at the right section - downstream

Vertical Stress – Main Section – Upstream

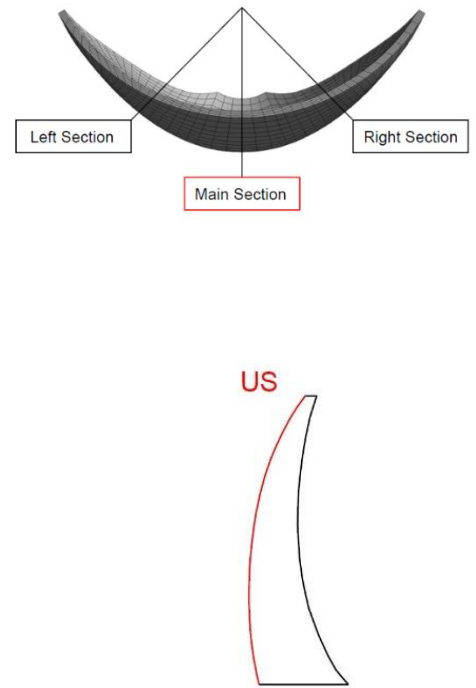
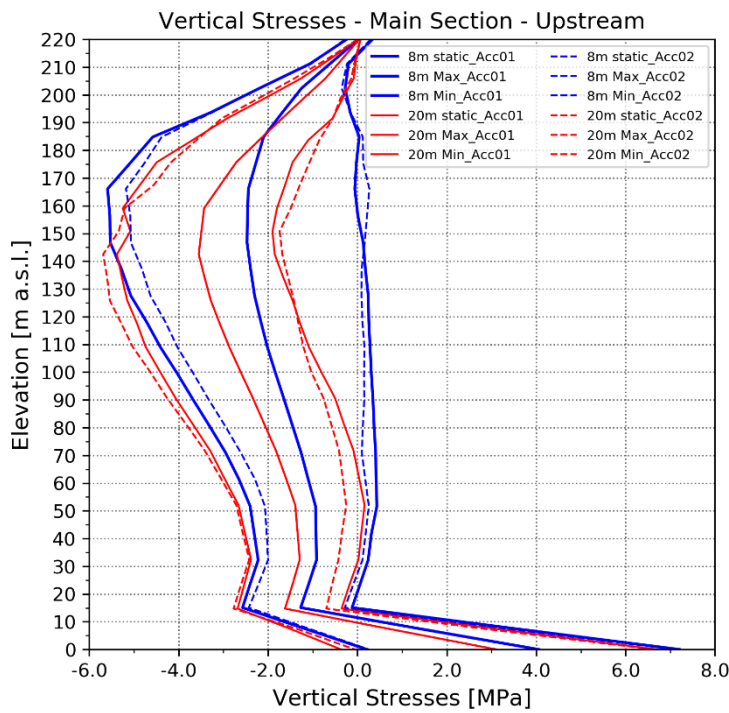


Figure 96: Vertical stresses of the dams with an 8 m crest width and a 20 m crest width in the main section along the upstream face

Vertical Stress – Main Section – Downstream

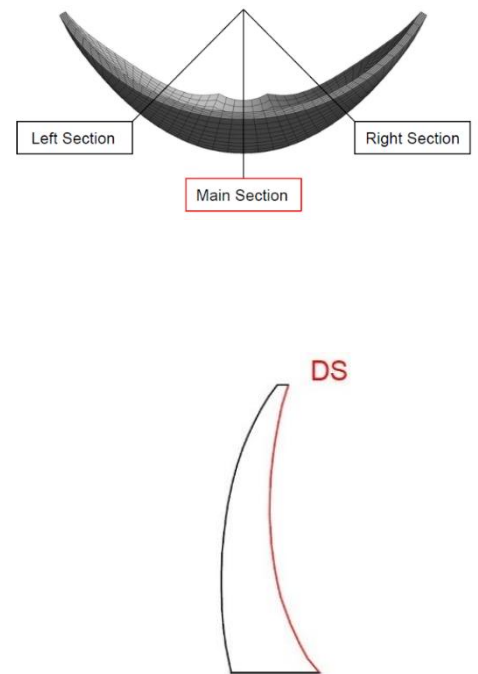
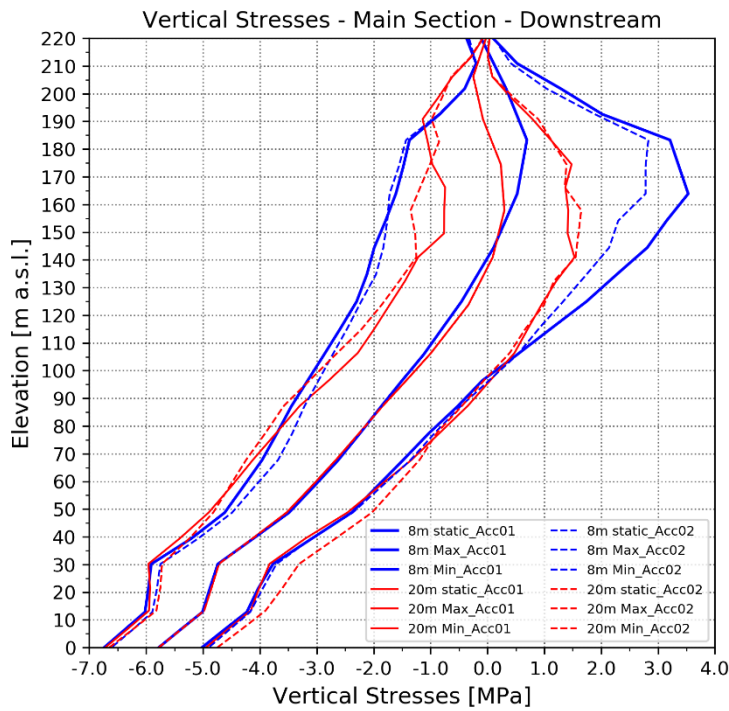


Figure 97: Vertical stresses of the dams with an 8 m crest width and a 20 m crest width in the main section along the downstream face

Vertical Stresses – Left Section – Upstream

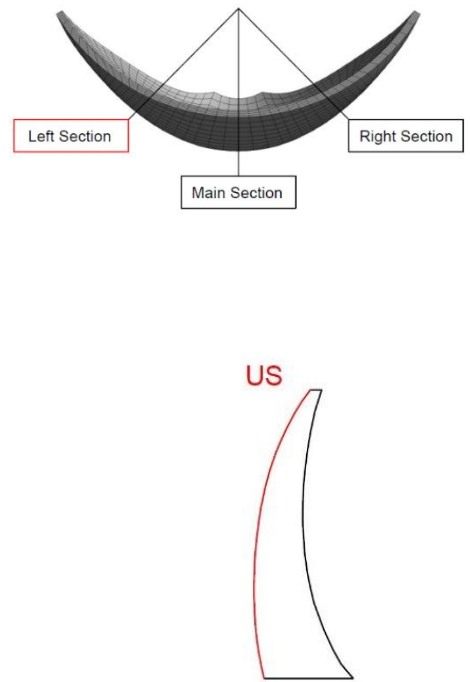
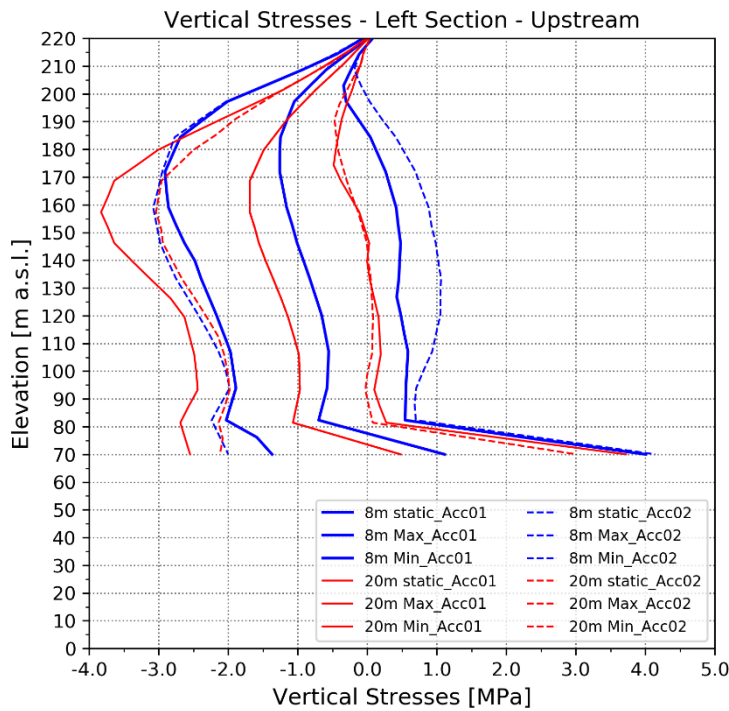


Figure 98: Vertical stresses of the dams with an 8 m crest width and a 20 m crest width in the left section along the upstream face

Vertical Stresses – Left Section – Downstream

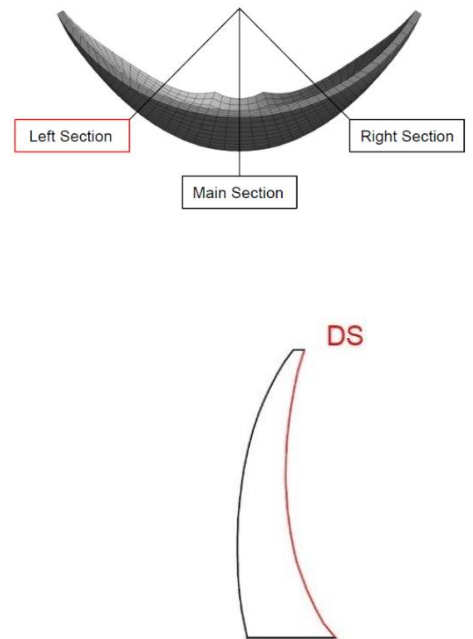
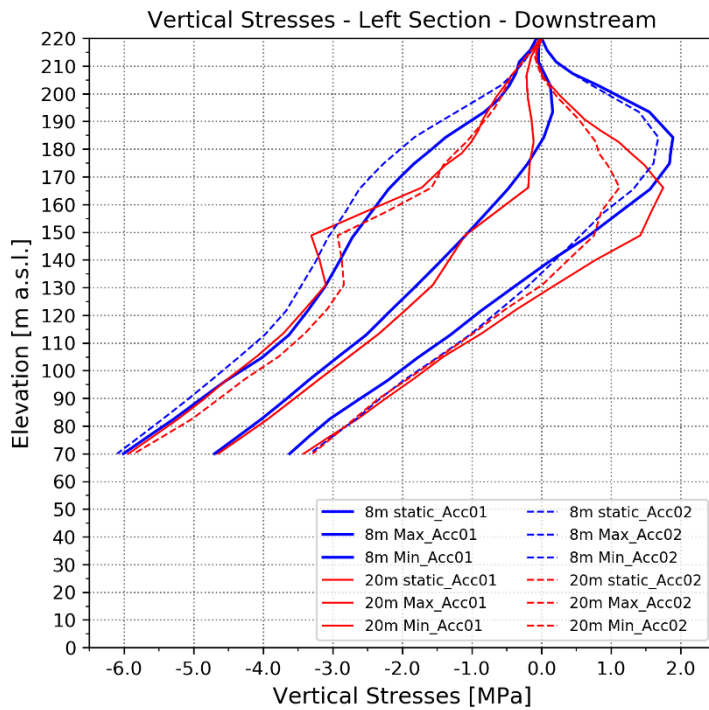


Figure 99: Vertical stresses of the dams with an 8 m crest width and a 20 m crest width in the left section along the downstream face

Vertical Stresses – Right Section – Upstream

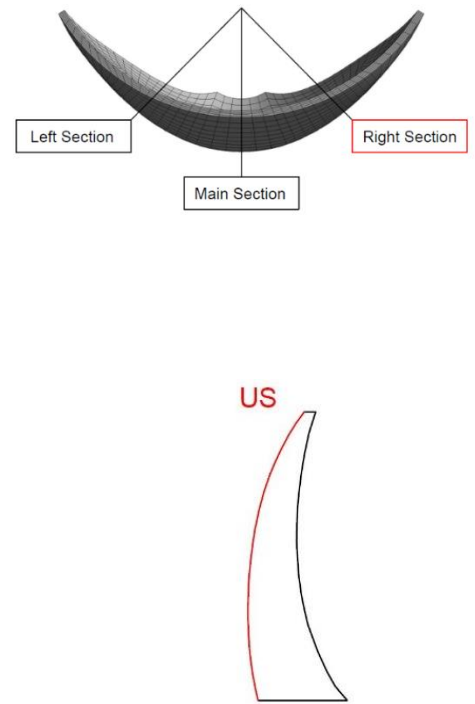
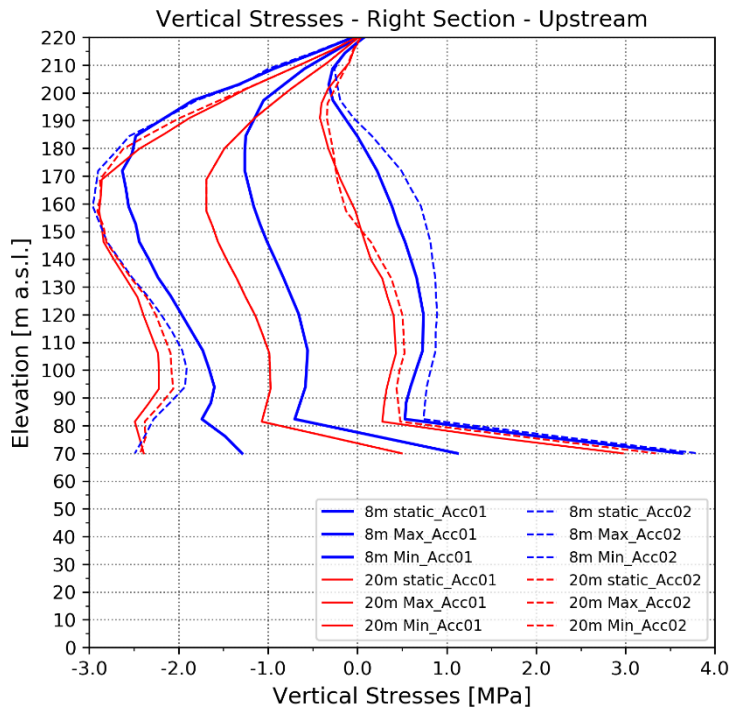


Figure 100: Vertical stresses of the dams with an 8 m crest width and a 20 m crest width in the right section along the upstream face

Vertical Stresses – Right Section – Downstream

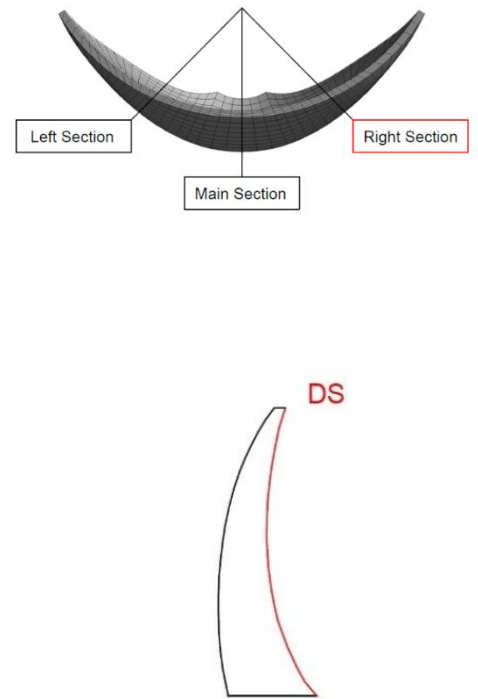
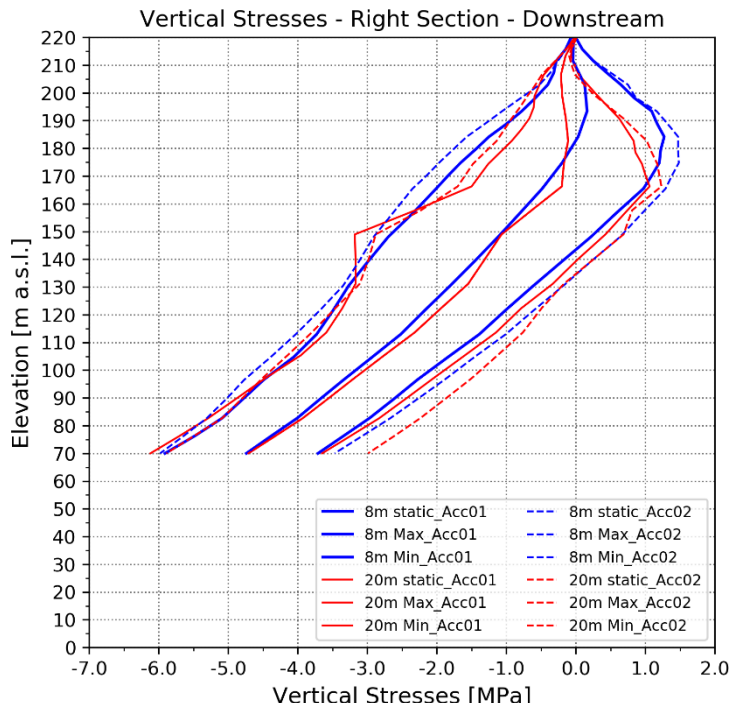


Figure 101: Vertical stresses of the dams with an 8 m crest width and a 20 m crest width in the right section along the downstream face

Vertical Stress - Main Section - US					
160 m	Static load	dynamic load			
Crest thickness	Vertical Stress [MPa]	min. Vertical Stress [MPa]	Difference from static load in %	max. Vertical Stress [MPa]	Difference from static load in %
8 m	-2.45	-5.10	100.0	0.22	100.0
9 m	-2.57	-5.00	91.7	0.06	98.5
10 m	-2.68	-5.20	95.1	-0.14	95.1
12 m	-2.87	-5.30	91.7	-0.63	83.9
14 m	-3.00	-5.30	86.8	-1.13	70.0
20 m	-3.43	-5.21	67.2	-1.49	72.7

Table 48: Vertical stresses at the main section - upstream

Vertical Stress - Main Section - DS					
170 m	Static load	dynamic load			
Crest thickness	Vertical Stress [MPa]	min. Vertical Stress [MPa]	Difference from static load in %	max. Vertical Stress [MPa]	Difference from static load in %
8 m	0.58	-1.60	100.0	2.78	100.0
9 m	0.60	-1.40	91.7	2.60	90.9
10 m	0.62	-1.30	88.1	2.50	85.5
12 m	0.60	-1.10	78.0	2.30	77.3
14 m	0.58	-0.90	67.9	2.00	64.5
20 m	0.25	-1.10	61.9	1.37	50.9

Table 49: Vertical stresses at the main section – downstream

Vertical Stress - Left Section - US					
160 m	Static load	dynamic load			
Crest thickness	Vertical Stress [MPa]	min. Vertical Stress [MPa]	Difference from static load in %	max. Vertical Stress [MPa]	Difference from static load in %
8 m	-1.16	-3.08	100.0	0.88	100.0
9 m	-1.24	-3.05	94.3	0.67	93.6
10 m	-1.32	-3.17	96.4	0.49	88.7
12 m	-1.44	-3.35	99.5	0.26	83.3
14 m	-1.53	-3.34	94.3	0.16	82.8
20 m	-1.69	-3.00	68.2	-0.13	76.5

Table 50: Vertical stresses at the left section – upstream

Vertical Stress - Left Section - DS					
180 m	Static load	dynamic load			
Crest thickness	Vertical Stress [MPa]	min. Vertical Stress [MPa]	Difference from static load in %	max. Vertical Stress [MPa]	Difference from static load in %
8 m	-0.08	-2.05	100.0	1.64	100.0
9 m	-0.04	-1.89	93.9	1.64	97.7
10 m	-0.02	-1.73	86.8	1.58	93.0
12 m	-0.01	-1.51	76.1	1.37	80.2
14 m	-0.02	-1.42	71.1	1.11	65.7
20 m	-0.14	-1.20	53.8	0.83	56.4

Table 51: Vertical stresses at the left section - downstream

Vertical Stress - Right Section - US					
160 m	Static load	dynamic load			
Crest thickness	Vertical Stress [MPa]	min. Vertical Stress [MPa]	Difference from static load in %	max. Vertical Stress [MPa]	Difference from static load in %
8 m	-1.16	-2.96	100.0	0.71	100.0
9 m	-1.24	-2.91	92.8	0.63	100.0
10 m	-1.32	-2.89	87.2	0.52	98.4
12 m	-1.44	-2.93	82.8	0.25	90.4
14 m	-1.53	-2.83	72.2	0.07	85.6
20 m	-1.69	-2.90	67.2	-0.12	84.0

Table 52: Vertical stresses at the right section – upstream

Vertical Stress - Right Section - DS					
180 m	Static load	dynamic load			
Crest thickness	Vertical Stress [MPa]	min. Vertical Stress [MPa]	Difference from static load in %	max. Vertical Stress [MPa]	Difference from static load in %
8 m	-0.08	-1.77	100.0	1.47	100.0
9 m	-0.04	-1.67	96.4	1.42	94.2
10 m	-0.02	-1.56	91.1	1.33	87.1
12 m	-0.01	-1.50	88.2	1.24	80.6
14 m	-0.02	-1.43	83.4	1.24	81.3
20 m	-0.14	-1.30	68.6	1.05	76.8

Table 53: Vertical stresses at the right section – downstream

Vertical Stress - Downstream

The results from the calculation before do not vary much from the results with the new acceleration. Only the results in the main section for the maxima time series shows a difference of around 1 MPa for the arch dam with a dam crest of 8 m.

The compressive stresses increase on the on the left side of the dam. The right side is different, as the tensile stresses for the minima time series decrease but increase for the maxima time series.

Vertical Stress - Upstream

Same as in the calculation before, the compressive stresses decrease in the left, right and main section, as the crest of the arch dam increases.

The results from the calculation before do not vary much from the results with the new acceleration in the main section.

Minimum Principal Stresses – Main Section – Upstream

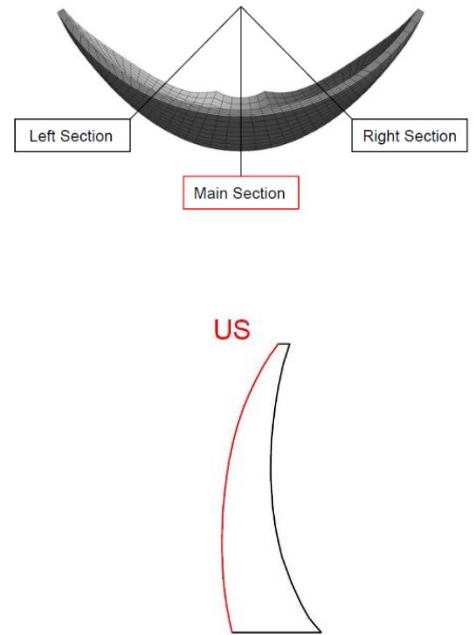
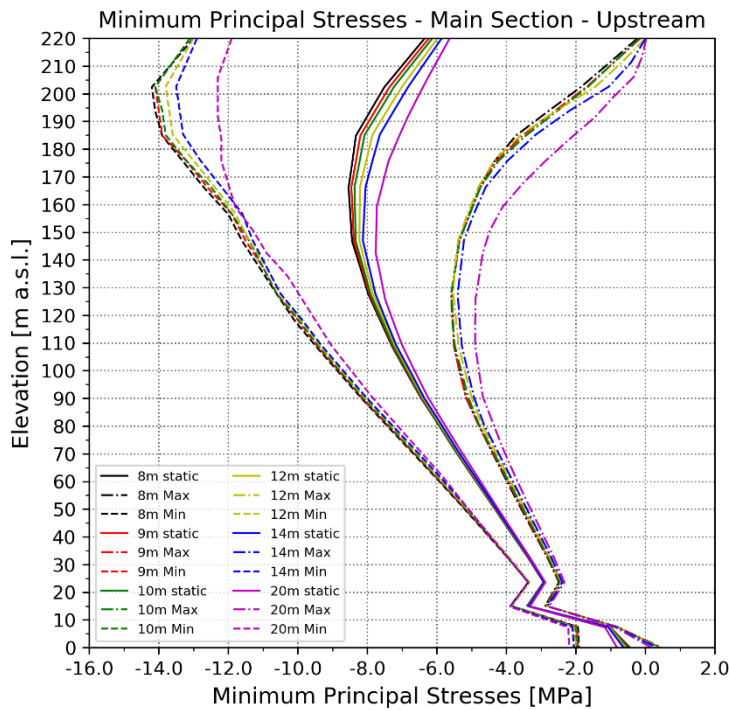


Figure 102: Minimum principal stresses at the main section - upstream

Minimum Principal Stresses – Main Section – Downstream

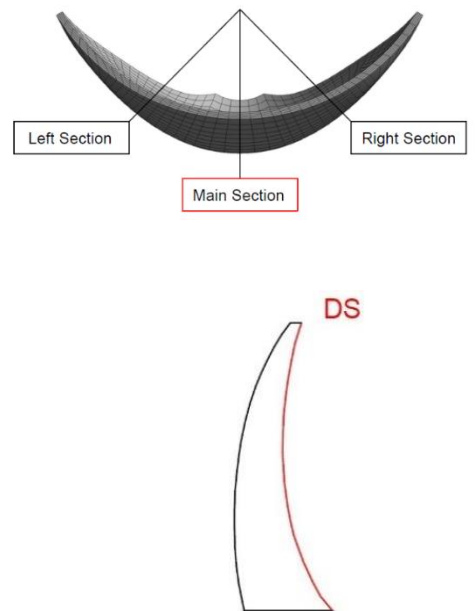
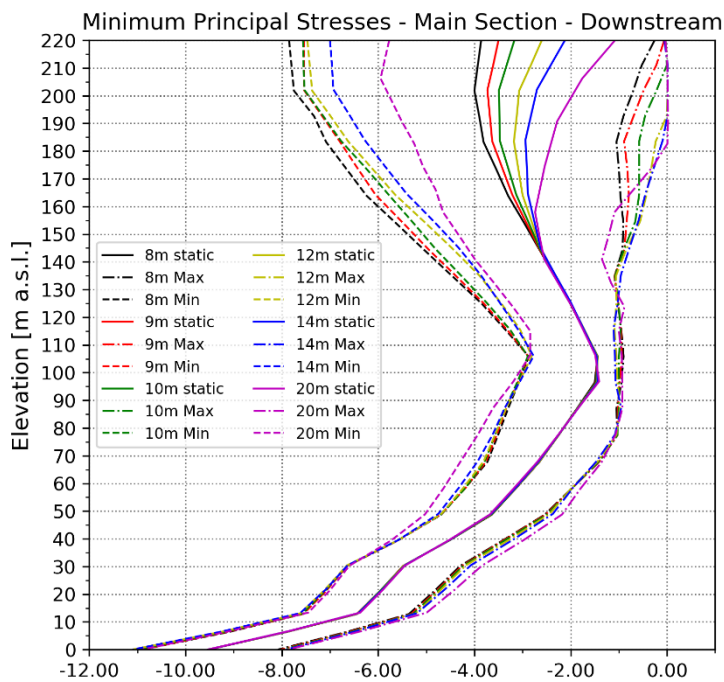


Figure 103: Minimum principal stresses at the main section - downstream

Minimum Principal Stresses – Left Section – Upstream

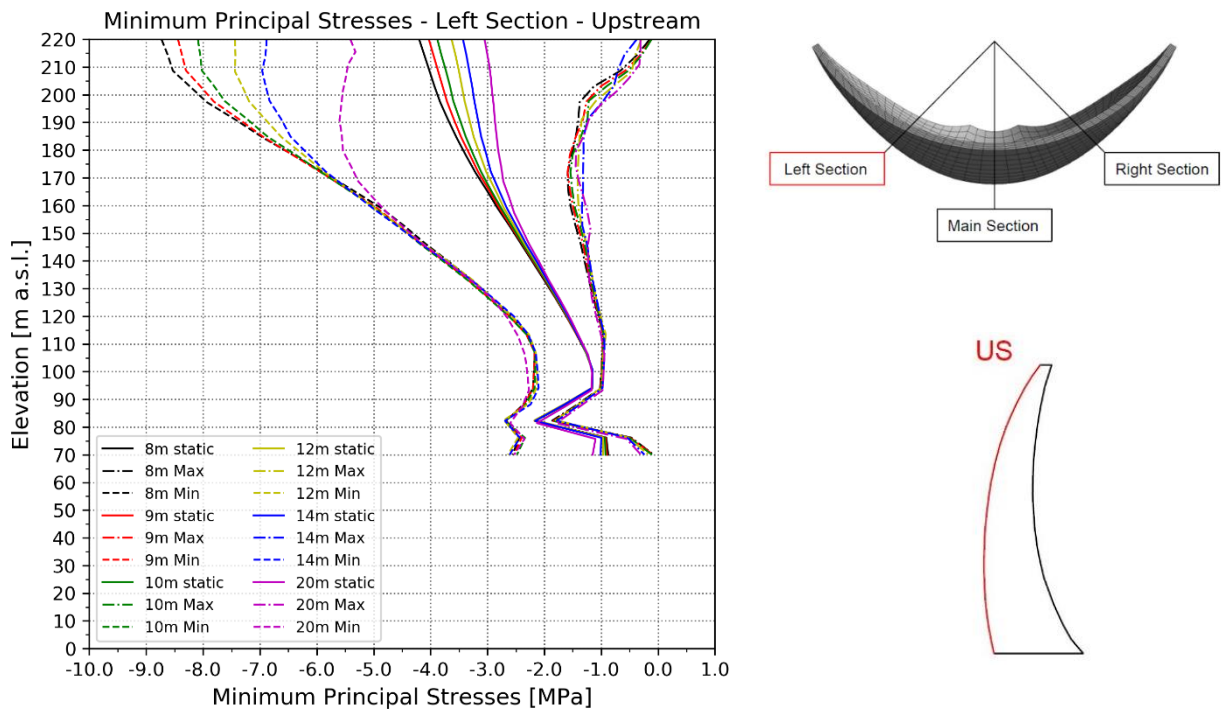


Figure 104: Minimum principal stresses at the left section - upstream

Minimum Principal Stresses – Left Section – Downstream

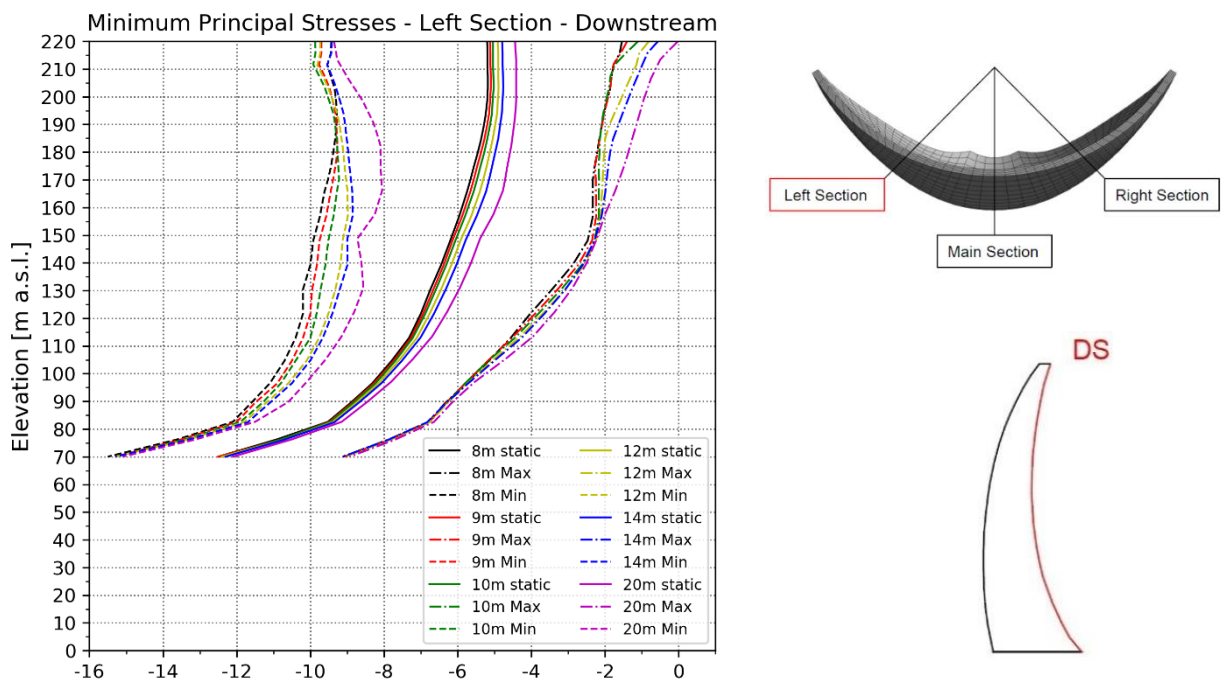


Figure 105: Minimum principal stresses at the left section - downstream

Minimum Principal Stresses – Right Section – Upstream

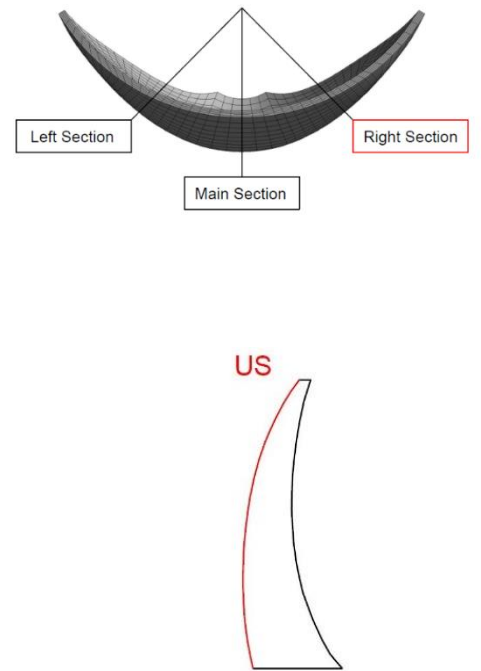
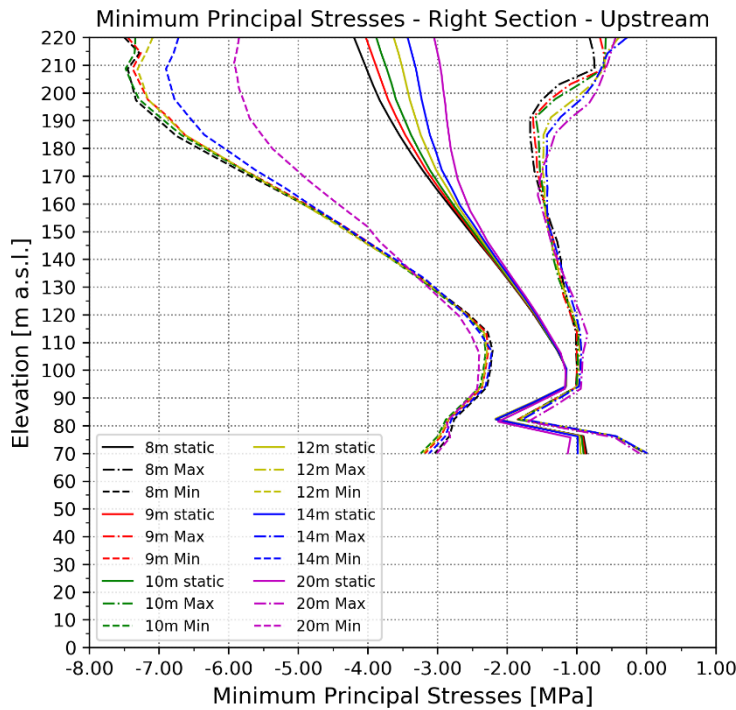


Figure 106: Minimum principal stresses at the right section - upstream

Minimum Principal Stresses – Right Section – Downstream

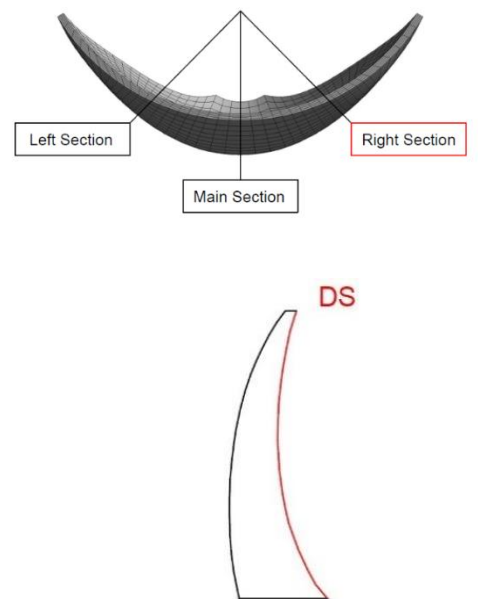
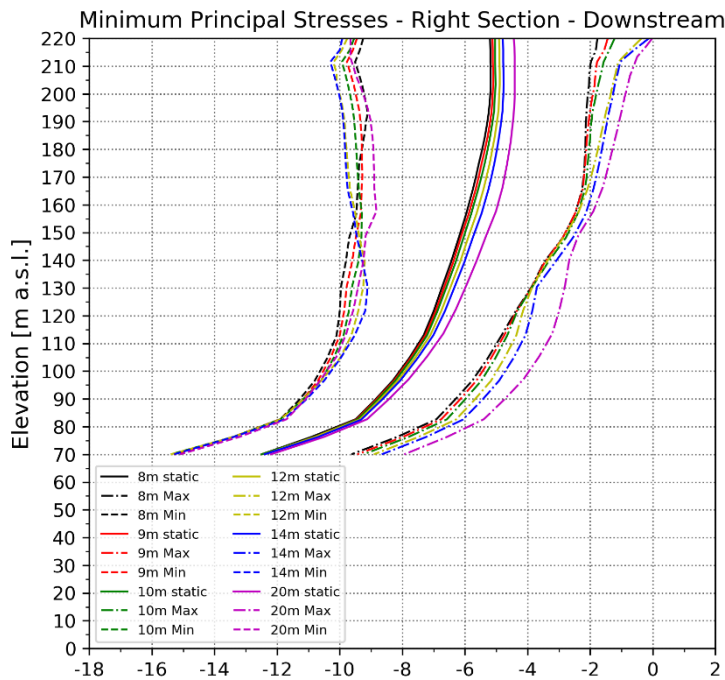


Figure 107: Minimum principal stresses at the right section - downstream

Minimum Principal Stresses – Main Section – Upstream

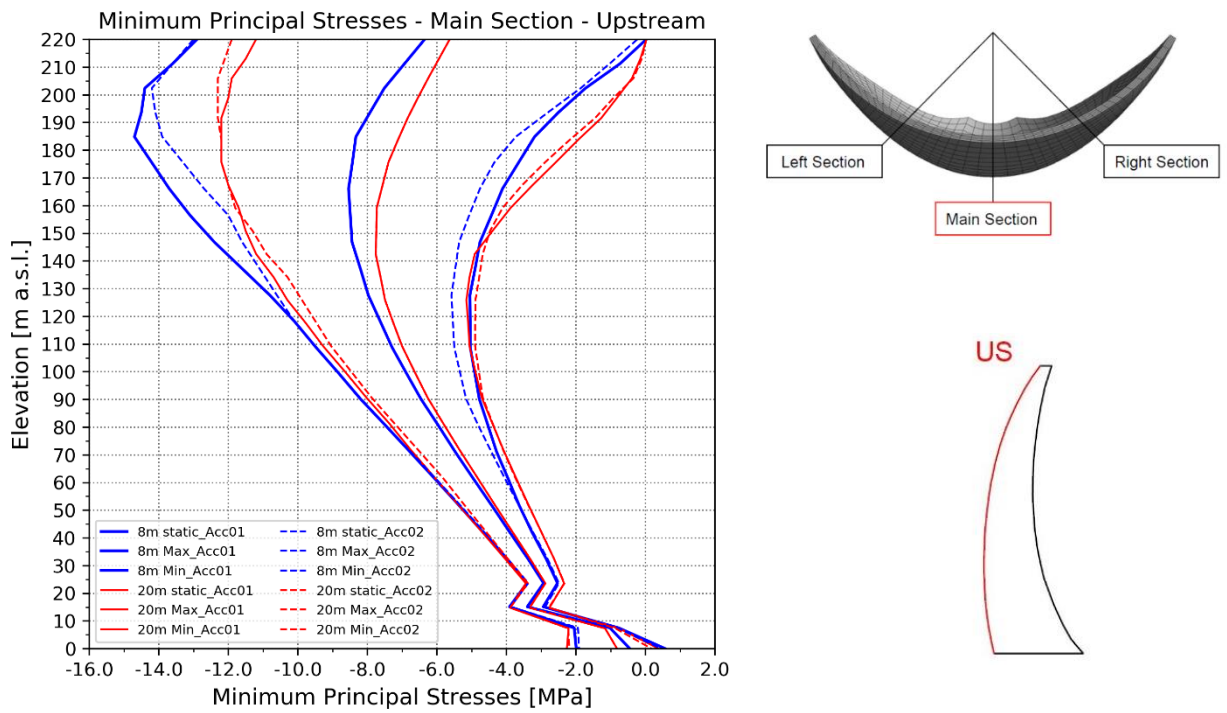


Figure 108: Minimum principal stresses of the dams with an 8 m crest width and a 20 m crest width in the main section along the upstream face

Minimum Principal Stresses – Main Section – Downstream

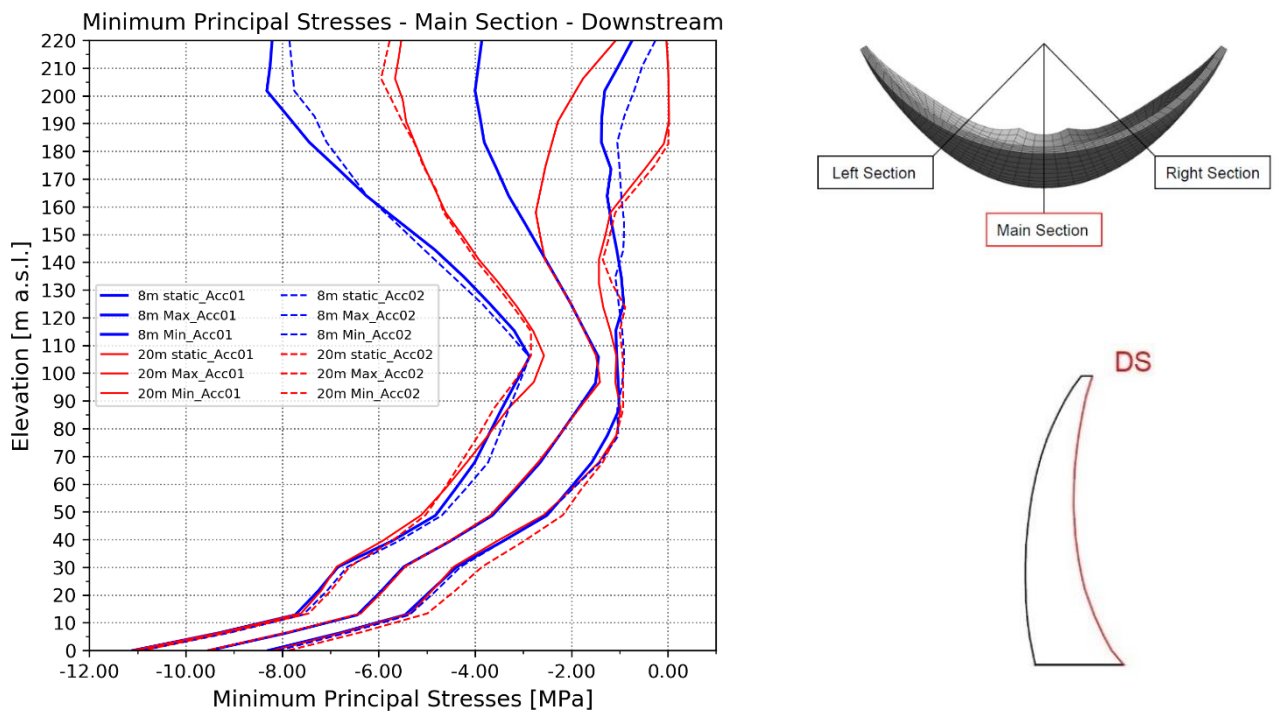


Figure 109: Minimum principal stresses of the dams with an 8 m crest width and a 20 m crest width in the main section along the downstream face

Minimum Principal Stresses – Left Section – Upstream

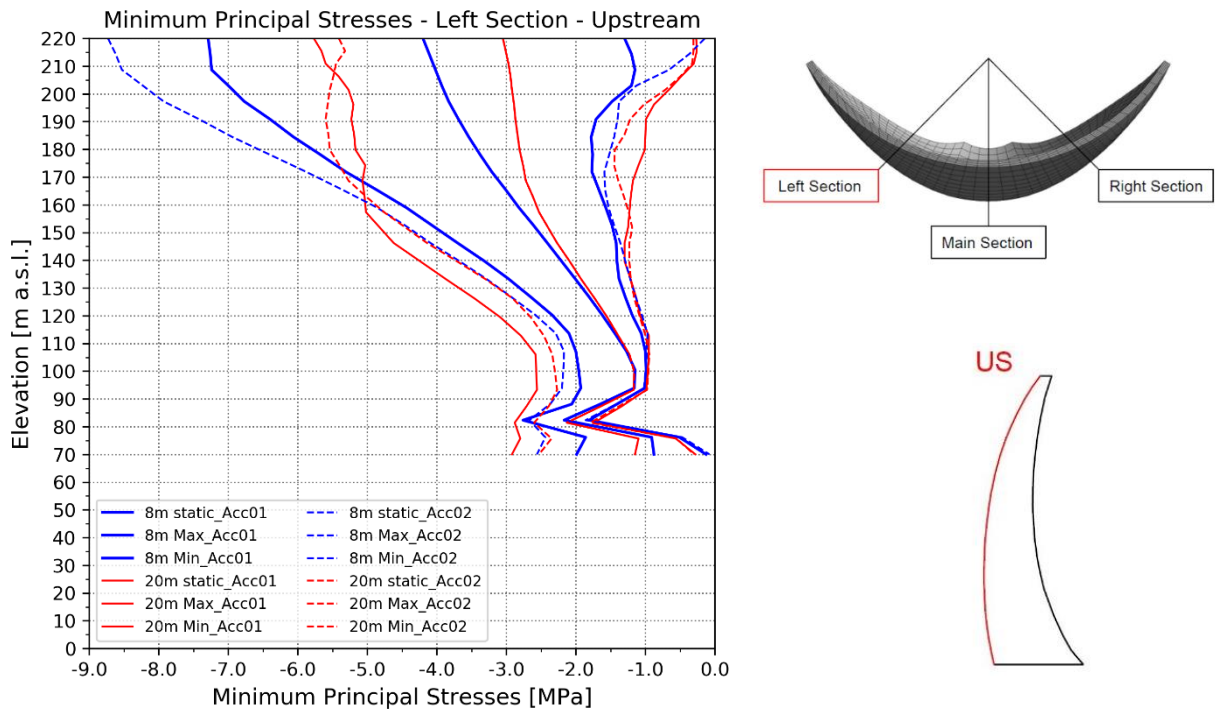


Figure 110: Minimum principal stresses of the dams with an 8 m crest width and a 20 m crest width in the left section along the upstream face

Minimum Principal Stresses – Left Section – Downstream

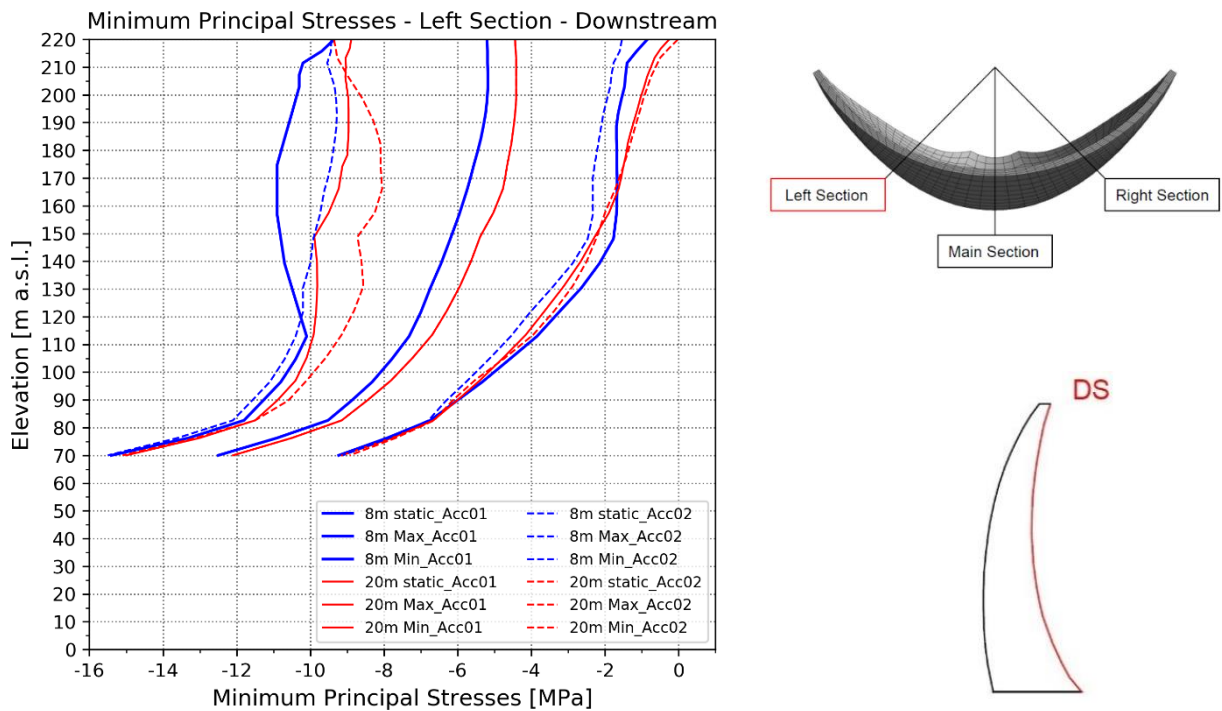


Figure 111: Minimum principal stresses of the dams with an 8 m crest width and a 20 m crest width in the left section along the downstream face

Minimum Principal Stresses – Right Section – Upstream

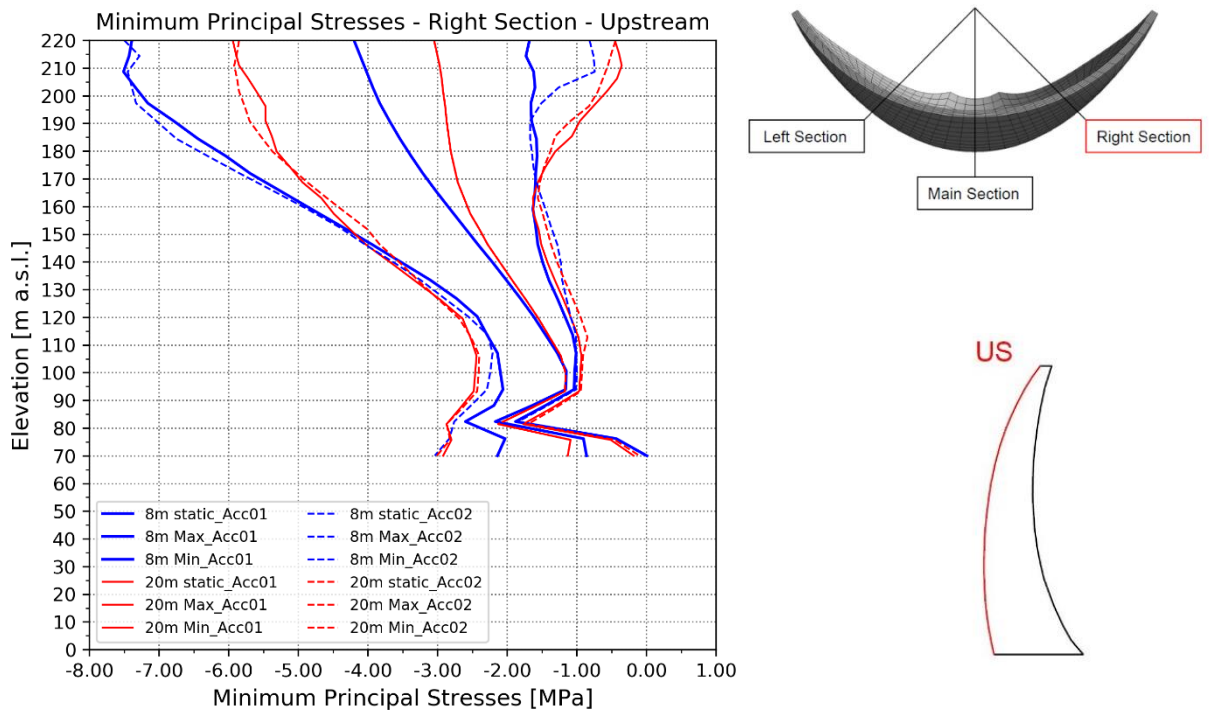


Figure 112: Minimum principal stresses of the dams with an 8 m crest width and a 20 m crest width in the right section along the upstream face

Minimum Principal Stresses – Right Section – Downstream

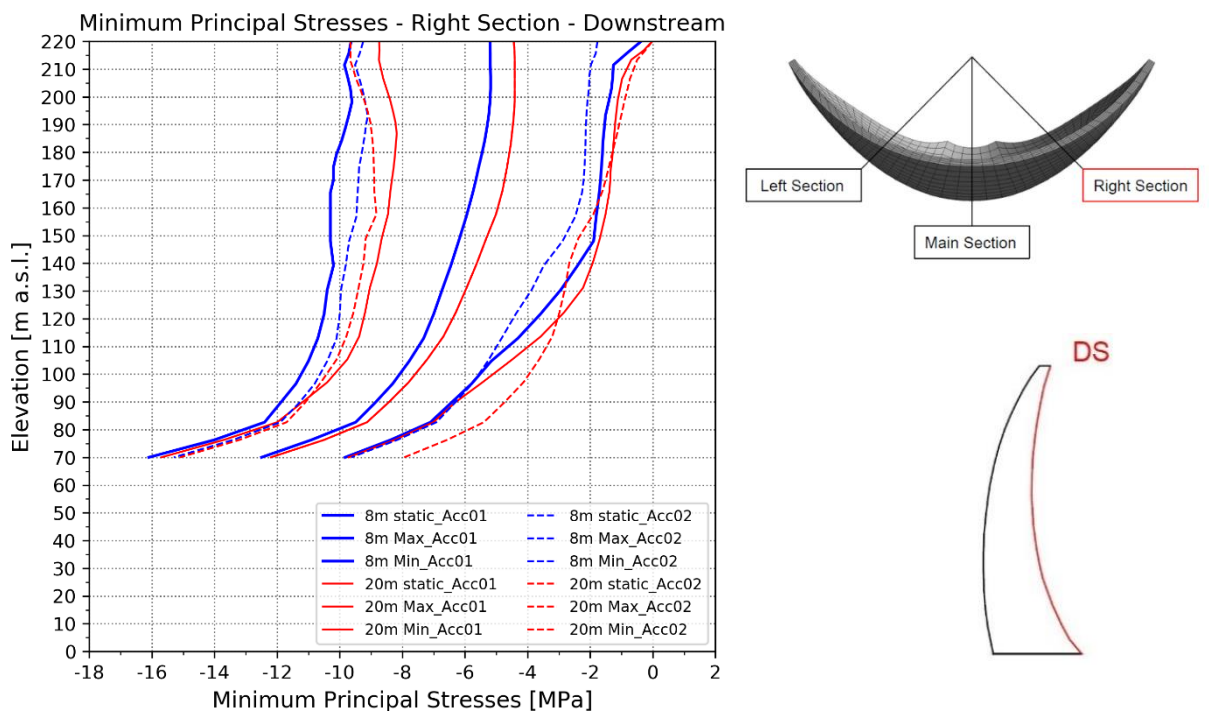


Figure 113: Minimum principal stresses of the dams with an 8 m crest width and a 20 m crest width in the right section along the downstream face

Minimum Principal Stress - Main Section - US					
180 m	Static load	dynamic load			
Crest thickness	Minimum Principal Stress [MPa]	min. Minimum Principal Stress [MPa]	Difference from static load in %	max. Minimum Principal Stress [MPa]	Difference from static load in %
8 m	-8.40	-13.30	100.0	-4.35	100.0
9 m	-8.20	-13.20	102.0	-4.30	96.3
10 m	-8.10	-13.20	104.1	-4.23	95.6
12 m	-8.00	-13.00	102.0	-4.35	90.1
14 m	-7.80	-12.80	102.0	-3.96	94.8
20 m	-7.30	-12.20	100.0	-2.88	109.1

Table 54: Minimum principal stresses at the main section - upstream

Minimum Principal Stress - Main Section - DS					
220 m	Static load	dynamic load			
Crest thickness	Minimum Principal Stress [MPa]	min. Minimum Principal Stress [MPa]	Difference from static load in %	max. Minimum Principal Stress [MPa]	Difference from static load in %
8 m	-3.86	-7.85	100.0	-0.26	100.0
9 m	-3.50	-7.54	101.3	-0.06	95.6
10 m	-3.17	-7.56	110.0	-0.03	87.2
12 m	-2.60	-7.47	122.1	-0.03	71.4
14 m	-2.12	-7.00	122.3	-0.05	57.5
20 m	-1.08	-5.77	117.5	-0.03	29.2

Table 55: Minimum principal stresses at the main section – downstream

Minimum Principal Stress - Left Section - US					
220 m	Static load	dynamic load			
Crest thickness	Minimum Principal Stress [MPa]	min. Minimum Principal Stress [MPa]	Difference from static load in %	max. Minimum Principal Stress [MPa]	Difference from static load in %
8 m	-4.20	-13.00	100.0	-0.23	100.0
9 m	-4.03	-13.10	103.1	-0.15	97.7
10 m	-3.88	-13.10	104.8	-0.19	92.9
12 m	-3.63	-13.00	106.5	0.00	91.4
14 m	-3.43	-12.90	107.6	0.00	86.4
20 m	-3.05	-11.90	100.6	0.01	77.1

Table 56: Minimum principal stresses at the left section – upstream

Minimum Principal Stress - Left Section - DS					
180 m	Static load	dynamic load			
Crest thickness	Minimum Principal Stress [MPa]	min. Minimum Principal Stress [MPa]	Difference from static load in %	max. Minimum Principal Stress [MPa]	Difference from static load in %
8 m	-5.46	-9.38	100.0	-2.22	100.0
9 m	-5.37	-9.27	99.5	-2.21	97.5
10 m	-5.28	-9.26	101.5	-2.15	96.6
12 m	-5.13	-9.10	101.3	-2.02	96.0
14 m	-4.98	-8.97	101.8	-1.86	96.3
20 m	-4.60	-8.09	89.0	-1.40	98.8

Table 57: Minimum principal stresses at the left section - downstream

Minimum Principal Stress - Right Section - US					
220 m	Static load	dynamic load			
Crest thickness	Minimum Principal Stress [MPa]	min. Minimum Principal Stress [MPa]	Difference from static load in %	max. Minimum Principal Stress [MPa]	Difference from static load in %
8 m	-4.20	-7.50	100.0	-0.82	100.0
9 m	-4.03	-7.45	103.6	-0.67	99.4
10 m	-3.88	-7.34	104.8	-0.58	97.6
12 m	-3.63	-7.09	104.8	-0.39	95.9
14 m	-3.43	-6.72	99.7	-0.28	93.2
20 m	-3.05	-5.85	84.8	-0.44	77.2

Table 58: Minimum principal stresses at the right section – upstream

Minimum Principal Stress - Right Section - DS					
180 m	Static load	dynamic load			
Crest thickness	Minimum Principal Stress [MPa]	min. Minimum Principal Stress [MPa]	Difference from static load in %	max. Minimum Principal Stress [MPa]	Difference from static load in %
8 m	-5.70	-9.30	100.0	-2.16	100.0
9 m	-5.56	-9.29	103.6	-2.13	96.9
10 m	-5.50	-9.47	110.3	-2.04	97.7
12 m	-5.30	-9.78	124.4	-1.76	100.0
14 m	-5.15	-9.83	130.0	-1.63	99.4
20 m	-4.73	-8.92	116.4	-1.32	96.3

Table 59: Minimum principal stresses at the right section – downstream

Minimum Principal Stress - Downstream

The tensile stresses increase in the left section for the minima time series but decrease for the maxima time for the newly calculated results with the acceleration which has the excitation frequency close to the Eigenfrequency. Same appears on the right side.

Figure 103 shows that tensile stresses in the main section increase, with the increasing volume of the investigated geometries.

The results from the calculation before do not vary much from the results with the new acceleration in the main section.

Minimum Principal Stress - Upstream

At the upstream side the tensile stresses increase, same as for the results with the calculation made before, on the left, right side and in the main section.

Compared to the results of the calculation before, the minimum dynamic load on the left side shows more compressive stresses.

Maximum Principal Stresses – Main Section – Upstream

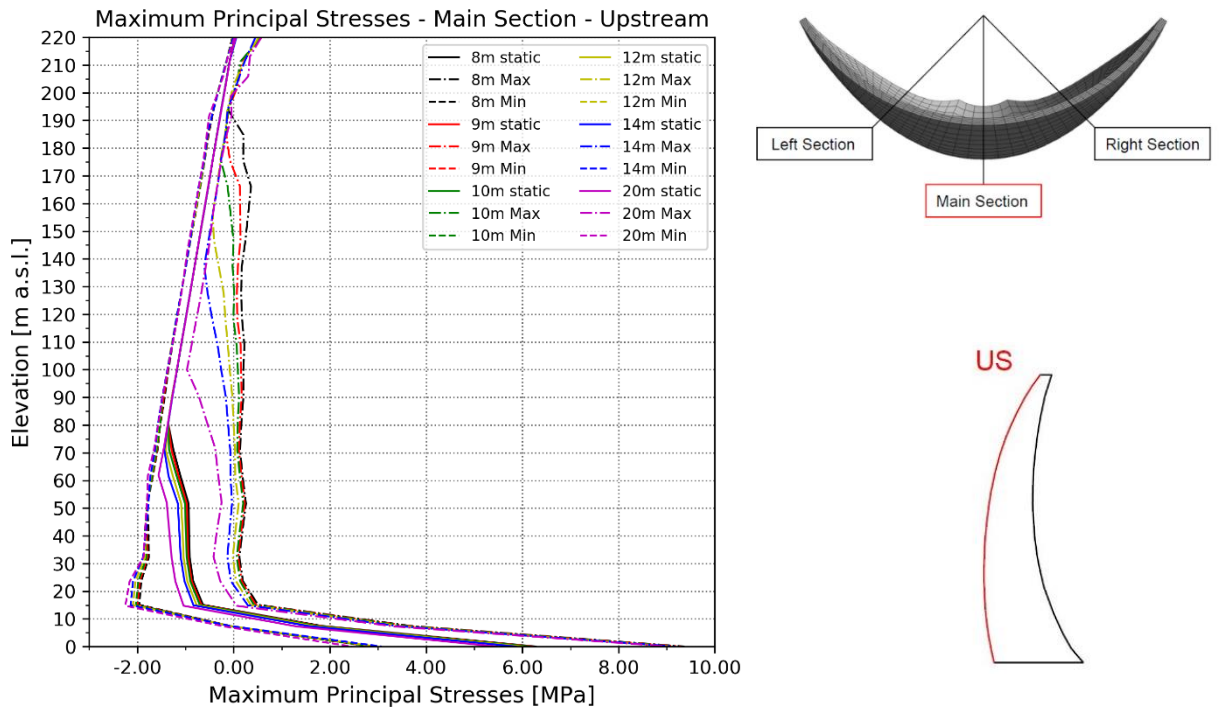


Figure 114: Maximum principal stresses at the main section - upstream

Maximum Principal Stresses – Main Section – Downstream

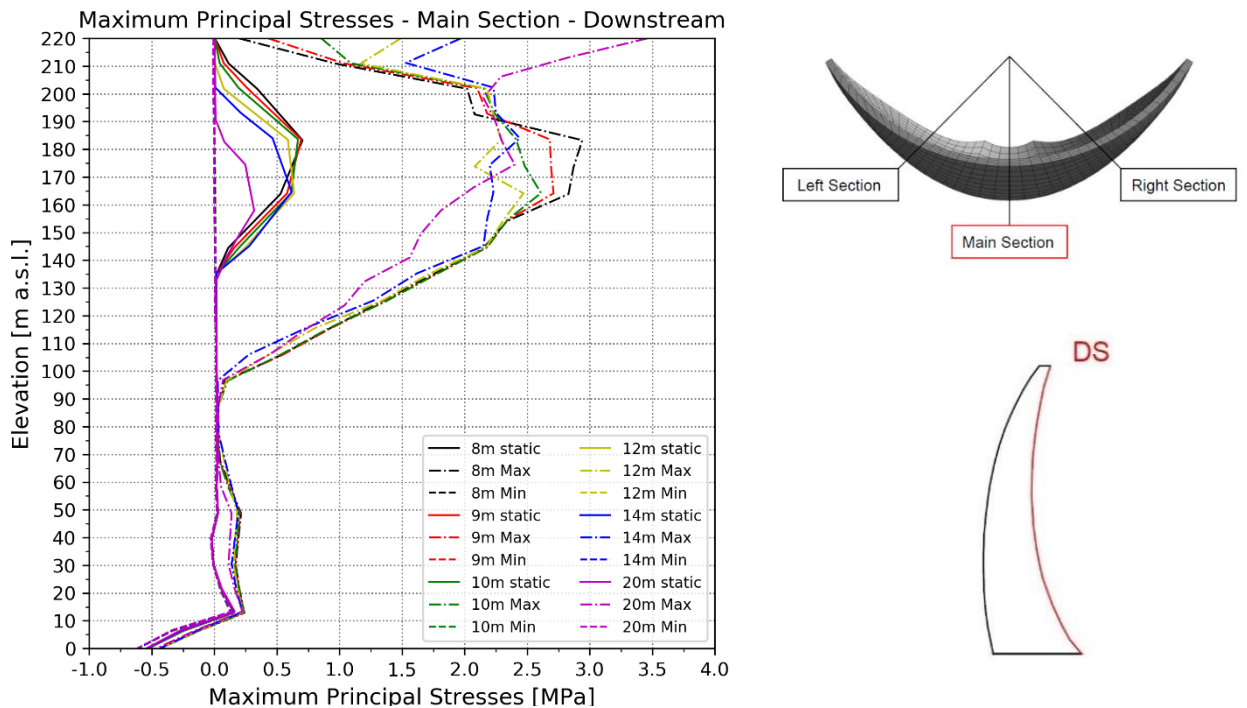


Figure 115: Maximum principal stresses at the main section - downstream

Maximum Principal Stresses – Left Section – Upstream

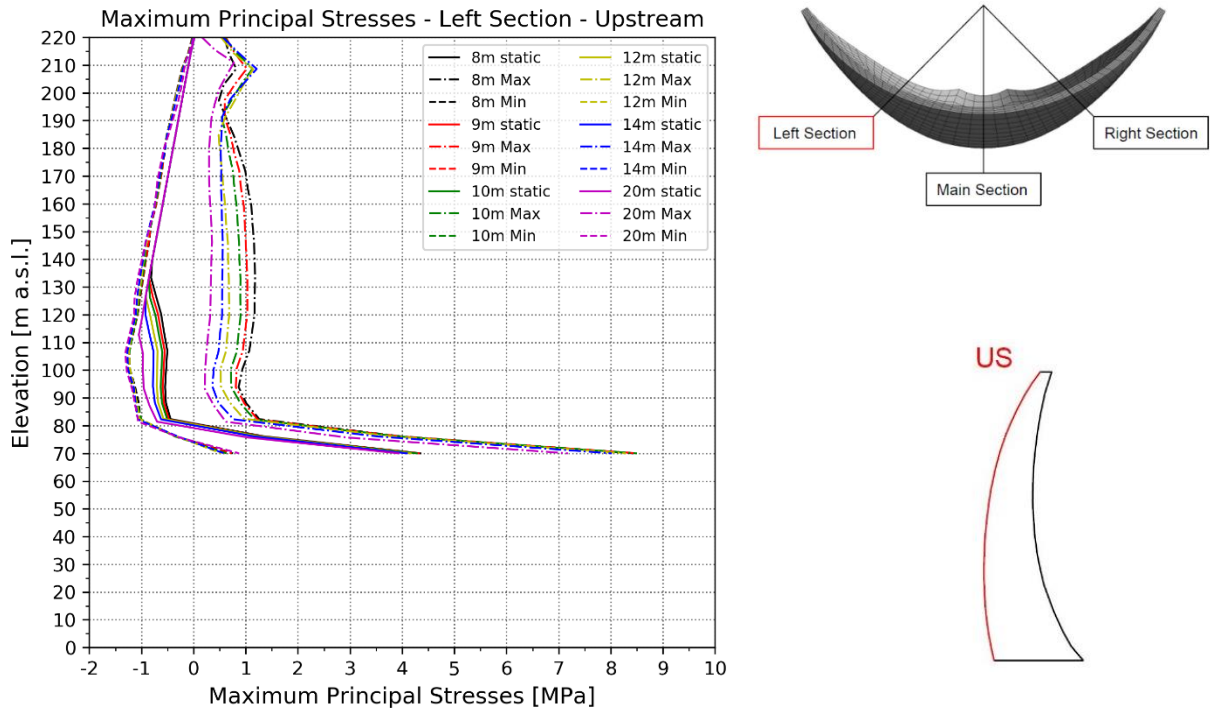


Figure 116: Maximum principal stresses at the left section - upstream

Maximum Principal Stresses – Left Section – Downstream

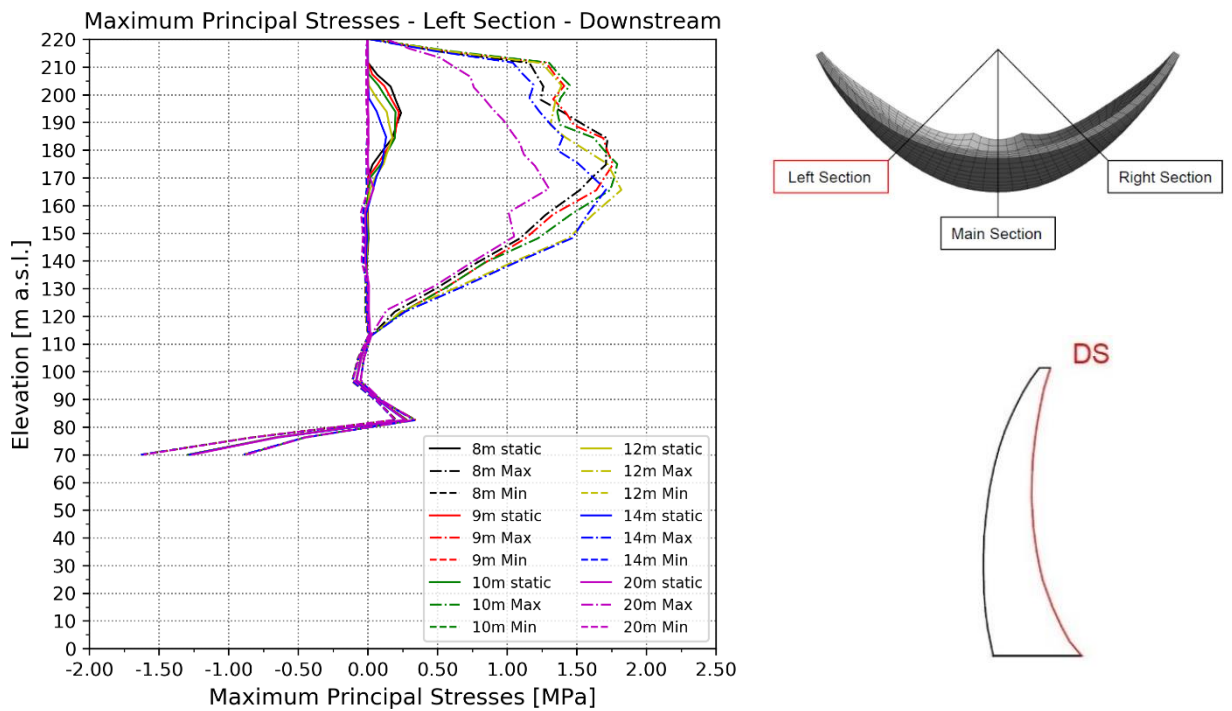


Figure 117: Maximum principal stresses at the left section - downstream

Maximum Principal Stresses – Right Section – Upstream

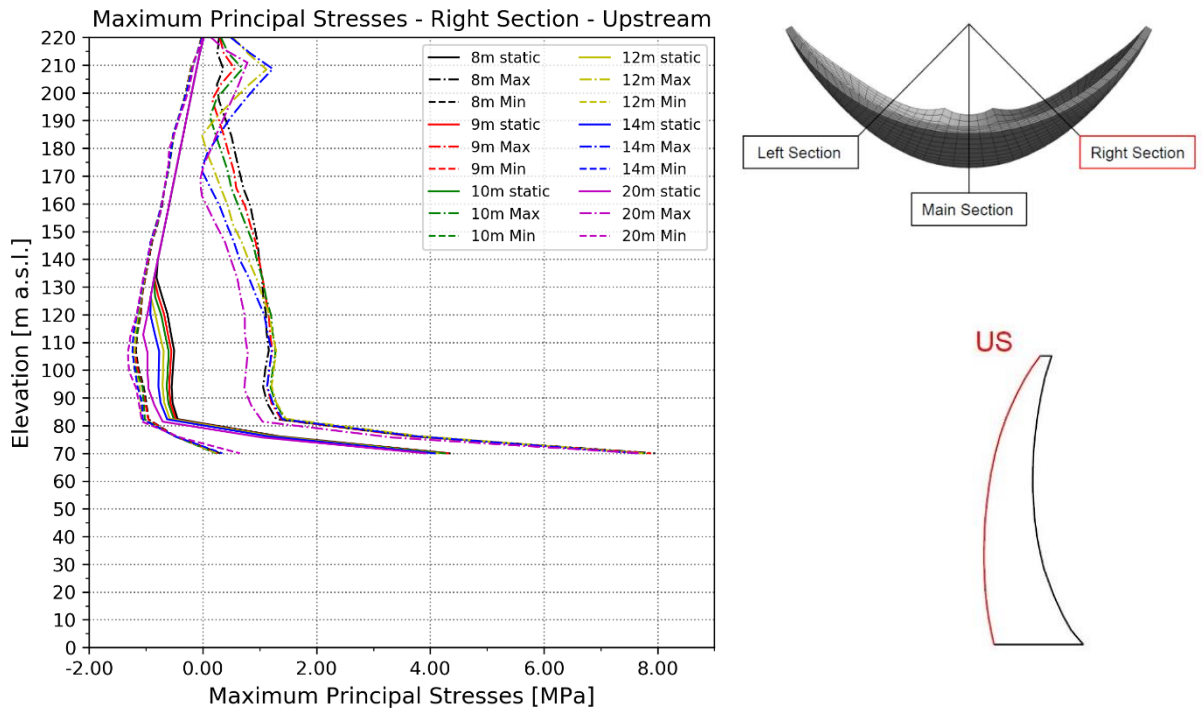


Figure 118: Maximum principal stresses at the right section - upstream

Maximum Principal Stresses – Right Section – Downstream

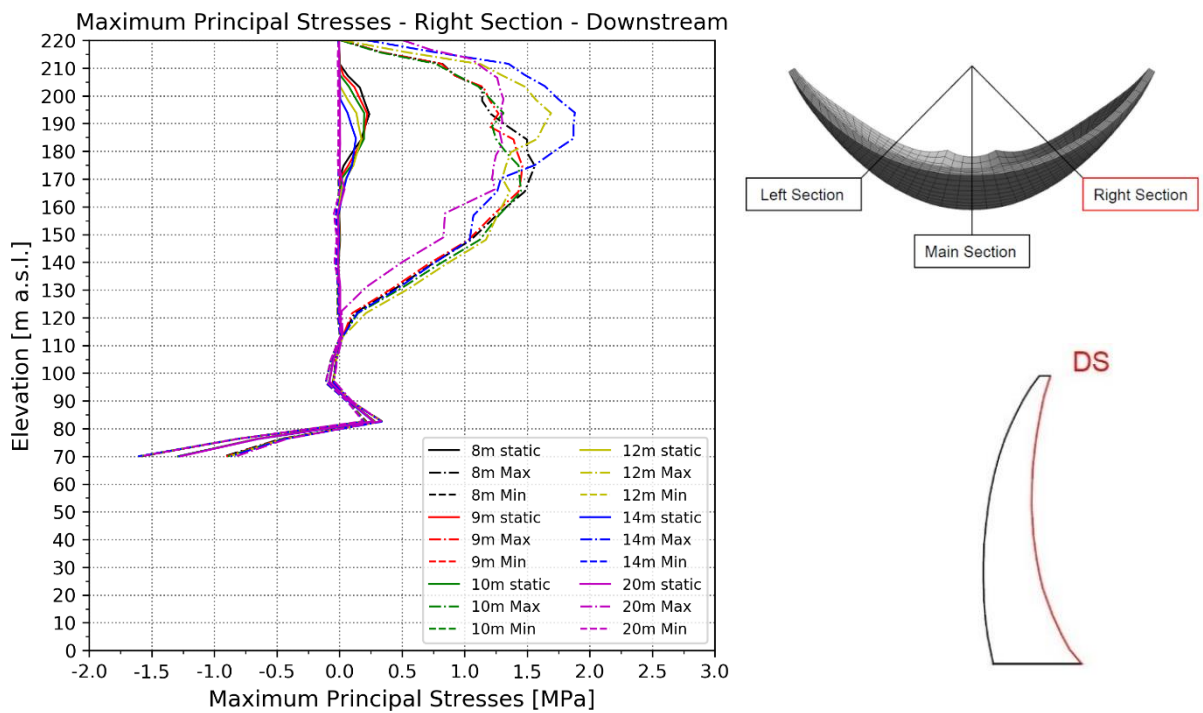


Figure 119: Maximum principal stresses at the right section - downstream

Maximum Principal Stresses – Main Section – Upstream

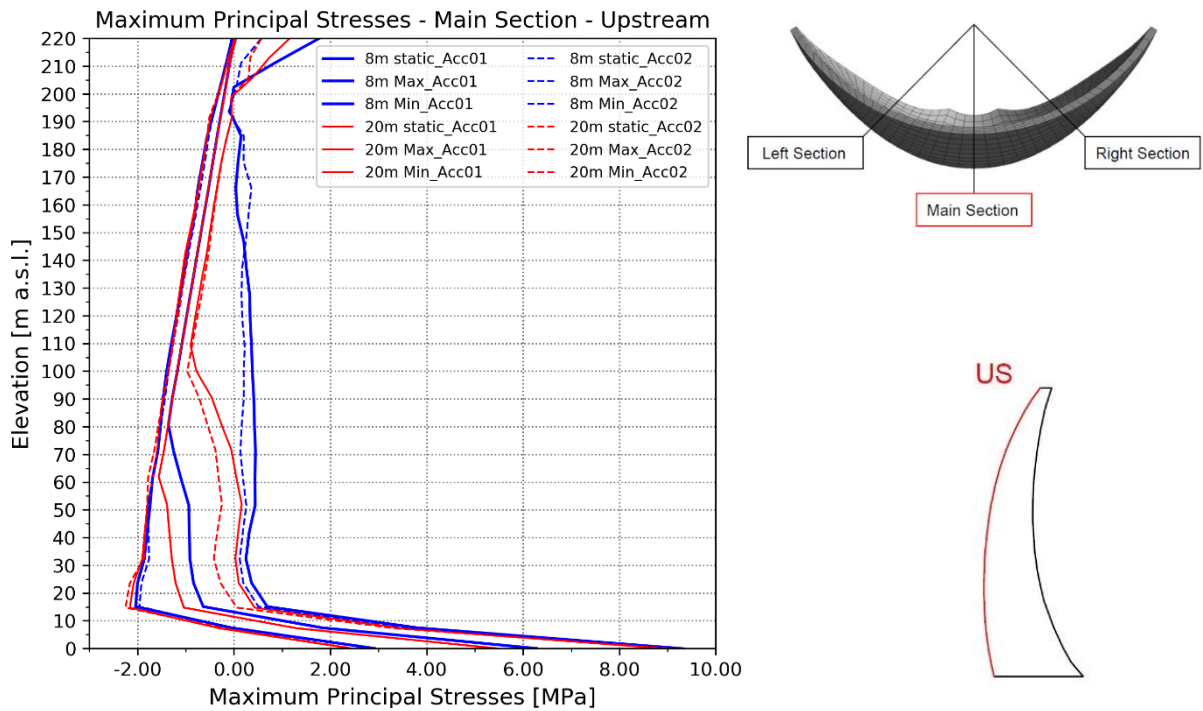


Figure 120: Maximum principal stresses of the dams with an 8 m crest width and a 20 m crest width in the main section along the upstream face

Maximum Principal Stresses – Main Section – Downstream

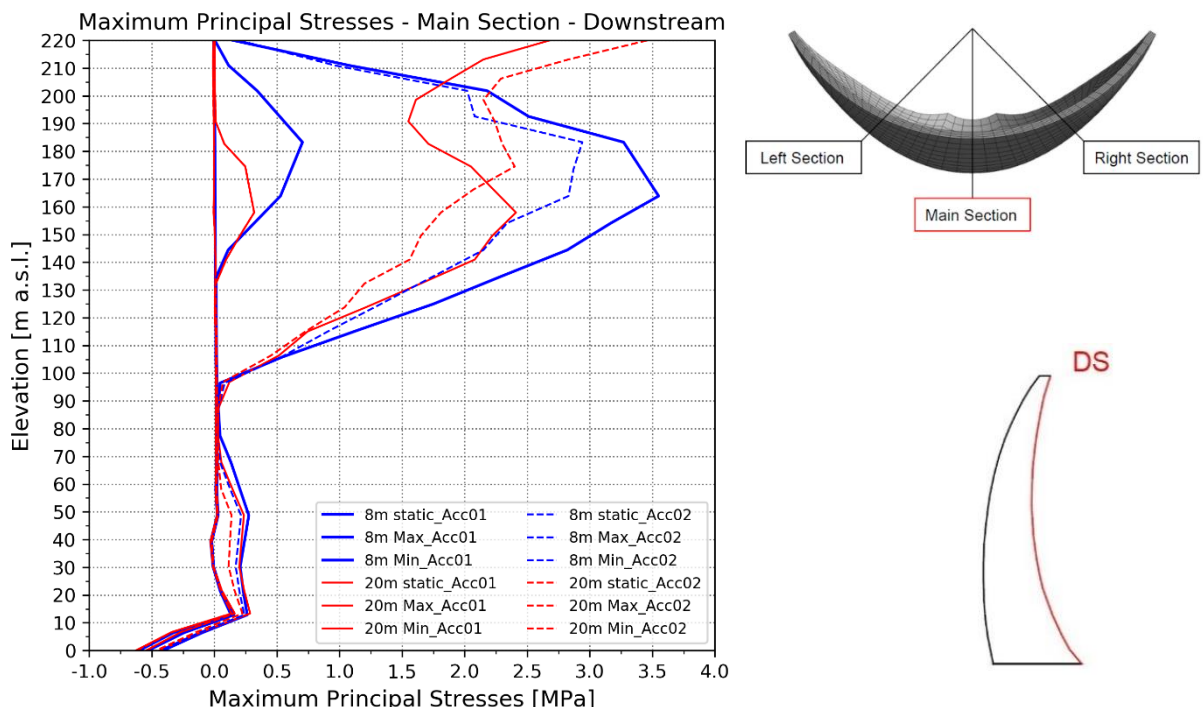


Figure 121: Maximum principal stresses of the dams with an 8 m crest width and a 20 m crest width in the main section along the downstream face

Maximum Principal Stresses – Left Section – Upstream

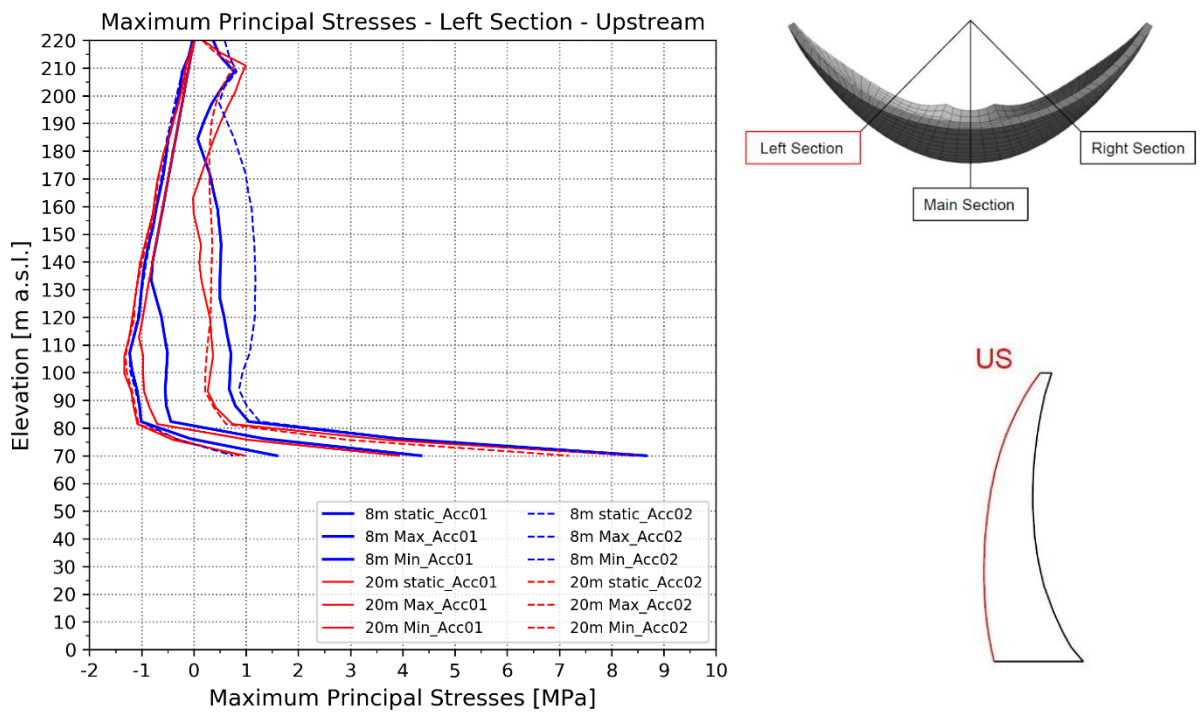


Figure 122: Maximum principal stresses of the dams with an 8 m crest width and a 20 m crest width in the left section along the upstream face

Maximum Principal Stresses – Left Section – Downstream

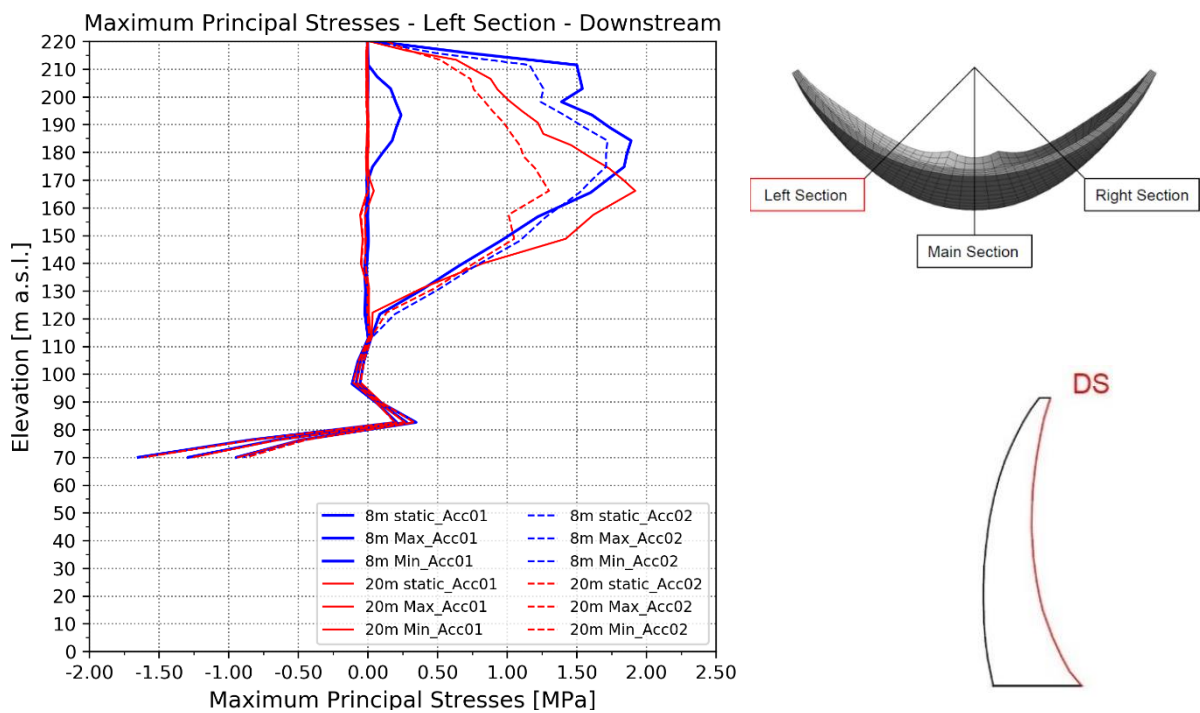


Figure 123: Maximum principal stresses of the dams with an 8 m crest width and a 20 m crest width in the left section along the downstream face

Maximum Principal Stresses – Right Section – Upstream

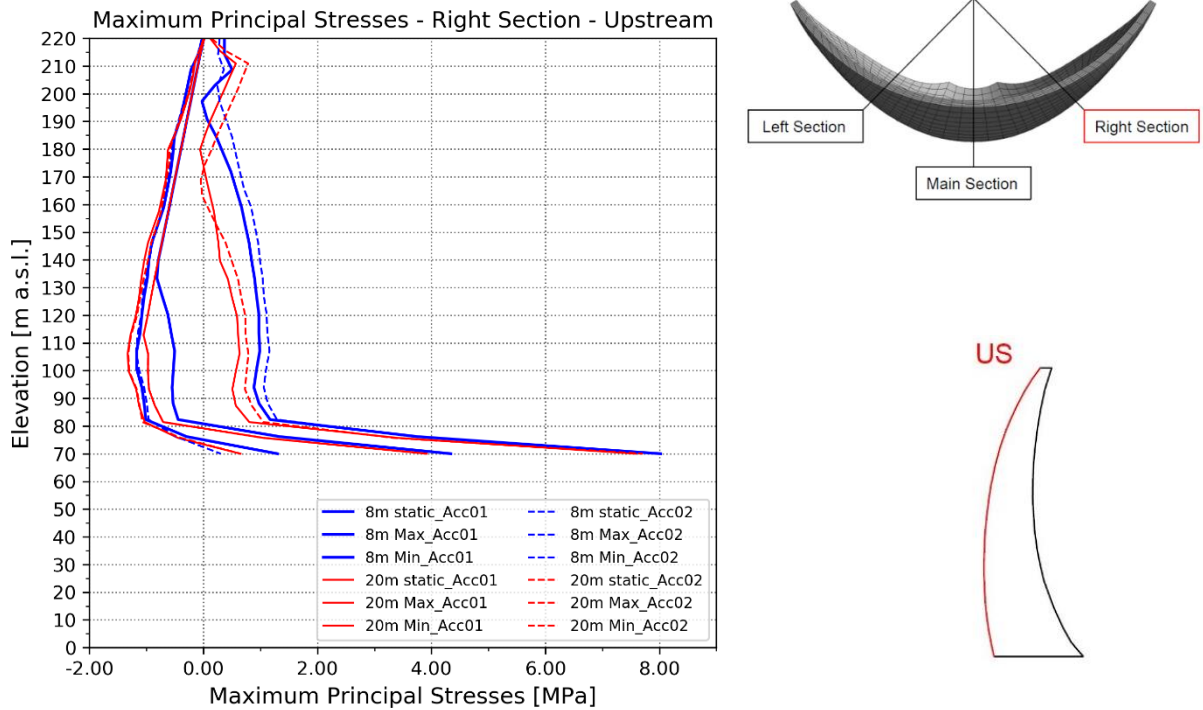


Figure 124: Maximum principal stresses of the dams with an 8 m crest width and a 20 m crest width in the right section along the upstream face

Maximum Principal Stresses – Right Section – Downstream

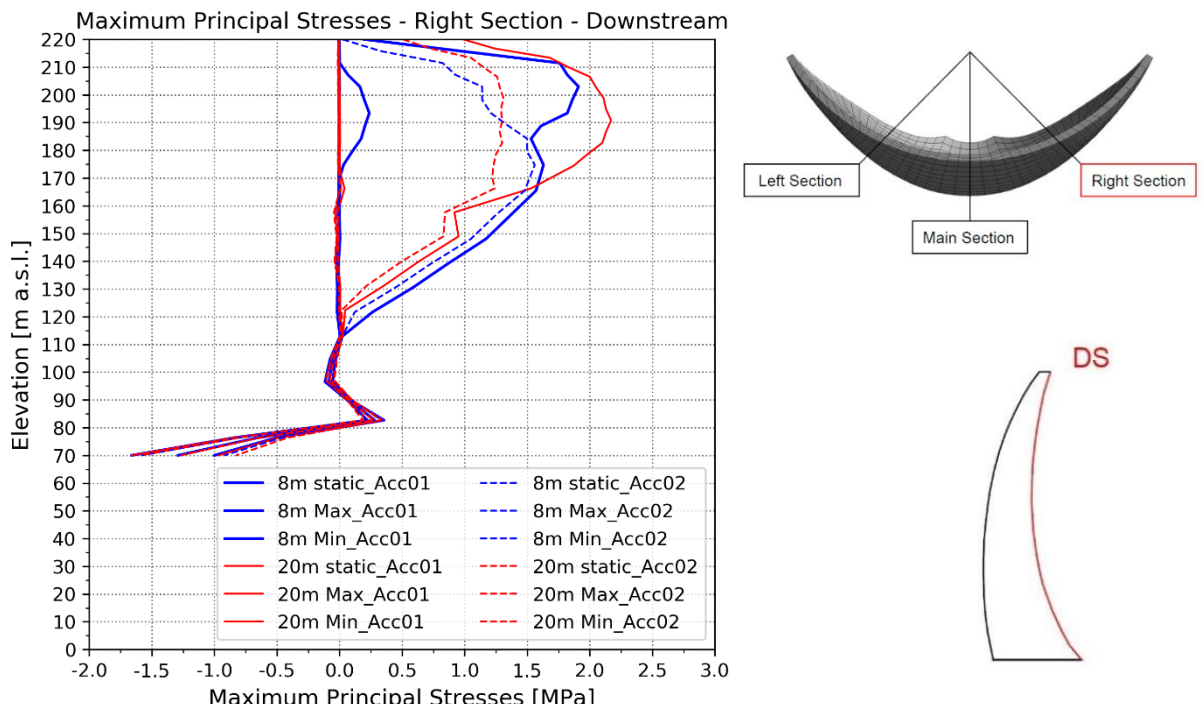


Figure 125: Maximum principal stresses of the dams with an 8 m crest width and a 20 m crest width in the right section along the downstream face

Maximum Principal Stress - Main Section - US					
50 m	Static load	dynamic load			
Crest thickness	Maximum Principal Stress [MPa]	min. Maximum Principal Stress [MPa]	Difference from static load in %	max. Maximum Principal Stress [MPa]	Difference from static load in %
8 m	-0.94	-1.78	100.0	0.26	100.0
9 m	-0.97	-1.80	98.8	0.23	100.0
10 m	-1.01	-1.79	92.9	0.20	100.8
12 m	-1.09	-1.78	82.1	0.10	99.2
14 m	-1.16	-1.77	72.6	-0.03	94.2
20 m	-1.35	-1.80	53.6	-0.30	87.5

Table 60: Maximum principal stresses at the main section - upstream

Maximum Principal Stress - Main Section - DS					
170m	Static load	dynamic load			
Crest thickness	Maximum Principal Stress [MPa]	min. Maximum Principal Stress [MPa]	Difference from static load in %	max. Maximum Principal Stress [MPa]	Difference from static load in %
8 m	0.62	0.00	100.0	2.85	100.0
9 m	0.63	0.00	101.6	2.70	92.8
10 m	0.64	0.00	103.2	2.60	87.9
12 m	0.61	0.00	98.4	2.40	80.3
14 m	0.55	0.00	88.7	2.20	74.0
20 m	0.26	0.00	41.9	2.10	82.5

Table 61: Maximum principal stresses at the main section – downstream

Maximum Principal Stress - Left Section - US					
100 m	Static load	dynamic load			
Crest thickness	Maximum Principal Stress [MPa]	min. Maximum Principal Stress [MPa]	Difference from static load in %	max. Maximum Principal Stress [MPa]	Difference from static load in %
8 m	-0.53	-1.22	100.0	0.94	100.0
9 m	-0.57	-1.24	97.1	0.82	94.6
10 m	-0.62	-1.24	89.9	0.71	90.5
12 m	-0.70	-1.22	75.4	0.52	83.0
14 m	-0.77	-1.26	71.0	0.39	78.9
20 m	-0.97	-1.28	44.9	0.22	81.0

Table 62: Maximum principal stresses at the left section – upstream

Maximum Principal Stress - Left Section - DS					
190m	Static load	dynamic load			
Crest thickness	Maximum Principal Stress [MPa]	min. Maximum Principal Stress [MPa]	Difference from static load in %	max. Maximum Principal Stress [MPa]	Difference from static load in %
8 m	0.20	0.00	100.0	1.55	100.0
9 m	0.20	0.00	100.0	1.47	94.1
10 m	0.20	0.00	100.0	1.38	87.4
12 m	0.15	0.00	75.0	1.31	85.9
14 m	0.09	0.00	45.0	1.31	90.4
20 m	0.00	0.00	0.0	1.00	74.1

Table 63: Maximum principal stresses at the left section - downstream

Maximum Principal Stress - Right Section - US					
100 m	Static load	dynamic load			
Crest thickness	Maximum Principal Stress [MPa]	min. Maximum Principal Stress [MPa]	Difference from static load in %	max. Maximum Principal Stress [MPa]	Difference from static load in %
8 m	-0.53	-1.13	100.0	1.10	100.0
9 m	-0.57	-1.15	96.7	1.17	106.7
10 m	-0.62	-1.18	93.3	1.23	113.5
12 m	-0.70	-1.21	85.0	1.25	119.6
14 m	-0.78	-1.20	70.0	1.17	119.6
20 m	-0.97	-1.30	55.0	0.76	106.1

Table 64: Maximum principal stresses at the right section – upstream

Maximum Principal Stress - Right Section - DS					
190m	Static load	dynamic load			
Crest thickness	Maximum Principal Stress [MPa]	min. Maximum Principal Stress [MPa]	Difference from static load in %	max. Maximum Principal Stress [MPa]	Difference from static load in %
8 m	0.20	0.00	100.0	1.33	100.0
9 m	0.20	0.00	100.0	1.20	88.5
10 m	0.19	0.00	95.0	1.22	91.2
12 m	0.15	0.00	75.0	1.63	131.0
14 m	0.09	0.00	45.0	1.87	157.5
20 m	0.00	0.00	0.0	1.28	113.3

Table 65: Maximum principal stresses at the right section - downstream

Maximum Principal Stress – Downstream

Figure 115, Figure 117 and Figure 119 show the maximum principal stresses along the downstream face. It can be seen that the tensile stresses decrease when the second acceleration is taken.

Maximum Principal Stress - Upstream

The results from the calculation before do not vary much from the results with the new acceleration. However, the tensile stresses on the upstream face at the main section decrease around 0.5 MPa.

It can be seen that on the left and the right section the tensile stresses increase for the new calculation with the acceleration that has the excitation frequency close to the Eigenfrequency.

The results show that the tendencies of the stresses and the deformation are the same as in the calculation made before. It can be seen that the deformation decreases more with the second acceleration.

The results show that the tensile stresses of the hoop stresses increase when the excitation frequency is close to the Eigenfrequency of the dams. Although, it is difficult to compare the hoop stresses with the results gained from the calculation before it can be said that the tensile stresses in general increase.

Same as in the calculation before, the tensile stresses according to the vertical stresses decrease in all sections along the upstream and the downstream face of the dam. A clear comparison of the results gained in the second calculation with the one before is also difficult to achieve. In general can be seen that the vertical stresses decrease with an acceleration which has its excitation frequency close to the Eigenfrequency of the dam.

The minimum principal stresses have the same tendency as in the results before. The tensile stresses increase with an increase of the volume of the height. The results of both calculations cannot be compared distinctly.

For the maximum principal stresses, the results show the same tendency as in the calculation before. The compressive stresses increase when the dam crest increases. The results of both calculations cannot be compared distinctly.

To get clearer results and to be able to compare the results better with the newly gained stresses and deformations, an acceleration with an amplitude higher than $1\text{m}^2/\text{s}$ should be taken. This could help by showing the differences in stresses between the investigated dam geometries.